



UNIVERSITÀ
DEGLI STUDI
DI PADOVA

Sede Amministrativa: Università degli Studi di Padova

Dipartimento di Geoscienze

SCUOLA DI DOTTORATO DI RICERCA IN SCIENZE DELLA TERRA
CICLO XXIII

THE CINQUE TORRI GROUP (THE DOLOMITES): ANALYSIS OF
PAST AND PRESENT-DAY GRAVITATIONAL PHENOMENA BY
LASER SCANNING AND NUMERICAL MODELING

Direttore della Scuola : Ch.mo Prof. Gilberto Artioli

Supervisore : Ch.mo Dott. Antonio Galgaro

Co-supervisore : Dott. Nereo Preto

Dottoranda: Alessia Viero

Padova, 31 Gennaio 2011

Ai miei cari

Table of contents

Abstract	5
Riassunto	11
1. Introduction	15
1.1. Scope	15
1.2. Problem definition.....	18
1.3. Research Rationale.....	20
1.4. Research Objective.....	21
1.5. Methodology.....	22
1.6. Thesis outline	24
2. The gravitational phenomena of the Cinque Torri group	27
2.1. Introduction to the study site	27
2.2. Local setting	30
2.3. The history of the Cinque Torri area	34
3. Laser scanning techniques	37
3.1. Introduction	37
3.2. Time of flight laser scanning: resolution and accuracy.....	40
3.3. Laser types: performances and specifications.....	41
3.4. Aerial laser scanning	43
3.5. Sources of error of 3D laser scan measurements	44
3.5.1 Horizontal and vertical sampling bias in terrestrial laser scanning..	45
3.6. Discussion and conclusions	46
4. Investigation on the Cinque Torri DSGSD by means of 3D geoelectrical tomography and passive seismic stratigraphy	49
4.1. Introduction	49
4.2. Data acquisition	50
4.2.1. Terrestrial laser scanner measurements	50
4.2.2. 3D Electrical Resistivity Tomography	50
4.2.3. Data inversion	52
4.3. Results of the ERT surveys and discussion	55
4.4. Passive seismic stratigraphy.....	61

4.4.1.	Results of the passive seismic stratigraphy.....	63
4.5.	Discussion and conclusions.....	65
5.	Laboratory analyses	67
5.1.	Introduction	67
5.2.	Atterberg limits	69
5.3.	X-ray analysis	73
5.4.	Ultrasonic velocities measurements	76
5.4.1.	Results of the ultrasonic tests measurements.....	78
5.5.	Uniaxial tests	80
5.5.1	Results of the uniaxial tests	81
5.6.	Discussion and conclusions	83
6.	Laser-scanning based recognition of rotational movements within the Cinque Torri Group	87
6.1.	Introduction.....	87
6.2.	Terrestrial and aerial laser scanning	88
6.2.1.	Laser scanner measurements.....	89
6.3.	Data analysis	91
6.3.1.	Method.....	91
6.3.2.	Structural analysis	93
6.4.	Quantification of discontinuity plane rotation.....	97
6.5.	Results	101
6.5.1.	Discontinuity sets and structural analysis.....	101
6.5.2.	Quantification of discontinuity plane rotations.....	105
6.6.	Discussion of the results and conclusion.....	109
7.	Rock properties extraction from point clouds and traditional field surveys	111
7.1.	Introduction.....	111
7.2.	Segmentation methodology.....	113
7.3.	Results for the Torre Inglese rock discontinuities extraction.....	117
7.4.	Computation of plane orientation and geometry	119
7.5.	Traditional geomechanical reliefs in the study area	122
7.5.1.	Rock discontinuities.....	123
7.6.	Introduction to rock mass properties derivation	124
7.6.1.	Hardness testing of rocks.....	125
7.6.2.	Scanline mapping and Rock Mass Rating.....	128
7.6.3.	Geological strength index (GSI).....	131
7.6.4.	Rock mass properties.....	133
7.7.	Discussion of the results and conclusion	137

8.	Numerical models of the Cinque Torri landslide: application and comparison of different approaches	141
8.1.	Introduction to numerical modeling.....	141
8.2.	Classes and objectives of numerical modeling.....	143
8.3.	Modeling with UDEC 4.1.....	144
8.3.1.	Effect of the monoliths.....	148
8.3.2.	Effects of the stratigraphy and deep angle of layers.....	158
8.3.3.	Shear strength reduction method.....	160
8.3.4.	Results of the numerical models in UDEC.....	163
8.4.	Modeling with Plaxis 8.5.....	165
8.4.1.	Plaxis elaborations.....	166
8.4.2.	Plaxis results.....	171
8.5.	Results and discussion.....	173
9.	Conclusions.....	175
9.1.	Analysis of the present-day setting.....	175
9.2.	Investigation of past movements through a novel methodology.....	177
9.3.	Interpretation of current and future instabilities.....	178
9.4.	The use of accurate geometrical reliefs.....	179
9.5.	The hydrogeological setting of the area: future perspectives.....	181
9.6.	Applications and limitations.....	182
9.7.	Concluding remarks.....	183
	References	185
	Appendices	195

Abstract

Many sites in the Dolomites are endangered by mountain slope instabilities, whose effects can lead to exposure of both human life and infrastructures to landslide hazard. In cases of reactivated or active landslides, the knowledge of the past gravitational phenomena can allow an indirect analysis of the present slope setting, therefore leading to an explanation of the triggering factors of the instability. In this cognitive process, the first step is the characterization of geometry and rock material properties of the studied unstable slope.

Among the wide variety of gravitational phenomena, the Deep Seated Gravitational Slope Deformations (DSGSDs) still represent an open issue in terms of triggering factors and slope behavior.

This study concerns the analysis of the dynamics that govern an unstable rock group named Cinque Torri, placed in the Dolomites (Eastern Alps, Italy). The rock group is an articulated system of carbonatic monoliths located in a very important touristic area, therefore characterized by a significant risk. The involved instability phenomena represent an example of lateral spreading developed over a larger DSGSD. After the recent fall of a monolith of more than 10 000 m³, a scientific study began to monitor the more unstable sectors and to characterize the past and present movements as a fundamental tool for predictions of future movements and hazard assessment.

The present research outlines how the geomorphology of the area is strongly influenced by the tectonic structures that resulted from the Alpine orogeny and the geotechnical contrast between lithologies. This DSGSD is mainly influenced by the contact of lithologies with different rheological attitudes. The setting is represented by a plastic bed mainly made up by mudstone layers, and above a dolomite cliff roof, which is extremely tectonized and separated in various rocky towers of different dimensions.

Attempting to achieve greater insight in the ongoing lateral spreading, a method aimed at producing a quantitative analysis of occurred rotations has been developed, applied and validated.

The introduction of numerical modeling as last stage of the research aims to investigate the present-day slope instability mechanisms, and indirectly to support the outcomes of the analyzed rotations. In particular, the combined use of the distinct-element and the finite-element codes allows a modeling of the stress-strain relations within the slope and the control exerted by both discrete structures and rock-mass strength. Moreover, these codes provide a powerful method to assess the influence of the controlling factors on the overall instability.

This research project is articulated in following steps:

1. Recognition and characterization of the main discontinuity systems through the use of laser scanner datasets (terrestrial, TLS, and aerial laser scanner, ALS), and their validation through traditional field measurements.
2. Rock properties classification through field surveys and laboratory analyses.
3. Geophysical investigations (Electrical Resistivity Tomography and passive seismic reliefs) aimed to discern the buried structural setting of the slope.

4. Use of the experimental software packages Coltop-3D (Jaboyedoff, 2007) and PCM (Vosselman, 2004) on TLS/ALS data, to discriminate the tectonic influence on local rock instability phenomena and provide a complete geometrical characterization of rock discontinuities respectively.
5. Structural correlation among the spreaded rock monoliths.
6. Estimation of the rotational components of the lateral spreading, in order to predict future instabilities and to interpret the buried features of the DSGSD.
7. Numerical modeling of the DSGSD based on a distinct element code (UDEC, 4.1) and a finite element code (Plaxis, 8.5). In order to create a conceptual model of the present and future instabilities, a comparison of the results of the modeling and the interpretation of the rotational component analysis is achieved.

In particular, the most significant achievement of this thesis concerns the role of rock discontinuities for indirect analysis of the initial slope conditions by providing a novel methodology for rotational movements computation based on laser scanner data treatment.

The input data frame is based on the accurate geometrical survey of the Cinque Torri area obtained by laser scanning. In June 2008, the Cinque Torri rock group was observed by using a long-range TLS and an ALS. The survey was performed covering a surface of about 22 km². In this way, a multi-scale model of the unstable rocky group and its surroundings is derived.

The results of the proposed methodology allows a primary identification of the tectonic fabric on the spread rock sectors in terms of representativeness of joint families inside the group with respect to a reference frame fixed on the external stable areas. Both bedding planes and representative joint-sets are used to derive the Euler angles that describe the rotational components of the lateral spreading. On the basis of these results, a new interpretation of the phenomena is achieved.

The variations from the regional trend provide a kinematic description of the past gravitational movement of the Cinque Torri group, which can be interpreted as initially controlled by the inherited tectonic features and subsequently differentiated into sectors. After such a differentiation, the movements are most likely induced by deep seated ground deformation and local topographic anomalies related to the lateral spreading development.

The geophysical data allow a confirmation and a completion of these interpretations. In particular, these data show that the tectonic action in the Cinque Torri area produced substantial changes in the strata bedding orientation which may have favored tilts and rotations of the uppermost brittle carbonates.

At a final stage, in order to decipher slope behavior, a reliable slope model is derived from accurate geometrical surveys of the outcropped rocks, analysis of compositional, mechanical and physical properties of the involved lithotypes. The slope modeling shows that three major factors control the behavior of the Cinque Torri DSGSD: (i) the monolith weight; (ii) the stratigraphical heterogeneity, and (iii) the inclination of strata. Two-dimensional finite difference and distinct-element modeling indicate small displacements of the overall DSGSD, confirming the typical velocities of this type of

landslide. These computations provide a model able to describe the geometries and gravitational mechanisms acting within the investigated slope.

The results of the field observations, rotational components analysis and numerical models suggest that the Cinque Torri DSGSD involves a complex mechanism with a rotational component of the movement, and a probable differentiation of the sliding surface of the DSGSD into segments with different amounts of rotation. In addition, the plastic deformation within the cohesive layers induces tilts, rotations and displacements of the topmost monoliths.

The results achieved during this research provide a comprehensive scheme of geometries and processes acting within the Cinque Torri slope. The obtained information can be used for hazard assessment purposes.

Keywords: Cinque Torri; Lateral spreading; Deep-seated Gravitational Slope Deformations; Rock Discontinuities; Rotation Angles; Laser Scanner; Applied Geophysics; Numerical Modeling.

Riassunto

IL territorio dolomitico è spesso interessato da fenomeni franosi di diversa entità che possono coinvolgere comunità e infrastrutture. Da ciò deriva la necessità di valutare costantemente le condizioni di instabilità, dunque di rischio, delle aree montane, al fine di poter predisporre adeguate misure di salvaguardia. Come dimostrato nella presente tesi di dottorato, l'analisi dei processi gravitativi avvenuti nel passato può essere importante per la comprensione dei fenomeni attuali o recenti, sia in termini di processo, sia in termini di volumi coinvolti. In genere, i fenomeni gravitativi possono essere decifrati attraverso il riconoscimento di un criterio geometrico che relazioni le porzioni di pendio mobilitate dal processo gravitativo, e che perciò fornisca indicazioni sull'assetto del pendio antecedente l'instabilità. Al fine di una corretta analisi delle dinamiche di versante è perciò fondamentale definire inizialmente geometrie e proprietà delle litologie che caratterizzano il pendio instabile.

Tra i molteplici fenomeni gravitativi esistenti in natura, le Deformazioni Gravitative Profonde di Versante (DGPV) rappresentano tutt'oggi un argomento di ampia discussione.

La presente tesi di dottorato si occupa dell'analisi dei fenomeni instabilità nell'area turistica del gruppo Cinque Torri (Dolomiti bellunesi, Alpi orientali, Italia). Un'ipotesi avvalorata dai precedenti studi vede il pendio su cui poggia il gruppo roccioso coinvolto da un processo di DGPV ampio, la cui espressione superficiale è rappresentata dall'espandimento laterale dei torrioni dolomitici a monte. Il recente crollo della Torre Trepfor, uno dei monoliti carbonatici che costituiscono il gruppo, avvenuto nel 2004, ha dato inizio ad un complesso studio scientifico concernente il monitoraggio dei settori più instabili e la caratterizzazione dei fenomeni d'instabilità attuali e passati come strumento di predizione e valutazione della pericolosità dell'area.

Le attività di ricerca si inseriscono in questo quadro come strumento di analisi approfondita delle dinamiche passate e in atto dell'espandimento laterale delle Cinque Torri. I processi gravitativi, così come la geomorfologia dell'area esaminata, sono strettamente legati all'assetto tettonico locale e alle caratteristiche meccaniche delle litologie ivi presenti. Difatti la DGPV dell'area Cinque Torri trova origine dal contrasto di competenza fra litologie a comportamento fragile (livelli carbonatici) e litologie a comportamento duttile (livelli marnosi).

Il punto chiave della ricerca vede lo sviluppo di una nuova metodologia di analisi basata sulla trattazione di dati geometrici derivati da acquisizioni laser scanner.

Nella fase finale di ricerca, l'introduzione di modelli numerici promuove un'analisi delle dinamiche in atto nel pendio offrendo uno strumento di validazione delle interpretazioni ottenute dall'analisi dei dati geometrici. Inoltre, l'approccio numerico permette la valutazione del grado di influenza di alcuni fattori predisponenti la DGPV in esame.

Le fasi del progetto di ricerca volte alla caratterizzazione di forme e processi nell'area in esame, possono essere così riassunte:

1. Identificazione dei principali sistemi di discontinuità degli affioramenti rocciosi attraverso l'uso di dati laser scanner (terrestre e aereo) e successiva validazione attraverso rilievi tradizionali di campagna;
2. Classificazione delle proprietà delle litologie coinvolte ottenuta da rilievi di campagna e prove di laboratorio;
3. Indagini geofisiche (tomografia elettrica e rilievi di sismica passiva) per l'identificazione indiretta dell'assetto strutturale del sottosuolo.
4. Utilizzo del pacchetto software sperimentale Coltop-3D (Jaboyedoff, 2007) per la caratterizzazione delle discontinuità e distinzione tra discontinuità tettoniche e gravitative e, inoltre, introduzione del software sperimentale PCM (Vosselman, 2004) per la caratterizzazione geometrica delle principali famiglie di discontinuità come criterio di confronto con il dato di campagna;
5. Correlazione strutturale tra monoliti rocciosi;
6. Calcolo delle componenti rotazionali dell'espansione laterale in atto, allo scopo di predire future instabilità e di interpretare le strutture sepolte;
7. Modellazione numerica della DGPV, realizzata attraverso codici di calcolo agli elementi distinti (UDEC, 4.1) e agli elementi finiti (Plaxis, 8.5). Paragonando i risultati ottenuti dalla modellazione numerica e le interpretazioni derivate dall'analisi delle componenti rotazionali si è potuto così ottenere un modello concettuale delle instabilità attuali e future.

In particolare, il risultato più significativo di questa tesi riguarda l'utilizzo dei rapporti geometrici esistenti fra le discontinuità tettoniche per l'analisi indiretta dei movimenti gravitativi. Infatti, attraverso l'analisi del dato laser scanner sono state ricostruite le componenti rotazionali dei movimenti che hanno determinato l'attuale assetto del gruppo Cinque Torri. Alla base di questa innovativa trattazione c'è il rilievo geometrico ad alta risoluzione, ottenuto attraverso l'impiego di tecniche laser scanner. Nel giugno 2008 infatti, la geometria del gruppo Cinque Torri è stata acquisita totalmente grazie un laser scanner terrestre (LST) a lunga portata ed inoltre un'acquisizione laser da aereo ha permesso di completare l'informazione geometrica sulle aree circostanti il gruppo roccioso. La combinazione dei due tipi di dato ha garantito la creazione di un modello geometrico multi-scala dell'area, con particolare attenzione alla rappresentazione di superfici planari sia orizzontali, sia verticali. Grazie a questo metodo sono state identificate le famiglie di discontinuità esistenti in ciascun monolite, successivamente correlate con dei set di riferimento estratti da affioramenti rocciosi esterni alla DGPV. Da tali correlazioni sono state poi dedotte le componenti angolari di spostamento dei set individuati rispetto a quelli di riferimento, fornendo le basi per nuova interpretazione dei fenomeni gravitativi in atto. Dai risultati della ricerca si evince che le dinamiche del pendio sono inizialmente controllate dalle principali direttrici tettoniche, che di fatto hanno frammentato il gruppo roccioso secondo chiare leggi geometriche. In una fase successiva la suddivisione del gruppo e l'allontanamento dei monoliti sono indotti dalla DGPV e da anomalie locali topografiche (legate con buona probabilità alla sviluppo dell'espansione laterale).

Questa interpretazione ha trovato riscontro nei risultati delle indagini geofisiche condotte nell'area in studio. Tali indagini hanno evidenziato il quadro tettonico del pendio sottostante il gruppo Cinque Torri, mettendo in luce dislocazioni metriche verticali subite dalla stratigrafia. E' ragionevole ipotizzare che questi gradini strutturali influenzino in parte le rotazioni e i basculamenti in atto nel gruppo Cinque Torri.

L'ultima parte della tesi è dedicata alla modellazione numerica del pendio, realizzata attraverso l'uso dell'accurato modello geometrico fornito dalle acquisizioni laser scanner e dai risultati delle prove di laboratorio e di campagna attuate per la caratterizzazione

delle litologie coinvolte. La modellazione numerica ha evidenziato che i fattori che maggiormente influenzano l'instabilità del pendio in studio risiedono nell'azione della forza peso agente sul pendio ad opera dei monoliti, nell'eterogeneità stratigrafica e nell'inclinazione degli strati. Inoltre, i risultati di tali modelli numerici confermano le interpretazioni dedotte dallo studio delle componenti rotazionali sulla geometria della DGPV.

In conclusione la tesi proposta fornisce un modello interpretativo dei fenomeni gravitativi dell'area Cinque Torri, che coinvolgono deformazioni gravitative profonde con componente pseudo-circolare e significative deformazioni plastiche all'interno degli strati marnosi. Queste ultime inducono basculamenti, rotazioni e traslazioni nelle porzioni sommitali del pendio, in altre parole, l'espandimento laterale.

L'insieme dei risultati così raggiunto fornisce un quadro nuovo per l'identificazione dei controlli strutturali e la comprensione dei processi agenti all'interno del pendio Cinque Torri, da cui un valido strumento per la valutazione e mitigazione del rischio.

1. Introduction

1.1. Scope

The Cinque Torri group (Fig. 1.1) is located in Dolomites, the recently elected UNESCO World heritage site (UNESCO, 2010), and consists in a dozen of carbonatic rock monoliths which creates impressive scenery. Due to the presence of ski resorts and numerous footpaths and rock climbing walls (Fig. 1.2), the area is an internationally well known tourist place. The rock group extends over an area of about 41000 m² and is characterized by frequent rock falls mainly induced by Deep Seated Gravitational Slope Deformation (DSSGD) and rock weathering.

At the present time the rock monoliths are subjected to the so called lateral spreading. Significant movements like tilts and rotations occur as a consequence of accommodation of the rigid blocks on a highly ductile substratum and to degradation phenomena as frost shattering.



Fig. 1.1. Cinque Torri group viewed from Rifugio Scoiattoli. Many tourists access the area all over the year.

Recent rock collapses and slope instabilities suggested to undertake a multidisciplinary investigation program, consisting of: geological and geomechanical field surveys, geophysical investigations, temperature and deformation sensors installation, GPS displacement monitoring, Terrestrial Laser Scanner (TLS) and Airborne Laser Scanner (ALS)-based geometrical and geomechanical characterization, numerical modeling for stability assessment. The aims of the whole investigation program are the hazard assessment of the area and a rock-fall early warning system.



Fig. 1.2. Pictures of Torre Mezzo pinnacle from East (left) and of the Torre Grande pinnacle from North-West (right). During summer many tourists access the area to climb the fully equipped rock walls of Cinque Torri group.

Among several possible types of approaches, the present PhD thesis deals with laser scanning data processing and numerical modeling. The former approach is used in order to guarantee both regional and local viewpoint to the investigation while the latter is mainly devoted to validation purposes. As this thesis demonstrates, the combination of TLS- and ALS-based data provides a multi-scale vision of the tectonic setting of the surfaces involved in the DSGSD, enabling a palinspastic analysis of the local instability phenomena. In order to obtain a general model able at describing superficial and deep deformations, the rotational components of lateral spreading processes have been investigated through an iterative methodology later validated by field surveys. Once obtained the Cinque Torri DSGSD geometrical model and by taking into account opportune assumptions on material models and on the hydrogeology context, this model is compared to the results of numerical computations and a final volume estimation of the whole instability is achieved.

In the last few decades, the DSGSDs have been defined on the basis of several classification parameters related to common geometries, geological and tectonic controls and similar kinematics. Even if a common general definition of DSGSD has been achieved by Dramis and Sorriso-Valvo (1994), every case study differs in the local setting and lithologies involved. Such a gravitational phenomenon is typically slow (0.4–5 mm y⁻¹; see e.g. Varnes et al., 1990; Agliardi et al., 2009), and mainly controlled by structural features such as bedding, foliation and fractures (Radbruch-Hall, 1978; Agliardi et al., 2001; Kellogg, 2001, Massironi et al., 2003).

Many investigation methods have been applied on DSGSD to achieve a better understanding on the geometrical patterns of a phenomenon that typically expresses its major deformation at high depths. In this study, a new method to investigate past movements inside a gravitational body by means of rock discontinuity analysis is proposed. In particular, to achieve greater insight on the ongoing lateral spreading process, a method for a quantitative analysis of rotational movements associated with the lateral spreading has been developed, applied and validated.

In order to support final interpretations, an integrated survey procedure based on geological field observations and geophysical measurements has been developed and tested in the area. This procedure investigates the structural patterns affecting the subsoil of DSGSD and therefore can be directly related to the phenomena which guide the lateral spreading of rock pinnacles. The present thesis also presents the results of the Electrical Resistivity Tomography (ERT) and passive seismic surveys carried out in order to gain a better insight in DSGSD of the Cinque Torri group. The geophysical investigations particularly addressed the location of the major faults and the lithological contact geometries. A secondary aim of these non-destructive surveys was to understand their potentials of application in similar sites in the Dolomites where analogue geological settings occur.

As a matter of fact although geophysical and geological imaging of near surface faults have been reported in several studies (Demagnet et al., 2001; Wise et al. 2003; Nguyen et al. 2005) a comprehensive 3D high-resolution electrical survey in the Dolomite area represents a novel application. Geophysical data clearly outline some tectonic and stratigraphical contacts along with and between the different lithological units. Based on these results the structural model of the study site is better defined finding some keys to provide a new interpretation.

Nowadays the mechanics of large gravitational slope deformations is not well understood and only a few studies on this topic have been carried out using numerical techniques (a.a. Hurlimann et al., 2006). The experience on numerical modeling for landslide reports that the main factors influencing the displacements of slopes mainly are the thickness and strength of the weak lithologies, inclination of slopes, rock discontinuities and groundwater level. The introduction of numerical modeling as last stage of the research aims to investigate the slope instability mechanisms by defining the principal inducing factors and indirectly to support the outcomes of the analyzed rotations (Chapter 6). In particular, the combined use of the distinct-element and the finite elements codes attempts to model the stress-strain relations within the slope and the control exerted by both discrete structures and rock-mass strength. Moreover these codes provide a powerful method to highlight the different aspects of the geotechnical and mechanical behaviors of the rock types constituting the unstable slope for different conditions.

In the case of the Cinque Torri landslide, the use of different models provided by UDEC software (Itasca, 2004) and Plaxis software (Brinkgreve et al., 2008) allows to assess and

relatively speaking quantify the influence of the above mentioned factors to the overall instability. The main purposes of the numerical modeling are:

- a) Creation of a possible model of the DSGSD in terms of mechanism, shape, dimensions and geotechnical relations among lithologies;
- c) Comparison and assessment of the modeling results (Chapter 8) with the interpretations derived from the analysis of the rotational components of the lateral spreading of the rock pinnacles (Chapter 6).

Because the slope data are limited in this case and are referred to few geotechnical and mineralogical analyses, general trends rather than quantitative values were expected from this modeling study.

1.2. Problem definition

In the Cortina d'Ampezzo area, DSGSDs are quite common and frequently occur at the contact between brittle and plastic lithologies. In the study area this contact is represented by the stratigraphic boundary between the Travenanzes Formation, which includes mainly reddish mudstones with minor intercalations of peritidal dolostones, and the overlying Dolomia Principale (DPR), consisting of well-bedded white and grey cyclic dolomites (Fisher, 1964; Bosellini, 1967). This heterogeneous stratigraphy produces a high variable behavior from a geomechanical viewpoint. The elected codes (UDEC, Plaxis) for slope dynamics analysis should create a model able at reproducing both fragile and plastic behaviors.

In the case of the complex geotechnical setting of the Cinque Torri slope, it is assumed that the displacement pattern in terms of position in the stratigraphic sequence is mainly controlled by the mechanical properties of the cohesive layers, while the number of joints characterizing the rock layers, controls the shape of the deformation.

Due to the wide variety of DSGSDs present in nature, a standard procedure in the analysis of such phenomena does not exist and its use would be conceptually incorrect. Every case of slope instability differs from geological, structural, hydrogeological and rheological viewpoints, therefore adequate field investigations should be required. For instance, when slope instability is likely to occur and mitigations countermeasures have to be planned, the investigations should be organized as follow:

- a) Traditional field surveys carried out in order to determine the characteristics of the lithotypes of the unstable slope and to locate the external boundaries of the landslide for a preliminary volume estimation;
- b) Monitoring programs focused on the recorded surface movements (GPS and rock extensometers), on the deep deformations (drilling programs and inclinometer equipment) and on hydrogeological conditions (electrical-equipped piezometers and explorative wells);
- c) Direct analysis of the drilling materials extracted at representative locations on the slope;

- d) Representative rock and soil sampling performed to provide, after laboratory measurements, a robust input model of the slope to be introduced in numerical analyses for stability assessment purposes.
- e) In case of ancient and recent landslides, rock and soil dating should be planned in order to temporally classify the phenomena and therefore to support or neglect the possible causes suggested by other investigations.

At the time of writing the direct information of the Cinque Torri slope conditions and monitoring campaigns falls down in the geotechnical and hydrogeological characterization, avoiding a reliable slope stability assessment.

In case of preliminary or validation analyses of rock and slope instabilities, when rotational movements occur, an alternative approach should be required. By investigating the surface features affecting a slope, interpretations of past and current instabilities can be achieved by analyzing and correlating the unstable rock masses with respect to the surrounding stable areas and among the different part of the slope instability itself. This can guide a deduction of the buried structures and dynamics involved in the unstable scenery resulting in a final solid model.

An important aspect that should be underlined is how any traditional investigation, such as drillings or laboratory tests, represents punctual information of the entire body rather than a statistical representation of its characteristics. Conversely, hydrogeological monitoring surveys which are typically carried out during a wide period cannot describe local variation of neutral pressures that can induce a significant decrease of the internal strengths of the slope materials in a specific part of the slope.

It can be easily considered how the unstable slope bears witness to the past and present phenomena acting within the slope itself and can be critically analyzed in order to deduce the processes and factors that led to the present-day setting, providing therefore a key study for future instabilities and a general comprehension of the group of phenomena acting in the slope.

In cases as the Cinque Torri area, where direct information of the subsoil is not provided, a method able to indirectly identify the behavior and geometries of the gravitational body is required. The surface expression of the deeper DSGSD is the lateral spreading of the Cinque Torri group and, through its analysis, the interaction with the DSGSD can be solved.

Indirect analyses of unstable areas generally provide interpretations of the past and present conditions rather than a method to predict future instabilities. Nonetheless these interpretations are fundamental in promoting new insights of DSGSDs occurring in sedimentary sequences once they are opportunely validated. In the present thesis an attempt of validation is achieved by comparing the interpretations of the slope dynamics to the results derived from numerical computations of slope conditions. With such an approach the slope behavior is assessed in relation to different conditions and the physic-mechanical relationships among the lithotypes allow explaining their role in the overall instability.

1.3. Research rationale

In the study case direct information of the slope conditions is missing, therefore any interpretation of the slope stability is purely qualitative and indicative. In this frame an alternative investigation technique based on remote sensing technologies and non-invasive geophysical surveys could provide a complete and accurate geometrical and structural model of the surveyed area which can be imported in numerical models for validation purposes.

The use of remote sensing techniques offers a logic alternative to manual survey of rock faces, since remote sensing avoids the potentially dangerous and ineffective physical contact with the rock slope. When dealing with rock bodies, a fundamental aspect is related to the rock body characterization by analyzing geometric properties of discontinuities which may be measured in the field with geologic compass and clinometer. Although these tools are effective, they introduce some errors due to their inaccuracy and human-induced biases (Slob et al., 2002). Erroneous data are very often introduced with such traditional method due to local variation of the parameters investigated when positioning the instruments on unrepresentative portions of the rocky outcrop with respect to the overall investigated feature. The traditional approach is besides a punctual investigation, and in order to reduce the local errors derived from the arbitrary choice of some representative rock discontinuities of the same discontinuity family, higher sampling are needed resulting in time-consuming and costly surveys.

Nowadays, TLS and ALS are often used for rock slope characterization because these techniques are able to provide detailed, dense, homogeneous and accurate 3D data of the acquired surfaces. Feng et al. (2001) firstly experienced the possibility to use a laser range finder, in the form of reflectorless total station to measure fracture orientations. The main advantage of laser scanning techniques is that it allows the rapid generation of a very detailed and accurate three-dimensional geometric representation of exposed rock faces. The acquired data are represented by geometric representation of the scanned surface, the so-called point cloud, made up by millions of points, each characterized by x , y , z values and by intensity scalars or mapped RGB colorization via photo coupling.

Data provided by TLS-based surveys allow the generation of accurate geometrical models of discontinuous rock masses as well as the detection of relative displacements of unstable zones through the use of multi-temporal images. The TLS can be used for deformation and structural analysis, as shown by Teza et al. (2007), and many others. Respect to topographical methods and the traditional scanline mapping this approach shows higher accuracy and its remote acquisition allows fast and safe surveys (Slob, 2005).

Generally such dense data sets are imported in computer programs devoted to numerically model rock mass properties in two and three dimensions (Itasca2010) with the final objective of slope stability assessment.

The heterogeneous stratigraphy of the study area produces a high variable behavior from a geomechanical viewpoint. In this scenery both discrete and finite element codes are suitable since the former create appropriate models for jointed rocks reproducing the deformation typical of fragile media while the latter are generally devoted to reproduce the ductile behavior of soil and soft rocks.

In particular, as experienced by Brideau et al. (2006), the combined use of the finite element and the distinct-element codes allowed modeling respectively the stress-strain relations within the slope and the control exerted by both discrete structures and rock-mass strength.

Since no slope stability assessment was foreseen within this research, only some field surveys and laboratory tests were carried out in order to ascertain the stratigraphical, geometrical and geotechnical relationships among the involved lithologies rather than a quantitative definition of their principal properties.

The main rationale behind this research is that in the geometrical pattern of the surface lateral spreading can be inferred the characteristics of the lower DSGSD. The Cinque Torri is a group of discontinuous rock monoliths whose surfaces originate from faults, joints or discontinuities. The basic principle in the manipulation of laser datasets is that the gravitational instability of the Cinque Torri is strongly conditioned by tectonic, and the recognition of structural features inside and outside the hazardous area furnishes the keystone for the past movements interpretation and therefore an effective tool in instability forecasting. The combined use of ASL and TLS data sets provide a large amount of highly accurate information on the geometric properties of discontinuities within the unstable areas and in the surroundings, allowing tectonic relationships and thus helping in the analysis of the past and current movements.

The main research question therefore is: how a multi-scale approach can be decisive in the understanding of the Cinque Torri DSGSD and how verify the reliability of the final interpretation?

1.4. Research objective

The main research objective is a verification of the effectiveness of correlations among rock discontinuities acquired by three-dimensional laser scanning for the analysis of gravitational phenomena showing similarities to the Cinque Torri case.

The present study focuses on a new method to investigate rotational components of gravitational movements by analyzing rock discontinuities. The combination of laser scanner techniques, a semi-automated back analysis based on a structural analysis and some MATLAB scripts for validation purposes, promotes accuracy, time saving and a more comprehensive explanation of the ongoing gravitational phenomena of the Cinque Torri area. This analysis allows to make assumptions on the roles of tectonic and gravity in the dismantling of the group, providing bases for the past movements interpretation. A crucial issue in this study is the reconstruction of a model able to explain the causes that triggered and fed the Cinque Torri landslide. In order to model the ongoing

phenomena and to assess the role of the factors that influence the DSGSD, numerical models of the slope behavior are carried out. Attempting to create a reliable model of the slope, geophysical investigations as well as laboratory and geotechnical relief results are accounted.

1.5. Methodology

Starting from an accurate geometrical characterization of the Cinque Torri rock monoliths a new method was developed in order to evaluate some hypotheses on the causes of the initial fragmentation of a former dolomitic plateau, afterwards dismantled in different rock cliffs- among the others, the Cinque Torri-owing to the action of different tectonic phases together with deglaciation and erosive processes.

In this work terrestrial TLS and ALS data were combined in order to obtain information about on steep and planar surfaces respectively. In this way, a complete geometrical picture of the observed system can be obtained.

The methodology of this part of the research consists of the following elements:

- 1) Acquisition of laser scanner data from the Cinque Torri area.
- 2) Analysis of the 3-D point cloud provided by laser scanner measurements through the application of the Coltop-3D software (Fig. 1.3)(Jaboyedoff et al., 2007, 2009).
- 3) Subdivision of the Cinque Torri area into different isolated sectors on the basis of morphological criteria and the previously defined rock discontinuities.
- 4) Comparison of the structural setting among the Cinque Torri sectors and between the Cinque Torri group and the regional tectonic framework to detect the joint sets with a definite tectonic origin.
- 5) Manual selection of planar and quasi-planar point cloud subsets and corresponding least square plane fitting, carried out in PolyWorks (Innovmetric, 2010). Such a fitting provides the normal unit vector and the corresponding main statistical parameters at each discontinuity set.
- 6) Estimation of the rotations of rock monoliths in terms of Euler angles by computing reorientation of reliable pairs of discontinuities identified by the structural analysis, belonging to different sectors.

In this way, the present settlement of the Cinque Torri system with respect to the surrounding stable areas is defined and significant information on the processes involved in the fragmentation and spreading of a former dolomitic plateau into different rock cliffs has been gained.

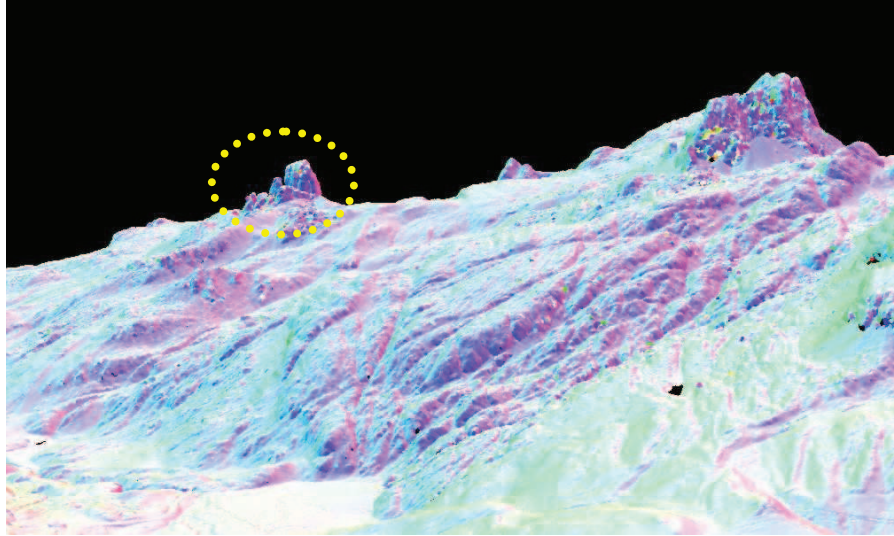


Fig. 1.3. A render view with Coltop-3D of the North-Western part of the ALS acquired area (Cinque Torri, Dolomites, Italy)

As the interpretations of the Cinque Torri DSGSD derived from rotational analysis need to be verified, numerical models of the slope behavior are developed and the role of the factors that influence the DSGSD has been assessed. In order to achieve such objectives a geometrical, stratigraphical, structural and geotechnical simplified model of the investigated slope is needed. Such information is derived from traditional field surveys and laboratory analyses.

Detailed topographical models coupled to geophysical surveys (Electrical Resistivity Tomography-ERT and passive seismic) allow investigating the buried structures of the slope, therefore providing some insights on the lithological and tectonic contacts involved in the DSGSD helping in the interpretation of the phenomena.

Laboratory tests are represented by:

- a) uniaxial compression tests on rock samples, aiding for rock strength parameters analysis;
- b) Atterberg limits for plastic and liquid limits determination of the weathered rock samples;
- c) X-ray diffraction analysis on the most of the samples analyzed on point b) in order to qualitatively determine the most representative mineral components and then find correlations with compressibility.

Moreover the introduction of TLS data processing by means of the experimental software Point Cloud Mapper (PCM) (Vosselman, 2004), combined to the Least Square estimation (Chap. 7), allows automated structural discontinuity analysis of the Torre Inglese, which is the most unstable rock pinnacle within the group. Moreover, the results about the main geometrical properties of the rock discontinuities, i.e. the dip angle and the dip direction, have been compared with the ones provided by traditional geomechanical field reliefs. In this way representative values of the discontinuity families such as normal set spacing, plane centroid and the maximum extends of x , y and z coordinates of each discontinuity plane can be corrected by biases encountered during

traditional field surveys and then introduced on numerical models for instability analysis.

The combination of all these approaches promotes accuracy and a more comprehensive explanation of the ongoing gravitational phenomena in the Cinque Torri area.

1.6. Thesis outline

This thesis consists of 9 Chapters:

Chapter 2 introduces the study site and the type of gravitational instability. It describes the local geological and structural setting and their role at predisposing DSGSD. It summarizes the importance of evaluating the characteristic of rock discontinuities to determine the instability prone character of rock bodies and to detect movements within the rock bodies. It further introduces the current remote sensing methods used to collect discontinuity data and their advantages with respect to traditional approaches. Finally, the main role of discontinuities and the importance of their correct representation in rock modeling are discussed here.

Chapter 3 analyses three-dimensional terrestrial and aerial laser scanning as survey techniques. Data quality aspects as well as types of acquisitions are summarized with emphasis to the advantages of the combination of both techniques for instability evaluation.

Chapter 4 deals with geophysical investigations of the subsoil in the surroundings of the Cinque Torri group. This chapter presents the results of the Electrical Resistivity Tomography (ERT) and passive seismic surveys carried out in order to gain a better insight in DSGSD of the Cinque Torri group. The innovative combination of these geophysical investigations addressed to the location of the major faults and the lithological contact geometries, aiding a stratigraphic and deformation analysis of the unstable slope. This combination results particularly helpful when direct analysis of the stratigraphy of an unstable slope is missing.

Chapter 5 describes the typologies of laboratory analyses carried out within the present research and focuses on the characterization of the lithologies involved in the Cinque Torri DSGSD by relatively investigating the geotechnical properties as well as mineral composition. The main purpose of these tests does not involve an absolute evaluation of the above mentioned properties, but a relative comparison of them in order to highlight the existing relationship in terms of strength and composition. In particular, to derive strengths properties, uniaxial tests were carried out and afterwards correlated to ultrasonic pulse velocities for validation purposes. Furthermore, by comparing the results of Atterberg limits and X-ray diffraction analysis a critical relationship between the geotechnical parameters such as compressibility of the ductile lithologies and the compositional variables of silty-clayey components can be achieved.

Chapter 6 explains the development and evaluation of laser-scanning based recognition of rotational movements within the Cinque Torri group. The chapter describes the

methodological phases and principles that govern the laser-data treatment. Within each level different kinds of software packages are introduced in order to iteratively process the point cloud, to derive geometric information of the identified rock discontinuities and then calculate the Euler angle as expression of the past rotations happened within the group. At a last stage these results are discussed and an interpretation of the DSGSD is achieved.

Chapter 7 proposes an application of the direct segmentation approach to the most unstable rock monolith within the rock group. With such a method discontinuity orientation and spacing information are generated and can be used as reference for numerical modeling. In addition, manual field measurements collected as part of this study are used to provide verification of the point cloud analysis.

Chapter 8 examines the use of distinct-element (UDEC) and finite element (Plaxis) codes for investigating the present-day slope instability mechanisms. The resulting models create an effort for the interpretation derived from rotational analysis and indirectly evaluate the average volume involved. The modeling carried out by using UDEC is particularly devoted to the detection of the instability pattern that characterizes the DSGSD and to evaluate the role of the influencing factors on instabilities. Due to the lack of in situ and laboratory tests, the numerical analysis is faced as a qualitative method of investigating the Cinque Torri instability rather than a quantitative assessment of displacements and stresses fields.

Chapter 9 provides a summary of this research in the form of conclusions and recommendations for further research in the Cinque Torri area and more in general some advices for risk management.

2. The gravitational phenomena of the Cinque Torri group

2.1 Introduction to the study site

The Cinque Torri group is located on the right flank of the Falzarego Valley (Fig. 2.1) in the Cortina d'Ampezzo municipality (Belluno Province, Italy). It extends over an area of 41 000 m² and is made up of 12 pinnacles (a 13th pinnacle collapsed in 2004) characterized by lateral spreading and frequent rock falls. These instabilities are mainly induced by deep seated gravitational deformation (DSGSD) (Neri, 2007), rock weathering, and the erosive processes which mainly acted since the last glacial period (Soldati and Pasuto, 1991). Soldati and Pasuto (1991) describe the DSGSD of the Cinque Torri group as a lateral spreading process evolving into a block slide, coupled with rock falls and topples. The group is located in the Dolomites (a recently elected UNESCO World heritage site; UNESCO, 2010), and are called "Five Towers" because only five of them can be seen from the city of Cortina d'Ampezzo (Fig. 1.1). The heterogeneity of the geological sequence together with the complex tectonic activity recorded in the monoliths determine their instability. The examination of photographs taken at the beginning of the last century allowed the interpretation of a minimum displacement of 1 m among the monoliths (Soldati and Pasuto, 1991).

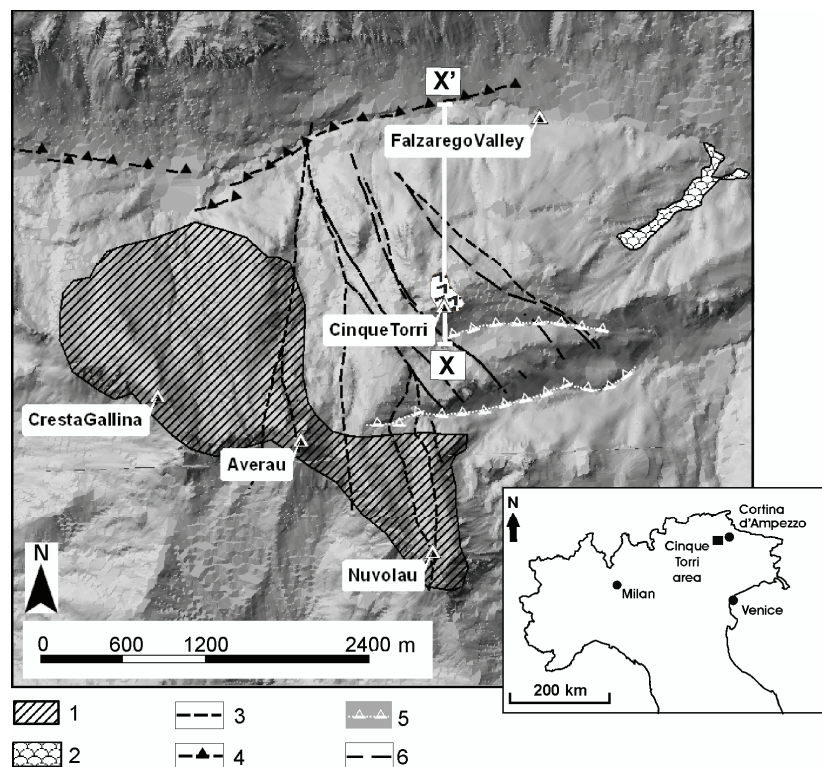


Fig. 2.1. Location of the Cinque Torri area in the Eastern Alps, Italy, and a shaded relief map of the study area. The main tectonic features and external reference area are also shown: (1) reference stable area, (2) mudflow, (3) N-S to NNW-SSE faults, (4) Falzarego Thrust, (5) counterscarps, and (6) NW trending gravitational graben.

Instabilities are also conditioned by weak surfaces involving the carbonatic sequence and by degradation phenomena such as freeze and thaw cycles.

Several rock cliff collapses have occurred at the DSGSD of the Cinque Torri group, the most recent of which was the fall of the Torre Trepbor at the beginning of June 2004 (Fig. 2.2). At present the rock monoliths are affected by perceptible movements such as tilts and rotations as a consequence of the settling of the rigid blocks on a highly ductile substratum. A GPS monitoring system was installed in 2007 on the top of the Torre Inglese, the most unstable monolith in the northern part of the rock group (Fig. 2.3). No movements are recorded yet, in confirmation of the typical low velocity of DSGSDs.

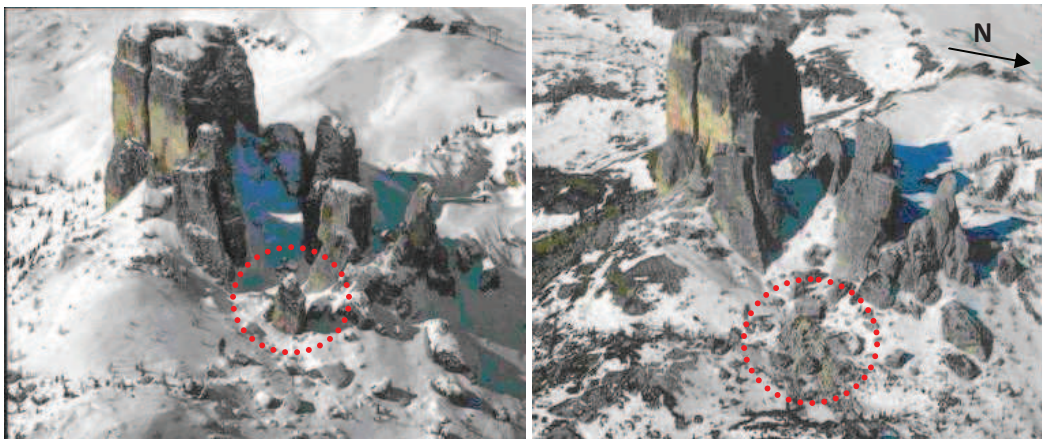


Fig. 2.2. Views of the Cinque Torri rocky group from the north-eastern side. In these pictures is evidenced the Torre Trepbor pinnacle before and after the collapse happened at the beginning of June 2004.

The advanced stage of evolution shown by the rock group which at the beginning was part of a wide carbonatic plateau can be explained only secondarily by the action of the erosive processes started from the last glacial period. As a matter of fact, in the Cortina area and its surroundings are also well documented several other gravitational bodies triggered by the retreat of the Würmian glaciers (Panizza, 1994). Differently from these cases the DSGSD of the Cinque Torri shows closer similarities to the so defined Subboreal landslides (Panizza et al., 1996). These landslides occurred just after the “Climatic Optimum” between 5000 yr and 4000 yr B.P. and they are mainly related to structural and lithological settings rather than climate conditions. The definition of structural landslides proposed by Kleczkowski (1955) and Bober (1984) as “...landslides occurring along certain natural geological planes, whose direction of shift is related to geological structure” is therefore applicable to the studied group and represents a crucial assumption for the research.

In the geologic framework of the study area, the Torre Trepbor collapse could be then considered as a normal event. In detail the event seems to be a combination of the local geological and tectonic settings, together with a freeze-thaw cycling effect and pore-water pressure increasing due to snow melting. The role of seismicity, although no significant earthquakes were reported at collapse time, is still an unresolved issue and a relation between earthquakes and the observed movements is also possible.

The potential instability of the other rock pinnacles, with volumes ranging between 25.000 m³ and 100.000 m³ (Table 2.1, Fig. 2.4), suggested to undertake a

multidisciplinary investigation program, consisting of geological and geomechanical field surveys, geophysical investigations, temperature and deformation sensors installation, GPS displacement monitoring, laser scanner geometrical and geomechanical characterization, numerical modeling for stability assessment. The aims of the whole investigation program are the hazard assessment of the area and a short term forecasting of rock-fall and pinnacle collapses.



Fig. 2.3. Phases of the GPS system on the top of the Torre Inglese pinnacle. This monolith is strongly bended and presents a wide steeped discontinuity plane parallel to stratigraphy that could become a sliding surface.

Table 2.1. Volume estimates of the rock pinnacles of the Cinque Torri group. The estimations were gathered by using the software package Polyworks (Fig. 2.4).

Monolith/s	Partial volume (m ³)	Total volume Cinque Torri group (m ³)
Torre Grande (North, South, West cliffs)	320000	540000
Torre Lusy, Barancio, Romana	40000	
Torre Latina	80000	
Torre Mezzo, Alta, Bassa	70000	
Torre Inglese, Avancorpo	30000	

At the margins of the DSGSD are sometimes reported “collateral” slope movements (Menotti et al., 1990) which may show an extremely rapid evolution. These phenomena, as suggested by Soldati et al. (1991), seem to be connected with the modifications of the groundwater flow and of the stress conditions of the slope induced by the acting deformations. An example of “collateral” events occurred during the summer of 1976, when a landslide of about 2400000 m³ broke off from the eastern side of the Cinque Torri group (the mudflow surface is reported in Fig. 2.1). This event took place after severe rainstorms and was triggered by the nearby Friuli Earthquake. Moreover, this event was influenced by the presence of bulges affecting the plastic material of the Travenanzes Formation caused by the overload of the dolomitic monoliths (Soldati et al., 1991). On 18 May 2009 this collateral phenomenon was affected by reactivation phase which produced a mudflow over an area of about 115.000 m² for a total volume of

about 500000 m³ involved and this event was related mainly to the snow melting and the quiescent instability of the gravitational deposits.

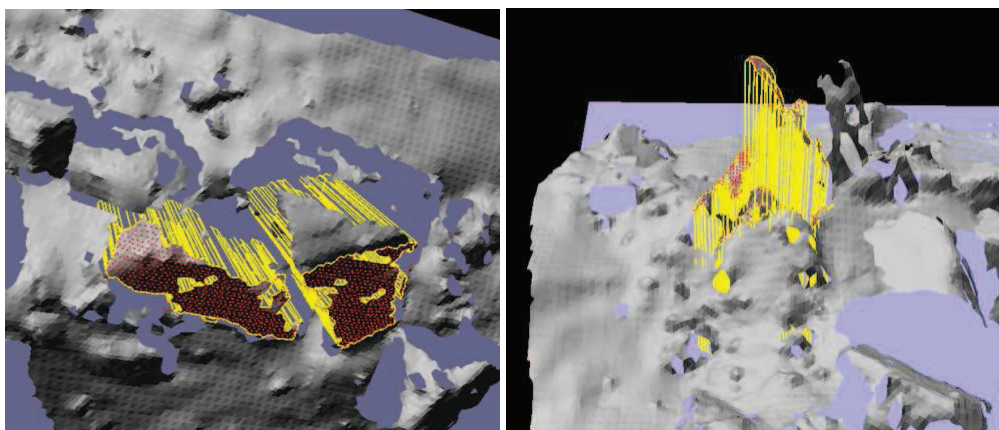


Fig. 2.4 Volume estimations of the Cinque Torri pinnacles. A Digital Terrain Model (DTM) of the rocky group topography obtained by surface reconstruction of the 3D point clouds (see Chap. 6 for details) and a reference plane which lies parallel to the stratigraphy at the base of the rocky towers are needed. The measurements basically extend the selection of the DTM which corresponds to the top surface of a tower towards the reference plane and calculate the volume.

2.2 Local setting

The Cinque Torri group belongs to the Italian Dolomites which are located in the Eastern Southern Alpine domain, a southern-vergent thrust and fold belt originated from N-S Alpine compression during the Cenozoic (e.g. Castellarin, 2006; Schönborn, 1999). In particular, the Cinque Torri group is located on a dolomitic platform interior on the footwall of the Falzarego Thrust, a southward-vergent Alpine thrust characterized by a northward dipping middle to low angle fault-plane.

The study area presents a Carnian (Upper Triassic) sedimentary succession constituted by the alternation of carbonate and silicoclastic lithologies resulting in a strong contrast in the geomechanical behavior of these materials. From the base to the top, the sedimentary sequence is formed by (Figs. 2.5, 2.6):

- i) Cassian Dolomite (Lower Carnian), consisting of small rimmed platforms (Cassian Dolomite, Assereto et al., 1977), formed by white greyish crystalline dolomites, generally massive.
- ii) Heiligkreuz Formation (Upper Carnian), consisting of white stromatolitic dolomites characterized by a decimetric layering and deposited in shallow marine conditions.
- iii) Travenanzes Formation (Upper Carnian), consisting of different lithologic layers. It includes polychrome pelites and marls, aphanitic limestones and microcrystalline dolomites. In the study area, it consists of prevalent reddish mudstones with sandstone to conglomerate intercalations, alternated with peritidal dolostones in thin beds (decimetric). The area surrounding the Cinque Torri group is mainly characterized by this formation, directly outcropping or by creating a gentle morphology. The base of the dolomitic outcrops forming the Cinque Torri is composed by the Travenanzes Formation.

iv) Dolomia Principale (Upper Carnian - Rhaetian), forming most of the dolomitic peaks of the Dolomites. It consists of white and grey cycling dolomites, with stromatolitic and massive lithozones; the sediments were deposited within carbonate tidal flats. The rocky pinnacles of the Cinque Torri s.s. are entirely composed of Dolomia Principale, organized in metric shallowing-upward cycles (Fisher, 1964; Bosellini, 1967).

From a tectonic point of view, the Cinque Torri area is interested by a diffuse deformation related to the Mesozoic-Cenozoic tectonics. The Mesozoic (Late Triassic-Jurassic) W-E extensional tectonics produced a system of NNW-SSE to N-S striking sub-vertical normal faults (Doglioni et al., 1992), that have been frequently reactivated with oblique movements during the compressive Cenozoic Alpine orogeny (Doglioni, 1992). The diffuse deformation is characterized by small-scale structures presenting different deformative behaviors in relation to the different geomechanical characteristics of the various lithotypes interested.

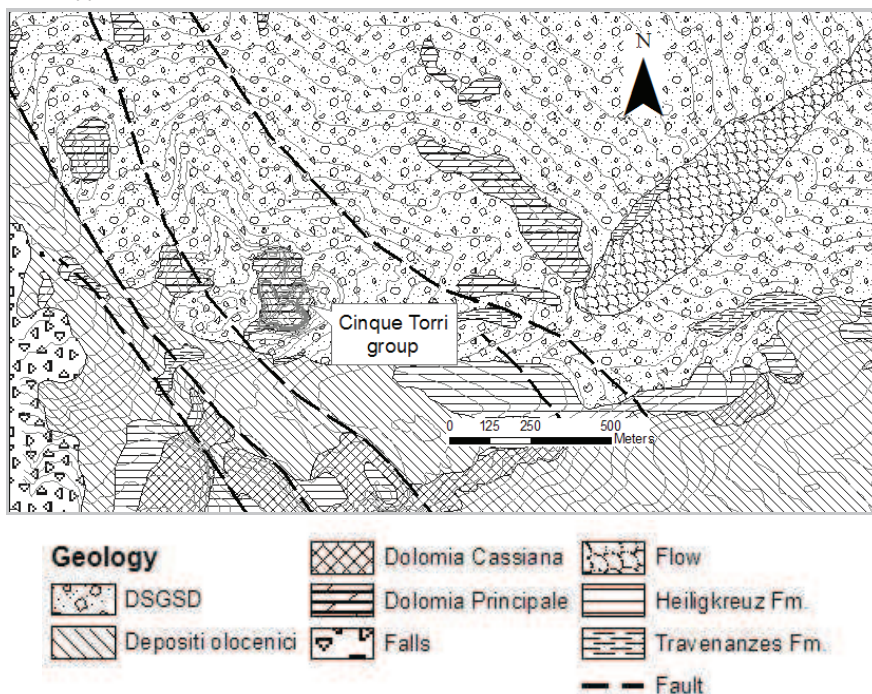


Fig.2.5. Geological map of the Cinque Torri area (modified from Neri et al, 2007)

Carbonate platforms display a rigid-fragile geomechanical behaviour as illustrated by the Cassian Dolomite outcropping southward of the Cinque Torri (Nuvolau Mount in Fig. 2.1). The exhumed top of these platforms is partitioned, by a system of sub-vertical NNW-SSE to N-S oriented normal faults, in a series of blocks progressively lowered eastwards (Neri et al., 2007).

The erosion of the dolomitic walls of the rock group is accelerated by the high topographic gradients and by the fast removal of debris produced by mechanical weathering.

In the Cortina d'Ampezzo area (Fig. 2.1), DSGSDs are quite common and frequently occur at the contact between brittle and plastic lithologies. In the study area this contact is represented by the stratigraphic boundary between the Travenanzes Formation (TVZ

in Fig. 2.4a,b), which includes mainly reddish mudstones with minor intercalations of peritidal dolostones, and the overlying Dolomia Principale (DPR), consisting of well-bedded white and grey cyclic dolomites (Fisher, 1964; Bosellini, 1967).

The total thickness of these sedimentary rocks is 150–250 m and they uniformly dip with a moderate inclination of 20° toward N10°E. The massive and heavy dolomite peaks are slowly sinking into the underneath ductile units causing severe instability with progressive spreading, sliding and rotation of the pinnacles. More specifically, the instability has a compound nature; at the surface it propagates with a lateral spreading mechanism, evolving into topple and block slide movements, while at depth the adverse hydraulic conditions and high imposed stresses cause translation movements on top of dolostone layers, and rotational sliding and bulges inside the homogeneous plastic strata (Soldati and Pasuto, 1991). In addition, fracturing of the upper brittle lithologies allows water infiltration which may cause the softening of the underlying marly and clayey formation (Panizza et al., 1994), and consequently further instability. In spring 2009, as a consequence of these conditions, combined with melting snow and the dormant instability of the gravitational deposits, a mudflow of about 500 000 m³, generated from the Travenanzes Formation, initiated on the eastern slope at a distance of 1400 m from the rock group (Fig. 2.6).



Fig. 2.6. Pictures of the reactivated mudflow which broke off on May 2009 during snow melting period. The mudflow is located about 1400 m from the Cinque Torri group, indicated on pictures (image courtesy of C. Baglioni).

As widely known, increased water infiltration leads to a rise in water-pressure and thus a drop in effective stress. Pore water pressure may play an important role in the Cinque Torri instability but at present neither water table monitoring data nor information about relation between pore water pressure and displacements are available. For the Cinque Torri DSGSD, a non-uniform behavior is expected as a response of water infiltration due the presence of fractured carbonates bounded by impermeable and deformed clay rich layers. In this case, as proposed by Matsuura et al. (2008) for a reactivated landslide in weathered mudstones, both melted and rainfall waters are directly related to pore water pressure, and a prolonged water supply is more effective in pore-water pressure changes than short and intense aquifer recharge. This statement is further supported by the fact that recent movements in the study area occurred

during spring (May and June), thus in a rainy period with active snow melting. Besides the effects of the water pressure increase, if relevant water adsorption events occur, plasticity and good adsorption capacity of the clay rich layers should be considered, since they are controlling factors of creeping phenomena.

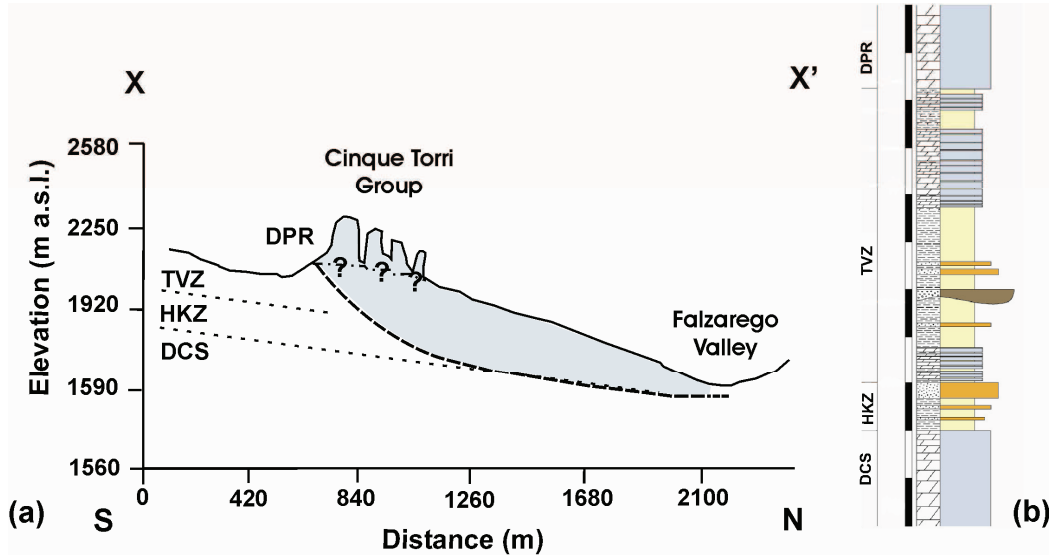


Fig. 2.6. Geological sections. (a) Cross-section through the Cinque Torri slope showing the main geological features (the trace of the profile is shown in Fig. 2.1). The hypothetical extension of the DSGSD structure at depth (grey area), based on the geological literature is also shown. (b) Stratigraphic column showing the main lithologies in the investigated area: DCS: Dolomia Cassiana; HKZ: Heiligkreuz Formation; TVZ: Travenanzes Formation; DPR: Dolomia Principale (image courtesy of A. Breda).

Although to date a complete description of the deeper deformations is not yet available, the surface characteristics clearly show that the instability phenomena of the Cinque Torri group originates from fragmentation of the original carbonate plateau into rock pinnacles, gradually sliding downhill as a consequence of the gravitational compression of the underlying ductile lithologies (Fig. 2.7). This is fully consistent with the general description of lateral spreadings proposed by Dramis and Sorriso Valvo (1994). The tectonic control of the gravitational phenomena of the Cinque Torri can be related to systems of sub-vertical conjugated faults and fractures, which belong to Mesozoic–Cenozoic tectonics and fragment the rock monoliths and the surrounding areas.

Within the rock group both large and local scale rock discontinuities can be distinguished. The first discontinuity type characterizes the surfaces of the rock monoliths therefore with a metric joint aperture, while the latter type subdivides the rock monolith in discrete elements and generally presents a millimetric aperture. These two types are intimately correlated, but differ in terms of both geotechnical and hierarchical aspects. Our fieldworks in the area showed three main joint families characterized by a general persistency larger than 1 m and an average joint spacing between 0.30 and 0.40 m, along with the bedding. The surfaces of the discontinuities are generally planar with gentle undulation. Weak weathering can be observed on most of the exposed surfaces as well as karst dissolution, which produces decimetric ellipsoidal shape holes displaying alteration products and moisture along the bedding.

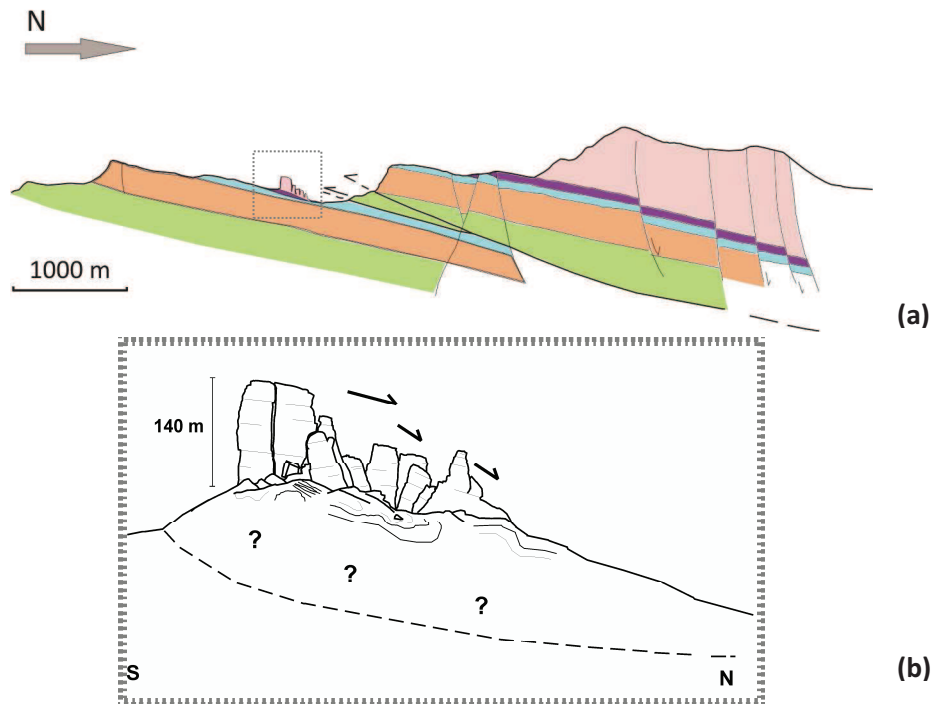


Fig. 2.7. The structural setting of the study area. (a) Sketched profile of a N-S section crossing the Cinque Torri group. (b) Detail of the present-day dynamics within the rocky group.

The Cinque Torri group occupies a high topographic level immediately to the North of an E–W trending scarp, but the limits of the main DSGSD area are still not well defined. The group itself is characterized by an NW trending gravitational graben perpendicularly cut by ENE asymmetric counterscarps (Fig. 2.1). The scarps are parallel to the slope and lead to a progressive downward lowering of the mobilized mass. Following the scheme of Nemcok and Pasek (1972), these kinds of features could be connected to the reactivation of previous fractures during post-glacial unloading. The slope leading from the base of the Cinque Torri group down to the valley floor ranges from 1800 to 2350 m a.s.l. (i.e. 550 m), with average inclinations of 36° (upper slope sector) and 20° (lower slope sector).

Although there are not evident signs, the basal shear zone probably coincides with the contact between the Heiligkreuz formations (HKZ in Fig. 3a,b) and the Dolomia Cassiana (DCS). This contact is masked at the Cinque Torri slope toe by talus accumulations; it is also buried by alluvial and glacial deposits along the Falzarego Valley, but outcrops extensively in the surrounding areas.

2.3 The history of the Cinque Torri area

A specific study devoted to the analysis of the group origin is not available at the time of writing. Many morphological features suggest a post-glacial evolution of the area due to the erosive processes started after the ice retreats. In figure 2.8 the author suggests a possible interpretation of the processes happened in the area until present.

Before glacial age (680000-12000 yr B.P.) the area probably was characterized at the top by a uniform platform made up mainly by Dolomia Principale (stage 1) which has been

fractured by several tectonic phases (stage 2). The Cinque Torri rock sequence therefore underwent to a gradual consolidation which lasted millions of years. With the settlement of the ice sheets in the alpine area all the reliefs were covered by ice and eroded by the ice progradation (stage 3).

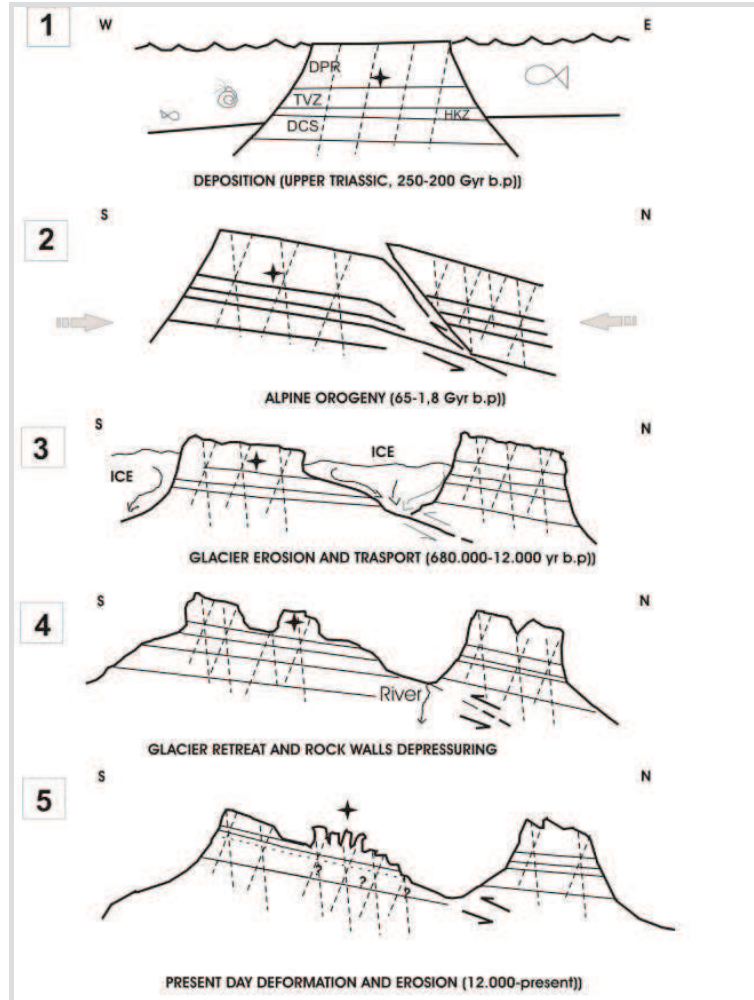


Fig. 2.8. Scheme of the Cinque Torri area history.

The main shapes of the actual reliefs and valleys were determined from these processes and from the phenomena that started during glacial retreat (stage 4). As a matter of fact, the ice melting along valleys caused alteration of the equilibrium of forces within slopes subsequently to the stress release along the shoulders of the valleys. Is possible that this release caused alterations also in the geotechnical properties of the lithologies. Furthermore the intense widening of rock fractures, the worsening of the strength properties and the significant change in the hydrogeological setting contributed to the present morphology and instabilities (stage 5).

3. Laser scanning techniques

3.1 Introduction

This chapter introduces three-dimensional terrestrial and aerial laser scanning as survey techniques. It starts by providing background on the theoretical and operational aspects of laser scanners. The types of laser scanners used in the field surveys are discussed. The focus is on the data quality aspects, since this has a great influence on the expected results of the point cloud analysis. The possibilities and difficulties for rock face scanning are discussed.

3-D laser scanning is a relatively new, but already revolutionary and very successful surveying technique. Like a radar system, the laser scanning technique allows the acquisition of an entire surface with a high sampling step. Nevertheless, in this case the signal is a laser beam (impulsive or continuous), highly collimated and spectrally well defined, from which high accuracy and resolution of the measurements can be achieved. Figure 3.1 the operational context of this research: the objective is the acquisition and reconstruction of a surface, which is a 2D object embedded in the 3D space. If is complex, the use of more than one viewpoint could be necessary. An instrumental survey is articulated in the following steps:

1. Planning and design of observations. This consists in the choice of a suitable instrument, essentially on the basis of size of the observed object, and in the identification of viewpoints that allow the acquisition of the entire interesting surfaces. In the case of a geological survey, this phase can require the choice of adequate techniques whose use is necessary to obtain the results georeferencing, or at least to introduce of a suitable reference frame.
2. In situ observation included the eventual application of georeferencing aimed techniques. The results of a survey are one or more set of points, each of them is called a point cloud, having information on coordinates of acquired points, as well as on corresponding reflectances and/or colors. Note that, if more than one viewpoint is considered, a series of point clouds with different local coordinates are obtained.
3. Data processing, to obtain a data set containing significant information for the user. A data filtering is generally necessary to reduce the effect of error and/or outliers. The registration of all the obtained point clouds, that is their linking on a common reference frame, is a very important operation because it directly influences the result accuracy. The registration can be performed using specific software, generally based on surface matching algorithms. In the case of geological surveys, the registration is often performed by means of a topographical network, introduced in order to georeference the data. The joint use of surface matching-based and topographic-based registration techniques can be considered in order to improve the results and/or to reduce the acquisition time or the elaboration time. After the generation of a unique point cloud defined on a suitable reference frame, a model of the observed surface is generated, using different methods. Such a model can be a 3D representation. If an analytical representation of the surface exists at least locally, it is of the type $f(x, y, z) = 0$. Note that the amount of data obtained in an instrumental session can be very large. Their elaboration requires suitable hardware and software resources.

4. Effective use of the data. The aim of a survey can be, for example, a mere geometrical characterization of the acquired object. Other possible applications are quantification of deformations and displacements in a time interval to characterize unstable areas. In this study the use of laser data accomplishes a semi-automated rock discontinuity analysis by recognizing planar features in the point cloud. Significant information on the tectonics control on a rock mass can be derived from rock discontinuity analysis. For this type of application are not required multi-temporal models. The fundamental tool is instead a multi-scale dataset and traditional field mapping for validation purposes. In the Chapter 6 an original method devoted to the calculation of the rotational components using a point cloud-based rock discontinuity analysis of the Cinque Torri lateral spreading is presented.

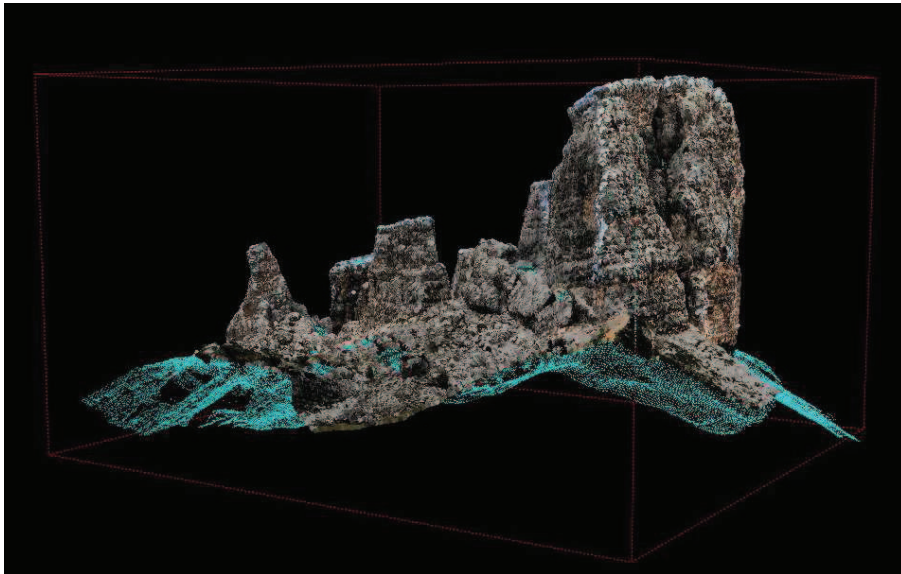


Fig. 3.1. Point cloud with RGB map colorization by photo coupling. The geometry of Cinque Torri group, Cortina d'Ampezzo, Belluno, Italy, is obtained through various viewpoints. For each view point, a partial point cloud is obtained. In such a case, the complete point cloud is generated by means of the registration (i.e., linking on a common reference framework) of the partial point clouds

On the basis of the acquisition technique, a laser scanner can be a:

a) *Triangulation laser scanner*. In this case, the 3D position of a point is reconstructed by geometric data only, without any time measurements. This kind of laser scanner is characterized by very high accuracy (micrometric also), but low range (few meters). A scheme is presented in figure 3.2a. A laser signal is projected onto an object surface and the position of the spot on the object is recorded by one or more CCD cameras. The angle of the light beam leaving the scanner is recorded and the fixed base length between laser source and camera is known from calibration. The distance from the object to the instrument is geometrically determined from the recorded angle and base length. The triangulation laser scanner is used, for example, in the survey of mechanical elements, surgery and acquisition of small particulars. This technique had not applied within the research described here. For this reason, it will no further considered.

b) *Time-of flight laser scanner*. It is a rangefinder equipped with a system allowing an accurate positioning of the laser beam. In this way, the spatial position of the acquired target is computed on the basis of angular coordinates of the laser beam as well as on

the target distance (figure 3.2b). In particular, a nanosecond laser pulse is sent towards a surface and backscattered by it. The direction of the laser beam is characterized by angular coordinates φ and α . The distance d of the target is computed from the time of flight of a laser pulse whose duration is few nanoseconds. The Cartesian coordinates (x, y, z) of the reflector are obtained from the spherical ones, that is (d, φ, α) . This is the instrumental configuration generally used in geological survey, and the range can be hundred of meters (mid range laser scanner) or about a thousand of meters also (long range laser scanner). The accuracy can be centimetric at the distance of about 100 m. All the instruments used within the Project are time-of-flight laser scanners.

c) *Phase-based laser scanners*. The other type of laser scanner, namely phase or modulated-based systems, instead of having the light source pulsing on and off they run it constantly. The light source is modulated with a sine wave, causing the amount of light that the laser emits to vary accordingly. In similar fashion to the time-of-flight method, the signal is transmitted from the laser and reflected from the object. To determine the length measured, the phase differences between the transmitted signal and the reflected signal are compared (Greaves, 2004). The range is restricted to a maximum of seventy to one hundred meters. Accuracy of the measured distances within some millimeters is possible and is therefore more accurate than the range-finding or time-based laser scanner. The speed of measurement is also much higher, up to 100 times faster than time-of flight laser scanners (Greaves, 2004). This allows the phase-based type of laser scanner to be used on mobile platforms for rapid surveying, for example mounted on a railway carriage inside a tunnel (Fröhlich and Mettenleiter, 2004).

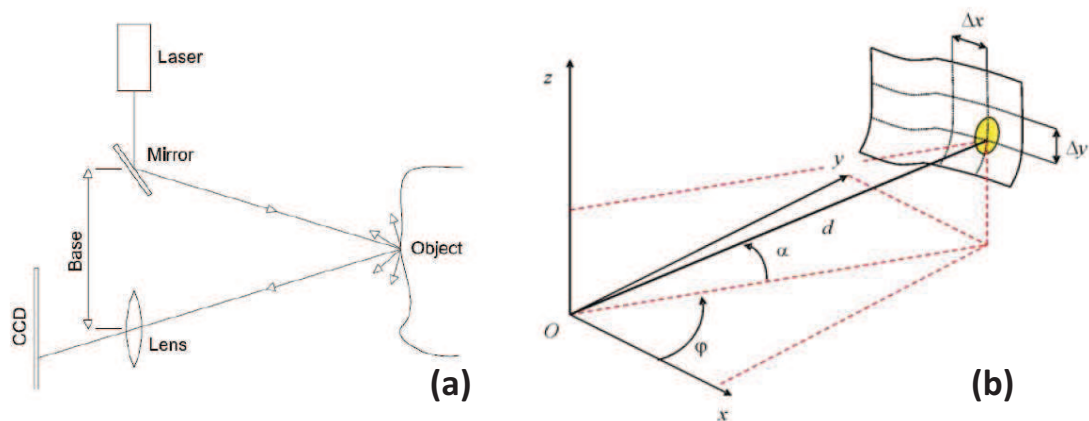


Fig. 3.2. Typologies of laser scanner. (a) Triangulation laser scanner (image from Boehler, 2001). (b) Time-of-flight laser scanner. The direction of the laser beam is characterized by angular coordinates φ and α , and the distance (or range) d provides the third spherical coordinate.

Finally, on the basis of the scanning and mounting system, a laser scanner can be:

- a) Terrestrial laser scanner (TLS), in which the instrument is mounted on a topographical tripod (or another mounting system) and the acquisition of an entire surface is performed by means of rotating mirrors, or other systems, along two orthogonal directions. The angles are incremented by discrete steps. In particular, the longitude angle is generally modified rotating the entire instrument, whereas the latitude angle is modified acting on rotating mirrors. Some instruments use rotating mirrors along both the directions.

- b) b) Aerial laser scanner (ALS), in which the instrument is mounted on an airplane or an helicopter flying at a suitable altitude (500-600 m over the soil). The coverage of the surface is performed using the same movement of the flying object along a direction, and a rotating mirror along the orthogonal direction. The instantaneous spatial position of the instrument is measured using GPS. A ground station, allowing differential measurements, is necessary to obtain accurate results.

All the LS instruments used within the research are time-of-flight laser scanner. For this reason, only this system will be described in the following paragraphs.

3.2. Time of flight laser scanning: resolution and accuracy

A time-of-flight TLS is a laser rangefinder equipped by a sub-system for the high accuracy scanning of an entire surface with high density sampling rate. Figure 3.2b shows the principle of such an instrument. A nanosecond pulse is emitted along a direction characterized by azimuthal (φ) and zenithal (α) angles, and the travel time instrument-target-instrument is measured in order to obtain the distance d . In this way, the spherical coordinates (d, φ, α) of the reflecting point are obtained. The Cartesian coordinates (x, y, z) of this point are obtained using the following transformations:

$$\begin{cases} x = d \cos \varphi \cos \alpha \\ y = d \sin \varphi \cos \alpha \\ z = d \sin \alpha \end{cases} \quad (3.1)$$

A fourth data is measured for each point. It is the intensity $I(x, y, z)$, that is the amount of reflected signal that reach the detector with respect to the emitted one. Commonly, I is normalized in the range $[0, 255]$, as in a 256 grey-level image. The intensity is related to the material reflectance, but it is also influenced by terrain moisture and observational conditions (for example, the angle of incidence). For this reason, it cannot be used in order to establish a correspondence between point clouds or digital models. Instead, I is very useful to detect and model high-reflectivity artificial targets positioned for georeferencing aims. These targets can be contemporarily acquired by total station or GPS and their absolute coordinates are therefore measured. Note that the introduction of an absolute reference frame is performed operating on data: an accurate knowledge of the instrument's position during the measurement is not necessary. The product of a scan is the point cloud $\{(x, y, z, I(x, y, z))\}$, generally with some millions of points. Finally, some TLS can provide for each point, besides the intensity $I(x, y, z)$, the three-elements vector $RGB(x, y, z)$ containing the color information. To obtain this information, a calibrated camera is necessary. In Fig. 2.1 an example point cloud coupled by RGB values is shown.

3.3. Laser types: performances and specifications

Various terrestrial laser scanning systems are presently on the market, both phase-based and time-based scanners are becoming more widely used throughout the world in all kinds of application. In the geosciences laser scanning is also becoming recognized as a potentially attractive survey method. At least seven manufacturers are developing both phase-based and time-based laser scanners, of which the time-based laser scanners are more widely used. As mentioned previously, the developments in the technology is very fast and it falls outside the scope compare the performance of all laser scanners here. Instead, the performance and characteristics of the two time-based laser scanners that are used in this study are summarized. In this study, data from two different terrestrial laser scanners are used: the Riegl LMS-420i and the Optech Ilris 3-D. Below the various performance parameters of the two scanners are given in Table 3.1.

Table 3.1. Laser scanner performance and technical specification

Parameter	Unit	Optech ILRIS-3D	Riegl LMS Z-420i
Laser wave-length	nm	1535 (infrared)	Infrared ^a
Laser class	NIR Class 1	1 (eyesafe)	1(eyesafe)
Range (80% reflectance)	m	1500	1000
Range (10% reflectance)	m	700	350
Field of view (horizontal)	°	40	360
Field of view (vertical)	°	40	270
Laser beam divergence	mrad	0.17	0.25
Spot diameter at 50 m	mm	20.5	12.5
Resolution at 50 m	mm	17.7	10.9 ^b
Single target acquisition accuracy at 50 m	mm	7	7
Minimum spot spacing at 50 m	mm	1.3	2.2
Scan velocity	pts/s	2000(fixed)	8000-12000

a: Riegl does not declare the wavelength. A value in the range 1300-1550 nm is very probable.

b: from Lichthi (2004). All the other data are from Optech (2010), Riegl (2010).

The long range TLS Optech ILRIS 3D (Optech, 2010) uses internal mirrors for both the angular directions to direct the laser beam within a maximum field of view of 40°x40°. The mechanism operates along rows defined by zenithal angles. The instrument uses the same scanning techniques along both the angular directions, with substantially the same accuracy. In addition, the moving masses are relatively small, so the instrument is compact and robust. Nevertheless, in order to acquire large surfaces, to operate inside a building or a natural cavity, or to allow the distribution on the space of the high-reflecting artificial targets located for georeferencing purposes when the observed surface is not accessible, a scan on a large angular extension can be required. For this reason, nowadays large part of the TLS can operate on an azimuthal angle until 360°. In the case of ILRIS 3D, this is obtained using a rotating/tilting unit on which the instrument is mounted. If the entire 360° extension is considered, 10 partially overlapped sub-scans with angular width (in azimuthal direction) of 40° are performed. The internal software operates in way to provide the sub-scans (roughly) on the same reference frame. Note

that the rotating/tilting unit simply rotates or tilts the instrument between a sub-scan and the other, and do not operates during the data acquisition. In order to obtain accurate data, these sub-scans must be registered on a common reference frame by means of an iterative surface matching algorithm implemented in the data processing software. This operation is relatively simple, and can be generally automated, because a rough alignment is provided by the internal software. The instrument, equipped by this rotating/tilting optional unit, is shown in figure 3.3. The scan velocity is 2000 points per second, fixed.



Fig. 3.3. Optech ILRIS 3D. Both the angles are defined using rotating mirrors, with 40°x40° maximum field of view. A rotating/tilting unit allows a coverage on the 360° azimuthal angle by means of successive re-positioning of the laser unit (image courtesy of Mr. A. Faccioli, Codevintec Italia).



Fig. 3.4. Riegl LMS Z-420i with mounted digital camera. A rotating mirror scans the zenithal directions, and the rotation of the entire laser unit covers the azimuthal angle. In this picture, the scanner is tilted upward. Operation of the scanner is by laptop PC (not shown) (after Riegl, 2010).

The long range TLS Riegl LMS Z-420i (Riegl, 2006) uses a different mechanism. The entire laser unit rotates to scan the azimuthal angle, so the moving mass is relatively high, fact which implies the necessity of a particular careful in the transport and use of the instrument. The practice with this instrument, as well as with other instruments that use the same scan technique, seems to testify that a regularly calibrated system warrants adequate accuracies along both the angular directions (the interval between two calibration sessions by the manufacturer is 1-2 years), that is the error related to the scanning sub-system is lower than the one related to the footprint extension. A 360°-measurement provides a point cloud only, and any pre-alignment is not required; so, the data processing is easy and quick. The instrument operates along the zenithal angle, that is it operates along vertical columns. The scan velocity can reach 8000 pts/s when the rotation happens, 12000 pts/s when only the rotating mirror operates. The LMS Z-420i instrument is shown in figure 3.4.

3.4. Aerial laser scanning

In this study, the surroundings of the Cinque Torri group were acquired by using the ALTM Gemini aerial laser scanner.

The ALTM Gemini is a high-altitude, wide area mapping sensor that can operate just as effectively at lower altitudes. This added functionality makes the ALTM Gemini flexible to operate in a variety of application areas. This ALS is integrated by numerous peripheral sensor options, including laser waveform capture for complex modeling capability and high-resolution digital image capture. The advantage respect other ALS systems is that ALTM Gemini incorporates the industry's only fully-automated Continuous Multipulse (CMP™) technology system, without the range-gated data loss associated with other multipulse systems (Optech, 2011). CMP™ can double the collection efficiency Capable of collecting data at twice the altitude of conventional single-pulse systems for a given sampling rate. The reasons of these potentials reside on its revolutionary approach to overcoming altitude constraints as a function of the timing limit associated with time-of-flight laser measurements. The timing limit refers to the time it takes for a pulse of light to travel from the laser transmitter to the target, and back to the receiver. Traditionally, laser sensors wait for the transmitted pulse to return to the receiver before emitting the next pulse. Consequently, the laser pulse rate directly limits the system operating altitude. CMP™ technology enables two or more pulse to be emitted and tracked, significantly increasing survey coverage rates, without the hassle of planning around the data "blind zones" common to other multipulse technologies. This determines unrestricted bank-angle capability while maintaining high data quality and the ability of the system to operate efficiently in all application areas and altitudes with maximum data density.

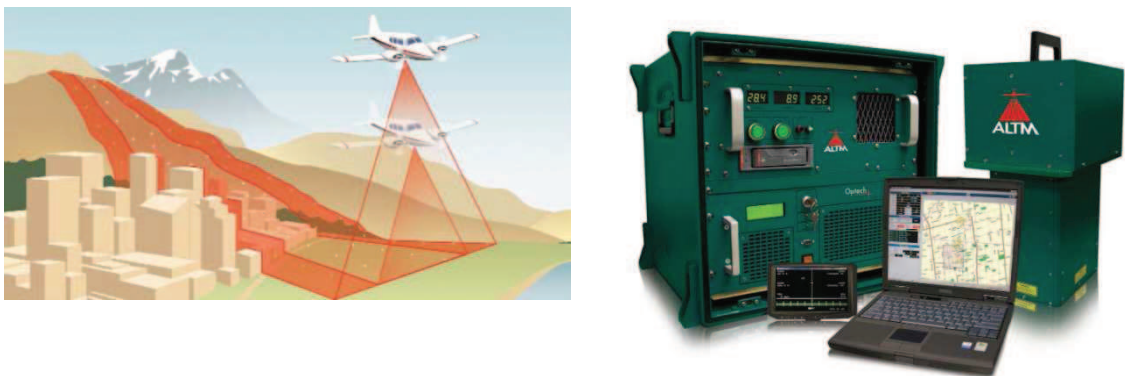


Fig. 3.5. Aerial laser scanning technique. On the left is sketched the survey principle showing the advantage in surveying from higher altitudes. On the right operational system of the Optech ALTM Gemini (from Optech, 2011).

Table 3.2. ALTM Gemini laser scanner performance and technical specifications (Optech, 2011b)

Parameter	Unit	
Laser wave-length	nm	1064 (infrared)
Operational envelope ¹	m	150-4000 AGL, nominal
Horizontal accuracy ²	m (AGL)	1/5, 500 x altitude
Elevation accuracy ²	m	<5-35 m; 1 σ
Effective laser repetition rate	kHz	Programmable, 33-167
Position and orientation system		POS AV™ 510 (OEM) includes embedded 72-channel GNSS receiver (GPS and GLONASS)
Scan width (FOV)	°	0-50
Scan frequency	Hz	0-70
Roll compensation	°	± 5 at full FOV
Range capture		up to 4 range measurements including 1st, 2nd, 3rd and last returns
Beam divergence	mrad	Dual divergence: 0.25 (1/e) and 0.8 (1/e), nominal
Intensity capture	bit	12 dynamic measurement range
Data storage		Ruggedized removable SCSI hard disk
Image capture	MP	60, medium format camera (optional)
Power requirements		28 V; 900 W; 35 A (peak)

¹ 10% reflective target

² Accuracy dependent on selected operational parameters using nominal 50° FOV (Field Of View) in standard atmospheric conditions

3.5. Sources of error of 3D laser scan measurements

According to Reshetyuk (2006) there are four main sources of error in the time-based laser measurements, which are: instrumental, object-related, environmental and methodological errors. A problem is that the sources for these errors influence each other and it is very hard to highlight the most important one. One of the most numerous errors is in fact introduced by the laser scanner itself. There is a limited precision with which the range can be measured. This is again related to the limited precision of the clock that measures the time difference. Secondly, there is a limited precision in measurement of the rotation angle of the beam deflection unit, the mirror that makes sure that the laser beam moves vertically and horizontally along zenith and azimuth. Both off course contribute directly to the location error. The error in the vertical direction (zenith) may be different than the error in the horizontal (azimuth) due to the different mechanics involved in the different rotations. All three errors together contribute to the point accuracy and precision or noise. Due to the complexity of the equipment, individual components in the scanner may also contribute to the total error budget. These errors require a detailed understanding of the scanner design, which, for proprietary reasons are not supplied by the manufacturer.

Since terrestrial laser scanning is a reflectorless surveying technique, the results of the range measurement depend on the amount of energy that is reflected by the surface. It was explained in section 3.1 that the reflectance is both a function of the material and geometric properties of the surface. Numerous benchmark studies revealed that different material, under different conditions (incidence angles, wetness and distance)

may result in slightly different range measurements. This depends again also on the wavelength of the emitted laser signal. A time delay or range delay is introduced by a reduced return pulse amplitude (low intensity), compared to a full amplitude pulse (Lichti et al., 2002). The distance of the object itself plays again an important role here, since the laser beam divergence causes the spot size to increase with distance. This results in less energy per surface area to be reflected and an averaging of the distance measurement over the entire spot size instead of a point-wise measurement at smaller distances. The accuracy and precision of the measured target coordinates generally decreases with increasing survey distance. Environmental aspects also influence the scanner's operations. Due to variations in the atmospheric conditions the velocity of the laser light can change. Also refraction and turbulence may change the trajectory of the beam slightly. In short range operation, the influence of atmosphere is negligible (Reshetyuk, 2006). However, laser scanners which can survey up to 1 km distance may experience significant atmospheric effect at these long ranges. Of course the platform of the scanner should be stable, and instabilities and even small vibrations may affect the position measurements, particularly at larger ranges. Finally, there are also methodological errors introduced due to the survey method that was used. The survey points are basically stored in scanner coordinates, i.e. the coordinates are relative to the scanner position and do not have any relation with local or regional reference grids. There are various methods to georeference a point cloud in scanner coordinates to reference coordinates. This can be done using build-in GPS and electronic compass facilities or using a minimum of 3 standard reflecting target objects, which can be measured-in with geodetic survey equipment. There will always be a certain inaccuracy in the georeferencing, which adds up to the total error budget. Apart from the georeferencing error, it is also possible that the chosen scanning resolution is inappropriate for the target's dimension, shape and distance, resulting in an under-sampling of the target's geometry.

3.5.1 Horizontal and vertical sampling bias in terrestrial laser scanning

An important issue in the survey of rock faces with laser scanning is the occurrence of sampling bias. This bias is caused by occlusion (shadow) of the scanned rock face, which happens when the laser beam is obstructed and not able to hit the target surface. It occurs when the parts of the rock face become semi-parallel or hidden from the incoming laser beam. The bias is that rock surfaces and thus also discontinuity surfaces that are parallel to the general trend of the rock face are over-represented in the data, while discontinuity surfaces that are perpendicular to the general trend of the rock surfaces are under-represented. The issue becomes more important in scans of highly irregular rock faces, particularly where the surveyed rock faces are high and steep or very wide. Both a vertical and horizontal sampling bias can be identified.

The vertical sampling bias occurs when a steep and high rock face is surveyed. Upper parts of the slope can contain occlusion areas due to the larger angle of incidence of the laser beam. The consequence is that discontinuity surfaces that are dipping out of the slope (day lighting) are generally more difficult to detect. However, for slope stability

analyses these discontinuities are in general the most important ones, since they may act as sliding surfaces. Also benched parts of the slope are more difficult to survey since the benched surfaces can be semi-parallel or even hidden from the laser beam. Some laser scanners have a limited vertical field of view, which makes upper parts of the slope impossible to reach. Other laser scanners have the possibility of tilting the laser scanner itself vertically to reach higher parts of the target to resolve this problem. The vertical sampling bias can be reduced by placing the laser scanner further away from the slope possibly in combination with placing the laser scanner on a higher platform. In practice it is often difficult to realize since this makes the survey more complex and expensive.

A horizontal sampling bias occurs when a very wide rock face is surveyed, possibly in combination with a relatively small scanning distance. The extreme left and right parts of the rock face are thus surveyed with a relatively large angle of incidence of the laser beam, which can result in occlusion areas. If it is possible, the laser scanner should be placed at a large distance from the slope, to minimize the angle of incidence, but the consequence is that it results in a lower data resolution and precision. A better solution is to scan the same rock face from different angles. In this way the occlusion areas in previous scans can be surveyed. The multiple scans of the same rock face can also be merged to get minimize the occlusion in the point cloud and thus the horizontal sampling bias. The vertical bias remains in the merged scans.

3.6. Discussion and conclusions

Terrestrial and aerial laser scanning are at present is the most logical solution for remote sensing of the 3D geometry of exposed rock slopes and faces. The combination of both techniques provides complete representation of a rock mass since steep and planar surface can be homogeneously acquired. Both with terrestrial and aerial laser scanning it is possible to generate a dense three-dimensional point cloud of the rock mass exposure. The combination of these techniques provides a complete model of a rock cliff. The limits experienced by TLS for acquisition of planar surfaces can be compensated for the use of ALS. Vice versa the spatial limit of ALS in acquiring steep surfaces is balance by accurate TLS surveys. Moreover, the availability of a point cloud covering both for the rock cliffs under study and the surrounding areas allow applying the same methodology for a local and a regional analysis. The differences in accuracy and precision between terrestrial and aerial laser scanning depends mainly on the range to the target and dimension and reflective property of the target. The different use of the point clouds derive from the two techniques well explain alone the different type of data quality. Although the equipment investment costs is high, terrestrial laser scanning is considered a superior method for surveying exposed rock masses than other remote techniques (i.e. terrestrial photogrammetry). Laser scanning is a relative new technology, but is experiencing currently a rapid development. As with many new technologies, the initial costs are relatively high, but as the technology becomes more widely applied and further developed, prices go down, while the functionalities and data quality improve. On the other hand, the much shorter data processing time and the operational advantages make the operational costs lower.

That is the main reason why terrestrial and aerial laser scanning has been selected in this research as the method for the acquisition of remotely sensed geometric point cloud data of exposed rock masses. There are two main types of laser scanners; time-based and pulse-based. The key differences between the two main types are related to range and rate. Time-based scanners, can measure much longer distances than phase-based systems, sometimes up to a kilometers. They typically capture data at a rate of between hundreds and thousands of points per second. The phase-based systems have a much more limited range, usually measuring at distances less than 25 metres. However, their rate of capture is more than 100 times faster than time-based scanners. Time-based laser scanners are more widely used and available than phase-based laser scanners. Because the time-based scanners can be used for larger ranges, there are more applications for this type of scanner.

The use of laser scanning techniques allows the characterization of rock masses in all the conditions, and allow the complete acquisition of large surfaces. In this way, a large amount of data can be obtained and the use of assumptions about the 3D position of the discontinuities could be reduced. In addition, the direct contact with the observed walls is not required. The TLS acquires in real time a rock surface whose distance from the viewpoint could be some hundred of meters; in this way, also a hardly accessible sector of the slope can be easily reached. In addition, the sampling density and the accuracy are sharply better respect to the case of classical survey, and the time saving is considerable (Slob et al., 2004).

4. Investigation on the Cinque Torri DSGSD by means of 3D geoelectrical tomography and passive seismic stratigraphy

4.1. Introduction

During last decades, many investigation methods have been applied on Deep Seated Gravitational Slope Deformations (DSGSDs) to achieve a better understanding on the geometrical patterns of a phenomenon that typically expresses its major deformation at high depths.

An integrated survey procedure based on geological field observations and geophysical measurements was developed and tested in the Cinque Torri site. In this way, the structural patterns affecting the subsoil of the DSGSD, which guides the lateral spreading of rock pinnacles at a top of a Mesozoic sedimentary sequence, can be investigated. The assessment procedure was developed with the secondary aim of exporting the methodology in many other areas of the Dolomites where similar geological settings occur. The sudden collapse of the Torre Trepfor, which was a monolith of about 11400 m³ of carbonate rocks located in a zone frequently accessed by tourists, occurred in the late spring of 2004. Major concerns for tourism safety rose up immediately after such an event and monitoring program was then undertaken.

In this framework 3D resistivity imaging was utilized to create a comprehensive surface and subsurface model of the area. The near surface stratigraphy and the tectonic settlement were defined down to a depth of about 50-60 m below the surface providing a better insight in the understanding of the triggering mechanism of the complex instability phenomena of the Cinque Torri area.

In the Cinque Torri group, the potential instability of the rock pinnacles, whose volumes range between 25.000 m³ and 80.000 m³, suggested to undertake a multidisciplinary investigation program. Within this program, geological and geomechanical field surveys, geophysical investigations, temperature and deformation sensors installation, GPS displacement monitoring, laser scanning surveys and numerical modeling were planned. The objectives of the whole investigation program are the hazard evaluation of the area and a short term forecasting of rock-falls and pinnacle collapses.

The present contribution presents the results of the Electrical Resistivity Tomography (ERT) and passive seismic surveys carried out in order to gain a better insight in DSGSD of the Cinque Torri group. The geophysical investigation particularly addressed the location of major faults and lithological contacts of the unstable slope to aid a stratigraphic and deformation processes analysis.

Although geophysical and geological imaging of near surface faults have been reported in several studies (Demanet et al., 2001; Wise et al., 2003; Nguyen et al., 2005), a comprehensive 3D high-resolution electrical survey combined to passive seismic reliefs in the Dolomite area represents a novel application.

Geophysical data clearly outlined some tectonic-driven displacements along with the major contacts between the different lithological units. Based on these results, the structural model of the study site could be then better defined finding some keys to provide a new interpretation of the Cinque Torri DSGSD and major details on the local stratigraphy for modeling purposes.

4.2. Data acquisition

During summer 2004 a land survey using Terrestrial Laser Scanner (TLS) and a geophysical survey, based on Electrical Resistivity Tomography (ERT), were performed in the study area. Subsequently, on 2010, the ERT datasets were integrated by passive seismic surveys to ascertain the depth of the lithological and tectonic contacts.

4.2.1. Terrestrial laser scanner measurements

The entire Cinque Torri group was surveyed using an Optech ILRIS-3D instrument. Survey design included seven different stations located at an average distance of approximately 50 m from the rock walls and surroundings. The chosen sampling step was 2 cm at 50 m. In this way a really fine spatial resolution was achieved. The TLS data were processed, following the standard procedures nowadays in use, by using the software package Innovmetric PolyWorks™ (Innovmetric, 2010). The scattered points were removed and the single point clouds were gathered on a common reference using an iterative surface matching algorithm implemented in the IMAAlign module of PolyWorks. The resulting dataset was then subsampled and converted into a surface via a triangulation process. The TLS model was a major aid for achieving a comprehensive representation of the study area and furthermore this model was used to improve the accuracy of the geophysical inversion. Thanks to the model, the surface propagation of electrical currents was properly taken into account.

4.2.2. 3D Electrical Resistivity Tomography

Previous studies in the area describe the local geological settings (Fig. 4.1) as characterized by sharp contacts of carbonate and mudstone layers of the Travenanzes Formation and complex geomorphological conditions. In such a frame the Electrical Resistivity Tomography technique (ERT) was considered to be the more appropriate geophysical approach to obtain a 3D image of the subsurface.

The problem related to complex 3D geophysical targets, when using standard 2D data acquisition techniques, was experienced by many authors (Dahlin et al., 1996; Dahlin et al., 2002; Bentley and Gharibi, 2004; Gunther et al., 2006; Rucker et al., 2009). A remarkable attempt of 3D processing on groups of parallel survey lines in a quasi-3D acquisition fashion was proposed by Rucker et al. (2009). This approach, with respect to a true 3D survey, where transmitting and receiving electrodes are distributed in all directions and used simultaneously, is advantageous in terms of logistics and speed of

acquisition, even though the recent spread of new multi-channel resistivity-meters has provided the capability of recording thousands of data-points in few hours.

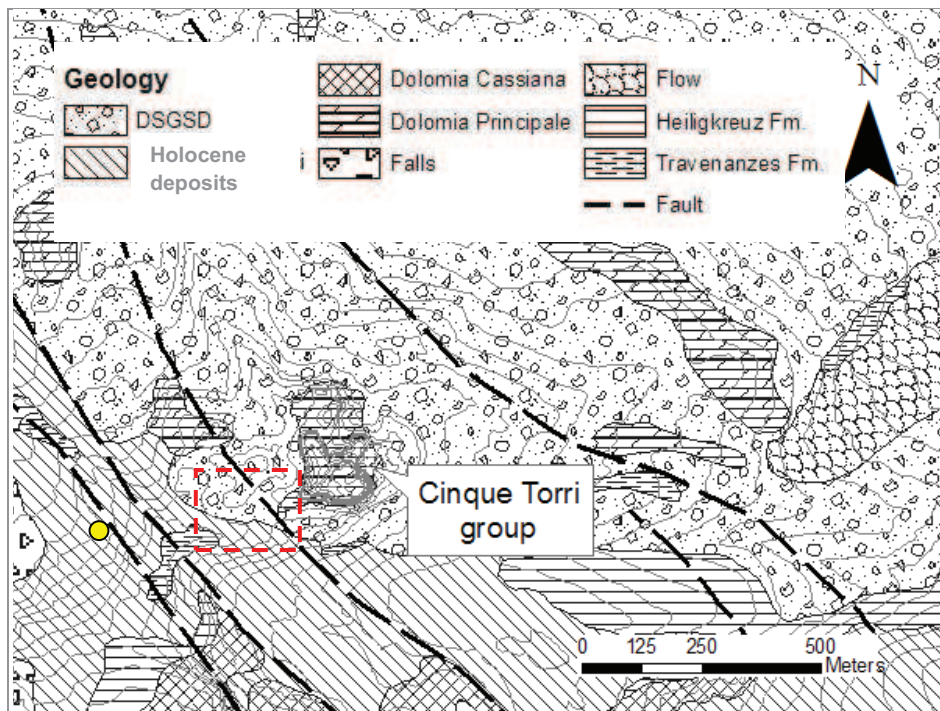


Fig. 4.1. Geological map of the studied area. The rectangle indicates the investigated site by 3D-ERT and the yellow circle the station of the ski resort.

The 3D ERT survey for the Cinque Torri case was the elected method for data treatment since the a priori geological framework suggested an approach based on lines possibly chosen to be parallel or perpendicular to the more evident lithological and structural features. The very complex morphology due to the presence of few pathways and trails, steep slopes, outcropping rocks, required to focus the investigations across the meadow which joins the western side of the rock group and the ski resort (Fig. 4.1). The surveys were carried out by employing two groups of crossing pseudo-lines, each with 48 electrodes, all connected to a 10-channels IRIS Syscal Pro resistivity-meter, capable of handling simultaneously 192 electrodes from a single switching box. The acquisition system was specifically designed for the IRD (Institut de Recherche pour le Développement, Bondy - France).

Data acquisition was carried out in two sessions of five sub parallel lines (L1, L2, L3, L4 and L5) and two sub orthogonal lines (L6 and L7) respectively. In this way, a total area of 260m x 310m was covered (Fig. 4.2). Due to practical reasons, the electrodes were settled according to a 2D fashion, while the acquired data are elaborated following a 3D approach (Constable et al., 1987). The in-line electrode spacing was set to 5.0 m for a total length of 235 meters for each segment, resulting in a global set of 336 electrodes. The electrodes locations and all the needed three-dimensional topographical data were obtained combining a Differential GPS (DGPS) survey with a terrestrial laser scanner campaign.

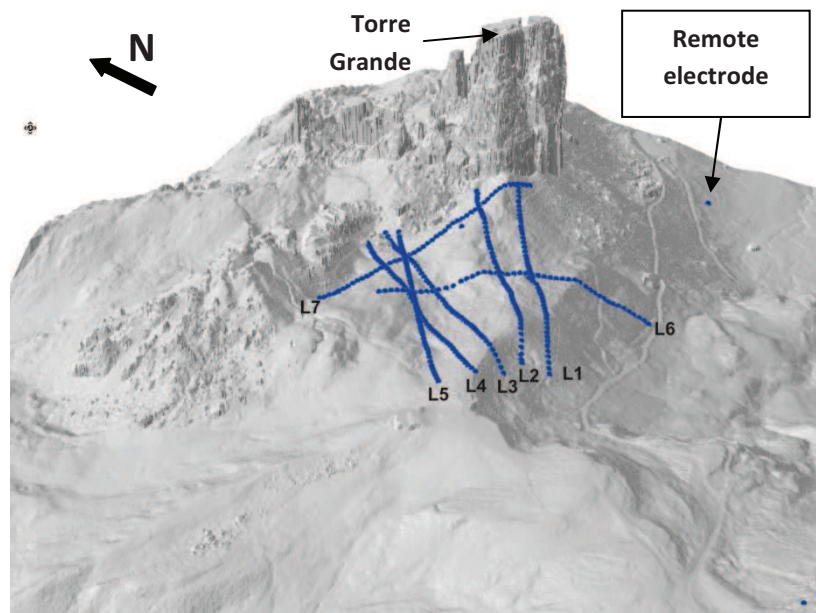


Fig. 4.2. Geophysical deployment on the topographic 3D model

Current injection and voltage measurements were scheduled using two different configurations: pole-dipole and pole-pole schemes which use respectively one or two remote electrodes located at “infinite” distance from the measuring lines, in order to increase the depth of investigation (Fig. 4.2). Additional dipole-dipole quadripoles were combined in the lines to improve the lateral resolution. The resulting dataset of about 15 000 quadripoles was obtained in two separate runs and combined into one global 3D inversion for the final processing.

Given the high measured voltages (average around 100 mV) and the general very low environmental noise on site, a very good signal-to-noise ratio was achieved, even for measurements with unusual electrode arrangements.

4.2.3. Data inversion

After data collection, the measured apparent resistivity values were statistically analyzed and displayed in a 3D generalized “pseudosection” view (Fig. 4.3b), prior to their use for the so called “tomographic inversion” procedure, needed to reconstruct the true resistivity distribution of the subsurface. Due to the non-linear behavior of the inverse problem for electromagnetic fields, the solutions were computed following an iterative procedure (Daily and Owen, 1991; LaBrecque et al., 1996). In such an approach, the “forward model” (simulation of electric field for a given resistivity distribution using a discrete domain) was recurrently solved while changing the subsurface electrical properties.

The 3D inversion approach adopted here and implemented in the software ERTLab (Geostudi Astier srl, Multi-Phase Technologies LLC) makes use of the so-called “Occam’s regularization” proposed in 1987 by Constable et al. and further developed by Morelli and LaBrecque (1996) for the optimal management of data noise. The iterative procedure needs an initial guess to start from and, in this approach, the best choice is

often a homogeneous half-space derived from the above mentioned statistical analysis of apparent resistivity. For this particular case, where two main lithologies within the Travenanzes Formation) with a very distinctive contrast of electrical properties (highly resistive carbonates and very conductive mudstones) are present, the inversion was tested starting from 20 to 250 Ω m according to the DOI (depth of investigation) approach (Oldenburg et al., 1999). Following the definition proposed by Oldenburg, the term DOI refers generically to “the depth below which surface data are insensitive to the value of the physical property of the earth”. In other words, this is the depth below which the earth structure is no longer constrained by the data, but the features outlined are artifacts of the inversion process.

When dealing with heterogeneous high-resistivity features as in the Cinque Torri area, the traditional inversion approaches are not suitable. Here the depth of investigation and, in general, the areas of high resolution are highlighted by means of a functional obtained from the ratio of different resistivity distributions deriving from different starting models. The final result was obtained starting from an initial homogeneous model of 120 Ω m, which represents the apparent resistivity value with the highest count in the global histogram of Fig. 4.3a, with a good sensitivity to explore down to 50-60 m depth. The inversion was carried out to the point at which the difference between consecutive root-mean square (RMS) errors was less than 5%. As there are no evident atrophic perturbations in mountains, the noise level was referred to the measurements errors or to 3D-structure effects.

For models with high resistivity contrasts, Olayinka and Yaramanci (1999) demonstrate that the best model is frequently the inverted model at a relatively low iteration number.

In order to derive the DOI index, R (eq. 4.1), the dataset inversion is computed following the indications proposed by Marescot et al., 2003:

$$R_{AB}(x, z) = \frac{q_A(x, z) - q_B(x, z)}{q_A - q_B} \quad (4.1)$$

where q_A is the first reference resistivity value calculated from the average of the logarithm of the observed apparent resistivity values (Fig.4.3a), and q_B is the second reference resistivity value, usually set at 10 times q_A .

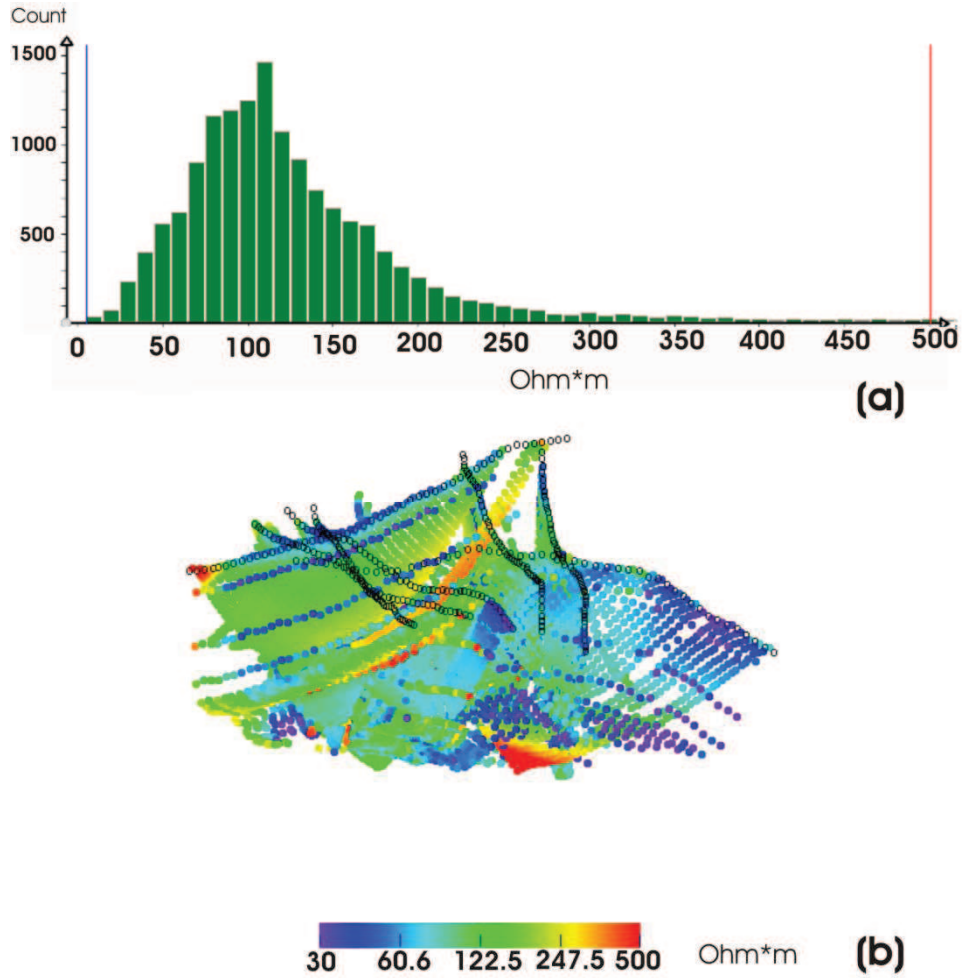


Fig. 4.3. Graph of the distribution of the apparent resistivity values recorded along pseudosections (a); pseudosections of the apparent resistivity. Black circles indicate the lines of acquisition. (b).

In the DOI calculation, the final apparent resistivity pseudosection is made up by model cells associated each to a particular DOI index. For values of R close to zero, the two inversions generate the same resistivity values, while cell resistivity close to unit indicates mismatching between the inversions, therefore a close similarity to the reference resistivity.

To determine the optimum depth range of investigation, the DOI calculations are repeated iteratively, in term of producing a median depth of investigation of the largest array spacing used. This method allows to calculate a scaled DOI ($R(x,z)$):

$$R(x,z) = \frac{q_A(x,z) - q_B(x,z)}{R_M(q_A - q_B)} \quad (4.2)$$

where R_M is the maximum DOI value calculated using equation 4.1.

4.3. Results of the ERT surveys and discussion

The recent surface geological analysis of the Cinque Torri group associated with the subsurface image provided by the 3D resistivity survey permitted a new interpretation of the stratigraphical and tectonic settings of the area. Several details imaged in the resistivity volume were crucial to re-define the boundaries of the different geological bodies.

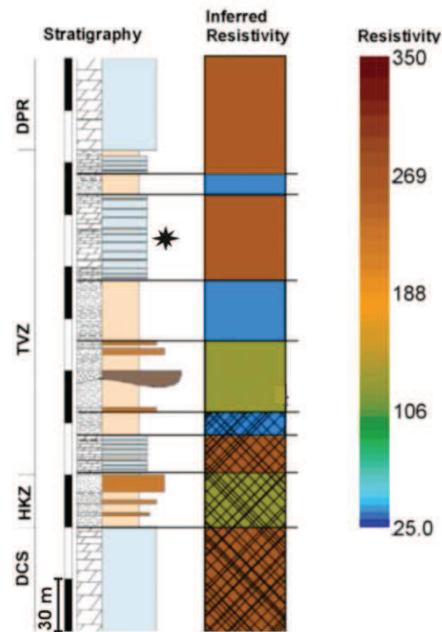


Fig. 4.4. Correlation between stratigraphy and electrical resistivity. From a physical viewpoint, the lithologies can be classified as: high resistive (DPR dolostones), alternation of conductive (mudstone layers) and resistive layers (dolostone) of the TVZ formation. The star close to the stratigraphy indicates the medium dolostone layers.

The resistivity cube covers an area of outcrops belonging to the Dolomia Principale and the Travenanzes Formation. Sections L1 and L2, extracted from the 3D volume at key locations (where there was a lack of stratigraphical background), show a quite complicated resistivity framework.

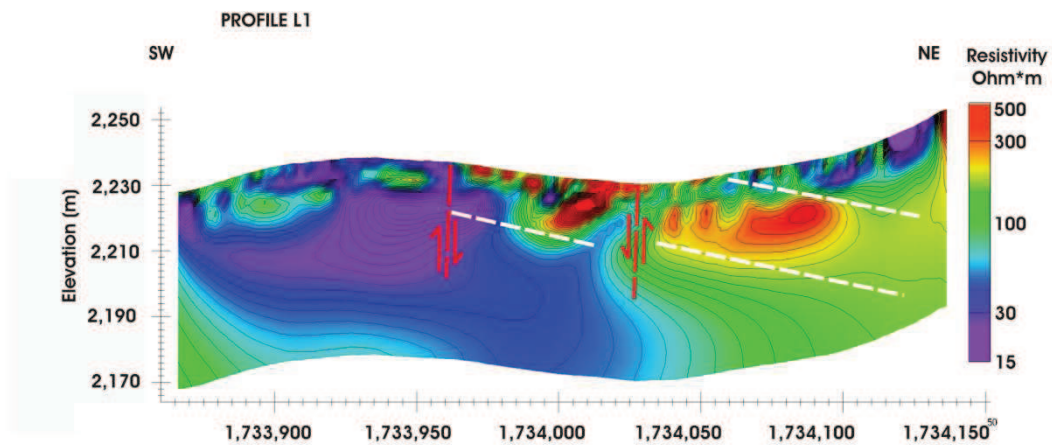


Fig. 4.5. Profile L1 extracted from L1 electrode line after inversion (see trace on Fig. 4.2). Lithological contacts as well as fault traces are highlighted.

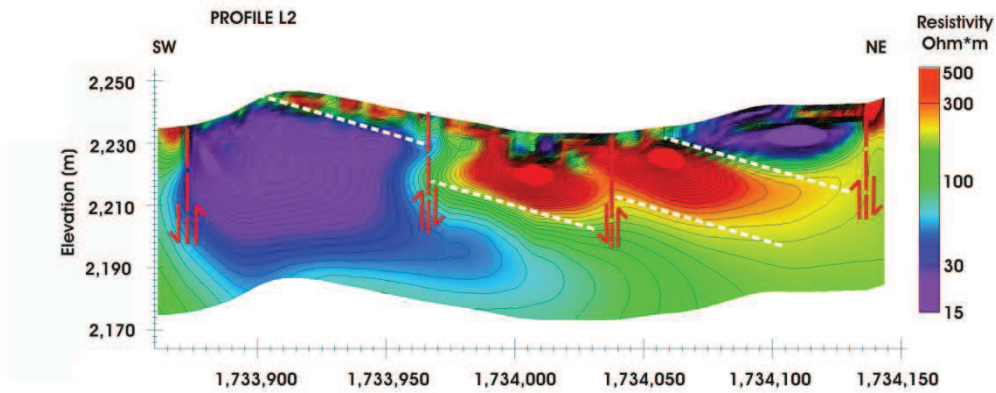


Fig. 4.6. Profile L2 extracted from L2 electrode line (see trace on Fig. 4.2) after inversion. Lithological contacts as well as faults are highlighted.

The distribution of resistivity values in profiles L1 and L2 is quite similar, as expected by a priori geological information, indicating a reasonable reliability of the inversion process.

At a general scale, a North-East trend of the resistivity contours is observable. This trend is fully comparable both with the local and the regional layering. On Fig. 4.6 from South-West to North-East the following features are recognizable: a resistive layer with values in the order of $300 \Omega m$; a very conductive layer with resistivity lower than $20 \Omega m$, three complex discontinuous layers with resistivity values ranging from $150 \Omega m$ to over several hundreds of Ωm ; a top conductive layer with resistivity lowering upwards to values of about $25 \Omega m$. The last unit in the far north-eastern side of the section marks a very resistive body showing a clear vertical contact with the previously described layers. The profiles L1 and L2, which cross the Travenanzes Formation, show rather uniform strata inclination. This trend can be related to the local strata dip direction, which ranges $N10^{\circ}E$, if the azimuthal difference existing between strata orientation and the ERT profile direction is accounted.

Tectonically the investigated meadow is crossed by a system of sub-vertical normal faults with meridian direction (Fig. 4.1). In the Dolomites these Triassic faults generally lower the eastern blocks, but during Alpine reactivation they can locally produce an opposite throw.

Along the profiles L1 and L2 (Fig. 4.5 and 4.6), at the longitudinal coordinate of about 1,734,040 m (Geographic coordinate system, Monte Mario Italy 1), the ERT survey shows a fault which clearly separates and displaces two portions of the medium dolostone level of the Travenanzes Formation (highlighted on Fig. 4.4). Despite the general trend, this fault lowers the block on the left side. This is an example of Alpine reactivation, with a left- transcurrent component and a metric vertical throw.

Towards the East of the profiles L1 and L2, it is remarked a high resistivity contrast. This is due to the presence of a sub-vertical normal fault that brings into contact the reddish

mudstones of the Travenanzes Formation with the western side of the Dolomia Principale of the Torre Grande (Fig. 4.2).

On the base of the ERT results it can be stated that, in this site, the outcropping root of the monolith is not represented by its typical basal sequence and moreover the upper part of the Travenanzes formation is partially erased by the reactivated faults. This interpretation is supported by the comparison between the regional stratigraphy (Fig. 4.4) and the evidences from stratigraphical field reliefs that converge into the interpretation of geoelectric data. Moreover, by inspecting the section of Fig. 4.6, two other sharp and vertical contacts are highlighted on the western side involving also a level of the mudstone layer which is probably deformed as a result of lithostatic pressure and gravitational phenomena acting within the slope.

More in general, from the analysis of the ERT sections, there is confirmation that the geological succession is partially erased by a system of meridian normal and inverse faults that crosses the meadow between the station of the ski resort and the Torre Grande (Fig. 4.1). Due to these tectonic features the usually gradual boundary of the Travenanzes Formation with the overlying Dolomia Principale, generally marked only by the complete disappearance of the silicoclastic input as observed by Breda et al. (2006), is here not observable. The interpreted stratigraphic sequence is shown on Fig. 4.7a, and in Fig. 4.7b the erased stratigraphy due to tectonic is highlighted.

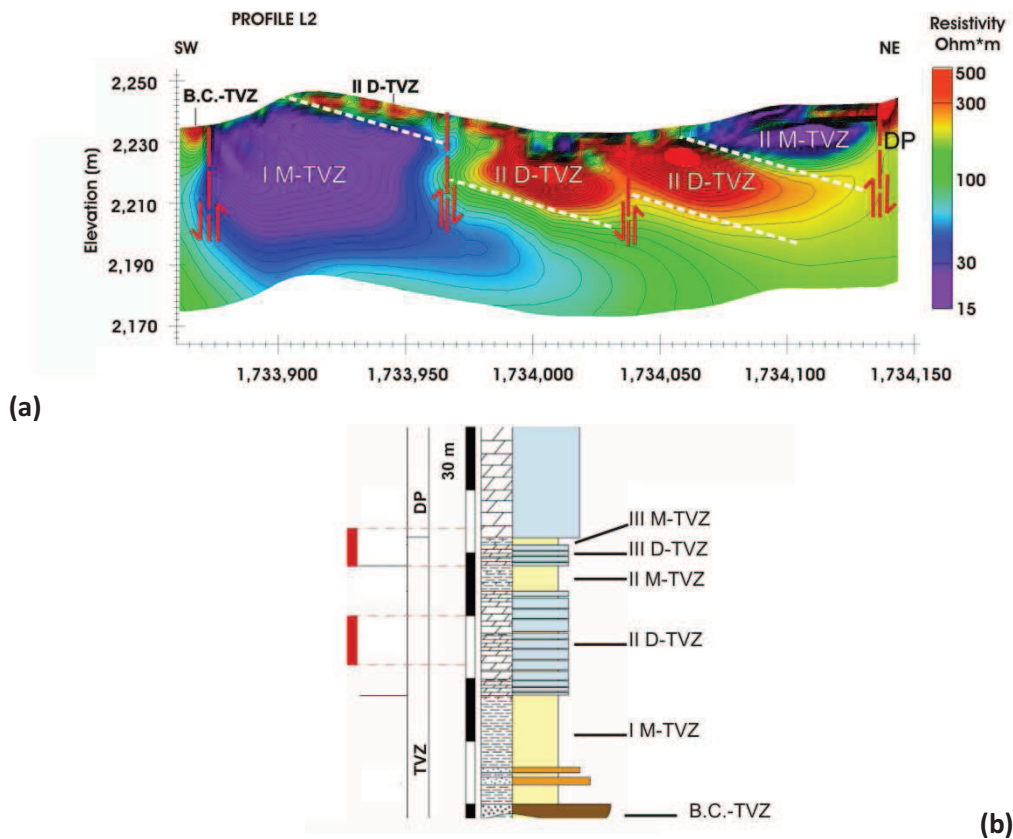


Fig. 4.7. Interpreted L2 section profile. The layers in the stratigraphic sequence abbreviations stand for: DP, Dolomia Principale; TVZ, Travenanzes formation; I, II, III M-TVZ, first, second, third mudstone layer of TVZ; I, II, III D-TVZ, first, second, third dolostone layer of TVZ; B.C.-TVZ, basal conglomerate of the TVZ. The red bands indicate the erased stratigraphic layers due to the fault system.

The Fig. 4.8 comprises two maps of the distribution of resistivity at different depths in the subsoil (depth-slides). It can be clearly observed the presence of superficial bodies with high resistivity values superimposed to conductive layers (Travenanzas Formation) (Fig. 4.8b).

As previously mentioned, the range of variation of the real resistivity changes from a minimum of 20-25 Ωm for the conductive soils, to values over 350 Ωm . According to these ranges, the figures clearly outline a homogeneous setting at 2190 m a.s.l. (Fig. 4.8a) which is related to a single lithological contact, in contrast to the superficial setting shown on Fig. 4.8b which shows two main lithological contacts and a random position of resistive bodies. These last features can be explained by the active deformations and lateral spreading that drive the resistive and fractured rock bodies to slide-on and sink inside the mudstone layers. In Fig. 4.8a and b, despite the clearness in displaying the lithological contacts, the presence of a sub-vertical electric anomaly, previously interpreted as a tectonic lineation, is less recognizable.

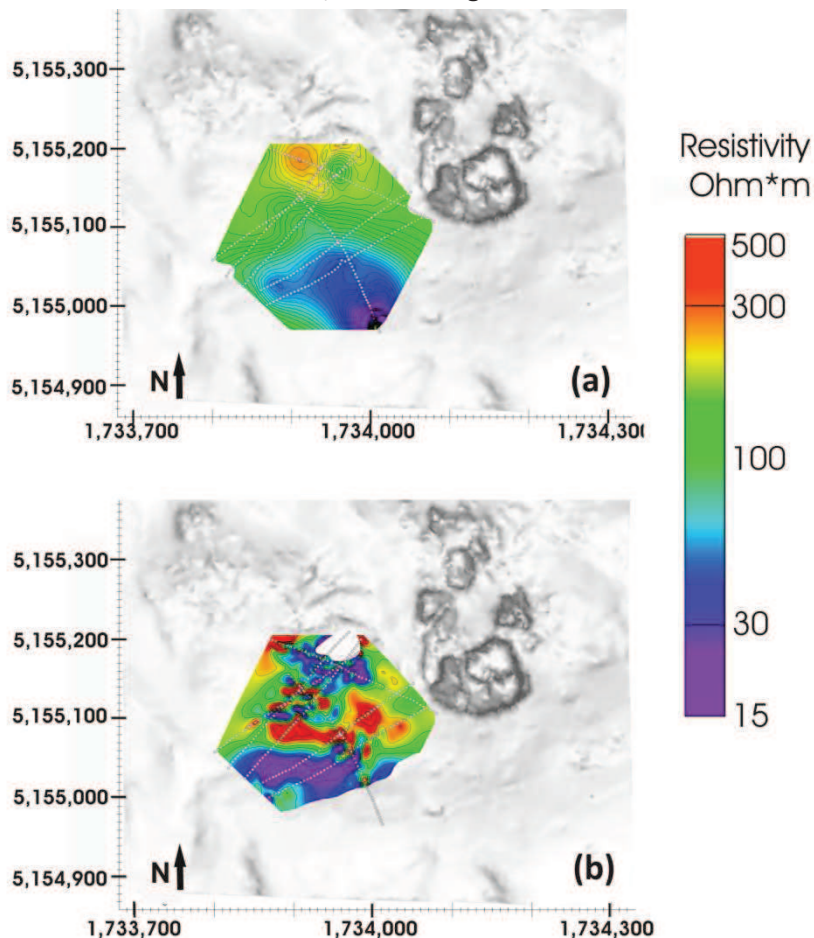


Fig. 4.8. Depth-slides of the 3D ERT extracted from the ERT-3D volume at different depths: 2190 m below the topographic surface (a) and at 2220 m (b) respectively.

More in details, from Fig. 4.8b it can be noticed two main conductive bodies characterized by values of resistivity ranging 20-25 Ωm ascribed to the mudstone layers at the opposite sides of a central resistive body (300-400 Ωm). This is a clear representation of the upper portions of the North dipping Travenanzas formation in

which the lower and the upper contacts of the medium dolostone level are bounded by mudstone layers.

The tomographic representation presents some limitations concerning the exact localization of contacts. Since these profiles are built using contour lines, the limit among layers having very different electric properties appears as an elevated gradient instead as a spotless line. It is therefore possible to assume that the strong gradient resulting from electrical profiles of Fig. 4.5 and 4.6 corresponds to straight contacts between different lithologies. Also the results shown in Fig. 4.9 need this type of interpretation and in addition they offer the example of misinterpretation which typically happens when the a priori geological information is not taken into account. As a matter of fact, the uniform dip direction of strata towards N10°E allows the exclusion of the presence of a resistive isolated body under the top conductive mudstone, which in turn should deepen according to an average dip angle between 10° and 20°.

Moreover, a differentiation of the conductive layers related to water stagnation within the mudstone layers of the TVZ formation can be observed (Fig. 4.8b), as recovered also on field by different types of vegetation that cover the investigated meadow. The presence of bushes or plants covering concave zones is often related to water stagnation.

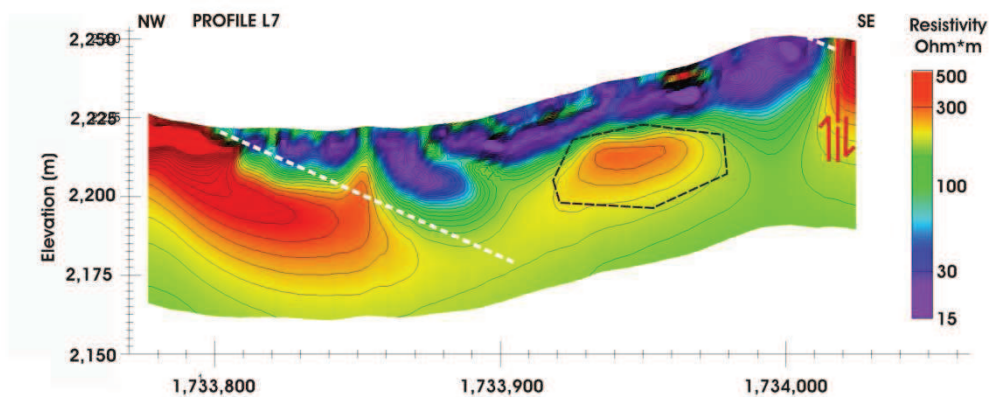


Fig. 4.9 Profile L7 extracted from L7 electrode line (see trace on Fig. 4.2) after inversion. Lithological contacts as well as fault are highlighted. The black polygon indicates a probable artifact and not a real resistive body.

The total 3D volume of the ERT survey and a 3D extraction of the most conductive layers are shown in Fig. 4.10a and Fig. 4.10b respectively. By observing on detail the total 3D resistivity volume it can be verified that the superficial complex frame of the data after inversion is directly related to the position of the measuring electrodes. As a matter of fact, the instrumented portions of the 3D volume show more detailed information which should be carefully interpreted. In particular, since the ends of the ERT lines do not find many other close electrodes for data interpolation, generally they produce artifacts that should not be accounted.

From Fig. 4.10b the 3D volume extraction of the resistivity values below 50 Ωm outlines very clearly two conductive bodies interpreted as mudstone layers of the Travenanzes

formation. The missing information comprised between these regions is the filtered values of resistivity related to the TVZ dolostone layers ($>250 \Omega m$).

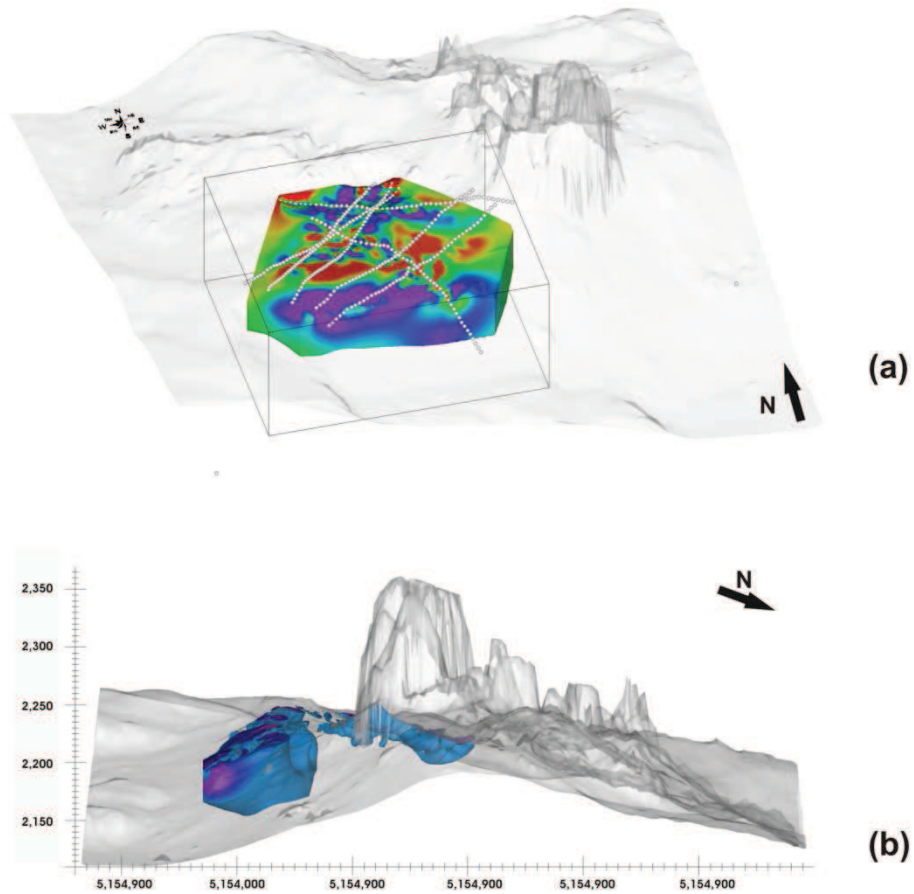


Fig. 4.10. View of the 3D ERT volume (a) and selection in the 3D resistivity volume of the values below $50 \Omega m$ viewed from the East. A clear separation of the two conductive bodies is clear suggesting the presence of two distinct strata that lies almost parallel to the northern slope (b).

4.4. Passive seismic stratigraphy

In the area of the ERT prospection, the passive seismic stratigraphy was also experimented. It is a non-invasive technique able to retrieve information on subsoil stratigraphy and on possible seismic site effects.

The survey established the presence and location of 2-D structures below the western meadow close to the rock group and determined the natural resonance frequencies of the subsoil in the area of investigation.

The passive seismic technique is based on recording and analysis of the seismic environmental noise. It is a very fast and economic technique since its application is totally non-invasive and does not need any drilling, deployment of cables or artificial energization but it only uses the natural seismic noise which is present everywhere.

In order to infer subsoil stratigraphy from seismic tremor, the most common method is the H/V (Horizontal to Vertical Spectral Ratio) technique (Castellaro et al., 2008). The method, firstly proposed by Nogoshi and Igarashi (1970) and later diffused by Nakamura (1989), is based on the evaluation of the ratio between the vertical and horizontal spectral components of the tremor recorded at a single station, providing a direct estimate of the resonance frequencies of subsoil. For the present study the horizontal components are referred to two orthogonal directions in the horizontal plane, and they coincide to North- South and East-West directions.

In order to obtain reliable estimations, a reference investigation of elastic wave velocities in the subsoil or of a calibration point is recommended as it allows correlating the H/V curves into stratigraphy (Castellaro, 2009).

The depth h of a seismic discontinuity, such as a lithological contact existing between carbonates and mudstone within the TVZ formation is derived from the free-surface resonance equation:

$$h = \frac{m v}{4 f} \quad (4.3)$$

where v is the seismic wave velocity of the upper layer, in the present case the mudstone layers of the TVZ formation, f is the resonance frequency, which appears as a peak in the H/V curve (Fig. 4.12), and $m = 1, 3, 5, \dots$ indicates the vibration mode (the fundamental mode, for which $m = 1$, is generally used). In case of a multi-layer system, the H/V curve contains information about the resonance frequencies of each layer (and therefore of each thickness). The formulation (4.3) is thus modified in order to fit a 'synthetic' H/V ratio (Castellaro, 2009) to the measured one, requiring a full modeling of the wavefield in the multi-layered system. The present contribution focuses on the detection of the first lithological contact below the topographic surface at the western side of the Cinque Torri group, therefore only a single layer should be accounted.



Fig. 4.11. Location of the sites of seismic ambient noise recordings (1-8) and of the ERT surveys (L1-L7). White dotted lines indicate faults traces.

The seismic ambient tremors were recorded at 8 sites at different levels of the meadow explored by the ERT surveys in order to cover homogeneously the surface and to thicken the stratigraphical information (Fig. 4.11).

The tremor recordings were acquired with a portable digital all-in-one tomograph (Micromed TROMINO), specifically designed to record seismic tremor. Seismic tremor was recorded for 15-20 minutes at each site with a sampling frequency of 128 Hz during daytime. Possible bias induced in the results by artificial noise is due to the close ski resort during daytime, therefore peaks with typical high frequency were expected.

4.4.1. Results of the passive seismic stratigraphy

Data were analyzed with the Micromed Grilla software package and fitted according to the 1-D layered soil theory (Castellaro et al., 2009).

In Figs. 4.12a,b,c a selection of H/V curves and single spectra of soil motion is illustrated, corresponding to passive seismic reliefs close to line L1 of the ERT survey (sites 5,7) and line 3 (sites 8).

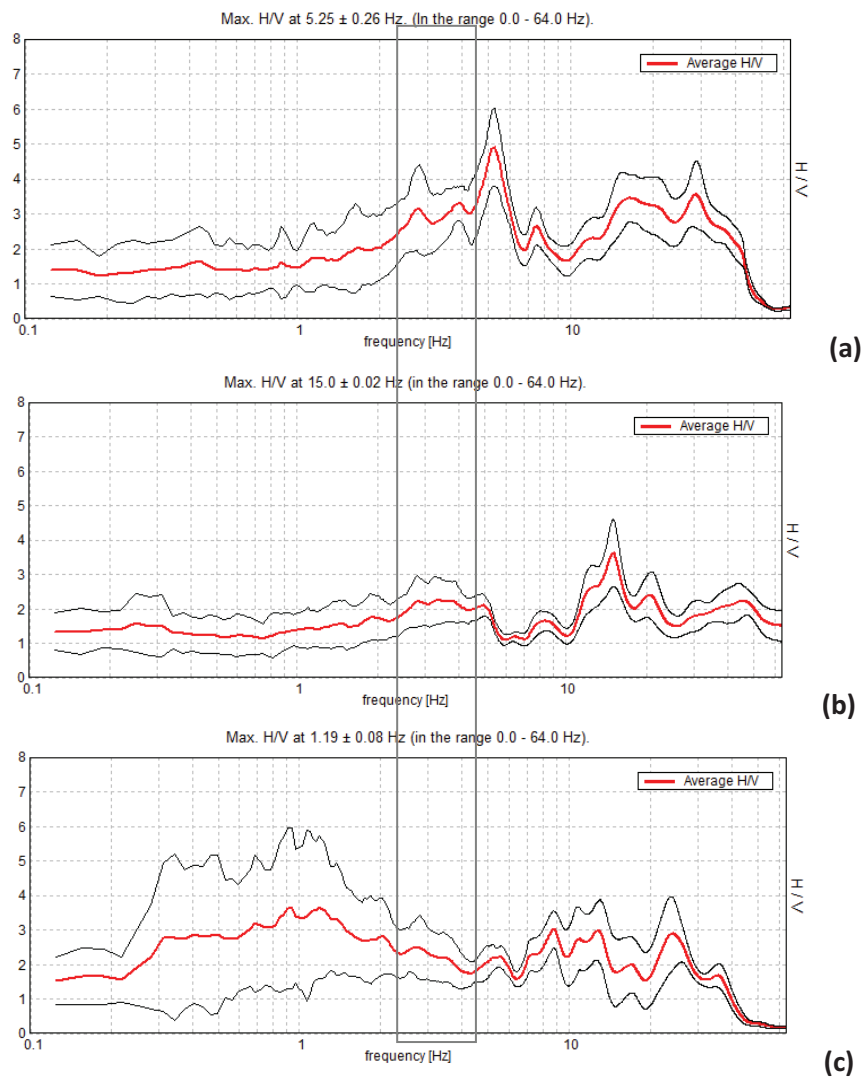


Fig. 4.12. H/V ratios recorded at sites 5 (a), 7 (b) and 8 (c). The common feature ranging 2.5-4.5 Hz is highlighted

In Figs. 4.12 the frequency is represented in a logarithmic scale, in order to enlarge the view of the first few meters (0-64 Hz), which are the most relevant to the present research. Frequency is related to depth: the higher the frequency, the minor the depth. The vertical scale in subplots of Figs. 4.12 is the adimensional Horizontal to Vertical spectral ratio (H/V ratio), while in Fig. 4.13 is the spectral amplitude in velocity (mm/(s Hz)).

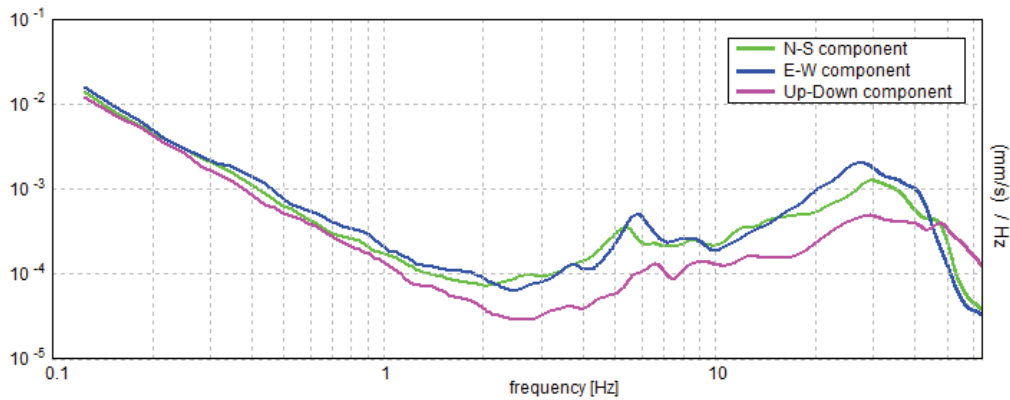


Fig. 4.13. Analysis of the N-S to vertical and E-W to vertical spectral ratios at site F0. The difference between the N-S and E-W components respect the Up-Down component strongly suggests the presence of directional 2-D subsoil structures.

From the analysis of the results of passive seismic, the curves of sites 4, 5, 6, 7, 8 show an H/V resonance peak at 2.5-4.5 Hz (Figs. 4.12.a,b,c). Assuming an average shear wave velocity typical for mudstones of about $V_s=250 \text{ mm s}^{-1}$, this peak can be attributed to a seismic discontinuity located between 20 m and 15 m (Fig. 4.14).

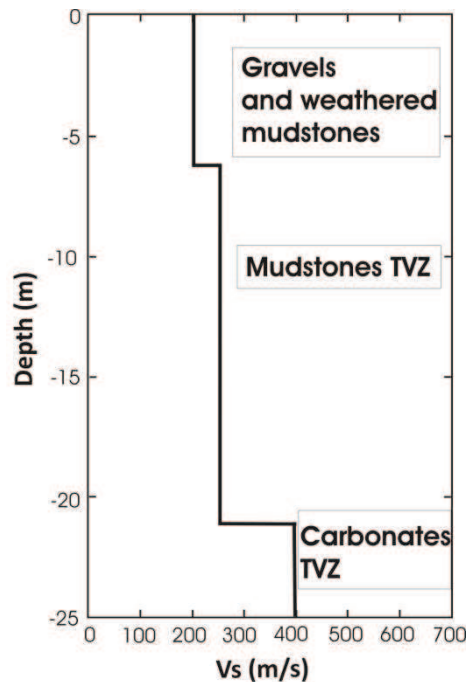


Fig. 4.14. Single-station passive seismic stratigraphy at sites 7 and 8. In the graph is plotted the shear wave velocity (V_s) model which produces the H/V theoretical curve in site 8).

The relative variability of the H/V curves expresses the inclination of the investigated lithological contact, which is additionally lowered by the faults highlighted by the ERT sections. The artifact caused by the proximal ski resort generates a peak at 6 Hz. For this reason, the peaks detected at such a frequency are not accounted in the interpretations. Sites 1 and 2 show high disturbance probably related to a wrong coupling of the instrumentation to the ground, resulting in a noisy spectrum with lack of distinctive

peaks testifying stratigraphical contacts. Site 3 lastly represents an exception to the overall trend. Since the local stratigraphy is characterized by a general trend of N10°E in direction and 20° of inclination, at site 3 the contact should be located at a depth of about 20 m. From the passive seismic results the recorded discontinuity is found at about 60 m from the surface (1 Hz), suggesting a probable anomaly in the dip angle of the strata. This interpretation needs to be further investigated, but it is in good agreement to the gravitational dynamics of the area which is severely influenced by tectonics and plastic deformations. In these conditions, local and sensible variations of the stratigraphy are reasonable and require additional reliefs.

Finally a consideration has to be underlined: in most of the recordings the peak ranging 2.5-4.5 Hz shows a clear directional mark (that is the N-S and E-W component very different from the Up-Down component on Fig. 4.13). This sign suggests the presence of bi-dimensional geometries in the subsoil therefore proving the detection of the contact between mudstones and the underlying dolostones.

4.5. Conclusions

The main aim of the geophysical surveys was to gather information on the subsoil stratigraphy. The 3D ERT surveys on the Cinque Torri Group delivered detailed images of the near-surface conditions which generally agree with tectonic and geological setting. The depth to the dolomitic root of the Cinque Torri was detected in the lateral part only, so there is not a high definition of the lower contact behind the pinnacles. In the 3D ERT volume within the central-western part of the 2D sections, some carbonatic bodies included in a more conductive matrix ascribed to the Travenanzes Formation can be defined also according to the geological a priori information. By defining the thickness of these strata, the local stratigraphic sequence was defined. Some obliterations due to tectonic activity were recognized. As a matter of fact the uppermost dolostones and mudstones layers of the TVZ formation (III D-TVZ and III M-TVZ in Fig. 4.7b) are here not observable.

ERT resolution analysis found that the pole-pole array furnishes the highest number of combinations of interpolation and the highest depth of investigation even if showing some deficiencies on measurement time.

The automatic classification outlined four subsurface units: the mudstone, dolostone and conglomeratic layers forming the Travenanzes Formation and surface layer with high resistivity values on the eastern side corresponding to the Dolomia Principale of the Torre Grande monolith. Taking into account the a priori geological information this model shows similarities to the regional stratigraphy, and moreover it confirms the presence of normal and reactivated faults on the western side of Torre Grande monolith. As these faults cause metric vertical displacements of the intersected layers a significant alteration to the slope setting is produced. These features can therefore favor the slope instabilities since they promote rock dismantling significant vertical movements of the subdivided units as well as erosive processes and possible changes in water circulation.

For future ERT investigations it is recommendable a 3D fashion of the electrode cover to decrease the influence of local factors on the overall resistivity volume, thus providing homogeneous and clear regions with different resistivity.

In the site was also explored the applicability of a single-station passive seismic technique, which is totally non-invasive and can reach large depths. Seismic noise was recorded at 8 sites located on the meadow previously investigated by the ERT survey.

The main resonance frequency of the subsoil was found to occur at about 2.5-4.5 Hz and it is related to the contact between the mudstone layers and the underlying dolostones. A different behavior is testified only by a site where the expected location of the lithological contact is reached at higher depths. This feature is not recoverable from ERT profiles probably due to the different resolutions of the two methods. Nonetheless this "outlier" can be related to local variations of stratigraphy due to tectonics and gravitational deformations. Finally, the H/V resonance peaks (2.5-4.5 Hz) at most of the sites emerges with evident directional features, which stand for 2-D geometries in the subsoil at about 15 m depth, consistent with the 3D ERT prospection.

The combined geophysical, TLS and passive seismic investigations have provided a suitable tool for investigating unstable slopes, in particular to extend the superficial geological data to the subsoil and to organize them in a 3D model. Implementation of this combined methodology is quite successful in locating stratigraphical and tectonic contacts without any invasive or costly technique.

These results are the input data for a numerical model aiding reliable prediction of the deep seated phenomena affecting the Cinque Torri area. This level of research will be useful to support a forecasting analysis and modeling of the movement of unstable pinnacles inside the Cinque Torri group and in general, to understand the causes of the collapses triggered by deep seated ground deformations.

5. Laboratory analyses

5.1. Introduction

The main triggering factors of landslides are related to geological structures, morphology, climate and climate changes of a region, worsening of the geotechnical properties of involved lithologies, exceeds in pore water pressure due to rainfalls or rapid snowmelt.

This chapter focuses on the lithological characterization of the Cinque Torri DSGSD by investigating the relative geotechnical properties among involved lithologies as well as mineral composition. The aim is not an precise assessment of these properties but the identification of the relationships existing among them in terms of strength and deformability. This purpose principally comes from the scarce number of available samples for laboratory testing.

As a matter of fact, according to Gill et al. (2005) the number and size of samples used to test for geotechnical properties evaluations should be taken as the smallest number of specimens for a lithology which insures small deviations from the averaging value of a chosen parameter. The authors concluded that the assumption of a priori optimal number of samples is unrealistic, but it can be obtained only through an iterative procedure which requires several dozen of samples. Since the number of available samples is limited and the main goal of numerical modeling is not slope stability assessment but investigation of deformation features (Chap. 8) to be compared to results of Chapter 6, the laboratory and field tests carried out on these samples are satisfactory for the outcome of this research.

Many studies observed the influence on the physical-mechanical characteristic of a lithology played by the mineralogical and textural composition of rocks as well as the interaction between the circulating solution and solid phases (see e.g. Summa et al., 2010). A landslide involving clay-rich layers is particularly dependent by the physical properties of the clays, i.e. consistency index and plasticity index, compression strength, shear strength, etc. These properties are in turn influenced by the water/clay interaction and clay fabric. By investigating the typology of clay mineral content even only from a qualitative viewpoint, some relationships with the ongoing movements can be explained. The results of laboratory tests can aid the recognition of a critical relationship between the compositional variables of silty-clay components and the geotechnical parameters such as compressibility of the ductile lithologies.

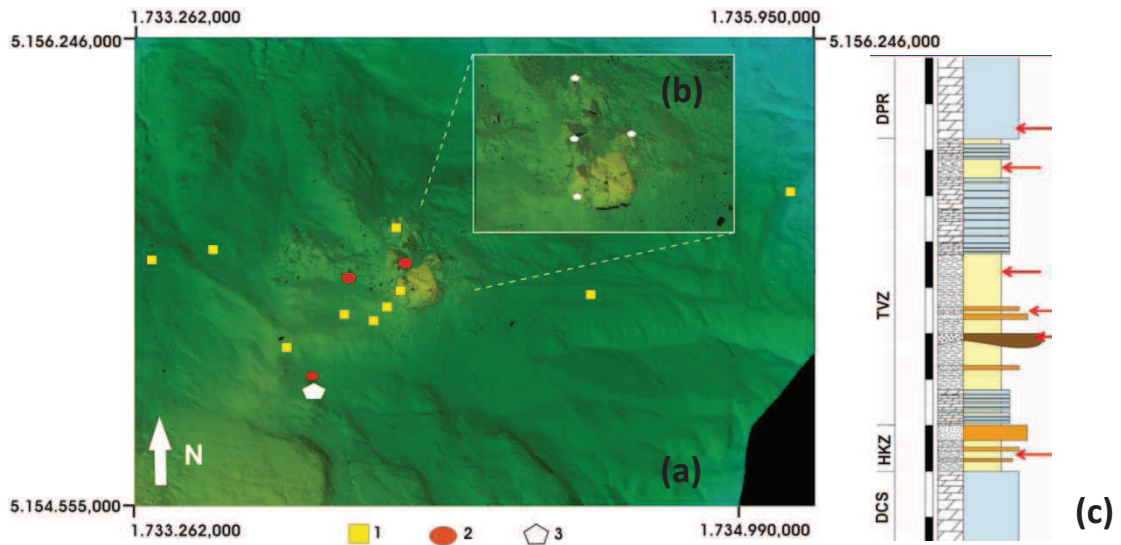


Fig. 5.1. Sampling and reliefs location in the surroundings of the Cinque Torri group (a) and within the rock group (b). Samples for Atterberg limits and XRD analysis (1), rock sampling for uniaxial test (2), geomechanical reliefs described in Chap. 7 (3). Analyzed levels of the local rock units (c).

The clayey formations are very susceptible to the volume change due to swelling and shrinkage that typically happen during the alternate wet and dry seasons. Such cyclic swell-shrink movements and total and differential volume changes in these layers result in considerable distresses and severe damages to overlying structures. Many studies have been carried out to assess the behavior of expansive layers with high clay content, outlining a fatigue of expansive layers after cyclic drying and wetting, due to continuous rearrangement of the solid particles, which leads to destruction of internal clay structure (see e.g. Tripathy et al, 2002).

As suggested by Gratchev et al. (2006), the Plasticity Index, determined by Atterberg limits, may be used as criterion for assessment of the aptitude to liquefaction of clay-rich lithologies. In addition, in the case of a mixed content of clay-silt and sand, a porous microfabric with clay particles forming bridges among sandy particles shows generally low resistance to liquefaction. On the contrary, a more compact microfabric with dominant clay matrix correlates with high resistance to liquefaction. This fact leads to a close relationship of liquefaction processes occurrence in relation to the clay content and clay mineralogy.

In the present research a dozen of samples collected from the mudstones layers of the Travenanzes Formation (TVZ) were analyzed through Atterberg limits determination and X-Ray Diffraction (XRD) analysis for mineralogical classification. The average geotechnical properties of samples are ascertained to be $WL=5\%$, $PI=9\%$ in accordance with American Standard Test Method ASTM M145-82.

The mineralogical analyses were carried out by X-ray diffraction (XRD) using a Siemens D5000 powder diffractometer ($CuK\alpha$ radiation, secondary monochromator and sample spinner). Mineralogical data analysis is based on the measure of integrated intensities of

all the crystalline phases. Quantitative or semi-quantitative estimation could not be carried out since a wider number of samples are needed for such purposes. Nevertheless, a qualitative characterization of the mineral content of the clay rich layers in the TVZ can provide some interesting correlations with the geotechnical parameters.

In order to characterize the rock units from a geotechnical viewpoint, some preliminary uniaxial compression strength tests were carried out in order to determine the peak compression strength (σ_c) as well as the elastic modulus (E) and the Poisson ratio (ν). On a second stage these parameters were compared to the results of ultrasonic tests carried out on the same rock samples to ascertain the obtained values. Even though the number of the analyzed rock samples is insufficient for a reliable classification of the rock properties, the combination of results provided by uniaxial and ultrasonic velocities tests and Schmidt hammer rebound tests (Chap. 7) can highlight qualitative relationships among different brittle lithologies. These comparisons allow defining average values of the rock mass properties of the tested lithologies. These values will be later introduced in numerical model of the slope to evaluate the influence of the stratigraphical heterogeneity to stress and strain distributions. In this way, some interesting interpretations of the Cinque Torri DSGSD can be deduced from the developed numerical models (Chap. 8).

5.2. Atterberg limits

Landslides with rotational components frequently have high clay-silt content (Summa et al, 2010). When the slope has a high clayey-silty component, it becomes prone to landslide because of the chemical and physical properties of these minerals. By absorbing water, clay minerals show a volume and strength parameters change, resulting into a reduction in the stability of natural slopes. The role of water can be related to an intense decrease in shear strength either by reducing the apparent soil cohesion or through the potential slip surfaces, a fact directly related to long-lasting rainfall events or considerable snow melting incomings. This is the case of Cinque Torri area.

Conversely, the susceptibility of the slope to failure depends on many factors including the gradient of the slope and the geotechnical properties of the material involved. As suggested by Cruden and Varnes (1996), a landslide is the alteration of the equilibrium relationship existing between acted stress and strength of materials in the slope. The strength is directly related to the internal cohesion, which is not influenced by the weight of the overlying material. Cohesion is produced by the mechanism of particles that enables the material to rest at an angle and by the internal friction which is the resistance of particles to slide across each other and is in turn depending on the weight of the overburden.

In such a frame, the water causes lubrication of the voids and therefore plays a significant role in the internal strength behavior. Weathered and saturated slopes are preferential environment for a landslide to occur.

The study area is known to have the typical wet weather of the Alpine region; the recent instabilities were recorded in late spring, a period typically characterized by high rainfall rate and intense snow melting. The area is exposed to high variations of precipitations during the year in the Belluno province, whose average total amount¹¹ is 1200 mm (ARPAV, 2010). The monthly average rainfall registered before the events of 2004 (Torre Trepbor collapse) and 2009 (mudflow reactivation) was close to 140 mm and 100 mm respectively.

The TVZ, which forms the main part of the Cinque Torri slope, is described in detail. The mudstone layers are made up by particles previously weathered, eroded, transported and deposited in basins. A considerable portion of these layers is made up by clay minerals, which give to the slope a landslide prone character due the complex nature of these materials. As a consequence of characteristics like plasticity, low permeability and time-dependent pore-pressure and volume changes, the composition and the geotechnical nature of clay-mixed slopes should be investigated first.

In order to determine the properties of the clay –rich materials, representative samples (Fig. 5.1) were collected for laboratory investigations including consistency of clay and X-ray diffraction (XRD) analyses (Sect. 5.3).

The consistency of fine material is defined as the capacity of a soil to be reshaped without changing in volume or cracking. This property is strictly related to the mineralogy of its minerals, presence of water or moisture content. In other terms consistency describes the physical state of a fine-grained soil at particular water content. As the geotechnical properties of clay and silt usually vary on the basis of their moisture content, the Atterberg limits can establish and describe the consistency of the cohesive soils. They can provide useful information regarding soil strength, behavior, stability, type and state of consolidation, or simply a classification of a clay-rich soil. The most interesting aspect in analyzing such properties is the detection of the entity range between plastic and liquid limits, which is related to their aptitude to rapidly change from semi-solid to liquid state, leading to a significant decrease of cohesion, angle of internal friction and bearing capacity after rain (Lambe and Whitman, 1979).

From a microscopic viewpoint, an increase of water content determines an increase in cations layer thickness and a decrease in the net attractive forces between particles and at the meantime a volume expansion (Yalcin, 2007).

Table 5.1 shows the results of the Atterberg limits carried out for 12 samples of weathered mudstones and dolostones.

¹¹ the monthly rainfall refers to 10 years (2000-2010) of recordings collected by three weather stations (ARPAV, regional environmental bureau) located within 10 km from the Cinque Torri area.

Sample ID	WL %	I _p %	Classification ASTM	
			M 145-82	Description
1A	4	4	A 4	L.C.S.
3B	6	16	A 6	L.C.C.
AV2	2	7	A 4	L.C.S.
4A	3	>10	A 7	H.C.C. & M./H.P.
1B	4	>10	A 7	H.C.C. & M./H.P.
3C	4	>10	A 7	H.C.C. & M./H.P.
2A	5	9	A 4	L.C.S.
5A	8	9	A 4	L.C.S.
6A	6	7	A 4	L.C.S.
FELIX	5	9	A 4	L.C.S.
BUCO ROSSO	6	9	A 4	L.C.S.
3A	5	>10	A 6	L.C.S.

Table. 5.1. Results and interpretation from Atterberg limits test. The samples are classified as low compressible silt (L.C.S.); low compressible clay (L.C.C.); high compressible clay from medium to high plasticity (H.C.C. & M./H.P.).

The tested samples are characterized by a low-plasticity, with liquid limits ranging between 2% and 6%, averaging 5%, whereas the average plastic limit values is 9%, ranging from 4% and 16%. According to the plasticity chart, 9 of the analyzed samples are in the CL group (low plasticity, inorganic clay), 2 samples are in the CL-ML group (low plasticity, inorganic clay and silt) and 1 sample is in the ML-OL (low plasticity, inorganic and organic silt and clay).

An important application of the Atterberg classification is the correlation of plasticity to the clay mineralogy (Casagrande, 1948; Yalcin 2007). On Fig. 5.2 is presented a chart for correlating liquid limit and plasticity index values to the montmorillonite, illite, kaolinite and chlorite content. From the same figure it can be observed that the Cinque Torri samples cannot be included into the general compositional classification. The analysis of the mineral content by means of XRD technique is therefore necessary to ascertain the presence of clay minerals, even if at low concentration.

Fig. 5.3 shows the recorded number of strokes for the liquid limit determination. It can be noticed that the general trend maintain below 8% of WL with small gradient, therefore the water content do not influence severely the behavior of these materials. The only exception is represented by the sample 1A for which an increment of the water content, according to the ASTM indications, is followed by a sensible decrease of WL. Therefore, significant changes of the material properties occur if water is adsorbed.

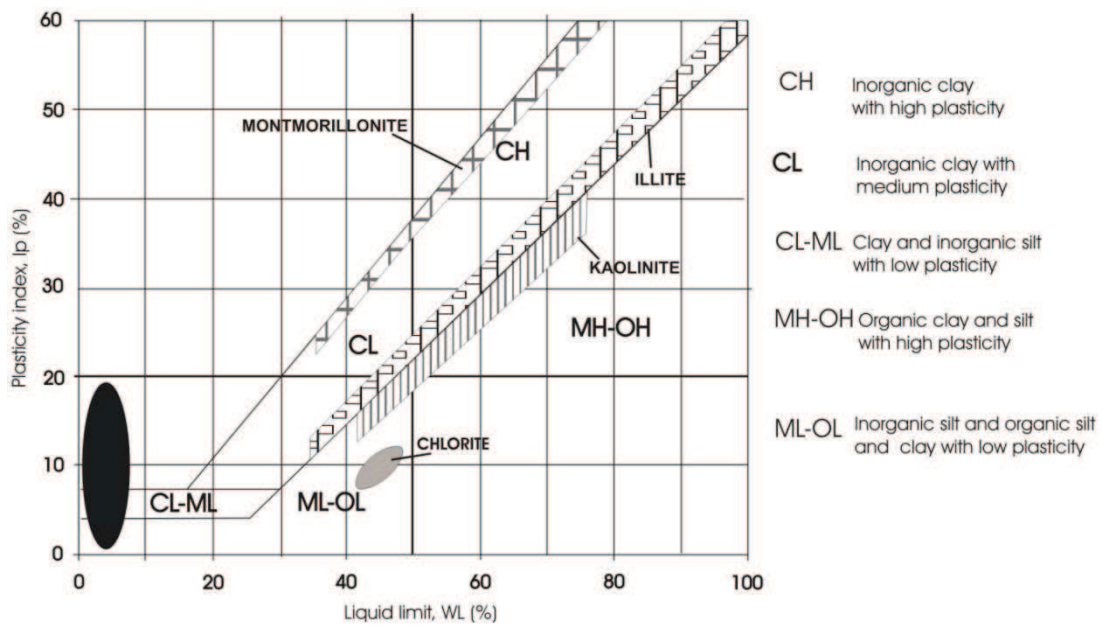


Fig. 5.2. Plasticity chart showing the relationship of the soil samples to clay mineralogy. The black ellipse represents the distribution of the Cinque Torri samples

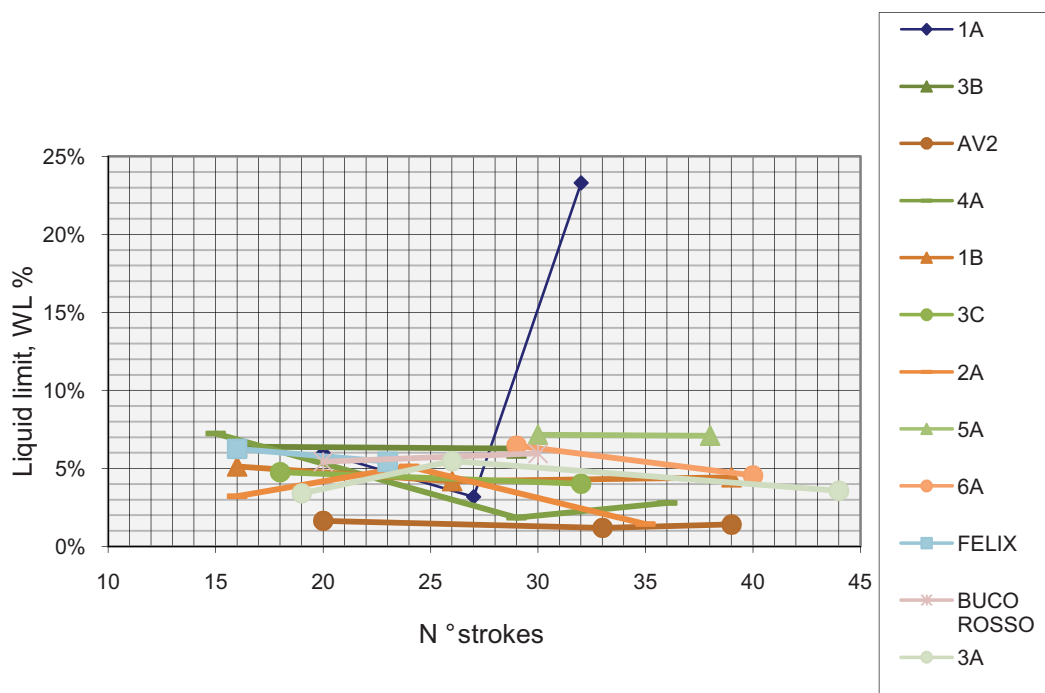


Fig. 5.3. Liquid limit values in relation to the number of strokes determined by using the Casagrande spoon

5.3. X-ray analysis

In the study area, the general heterogeneity of the stratigraphy composition and the weathering process acting on outcrops make the interpretation of data rather complex but as well some results can be outline on the basis of a relative comparison and correlations with the results of the Atterberg limits.

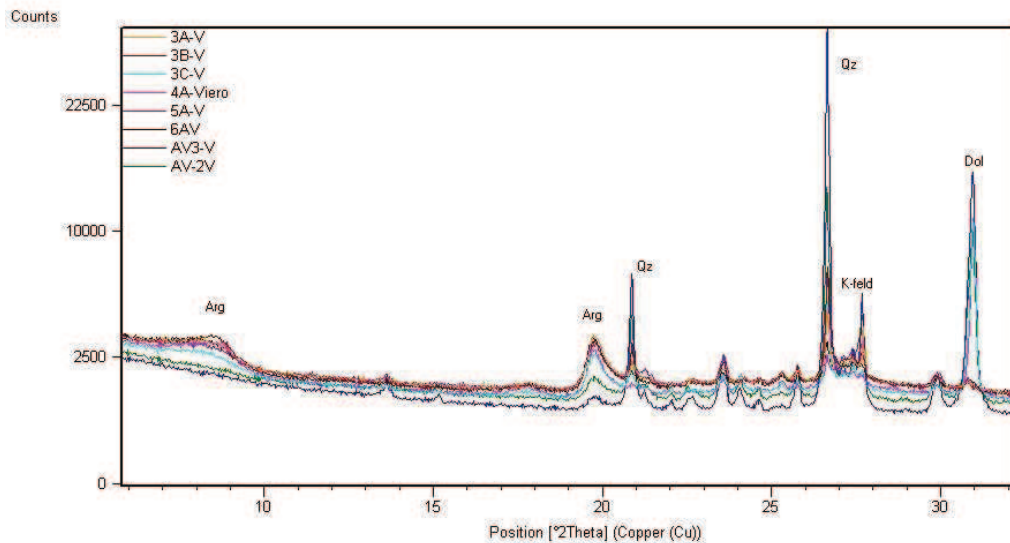


Fig. 5.4. Powder diffractogram showing the mineralogical composition of a part of the samples analyzed by means X-ray diffraction (XRD) technique. $CuK\alpha$ radiation. For clarity, only the range to $32^\circ 2\theta$ is shown.

Mineralogical analyses on a total of 14 samples were carried out by X-ray diffraction analysis (XRD, Siemens Cristalloflex 810 diffractometer, using $Cu\text{-}k\alpha$ radiation) on powder bulk sediment and weathered rocks.

Although well accepted as a definitive tool for mineral identification, XRD is traditionally regarded as having limitations in the evaluation of mineralogical data on a quantitative basis. The limitations include changes in diffractogram characteristics (Fig. 5.4) caused by ionic substitution, variations in mineral crystallinity, preferred orientation in the sample mount, grain size of the different particles and differential absorption of the X-rays by the various minerals in the mixture.

The main mineral phases are phyllosilicates (illite, smectite), dolomite and quartz, while K-feldspars and aragonite are presents as minor compounds.

Several compositional parameters, such as the percentage of smectite-illite and dolomite (Table 5.2, Fig. 5.5), indicate stratigraphic compositional variations. The results sketched on Fig. 5.5 depict a relative increase of clay content from the lower mudstone layers to the top ones in the stratigraphic sequence and a coherent decrease of dolomite component. This trend follows the uniform dip immersion of strata ($N10^\circ E$).

These mineralogical characteristics show a correspondent behavior from a geotechnical viewpoint since an increase of compressibility is recorded from SSW to NNE (Fig. 5.6), implying a direct correlation between clay content and plasticity.

Sample	Composition
1A, AV2, 2A, AV3	Low clay content
3A, 3B, 5A, 6A	Smectite and illite rich, no dolomite
4A, 3C	Smectite and illite rich
1B, AV6	Smectite and dolomite rich
Buco Fex	Dolomite rich
BUCO Rosso	Dolomite, kaolin, illite, clinocloline and anathase rich

Table. 5.2. General classification of the Cinque Torri samples according to the relative comparison o the XRD results. Samples AV2, AV3, AV6 are collected from outcrops of the TVZ formation in the vicinity of Averau mount (Fig. 2.1.).

Some studies related to the clay content and geotechnical properties testify that illite and montmorillonite clay minerals have lower shear strengths and higher swelling potentials and are therefore more prone to landslide with respect to kaolinite and chlorite-rich slopes (Ohlmacher, 2000, Yalcin, 2007).

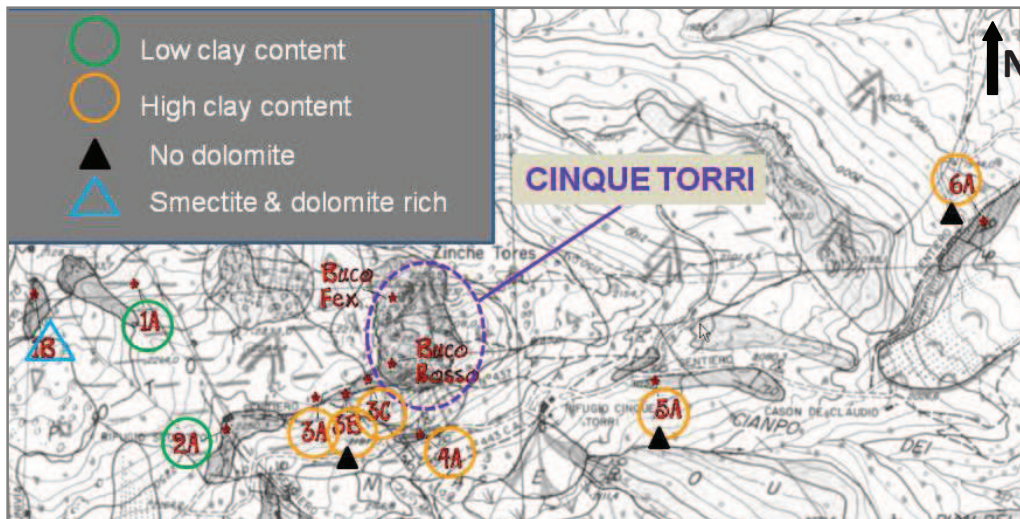


Fig. 5.5. Distribution on map of the mineralogical content, according to the XRD analysis results

If deformations occur, the textural features can be modified and the mechanical removal of the finer particles promoted. Circulating fluids moreover deposits new minerals such as sulphates and iron oxides. In the present case, the active role of circulating fluids is suggested by an increase in the illite-smectite content in samples 5A

and 6A that were collected from the same mudstone layer of samples 1A and 2A even if characterized by different clay content as qualitatively ascertained from preliminary XRD analysis.

It should be noted that the presence of smectite minerals is often associated to an high water content (see e.g. Abdullah et al., 1999). Smectite minerals incorporate water in the electrical diffuse double layer which is thicker with compared to illite minerals. In the Cinque Torri case, this statement is further explained by an increase in compressibility index (see samples 3C, 4A, Fig. 5.6) since smectites have a higher affinity for water hosting exchangeable cations. Therefore it can be stated that among the clay minerals, smectites play the strongest influence on the Atterberg limits and, as suggested by Kaya (2009), the smectite content is also linearly correlated to the residual friction angle ϕ'_r of soils and weak rocks on the basis of its crystalline structure.

At a last stage, a short paragraph should be devoted to the organic material contents and its influence on the Cinque Torri DSGSD. Even if a specific test on the sampled material was not carried out, it can be assumed that the presence of organic material has a minimal influence on the top lateral spreading since there is a low vegetation cover around the rocky group and, in general, the organic material is not prone to fast chemical interaction with clays and water.

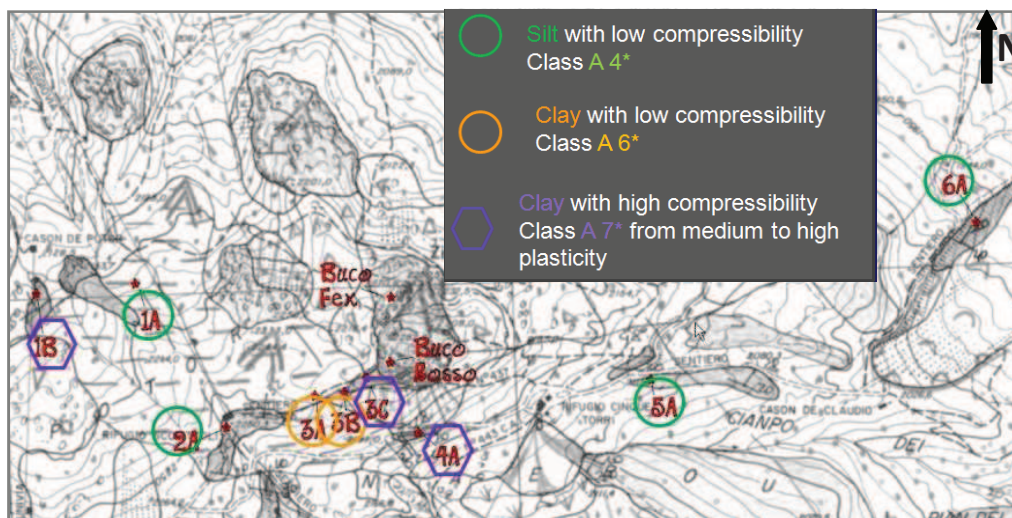


Fig. 5.6. Distribution on map of the compressibility and plasticity classes, according to the Atterberg limits results.

5.4. Ultrasonic velocities measurements

The velocity of ultrasonic pulses travelling in a solid material depends on the density and elastic properties of the material. Ultrasonic pulse velocity (UPV) testing has been reported by several authors as a useful and reliable non destructive tool of assessing the mechanical characteristics of materials like concrete and natural rocks (Hassan et al., 1995, Sack et al., 1995). In particular, the Young's modulus and the compressive strength are obtained. The UPV testing is based on empirical correlations between the ultrasonic pulse velocity and the compressive strength and modulus of elasticity (Uchida et al., 1999; Yasar et al., 2004). The UPV technique can also detect microfracturing in materials subjected to compressive or tensile loading. The fact that the UPV decreases as the damage due to stress induced cracking grows has been reported by Meglis et al. (2005). Experience on rock mechanics elects Acoustic emissions (AEs)² as the most appropriate in the evaluation of the crack damage in concrete and especially in rocks under uniaxial compression, as experienced by Pettitt et al. (2004).

In this research the UPV tests were carried out to help assignment of the mechanical properties of the Cinque Torri lithologies by correlating them to the results of uniaxial compression test.

The available instrumentation provided by Controls (models 58-E0048, E0046) is specifically designed for concrete testing, since only compressional wave velocities can be evaluated. In the case of rock samples, the relation (eq. 5.1) that allow the mechanical properties determination from UPV are here not applicable since they require both compressional and shear velocities estimates, related to P-waves and S-waves respectively (ASTM D2845-05):

$$E = [\rho V_S^2 (3 V_P^2 - 4 V_S^2)] / (V_P^2 - V_S^2) \quad (5.1)$$

The main goal of the present study can as well be achieved by evaluating the possible linear relations between the estimated v_p velocities and the Young's modulus provided by uniaxial tests for each rock sample.

The samples used in the present study were mostly collected in the surroundings of the Cinque Torri group (see Fig. 5.1) and some of them from the southern side of the Averau mount (Fig. 2.1). The selection of the sampling sites was based on practical and representativeness reasons. Thus, Dolomia Principale (DP), TVZ dolostones and TVZ conglomerates were selected.

As mentioned above, the main goal of using UPV testing as a non destructive technique is the correlation of compressional wave velocities with elastic and strength properties of the lithologies under study. This implies that measurements of these mechanical properties and the UPV should be made on the same specimens. Thus, before the compressive tests, the ultrasonic pulse velocity was measured in each specimen.

² AEs are transient ultrasonic waves generated by the sudden release of strain energy as affect of damage formation in a loaded material.



Fig. 5.7. Test equipment for ultrasonic measurements and example of specimen

According to ISRM (1981) (ISRM, 1981), ASTM D2845-05 (2005) (ASTM, 2005), the ultrasonic pulse velocity is affected by the shape and size of the specimens. Moreover, the resonance frequency of the transducers, the minimum lateral dimension and the grain size of the rock are interrelated factors that affect test results.

More in details, according to ASTM D2845 (2005), the minimum lateral size of the specimen, D , should be greater than five times the average grain size of sample under study, d :

$$D \geq 5 \left(\frac{v}{f} \right) \geq 5d, \quad (5.2)$$

where v is the pulse velocity and f is the frequency of the transducers. Since the pulse propagation velocity and the average grain size of the material are intrinsic properties of the material, the values of the minimum lateral size and the resonance frequency of the transducers must be selected in order to allow accurate measurements. The average sizes of the cylindrical specimens ($D = 37.6$ mm, $L = 80$ mm) are satisfactory to attain reliable results. The main physical properties of the prepared rock samples are shown on Appedix A.

In general, moisture content plays considerable influence on the ultrasonic pulse velocity since saturation increases compressional velocities. The UPV measurements were carried out by using the E46 (Fig. 5.7) and the newer E48 equipments from Controls. The equipment it is composed by a central pulse generator unit with a measuring resolution of $0.1 \mu\text{s}$, a pulse rate of 1 s^{-1} and a pulse voltage of 1.5 kV . Piezoelectric transducer of resonance frequency of 54 kHz was used in the measurements. The ultrasonic pulse velocity was obtained by direct transmission, being the transmitter and the receiver transducers located directly opposite each other on parallel surfaces (Fig. 5.7). The connection of the transducers to the specimen was improved through the application of an appropriate coupling gel, i.e. Vaseline, in order

to reduce the influence of voids between the material and the transducers. The transit time was recorded for each specimen as the average of four independent measures for each UPV equipment.

5.4.1. Results of the ultrasonic tests

The mean values of the UPV were obtained by averaging eight measurements of the transit time, t , recorded during the test. After measuring the path length, L , the values of the velocity were calculated as $UPV = L/t$. The mean values of the ultrasonic pulse velocity measured in the cylindrical specimens are shown in Table 5.3. The variations among the recorded travel times of compression waves can be appreciated in Fig. 5.8.

It can be observed that the differences between the values of the ultrasonic pulse velocity obtained are very small with a maximum of 5% and an average of 2%.

The observed low data scattering reflects the homogeneity of the test specimens, sometimes cored from the same rock block, and confirms the reliability of UPV testing. Due to this homogeneity, statistical correlations between the UPV and the mechanical parameters measured in each specimen can be proposed.

ID	Sample Name	Average travel time t (μ s)	Sample Length L (m)	UPV (m/s)
1	HKZ 1	19.5	0.0924	4752.
2	HKZ 1 (perp strata)	15.2	0.0736	4848.
3	5T 1	16.3	0.0956	5871.
4	T M 1 (obliq)	13.4	0.0806	6017.
5	T M (perp strata)	11.5	0.0679	5886.
6	AV1 (pll strata coarse)	32.9	0.0754	2293.
7	AV1 (pll strata fine)	42.8	0.0934	2184.
8	AV1 (pll strata fine)	32.0	0.0783	2451.

Table 5.3. Mean values of the traveling time, length of the analyzed samples and the calculated ultrasonic pulse velocities. Samples 1, 2 are representative of Heiligkreuz Formation (HKZ, made up mainly by carbonates), samples 3, 4 and 5 are representative of Dolomia Principale (DPR, dolostones) and samples 6, 7 and 8 are representative of the sandstones and conglomerates of the Travenanzes Formation (TVZ).

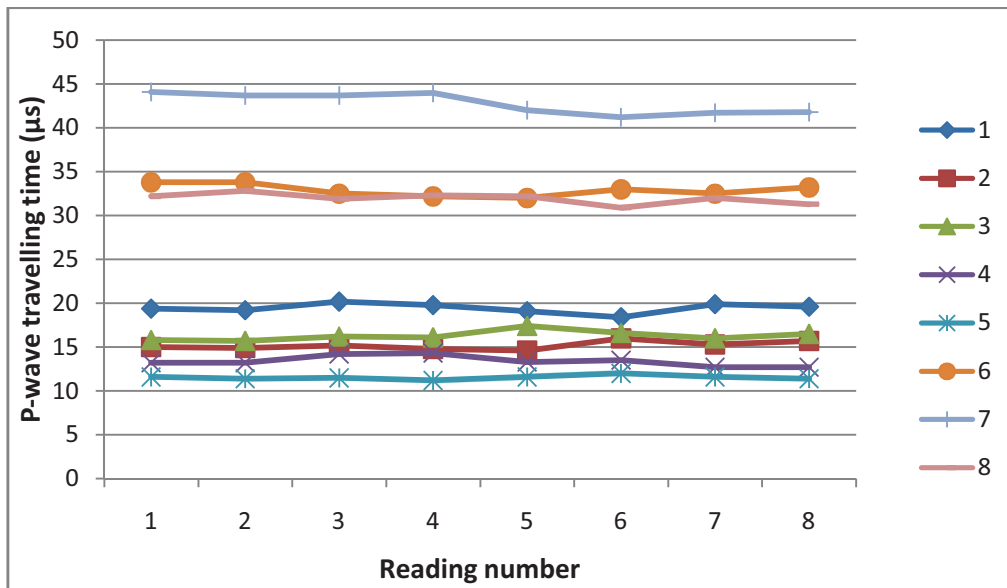


Fig. 5.8. Comparison of the ultrasonic pulse velocity for the analyzed rock samples. Legend refers to the sample ID on Table 5.3.

Under free stress conditions, the anisotropic velocity reflects the internal structure of the material related to the preferential alignment of minerals or cracks. In general, UPV is expected to be higher in the direction parallel to the strata bedding. As a bedding plane is a rock discontinuity, the trajectory of a perpendicular wave which is crossing it undergoes to deviation. The presence of air inside the rock discontinuity results in an additional dampening. Similarly to what was referred about the weathering state, also the anisotropy resulting from the internal structure is attenuated by water saturation. For the present case study, only dry samples were considered therefore the action of water cannot be assessed.

Among the results, more remarkable differences are recorded in case of sample 7. This behavior can be related to the degree of deformation which does not assure a correct parallelism of its surfaces, thus determining an incorrect coupling of the transducers. The higher values of the travel times for samples 6, 7 and 8 is due to their composition: Travenanzas conglomerates present higher porosity with respect to DPR dolostones therefore, as was previously mentioned, the increase in the porosity means a dampening of the P-wave transmission which can be directly related to a reduction of the internal stiffness and strength. The porosity also reflects weathering, tectonic and gravitational processes that act, from a microscopic viewpoint, through a degradation of the rock forming minerals strength and of the grain boundaries stiffness. The higher amount of voids, pores and fractures reflects the slower propagation of the elastic waves. By observing Table 5.3 as confirmation of what these relations, the dolostone specimens (ID 3, 4, 5) which appear scarcely fractured, show the highest values of P-wave velocity. Among them, sample 3 is the only cored parallel to strata direction, but nonetheless is characterized by the lowest recorded velocity. This result suggests a scarce influence, at the scale of the specimen, of strata bedding to P-waves propagation.

5.5. Uniaxial tests

Mechanical testing is considered as a suitable tool for estimating rock and soil properties for modeling purposes. In the present research the uniaxial compressive test together with ultrasonic velocity recordings were carried out in order to calculate intact rock properties of the most competent lithologies of the studied area. In a second stage, the use of empirical correlations (Chap. 7) allowed to derive from intact rock properties the rock mass properties to be introduced in the numerical models for slope instability analysis (Chap. 8).

Due to problems of accessibility during field surveys, sampling collection and scanline mapping were not carried out for all the lithologies. To overcome this deficiency, rock mass properties were derived through a different approach. If no sample was available, the rock properties were derived from empirical relations based on the results of Schmidt hammer rebound test and scanline mapping (Chap. 7). Subsequently the calculated rock mass properties were compared or correlated to the rock mass properties of other lithologies of known intact rock properties. Therefore, the uniaxial tests were useful to first derive intact rock properties, to be then used as a frame for the estimation of the missing values, needed in numerical modeling of instabilities (Chap. 8). The mechanical characterization of the Cinque Torri samples therefore provided an overview of significant engineering geology properties, i.e. modulus of elasticity and compressive strength.

The uniaxial compression test is the most common procedure to characterize rock samples, and indirectly infer the processes which acted from deposition to present day-alteration.

The weathering state, planar anisotropy and even the grain size of a rock sample influence considerably the strength and elastic properties. Generally the weathering state leads to a significant reduction of compressive strength, as well as of the modulus of elasticity. On the other hand, the normalized fracture energy (or ductility) increases with weathering.

The uniaxial tests were carried out by using the compression testing frame Mod. 50-C6600 provided by Controls (Fig. 5.10a). A compression rate of 0.300 MPa/s was used. The correct parallelism between opposite edges of the cylindrical specimens was insured by using a rock polisher. Strain gauges of different size were placed on the surface of specimens in order to record vertical and axial deformations every 0.2 s. Strain gauges can be bonded satisfactorily to almost any solid material if the material surface is prepared properly. The conventional preparatory phase of the surface sample is followed (solvent degreasing- abrading, conditioning, neutralizing and adhesive solution).

5.5.1. Results of the uniaxial tests

The average values of the tensile and compressive strength and the modulus of elasticity for the different types of rock calculated by the Datamanager software package dedicated in SERCOMP 7 (Controls) is shown on Table 5.4.

ID	Sample name	UCS (MPa)	E_{tan} (GPa)	E_{sec} (GPa)	Poisson	ν (MPa/s)	n. strain gauges	Dir.
1	HKZ 1_a	113.53	142.11	143.28	0.860	0.300	3	Perp.
2	HGZ 1_b	279.01	168.44	140.25	0.260	0.300	3	Perp.
3	5T 1	62.23	125.67	121.76	2.720	0.300	3	Parall.
4	T M 1	120.35	86.27	90.12	0.250	0.300	3	Obliq.
5	T M	86.18	77.86	61.22	0.135	0.300	3	Perp.
6	AV1_a (coarse)	85.32	15.15	12.85	0.210	0.300	3	Parall.
7	AV1_b(fine)	108.32	22.10	14.76	0.160	0.300	3	Parall.
8	AV1_c (fine)	91.03	35.65	30.29	0.050	0.300	2	Parall.

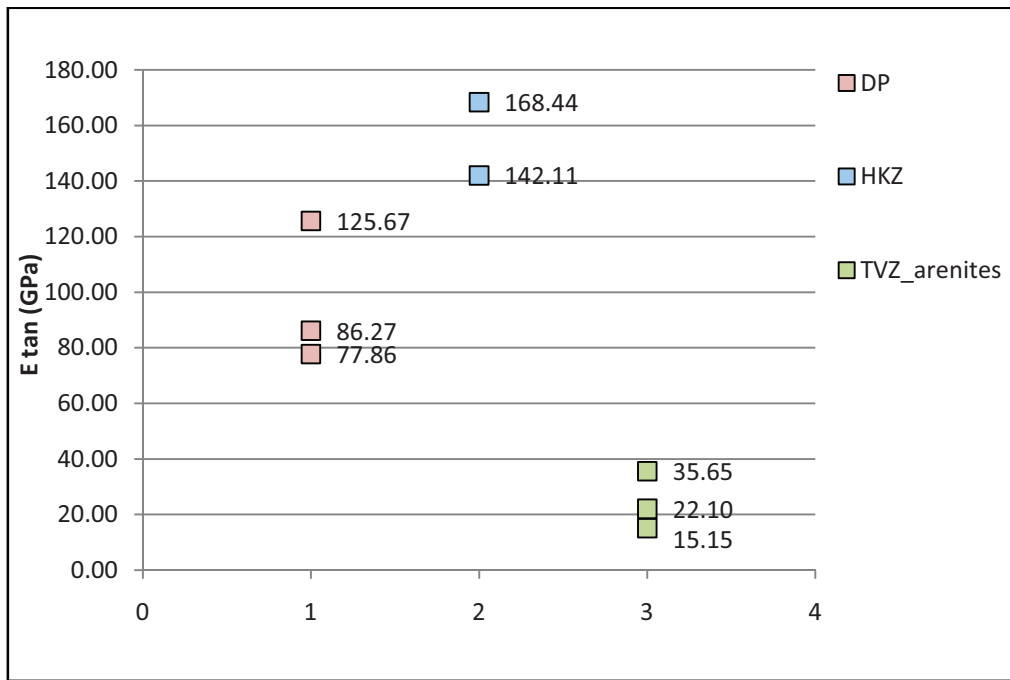
Table 5.4. Mechanical parameters characterizing the compressive behavior of the examined rock samples. 'UCS' stands for uniaxial compressive strength, ' E_{tan} ' and ' E_{sec} ' refer to tangent and secant Young's modulus respectively, ' ν ' is the compression rate and the column of 'Dir.' refers to the direction of sample coring with respect to strata direction.

Table 5.4 shows that a significant variability of the data occurs. This fact reflects the different kind of lithology, as well as a peculiar behavior due to specific characteristics of specimens taken within each lithology (Fig. 5.9).

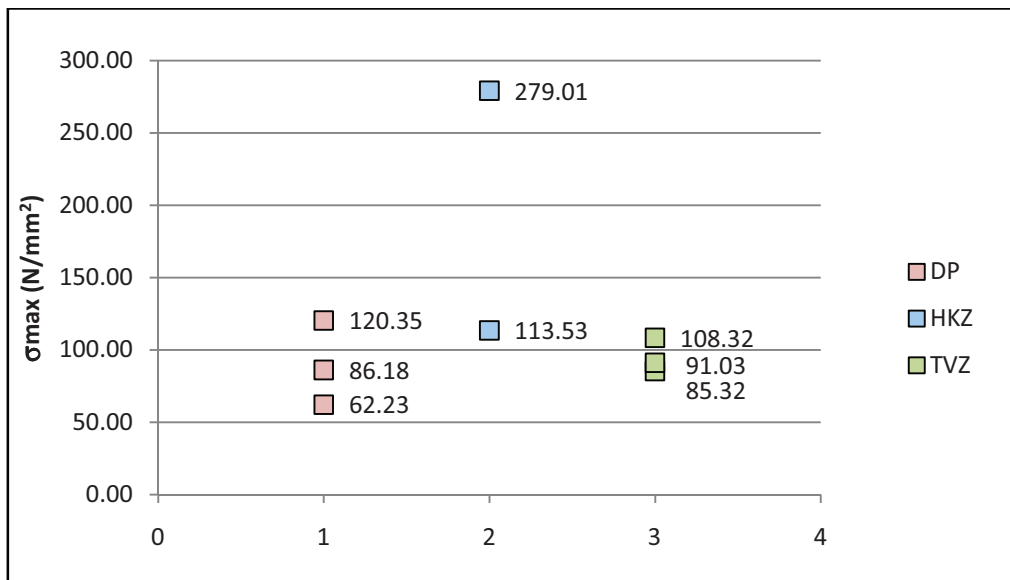
As expected, the lowest strength values are related to TVZ sandstones and conglomerates that, in turn, show lower dispersion of values. The highest strength is recorded by the samples of the Heiligkreuz Formation (HKZ) (Fig. 5.10b), suggesting a minor role of this formation in the dynamics of the instability, also related to its basal location within the slope.

In Table 5.4 some results cannot be taken into account due to their anomalous values. For instance, an incorrect positioning of the axial strain gauge on sample 3 determined the anomalous Poisson ratio value. It cannot be excluded that the highest length to diameter ratio (Appendix A.) could influence the wide differences in terms of E_{tan} and UCS compared to the other DP samples (Fig. 5.9a,b).

Any attempt to furnish an average value of the mechanical properties shown in Table 5.4 is erroneous due to the scarce population of data and to their dispersion. Nonetheless the most representative samples can be elected for each rock type; in particular sample 1, 4 and 7 are respectively representative of HKZ, DP and TVZ arenites.



(a)



(b)

Fig. 5.9. Plotted results of the uniaxial compression test for tangent Young's modulus (a) and peak compression strength (b).

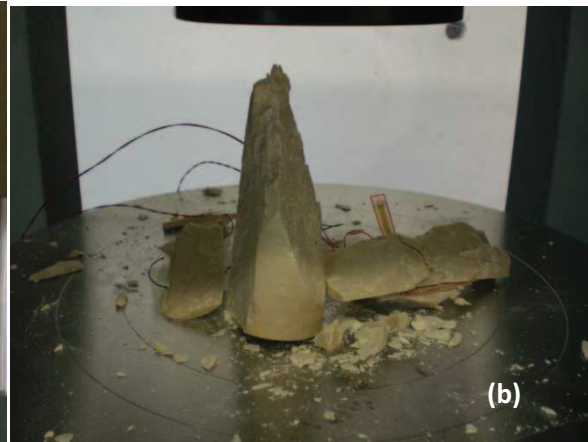
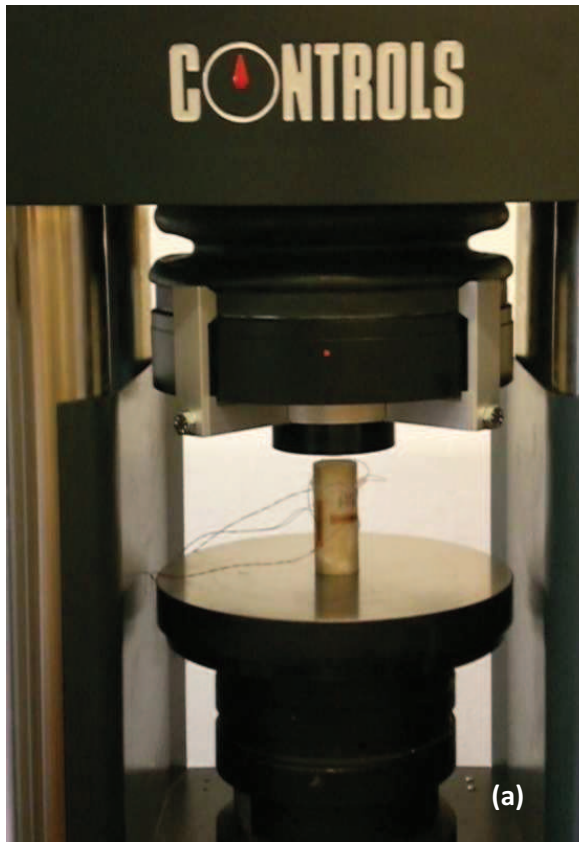


Fig. 5.10. Test setup of the mechanical characterization through uniaxial compressive test. compression testing frame Mod. 50-C6600 provided by Controls (a). Rock specimen (HKZ carbonate) after uniaxial test.

5.6. Discussion and conclusions

The present chapter focused on the characterization of the lithologies involved in the Cinque Torri DSGSD by investigating the geotechnical properties as well as mineral composition. The main purpose of the laboratory tests does not involve a complete quantitative evaluation of these properties, but a relative comparison of them in order to highlight the existing relationship in terms of mechanical properties and composition. By comparing the results of Atterberg limits and X-ray diffraction analysis, a critical relationship between the geotechnical parameters such as compressibility of the ductile lithologies and the compositional variables of silty-clayey components is achieved. As a matter of fact, the mudstone layers of the Travenanzes formation can be stratigraphically differentiated on the basis of clay minerals content and different plasticity. Even though the tests had not a quantitative purpose it can be observed that the topmost mudstone levels (close to the Cinque Torri group) are characterized by higher clay content which reflects in higher plasticity and compressibility. This result should be taken into account for the interpretation of the present deformations affecting the Cinque Torri slope. Moreover, this fact could be a predisposing factor for tilt, rotations and sliding affecting the Cinque Torri group. The high smectite minerals

content revealed by the XRD analysis is often associated to high water content since this type of clay mineral incorporate water in the interlayer space. In literature this behavior is often related to high compressibility and plasticity indexes of the smectite-rich lithotypes. These considerations can help at describing the reasons of the slow movements of the Cinque Torri DSGSD and the unsolved dynamics happening within the slope.

Concerning the assessment of the rock properties by means of simple non destructive techniques, different results revealed the dependence of the mechanical properties, i.e. the modulus of elasticity and compressive strength on UPV.

In this chapter the ultrasonic pulse velocity (UPV) was experienced as a simple and economical nondestructive technique to predict and confirm relations among elastic and strength properties of the Cinque Torri rock types. The statistical correlations that enable the correlation of the Cinque Torri rock mechanical properties with UPV are now studied. The experimental data collected in the present testing program includes UPV measurements from cylindrical specimens. The relationship between the velocity of the longitudinal ultrasonic waves and the Young's modulus derived from uniaxial tests is shown in Fig. 5.11.

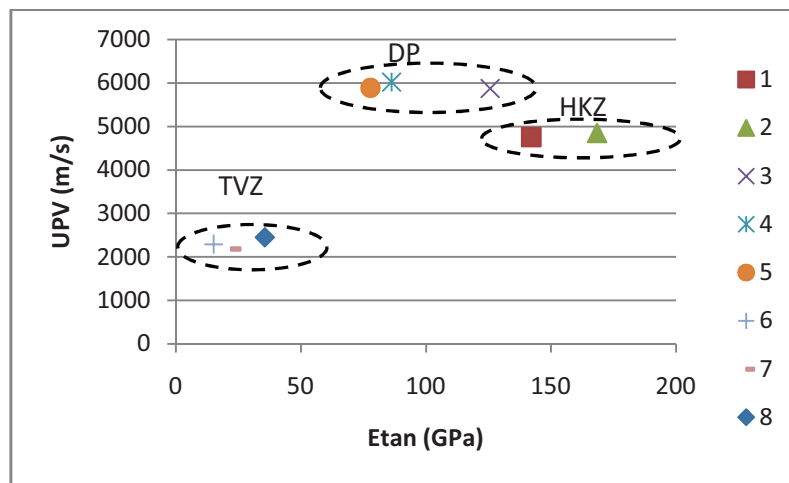


Fig. 5.11. Relationship between ultrasonic pulse velocity, UPV , and modulus of elasticity, E_{tan} .

Despite the difficulty in trying to find a relationship between the variables of Fig. 5.11 due to the small population of data, a correlation can be detected. Ultrasonic pulse velocity can help in finding correlations among rock samples with known rock mechanical properties.

High elastic lithologies have associated high values of velocity but the highest values of UPV are not associated to the highest E_{tan} . In these conditions no linear expression for estimation E_{tan} from UPV was found, but the dependency of the propagation velocity on the dynamic modulus of elasticity of the continuum medium is still clear.

As a main result, it is important to stress the possibility of making comparison among elastic properties of sedimentary rocks through a preliminary measurement of the UPV.

The possibility to find a clear correlation between UPV and compressive strength is even worsen with respect to the previous correlation due to outliers and close similarities among UPV values within each lithology (Fig. 5.12). In spite to determine an absolute correlation for each rock type, it can be observed a small increment of UPV followed by a sensible increment in compressive strength. UPV is therefore directly related to compressive strength but this relation is damped.

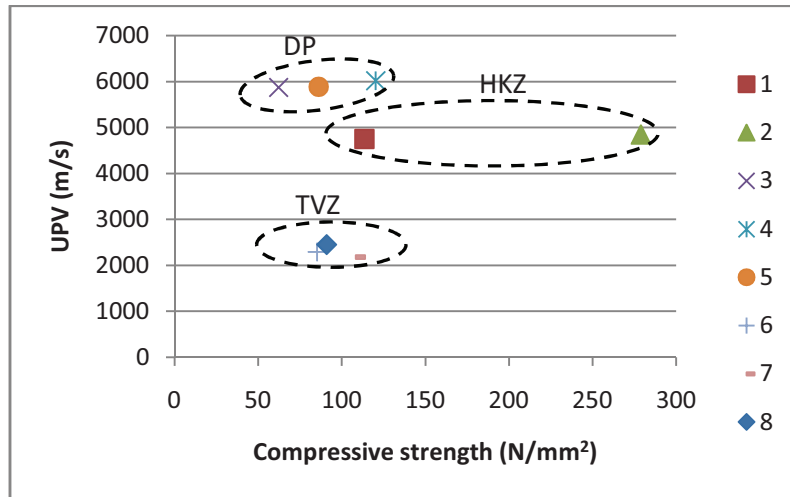


Fig. 5.12. Relationship between ultrasonic pulse velocity, UPV, and compressive strength.

Since the chosen UPV instrumentation is specifically conceived for concrete characterization and evaluates only compression waves, its use in mechanical characterization of cylindrical rock specimen has some limitations.

Despite the scarce number of available rock samples some trends can be outlined from the comparison of the uniaxial compressive test results and UPVs. In particular, TVZ arenites and conglomerates characterized by the lowest values for both the Young's modulus and the compressive strength are also characterized by the lowest UPV values. Carbonates represented by DP and HKZ lithologies have in turn the highest values but despite the higher UPV of the DP, HKZ shows higher E_{tan} . This result is interesting as confers to HKZ a good reaction to deformability. Since HKZ is at the base of the TVZ formation it can be assumed a positive influence of this lithology to the slope stability.

The reason of this different behavior could be explained by a different exposure of the rocky outcrops from which the samples were collected. Factors like weathering state affect remarkably the values of the UPV. Weathered rocks exhibit lower values for UPV than fresh rocks and saturated rocks exhibit higher values for UPV than dry rocks. In addition, the internal microstructure related to planar stratigraphy does not lead to remarkable anisotropy of the UPV. In spite of the expected higher values of velocity in the direction parallel to the stratigraphy for the case of DP specimens, an opposite behavior was found. The reason lies on the homogenous properties of the rock at the

scale of the rock specimen which is provided by the typical decimetric stratification of the Triassic dolostones of Alpine regions.

In final part of this chapter some significant correlations are established between the ultrasonic pulse velocity and the mechanical properties, namely compressive strength and modulus of elasticity, indicating that the values of these parameters can be reasonably validated by means of this nondestructive method. The combination of these analyses therefore provides further information to make assumptions in slope stability analysis and interpretation (see Chaps.7 and 8 for details).

6. Laser-scanning based recognition of rotational movements within the Cinque Torri Group

6.1. Introduction

In the last few decades Deep Seated Gravitational Slope Deformations (DSGSDs) have been defined on the basis of several classification parameters related to common geometries, geological and tectonic controls and similar kinematics. Even if a common general definition of DSGSD has been achieved by Dramis and Sorriso-Valvo (1994), every case study differs in the local setting and lithologies involved. Such a gravitational phenomenon is typically slow ($0.4\text{--}5\text{ mm y}^{-1}$; see e.g. Varnes et al., 1990; Agliardi et al., 2009), and mainly controlled by structural features such as bedding, foliation and fractures (Radbruch-Hall, 1978; Agliardi et al., 2001; Kellogg, 2001; Massironi et al., 2003).

Soldati and Pasuto (1991) describe the DSGSD of the Cinque Torri group (Veneto Region, North-Eastern Italian Alps) as a lateral spread evolving into a block slide, coupled with rock falls and topples.

The definition of structural landslides proposed by Kleczkowski (1955) and Bober (1984) as “...landslides occurring along certain natural geological planes, whose direction of shift is related to geological structure” is applicable to the studied group and represents a crucial assumption for data treatment. Indeed the major role of the tectonic framework in the Cinque Torri instability resides in the definition of lateral spreading itself and can be easily verified by orthophotos (Fig. 6.3), since the regular facets of some monoliths show angular relationships that have also been confirmed during fieldwork in the stable outcrops that surround the rock group. An important issue is the identification of the past movements in order to reconstruct a model able to explain the causes that triggered and fed the gravitational phenomena.

In this study, a new method to investigate past movements inside a gravitational body by means of rock discontinuity analysis is proposed. The methodology is based on the following steps (Viero et al, 2010a): (1) an automated collection of geometric data by means of laser scanner techniques; (2) a structural semi-automated back analysis approach to determine the rotational components of the movements in the rock group up to present by using the data processed in the previous step; (3) computation of the occurred rotations by means of some MATLAB scripts; and (4) validation of the results. The combination of these approaches promotes accuracy and a more comprehensive explanation of the ongoing gravitational phenomena in the Cinque Torri area.

6.2. Terrestrial and aerial laser scanning

Nowadays, terrestrial (TLS) and aerial laser scanners (ALS) are often used for rock instability characterization because these techniques are able to provide detailed, dense, homogeneous and accurate 3D data of the acquired surfaces. In a time-of-flight TLS, which is typically used in geological surveys, a ~ 10 -ns length, 1-ns rise time laser pulse is sent along a direction accurately determined by means of a system based on rotating mirrors and/or rotating elements and the backscattered signal is detected to measure the distance of the reflecting target and therefore to compute their coordinates in the instrumental reference frame. A surface is scanned with a radar-like procedure, i.e. the direction of consecutive emitted pulses is changed by discrete steps. In an ALS measurement, a mirror system operates in the direction of the emitted pulse and perpendicular to the flight acquisition. A surface is therefore scanned by combining the motion of the laser beam and the aerial platform on the basis of the data provided by on-board inertial platform and GPS systems as well as by a ground topographical network.

A TLS/ALS observation provides a point cloud, i.e. the set $\{(x_k, y_k, z_k), I_k : k = 1, 2, \dots, N\}$, where (x_k, y_k, z_k) are the coordinates of the k -th acquired point in a local or a global reference frame, $I_k = I(x_k, y_k, z_k)$ is the corresponding intensity, and N can reach some millions.

In a typical TLS observation carried out from a ~ 200 m mean distance, the spatial sampling is 5–10 cm to provide about 100–400 points per square meter (pt m⁻²), with ~ 2 –3 cm accuracy, whereas the spatial sampling in a typical ALS measurement from a 600 m altitude with respect to the ground is ~ 30 –50 cm to provide ~ 4 –10 pt m⁻² with ~ 10 –15 cm accuracy. In both cases, the potential capacity of the instruments is optimized (Licthi and Jamtso, 2006; Teza et al., 2008a). In geological applications, laser scanner data are typically used to evaluate the geometry and kinematics of unstable masses (Teza et al., 2007, 2008b; Oppikofer et al., 2009a,b), including volume calculations, or also to carry out remote geomechanical evaluations (Slob et al., 2005). Both geometric and radiometric data provided by laser scanner measurements can be used jointly for pattern recognition and strata identification purposes (Pesci et al., 2008; Franceschi et al., 2009).

The TLS and ALS data can be usefully integrated to provide a multi-scale model of the study area by means of a clean and georeferenced point cloud suitable for geometrical analysis of rock discontinuities. In particular, the TLS data are able to represent in detail the steep surfaces of the unstable area, whereas the ALS data can represent the global environment, and therefore the surrounding stable slopes. In addition, the availability of homogeneous and very dense information related to the whole rock walls allows accurate plane fitting and high order statistics that decrease the biases related to the traditional field surveys based on limited compass measurements. The outcomes of the combination of TLS- and ALS-based data can provide more complete information on steep and planar surfaces and a multi-scale 3D model of the study area, enabling the analysis of the tectonic structures on the local rock-instability phenomena.

6.2.1 Laser scanner measurements

In June 2008, the Cinque Torri rock group was observed by using a Riegl LMS Z420i TLS (Fig. 6.1) (Riegl, 2010a), providing 16 partial point clouds for a total of ~10 million points. The accuracy of such an instrument in the single point acquisition is 1.4 cm at 100 m, the corresponding spatial resolution is ~2 cm (Licthi and Jamtsho, 2006), and the acquisition rate ranges from 8000 to 12000 pt s⁻¹. A reasonable compromise between observation time and density of the spatial information was obtained by setting the sampling step at 10–11 cm at 200-m distance. Low resolution scans, with 50-cm sampling steps at 200-m distance, were also performed in some cases where the aim was to provide a reference geometry only. Together with the TLS acquisitions, GPS measurements were carried out for data registration/georeferencing purposes. In particular, in each point cloud two points were positioned in the ETRF2000 reference frame by means of rover GPS receivers in rapid static differential measurements. The two points chosen were the instrument center and the center of a target whose shape can be easily recognized and modeled in the point cloud. Both points were referred to a master GPS receiver placed on a topographic benchmark.

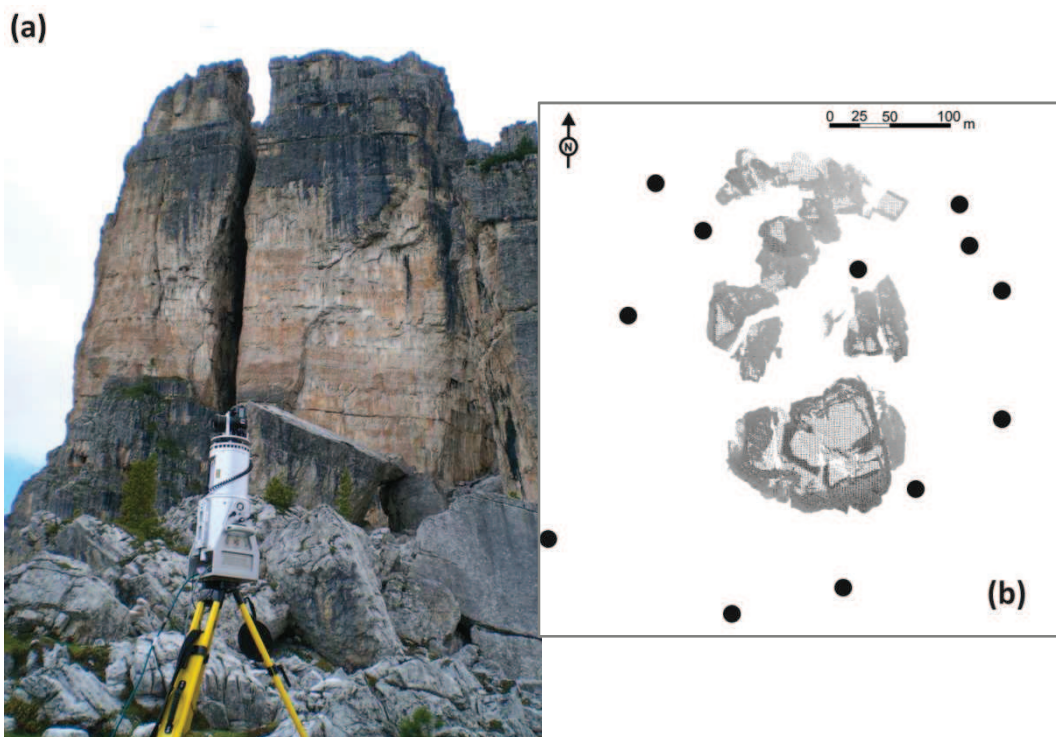


Fig. 6.1. Riegl LMS-Z420i scanner with mounted digital camera during acquisition. A rotating mirror scans the zenithal direction, and the rotation of the entire laser unit covers the azimuthal angle. Operation of the scanner is by laptop PC (not shown) (a). Distribution around the rocky group of most of the scanning positions represented on the map view of the filtered point cloud (TLS+ALS datasets) (b). Three additional point clouds were acquired from distal areas in the western side of the rocky group for reference purposes.

After a first phase of cleaning and filtering from vegetation and scatters, the partial point clouds were co-registered by means of Riegl RiSCAN Pro software (Riegl, 2010b) on the basis of the above mentioned GPS data, to obtain a single, georeferenced point

cloud. The data were then exported to PolyWorks 9.0 software (Innovmetric, 2010) to improve the co-registration in the external reference frame by means of a surface-to-surface ICP (Iterative Closest Point) algorithm (Bergevin et al., 1996).

In the same period as the TLS surveys, the ALS acquisition was also performed covering a $\sim 3.5 \text{ km}^2$ area (Fig. 6.2) using an Optech ALTM Gemini (Optech, 2010) from a mean relative altitude of $\sim 900 \text{ m}$, with a point density ranging from 1 to 3 pt m^{-2} depending on the slope gradient and providing a point cloud with 15.5 million points. The observed area comprised both the Cinque Torri group, which covers only $41\,000 \text{ m}^2$, and the surrounding reference area not involved in the gravitational phenomena. The latter corresponds to the entire section of slope confined by the Falzarego River (North and Northeast), the Nuvolau cliffs (South) and Cresta Gallina (West), as shown in Fig. 2.1.

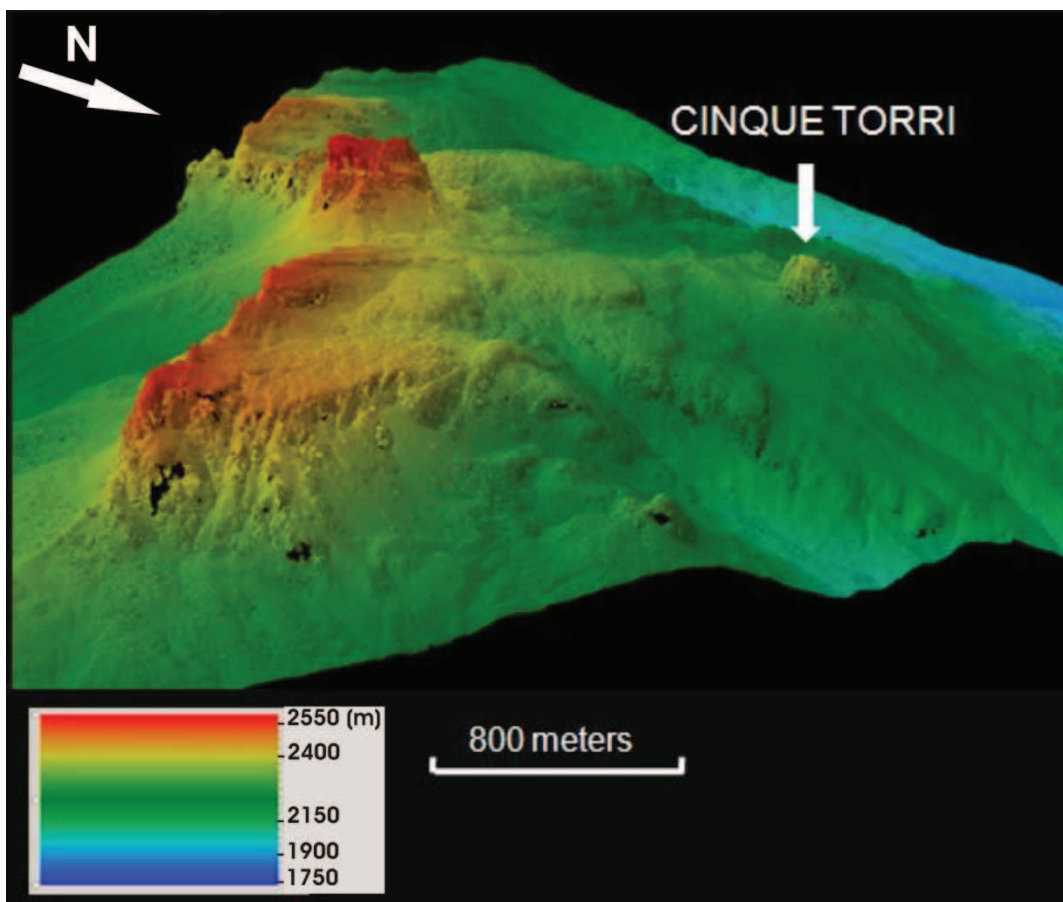


Fig. 6.2. Point cloud of the surveyed area by Aerial Laser Scanning. The point cloud is rendered according to the z coordinate associated to each point (elevation coordinate respect sea level)

6.3 Data analysis

6.3.1. Method

The basic principle of the laser scanning-based geometric and kinematic study of the Cinque Torri gravitational instability is the fact that the deformation mechanism is strongly controlled by the pre-existing tectonic structures. The frequently reported observation that the presence of tectonic structures is frequently associated with rock slope failure (e.g. Guzzetti et al., 1996; Agliardi et al., 2001, 2009; Badger, 2002; Massironi et al., 2003; Ambrosi and Crosta, 2006) underlines the importance of characterizing joints and structural features in order to deduce rock-mass quality and landslide susceptibility.

In this study, the authors would like to stress another important potential for using joints as a gauge of gravitational movements (Viero et al., 2010a,b). The recognition of faults and fractures as well as strata attitudes inside and outside the hazardous area allows a good characterization of the past movements and can be an effective tool in instability forecasting.

A given discontinuous rock body is characterized by a precise number of joint families. When a compound movement starts on a slope, the rock body is fragmented into different rock elements leading to a new settlement. Provided that the gravitational phenomena do not cause severe crumbling of the rock mass, it is possible to rebuild the initial structural setting by investigating the inherited tectonic fabric in each fragment. This can be achieved by measuring the joints and discontinuities, often represented by the surfaces of the dismantled rock body (Fig. 6.3), and by computing angular relationships between the discontinuity sets. In the present case study, the angular relationships between bedding and selected discontinuities offer distinctive markers to assess the orientation of each block with respect to the original structural setting typical of the stable areas outside the landslide. Additional information can be obtained by comparing the fragment motions with respect to each other inside the gravitational deformation area in order to emphasize the occurrence of local-scale rotations and thereby predict future collapse trajectories.

According to the above arguments, the data analysis is carried out using the following steps:

- 1) Analysis of the georeferenced point cloud provided by laser scanner (LS) measurements through the application of the Coltop-3D software (Jaboyedoff et al., 2007, 2009; Metzger et al., 2009). This package performs a classification of the point cloud by means of automatic recognition of the planar or quasi-planar regions (facets) and characterization of the corresponding attitude (dip direction and dip angle). A color level is assigned to the modeled surfaces, on the basis of their orientations. Hence rock discontinuities are defined by specific clusters of orientations that can be selected and drawn on stereoplots.

2) Subdivision of the Cinque Torri area into different isolated sectors on the basis of morphological criteria and the previously defined rock discontinuities. This procedure allows common structural domains among the different sectors to be identified.

3) Comparison of the structural setting among the Cinque Torri sectors and between the Cinque Torri group and the regional tectonic framework to detect the joint sets with a definite tectonic origin. Since only these sets precede the gravitational phenomena, they allow the numerical computation of the rotational movements which have occurred within the gravitational area. The structural correlations have been achieved through the identification of the attitude relationships between strata and joints and the Mohr-Coloumb angular relationship between fractures planes and the principal stress directions (Viero et al., 2009a).

4) Manual selection of planar and quasi-planar point cloud subsets and corresponding least square plane fitting, carried out in PolyWorks (Innovmetric, 2010). Such a fitting provides the normal unit vector and the corresponding main statistical parameters at each discontinuity set (i.e. number of points of the plane, standard deviation of the parameters of the modeled plane, RMS of the normal distances of the points with respect to this plane).

5) Estimation of the rotations of rock monoliths by computing reorientation of reliable pairs of discontinuities identified by the structural analysis, belonging to different sectors. In particular, for each pair of discontinuities assumed originally be part of the same discontinuity set before the gravitational process, the best fit rotation between the corresponding reference frames is derived.

To sum up, steps 1, 2, and 3 are based on a semi-automated inspection of point clouds and a manual selection of common families of discontinuities via traditional graphical tools. In particular, step 3 allows the planes with a definite tectonic origin to be detected within the Cinque Torri sectors. These discontinuities are used in steps 4 and 5 that implement a novel semi-automatic approach in the analysis of 3D rock body rotations.

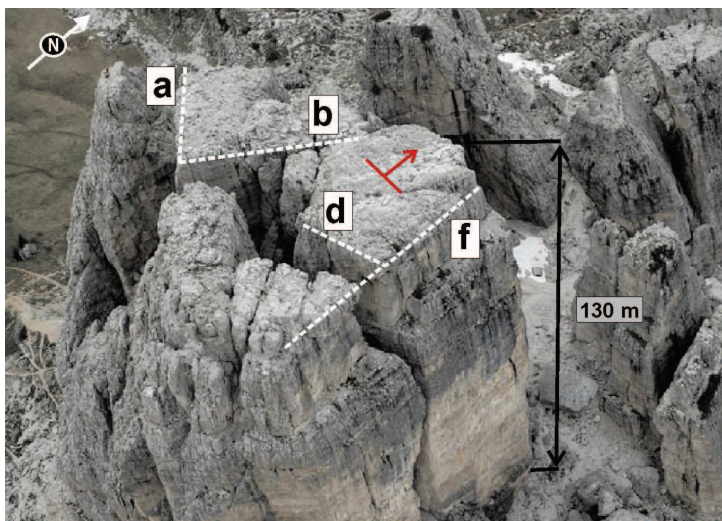


Fig. 6.3 Photograph of the southern part of the rock group viewed from a helicopter (Photo by E. Manfrè). The main discontinuity sets (A, B, D and F) are highlighted together with strata direction. The tectonic control on the fragmentation as seen in the crests of the towers is clear.

6.3.2. Structural analysis

In order to define the actual settlement of the rock monoliths with respect to a stable reference frame, the Cinque Torri group has been divided into subgroups according to morphological and structural criteria. This partitioning is useful for comparing the relative rotations among the sectors themselves, aiding the prediction of future trajectories of movement. The presence among the monoliths of detritic deposits, detritic fans, and blocks derived from precedent collapses and rock weathering allows a first morphological division into groups of towers. In addition, the existence of a common average trend among rock discontinuities inside each group provided a further constraint on the subdivision of the rock group into sectors.

The spatial distribution of the discontinuities was obtained using the Coltop-3D software, which is able to perform a detailed structural analysis of an acquired surface starting from the original point cloud (Fig. 6.5a). A color level is added to the point cloud on the basis of the spatial orientation, in terms of the dip angle and dip direction, of the plane fitted to individual points and their neighbors (Jaboyedoff et al., 2007). In order to decrease the error, the results provided by Coltop-3D are local spatial averages.

More in details, Coltop3D attributes a unique RGB color to each spatial orientation, which permits the user to visually identify the discontinuity sets and to select areas with the same color and consequently also the same orientation for the computation of the average dip direction and dip angle (semiautomatic approach) (Jaboyedoff et al., 2004, 2007).

The software principle can be easily outlined by its initial capability (Jaboyedoff and Couture, 2007) in representing square grids DEM (Fig. 6.4A) using Hue Saturation Intensity (HSI) wheel (Fig. 6.4B). The HIS can be referred as a projection system which makes a direct link between the color and the direction of the normal of the DEM cells and then converted into a color-coded stereonet (Fig.6.4C).

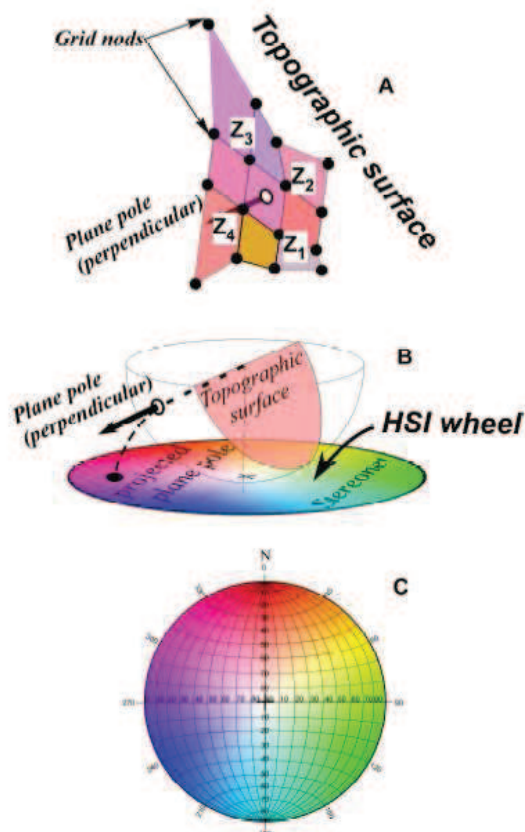


Fig. 6.4. Principle of Coltop color scheme for the digital surface models processing. (A) The color is affected to cells defined by four nearest neighbors on a square grid. With T_{in} it will be 3 points. (B) Relationship between Schmidt-Lambert projection and HSI wheel. (C) The HSI wheel plotted on a stereonet. (Jaboyedoff et al. 2007)

After the automatic classification, structural features inside the colored point cloud can be manually recognized (Fig. 6.3a). The poles of the corresponding planes are then plotted by means of the structural software Dips (Rocscience, 2010) (Fig.6.5b) and grouped into joint sets to allow a comparison between regional and local tectonics.

In Table 6.1 are summarized mean orientations and related statics of the all the recognized discontinuity sets for each rock sector. Facet orientations of a monolith are assumed to belong to the same discontinuity system if the average values of dip and dip directions show a low dispersion (generally below 15% of the corresponding standard deviation, see e.g. Oppikofer, 2009b) and the facet distances of neighboring blocks are less than 5 m, according to observational data. Following these criteria, the subdivision of the Cinque Torri into groups of monoliths became feasible and for each sector a stereoplot, where the main discontinuity sets are plotted, was obtained. The computation of the sets provided an average dip direction and dip angle with dispersions expressed by the aperture angle of the 1σ confidence cone centered on the mean orientation of the discontinuity set (Wyllie and Mah, 2004; Rocscience, 2010). Every set is represented by a pole that may derive from the semi-automated fit of the orientation of thousands of points. As reported on Table 6.1 the dispersion factor expressed by the Fisher's constant which indicates how well a sampled set of cluster values defines a specific discontinuity set (Priest, 1993).

Table 6.1. Summary statistics of the discontinuity sets properties in the sectors of the Cinque Torri group obtained by Coltop-3D-based classification of the point cloud. The difference between extracted poles and clustered poles for derivation of sets orientation is evidenced.

SET ID	Dip Direction (°)	Dip Angle (°)	Number of input poles	Number of interpolated poles	Fisher's K	Standard Deviation σ (°)
SECTOR 1- torre Grande						
1-1	271	85	11519	7508	42	13
1-2	210	79	28782	14406	30	16
1-3	335	90	14973	7890	45	13
1-4	181	86	11748	5517	27	17
1-5	116	88	10004	4693	48	13
1-6	255	90	650578	308412	42	13
1-7 (strata)	6	18	402	247	88	9
SECTOR 2- torre Latina						
2-1	229	89	73568	39737	18	21
2-2	273	88	302432	132758	40	14
2-3	355	79	83030	32209	66	11
2-4	48	88	73568	25402	30	16
2-5	291	86	50205	19061	61	11
2-6	100	79	29103	17794	55	12
2-7	150	86	6760	3082	27	17
2-8	186	86	4614	2594	36	15
2-9 (strata)	75	15	217	128	83	10
SECTOR 3- torre Lusy, Barancio, Romana						
3-1	64	86	549907	186133	64	11
3-2	349	82	296318	102972	65	11
3-3	329	83	148826	34854	39	14
3-4	267	87	66170	33715	98	9
3-5 (strata)	52	2	186	99	90	9
SECTOR 4- torre Mezzo, Quarta Alta, Quarta Bassa						
4-1	83	75	674223	313393	41	14
4-2	164	67	130677	62362	56	12
4-3	21	74	71906	43988	79	10
4-4	194	75	11216	7558	66	11
4-5	31	67	42269	28890	44	13
4-6	101	78	128647	67041	33	15
4-7	149	87	48185	25440	37	14
4-8 (strata Quarta Alta& Bassa)	316	18	547	456	68	11
4-9 (strata Mezzo)	257	19	4683	4529	1404	2
SECTOR 5- torre Inglese						
5-1	81	79	111128	56290	101	9
5-2	306	88	43157	16671	24	18
5-3	203	77	6872	4023	52	12
5-4	37	88	142939	69067	47	13
5-5	182	86	11028	4888	51	12
5-6	159	74	40489	15858	72	10
5-7 (strata)	336	30	3138	2506	122	8

More in details of the Fisher's constant can be calculated by the equation (6.1):

$$K = \frac{N-2}{N-R} \quad (6.1)$$

where K is the Fisher's constant, N is the number of the analyzed poles ($N \geq 10$) and R is the resultant normal vector of plane fitted on the basis of the manual clustering of poles. It can therefore be stated that a large dispersion of pole vectors produces a small resultant vector (R); thus the numerator ($N - 2$) and the denominator ($N - R$) are almost equal, and therefore Fisher's constant K is close to 1.0. In contrast, if the dispersion is small and all vectors point in approximately the same direction, then the magnitude of the resultant vector R will be very high, approaching N, and the denominator will approach zero. Thus the Fisher's constant K will become extremely large, approaching infinity in the limit.

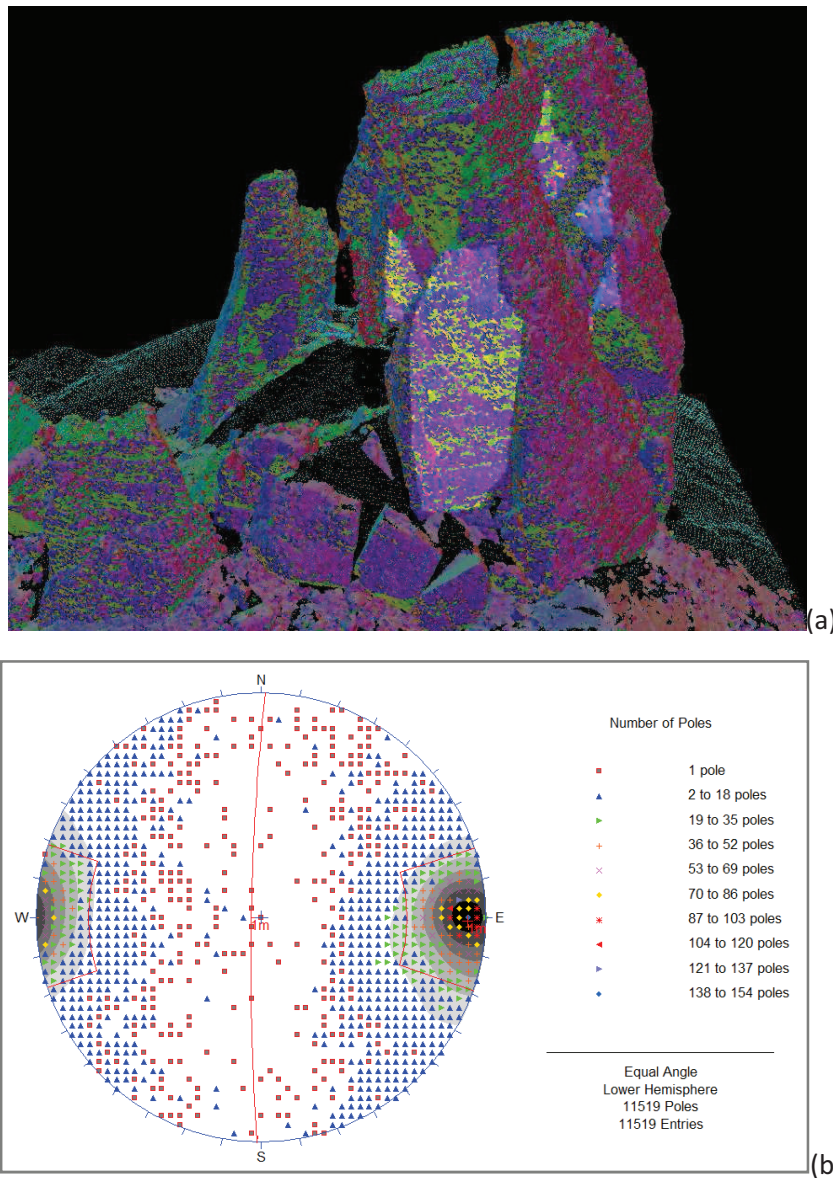


Fig. 6.5. Example of discontinuity family selection within the point cloud of Torre Grande monolith (Sector 1 according to rock group subdivision) by means of Coltop-3D software (a). Corresponding stereoplot of the spatial information associated to the selected points (b)

Likewise, for the Cinque Torri sectors a complete structural definition was obtained for distal stable areas surveyed by the ALS (Table 6.2). Afterwards, the comparison between the discontinuity sets from stable areas (regional data) and the Cinque Torri sectors (local data) was achieved by a first inspection of stereo plots. The structural comparison between sectors and stable areas and among sectors themselves was obtained through a software-based matching of the recognized common sets. This operation requires an iterative procedure that realizes stereo plot matching through the use of software packages able to compute stereonet rotations (Georient, 2010) and to evaluate the results (TectonicsFP, 2010). In this way, the selection and reorientation of the common sets can be carried out and the choice of the optimal sets for the last step of the proposed methodology achieved.

Table 6.2. Summary statistics of the discontinuity sets properties for the reference external areas obtained by Coltop-3D-based classification of the corresponding point cloud.

External reference areas						
SET ID	Dip Direction (°)	Dip Angle (°)	Number of input poles	Number of interpolated poles	Fisher's K	Standard Deviation σ (°)
E-1	275	40	134366	74564	53	12
E-2	216	54	24698	13655	54	12
E-3	198	47	19771	10368	37	14
E-4	64	54	22019	20178	87	9
E-5 (strata)	24	24	59062	43292	24	10

6.4. Quantification of discontinuity plane rotation

The computation of rotations requires assumptions concerning the choice of rotational parameters, i.e. axes and angles, and biases induced by the analyst's choices can therefore affect the results. To prevent these biases and use the whole amount of TLS- and ALS-based data providing solid statistics, a new approach, based on recognition of common structural features, was used. If two discontinuity planes (DPs) π_{D1} and π_{D2} are derived from the same plane π , or a family of parallel planes represented by π , by means of sliding, toppling or other gravitational phenomena, the objective is to compute the quantities that characterize the transformation from π_{D1} to π_{D2} , as well as from π to π_{Di} , $i = 1, 2$.

Euler's theorem states that the general affine transformation in the R3 space is the composition of a translation and a rotation around an axis. The proposed analysis method is based on evaluation of rotation only, whereas the translational component of the motion will be the subject of further work requiring comparison of stratigraphic sequences within the system. The evaluation of the rotation between two discontinuity planes π_{D1} and π_{D2} is carried out in three steps: i) recognition and modeling of the discontinuity/bedding planes pairs (see Section 6.3.2), ii) characterization of a suitable reference frame for each DP, and iii) computation of the rotation parameters.

Inspection of the point cloud, carried out using PolyWorks (Fig. 6.6) or similar software packages, allows the DP to be recognized and modeled. After the selection of the points related to a DP, a linear least square fit provides its equation $a_Dx + b_Dy + c_Dz + d_D = 0$ on a reference frame $Oxyz$. The corresponding unit normal vector, $\hat{\mathbf{n}}_D = [n_{Dx}, n_{Dy}, n_{Dz}]^T = [a_D, b_D, c_D]^T / \sqrt{a_D^2 + b_D^2 + c_D^2}$, where T indicates the vector transposition. In the same way, a bedding plane (BP) intersecting the selected DP can be recognized. Let $\hat{\mathbf{n}}_B$ be its unit normal vector. The positive sense of this unit vector is chosen according to the conventional lower hemisphere projection on a stereoplot.

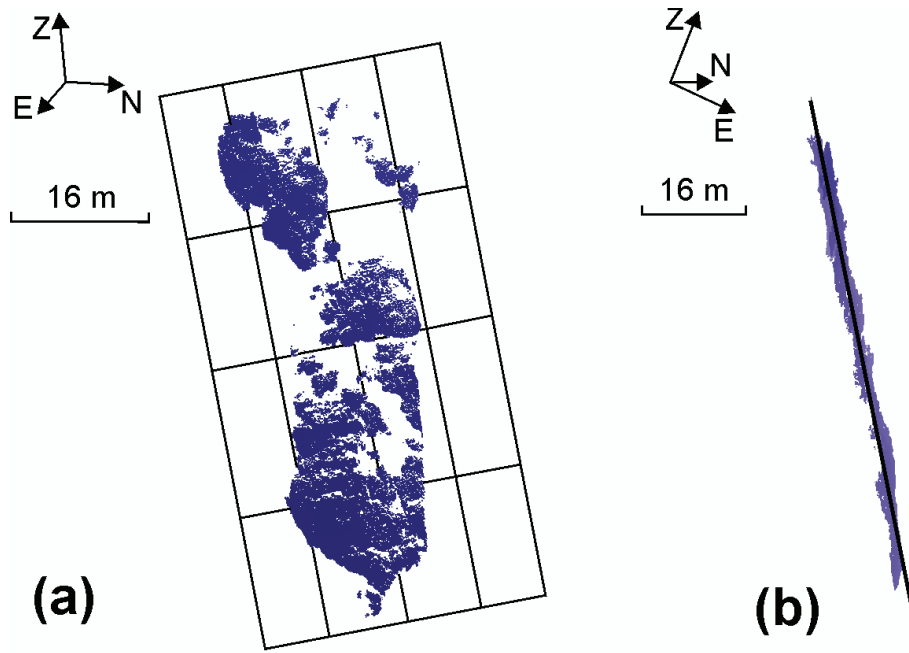


Fig. 6.6. Example of least square plane fitting of a point cloud subset carried out using Polyworks software. (a) Normal view of the fitted plane of a monolith. Very often the analyzed discontinuity is a whole monolith facet represented by thousands of points. (b) Corresponding trace showing the dispersion of the point cloud with respect to the fitted plane.

An orthogonal, right-handed triad $\hat{\mathbf{i}}_D, \hat{\mathbf{j}}_D, \hat{\mathbf{k}}_D$ of unit vectors can be obtained taking $\hat{\mathbf{k}}_D = \hat{\mathbf{n}}_D$, assuming $\hat{\mathbf{j}}_D$ to be the unit vector of the intersection between the DP and the corresponding BP ($\hat{\mathbf{j}}_D = \hat{\mathbf{n}}_D \times \hat{\mathbf{n}}_B$, where \times indicates the cross product) and, finally, taking $\hat{\mathbf{i}}_D = \hat{\mathbf{j}}_D \times \hat{\mathbf{k}}_D$. In this way, a reference frame solid for a DP able to completely characterize its spatial position and its intersection with the BP can be provided, as depicted in Fig. 6.7a.

The above operation is carried out for each pair of discontinuity/bedding planes. Therefore, if two DPs π_{D1} and π_{D2} are related, the rotation leading to π_{D2} (unit vectors: $\hat{\mathbf{i}}_{D2}, \hat{\mathbf{j}}_{D2}, \hat{\mathbf{k}}_{D2}$) starting from π_{D1} (unit vectors: $\hat{\mathbf{i}}_{D1}, \hat{\mathbf{j}}_{D1}, \hat{\mathbf{k}}_{D1}$) can be easily computed. Let A be the direction cosine matrix (DCM) related to this rotation in the reference frame solid for π_{D1} (see Appendix B). The ij -th element of $A = [a_{ij}]$ is the

projection of the i -th vector of the second triad on the j -th vectors of the first triad. For example, $a_{12} = \hat{\mathbf{i}}_2 \cdot \hat{\mathbf{j}}_1$, where \cdot indicates the dot product. The rotation in the $Oxyz$ reference frame is therefore $R = B^{-1}AB = B^T AB$ where B is the rotation from the triad $\hat{\mathbf{i}} = [1, 0, 0]^T$, $\hat{\mathbf{j}} = [0, 1, 0]^T$, $\hat{\mathbf{k}} = [0, 0, 1]^T$ to $\hat{\mathbf{i}}_{D1}$, $\hat{\mathbf{j}}_{D1}$, $\hat{\mathbf{k}}_{D1}$. The transformation R can be conceived as rotation by the angle α around the Euler unit vector $\hat{\mathbf{v}}$, i.e. $R = R_v(\alpha)$. Such a representation generally has a clear physical interpretation, but in this case a better representation, able to characterize the fundamental motion of a DP, is the sequence 3-2-1 of the Euler angle rotations, as in the case of aircraft attitude control (see e.g. Markley, 1980; Appendix B).

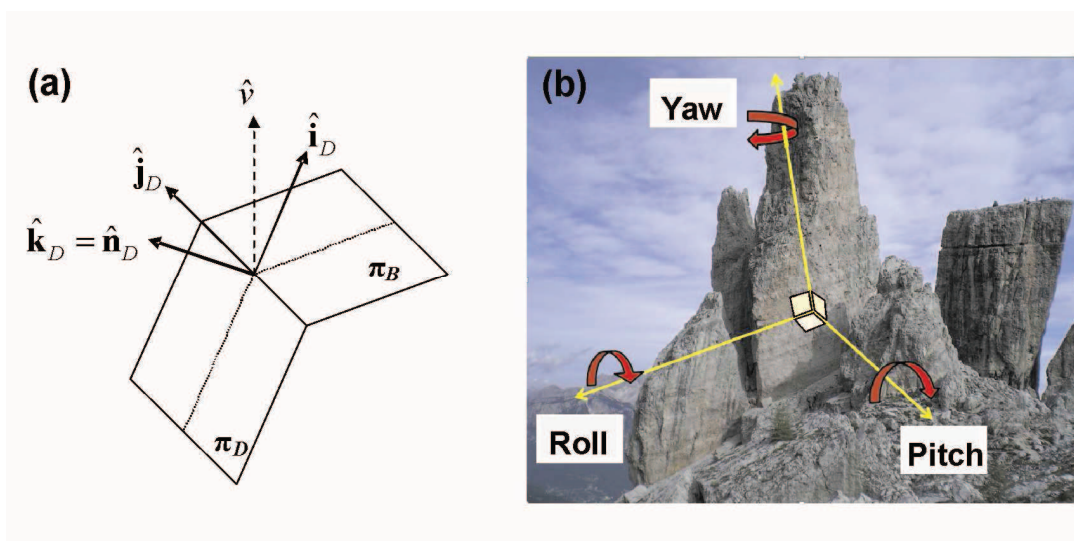


Fig. 6.7. Quantification of discontinuity plane rotation. (a) Example of intersection between a bedding plane π_B (sub-horizontal) and a discontinuity plane π_D (sub-vertical). The right-handed triad $\hat{\mathbf{i}}_D$, $\hat{\mathbf{j}}_D$, $\hat{\mathbf{k}}_D$ of unit vectors is also shown; $\hat{\mathbf{j}}_D$ is the unit vector of the intersection between π_D and π_B , and $\hat{\mathbf{i}}_D$, $\hat{\mathbf{k}}_D$ are respectively the bedding normal and the discontinuity normal unit vectors. (b) Scheme of the rotational components with reference to photograph of sector 5 (Torre Inglese). The rotation is described by the roll, pitch and yaw angles and represents the rotation of a considered intersection plane around the dip direction, strike and normal of the bedding planes respectively. Note: due to the application of the right-hand rule, negative and positive tilt angles stand for clockwise and counter-clockwise rotations.

If the sequence 3-2-1 is used, then $R = R(\phi, \theta, \psi) = R_x(\phi)R_y(\theta)R_z(\psi)$, where ϕ , θ , and ψ are the roll, pitch and yaw angles respectively and represent the rotation of the considered plane intersection around the dip direction, strike and normal to the bedding planes respectively (Fig. 6.7b).

The computations were carried out in MATLAB; the function SpinCalc (Fuller, 2009) implements the rotation, and other scripts have been written to compute the triads of unit vectors and characterize the results.

An important issue that has to be addressed in such an analysis is the estimate of the uncertainties related to computed angles. The discontinuities are assumed to be planar and, for each discontinuity, the corresponding least squares fit is carried out. Nevertheless, possible partial deformation with respect the pure planar form, existence of unrecognized outliers and also centimetric fluctuations due to TLS measurement errors, could affect the results. In order to carry out this estimation, a Monte Carlo approach was applied. A series of plane fitting tests were carried out, changing the selection area and showed that the error on determination of the unit normal vector depends on the magnitude of its components and ranges from 2% to 5% in the case of a component significantly greater than 0.1 (absolute value) and can reach 15–20% if a component is lower than or equal to 0.1. The simulations showed that a realistic error in the unit normal vector components can lead to uncertainties of $\sim 2^\circ$ on Euler angles of $\sim 50^\circ$ (4–5%), $\sim 0.8\text{--}1.2^\circ$ on small Euler angles (2–5°, i.e. 25–40%) and reaches 100% for very small Euler angles. These results can be used as a reference in data analysis.

6.5. Results

6.5.1. Discontinuity sets and structural analysis

The Cinque Torri area was subdivided into five sectors (sectors 1, 2, 3, 4, and 5), according to morphological and structural criteria (Fig. 6.8A). Each sector is made up of the following pinnacles: (1) Torre Grande (Cima Nord, Ovest and Sud); (2) Torre Lusy, Barancio, and Romana; (3) Torre Latina; (4) Torre Quarta Alta, Quarta Bassa, and Di Mezzo; (5) Torre Inglese and Avancorpo.

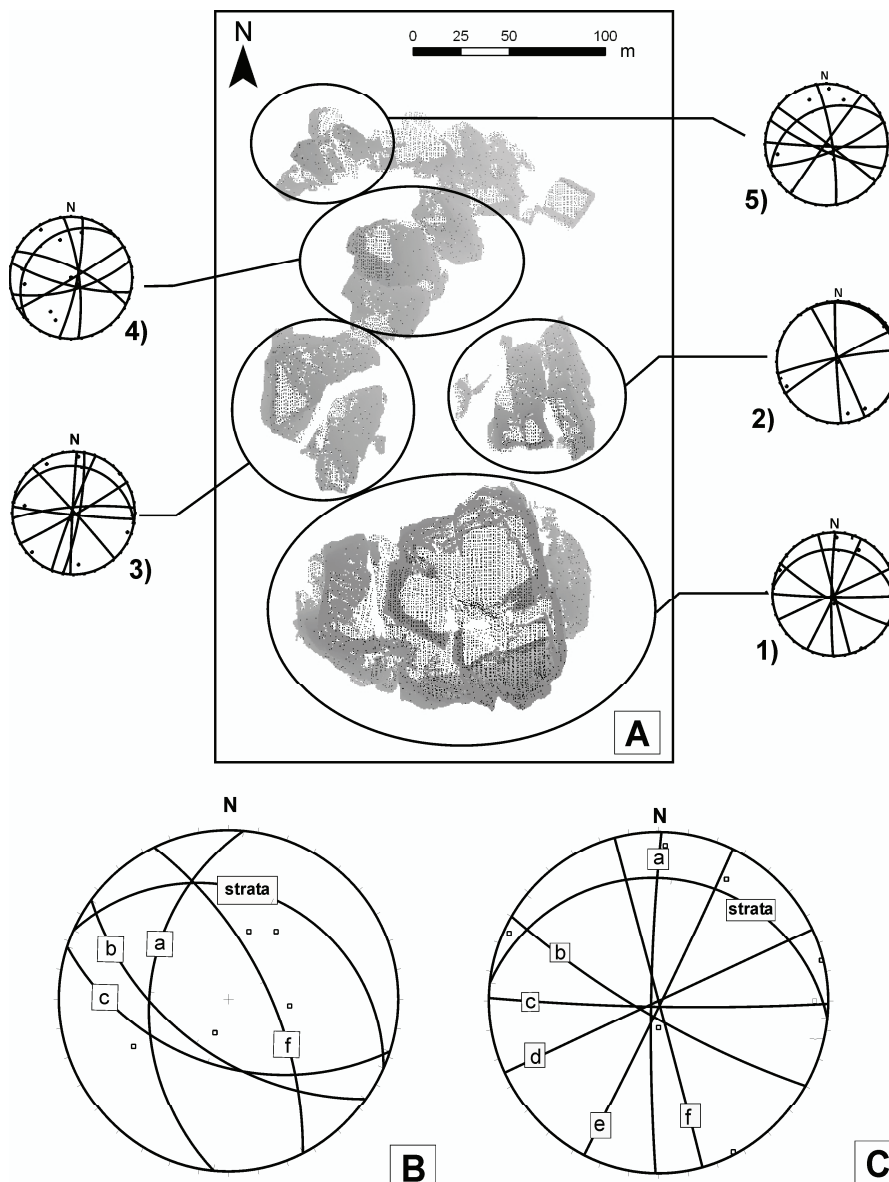


Fig. 6.8. Stereonets of discontinuity. (A) Lower hemisphere stereonet of all recognized discontinuity sets for the individual sectors. Two discontinuity sets are highlighted: the strata, plotted as dashed line and the discontinuity set C, plotted as dashed-dotted line. Each sector is made up of the following pinnacles: (1) Torre Grande (Cima Nord, Ovest and Sud); (2) Torre Lusy, Barancio, and Romana; (3) Torre Latina; (4) Torre Quarta Alta, Quarta Bassa, and Di Mezzo; (5) Torre Inglese and Avancorpo. (B) Stereonet showing major features in the external reference areas. (C) Discontinuity sets (A to F and Strata) in sector 1.

The southern sector (sector 1) is represented by the biggest rock volume within the group and considered to be the best preserved in terms of its dimensions, position and clear structural framework. Therefore, it is used as a reference sector of the structural analysis for comparison with mobilized sectors. With the exception of sector 3, all the other sectors are characterized by more than one monolith or an initial monolith fragmented into distinct portions. Sector 5 is the northernmost sector and at present is a significant hazard, mainly due to the instability of the monolith named Torre Inglese.

The presence of relatively fresh surfaces within the unstable rock groups allows a reliable recognition of the principal structural features dominating in the area. The analysis of gravitationally stable areas was performed using the ALS point cloud. In Fig. 1 the area to the South of the Cinque Torri group, which was used as reference for the structural analysis, is highlighted. Since the spatial sampling in the ALS observation was significantly lower than in the TLS survey, and the acquired area is significantly wider, a large dispersion of the dip direction and dip angle of a single joint set was recorded. In addition, the distal stable areas show a generally lower dip angle than recorded in the Cinque Torri Group.

This difference is mainly due to longer exposure to erosive agents and resulting slope rectification, particularly significant where differential weathering has acted on sequences of superimposed lithologies with contrasting geotechnical properties. However, although perceptible, this effect does not adversely influence comparison of the discontinuity planes in the stable area with those in the mobilized blocks of the Cinque Torri group.

Analysis of the TLS/ALS data using Coltop-3D, as well as field surveys carried out both inside the group and the near surroundings, reveals the occurrence of several types of rock discontinuities (see Fig. 6.8A and Table 6.3 for rock discontinuity details). Fig. 6.10 shows an example of discontinuity set selection in Coltop-3D in each recognized sector, while Fig. 6.8B,C represent the regional faults and fractures on a stereo plot and the detail of sector 1 discontinuities respectively.

Table 6.3. Discontinuity sets in the reference area and in the sectors of the Cinque Torri group obtained by Coltop-3D-based classification of the point cloud. The discontinuity parameters are dip direction, dip angle. Please refer to Tables 6.1,2 for the corresponding standard deviations.

Sector/ area	Set A	Set B	Set C	Set D	Set E	Set F	Strata
Reference area	275°/40°	216°/54°	198°/47°	/	/	64°/65°	24°/24°
1	271°/85°	210°/79°	181°/86°	335°/90°	116°/88°	255°/90°	6°/18°
2	329°/83°	267°/87°	64°/86°	/	349°/82°	/	52°/2°
3	273°/88°	229°/89°	186°/86°	150°/86°	291°/86°	/	10°/15°
4	26°/71°	164°/67°	149°/87°	101°/78°	83°/75°	194°/75°	317°/18°
5	203°/77°	182°/86°	159°/74°	306°/88°	81°/79°	37°/88°	336°/30°

Fig. 6.10 illustrates an example of the results of the matching between features considered to have the same origin. The results are obtained by rotating the discontinuities of the rotated sectors until the overlap with the discontinuities recognized in the regional reference stable area is reached. The bedding plane due to its

uniform orientation in the whole investigated area was considered as the primary reference set to accomplish the matching between rotated and non-rotated sets. The accuracy in the best fit determination is less than 3° for the dip angle and less than 7° for the dip direction.

Among the recognized discontinuity sets, four have a clear tectonic origin, whereas the others are probably gravity-induced. In particular, in the restored sector 1 (in Fig. 6.8C the corresponding not restored stereonet is shown) the following sets are of definite tectonic origin: sets A and F, are related to N–S to NNW–SSE joints and faults, originated during the Mesozoic E–W extensional phase and frequently reactivated during the compressive Cenozoic Alpine orogeny with transcurrent movements; set B, contains alpine NW–SE synthetic Riedel conjugates of the previous sets; set C is made up of W–E trending faults possibly related to the Alpine compressive phase. The remaining sets, i.e. D and E, most probably have a gravitational origin since they do not correspond to any regionally observed fault or joint sets.

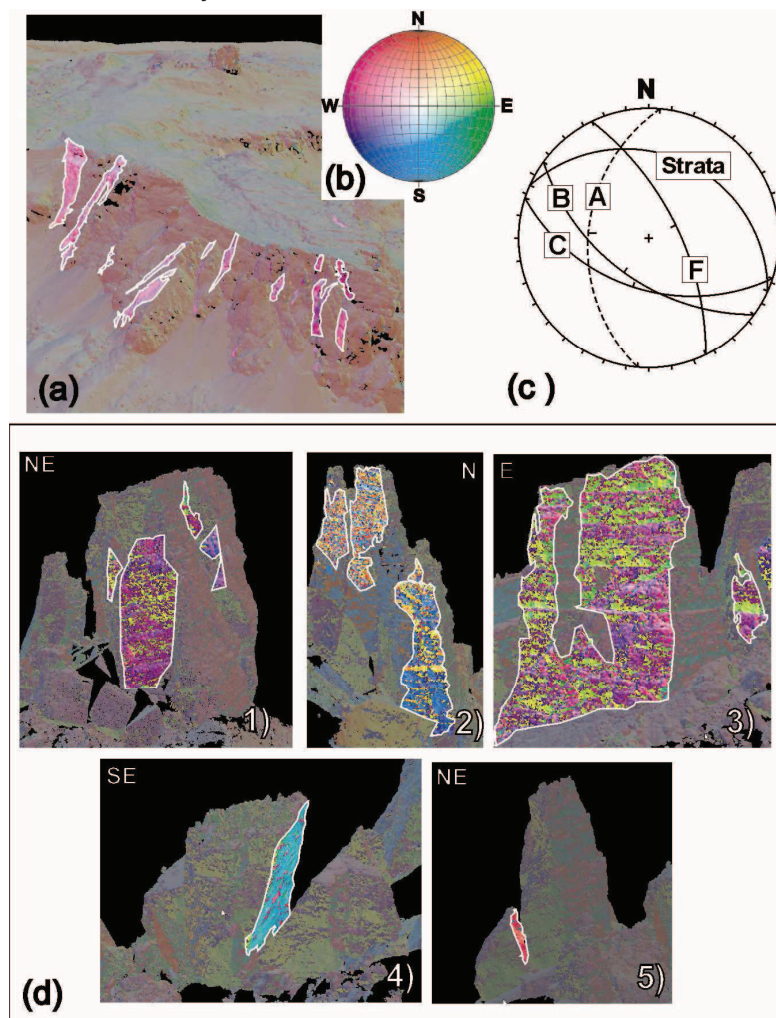


Fig. 6.9. Discontinuity set analysis in Coltop-3D. (a) N–S discontinuity set recognized in the distal stable areas recognized in the ALS point cloud. (b) Stereonet indicating the color scheme of the map based on the pole of the surface orientation. (c) Stereonet of the discontinuity sets recognized in the distal stable areas. The N–S discontinuity is highlighted by the dashed line. (d) Example of the selection of a same discontinuity set in the five sectors.

The sets of sector 1 are also recognized in the other sectors, and a total of 118 discontinuity planes were fitted on the basis of 3.9 million points. In Figs. 6.11 and 6.12 the histograms of the main sets derived from both the regional-scale ALS data and the Cinque Torri group point cloud are shown. Fig. 6.11 highlights the predominant presence of the N–S set (set A), which indicates a greater control of the reactivated Mesozoic faults over distal and stable areas. By comparing the regional sets with those in sector 1 it appears that the entire regional tectonic imprint is represented on the local scale. In Fig. 6.12 the dominance of the gravitational sets E and F is clear, the latter representative of the extensional Mesozoic phase. In addition, a significant number of planes belonging to sets A and D are also observable. Set F is meaningful since it follows the direction of normal faults, reactivated during the Alpine orogenesis which can be found in the western side of the investigated area. All the recognized planes in each of the monolith groups belonging to sets with a definite tectonic origin (i.e. sets A, B, C and F) were introduced in the MATLAB interface for plane rotation computation.

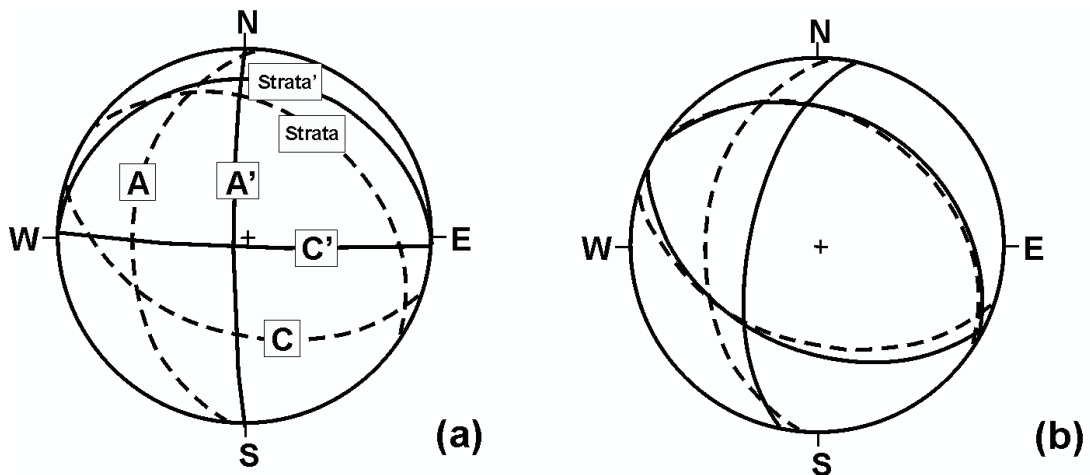


Fig. 6.10. Example of stereonet matching through a best-fit reorientation of rock discontinuities. (a) Superposition of selected sets of tectonic origin and bedding planes recognizable both on sector 1 (solid lines) and on the external reference frame (dashed lines). (b) Graphical output of the stereonet matching obtained by rotating the discontinuities of the rotated sectors until they overlap with the discontinuities recognized in the regional reference stable area.

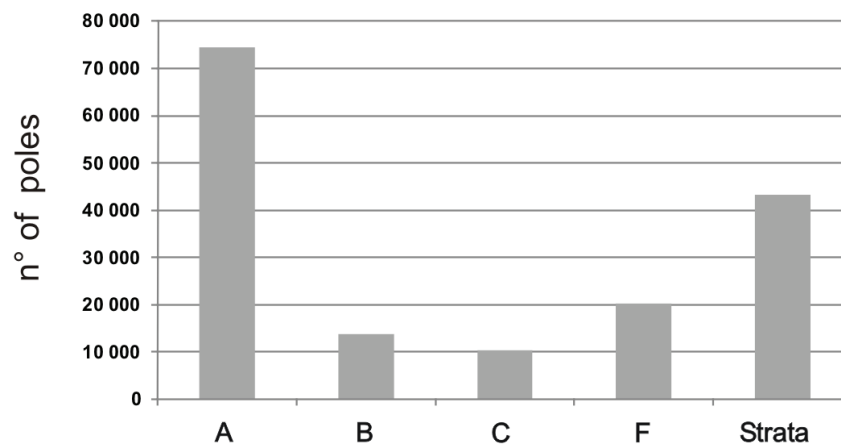


Fig. 6.11. Distribution of the poles in the distal reference areas according to the discontinuity sets shown in Fig. 6.8B.

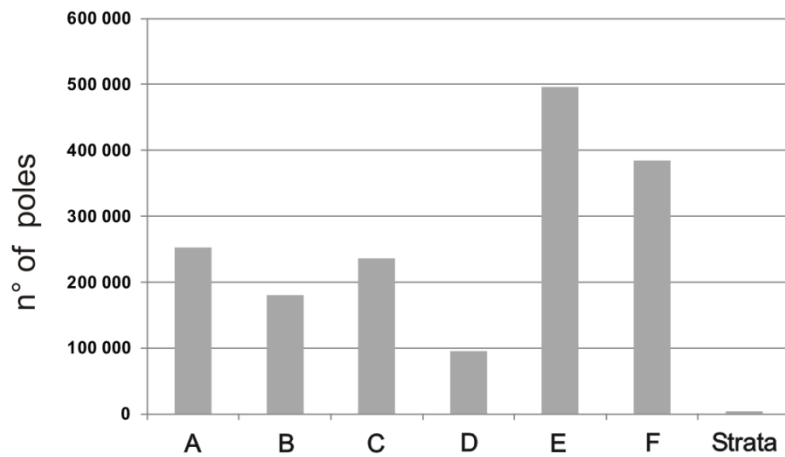


Fig. 6.12. Distribution of the poles in the Cinque Torri area according to the discontinuity sets shown in Fig. 6.8C.

6.5.2. Quantification of discontinuity plane rotations

As described in Section 6.3.2, the rotation computations require the results of structural analysis for each discontinuity family, with a reference frame being derived from the corresponding DP and bedding plane. The best-fit reorientation described in Section 6.3.2 was obtained regardless of the third degree of freedom of the rock body, i.e. the rotations around the dip vector were not taken into account, whereas the results explained in the present section were obtained using MATLAB and are based on a complete 3D structural repositioning of each sector.

The results obtained with the 3D approach summarized in Table 6.4 and Figs. 6.13, 6.14, and 6.15. In particular, from Fig. 6.13 a variable rotation of the yaw angles stands out. By contrast, the sectors show a general tilt towards the East according to the roll angle values and towards the South according to pitch angle values.

Table 6.4. Inferred discontinuity plane rotations for five sectors compared to the external stable areas (i.e. ALS-based georeferenced point cloud). Yaw, pitch and roll angle values are expressed in terms of both unweighted (u) and weighted (w) values together with their standard deviation.

Sector	Yaw (°)			Pitch (°)			Roll (°)		
	ψ_u	ψ_w	σ_ψ	θ_u	θ_w	σ_θ	φ_u	φ_w	σ_ϕ
1	3	3	3	-20	-19	3	18	17	3
2	-69	-66	3	-4	-7	5	21	28	3
3	-3	-19	3	-18	-17	3	15	10	2
4	47	46	3	-1	-20	3	3	11	2
5	23	22	3	14	2	2	2	-1	1

Sectors 1 and 3 show an overall minor angular difference with respect to the regional trend; sector 2 shows the highest yaw angle value with a clear clockwise rotation; sectors 4 and 5 correspond to the distal sectors from the hypothetical detachment area located near sector 1 and have in contrast anticlockwise yaw angle values. In Figs. 6.14 and 6.15 a common trend among pitch and roll values is evident. Fig. 6.13 shows a non-uniform trend of yaw values and in this frame, sector 3 represents a gravitational divide between the other two sectors. The central sectors (2 and 4) are clearly affected by rotations with a high magnitude but in a completely opposite sense to each other.

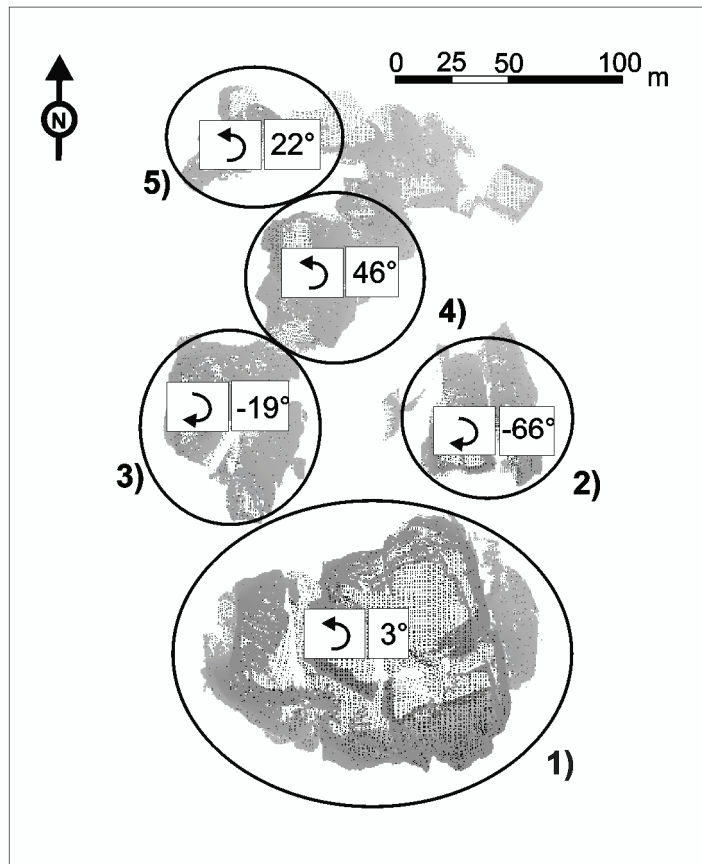


Fig.6.13. Sketch of the inferred Yaw angles for the five sectors indicating the rotation around the normal vector of the bedding plane of each sector, rendered on the point cloud.

The apparent anomaly in these results is related to the trend of pitch values. Even if the pitch angles show a regular sense of rotation with respect to the regional setting, a high dispersion in the angular amount is observed.

On the other hand, by observing the roll angles, the gravitational sectors show a general tilt rotation towards the East, with the exception of the lowest slope sector (sector 5).

The dispersion of the angular values is also significant in this case, and is indicative of a complex subsurface geological structure.

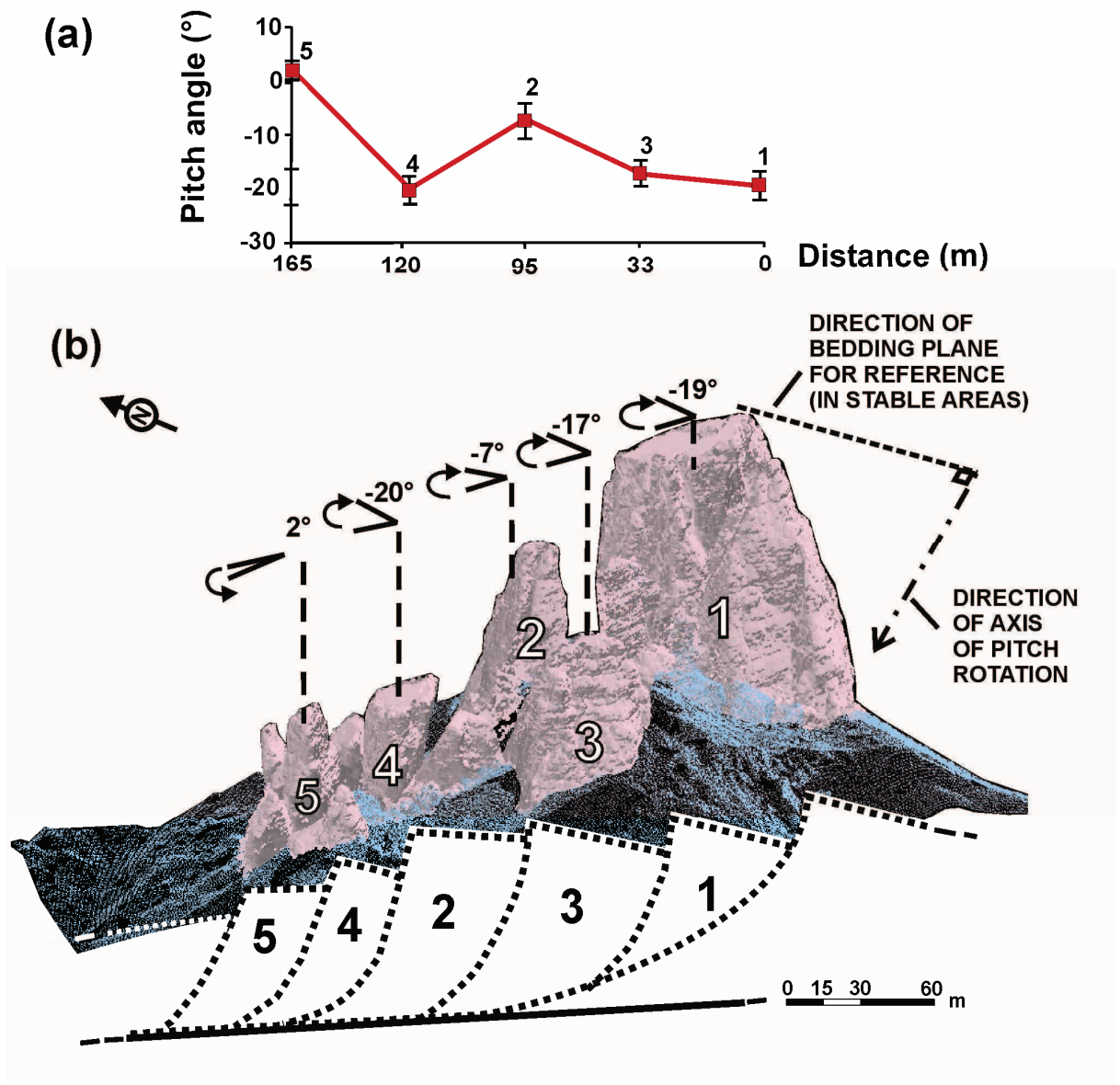


Fig. 6.14. Distribution of the pitch angles. (a) Distribution as a function of the spatial distance among the centre of gravity of sectors (with respect to sector 1) projected along an SW–NE profile. Sectors are labeled on the top of the graph. (b) Sketch of the inferred Pitch angles indicating the rotation around the normal vector of the bedding plane of each sector, rendered on the point cloud. The direction of the rotation axis coincides with the strike of strata. Interpretative cross-section through the Cinque Torri area slope is also shown.

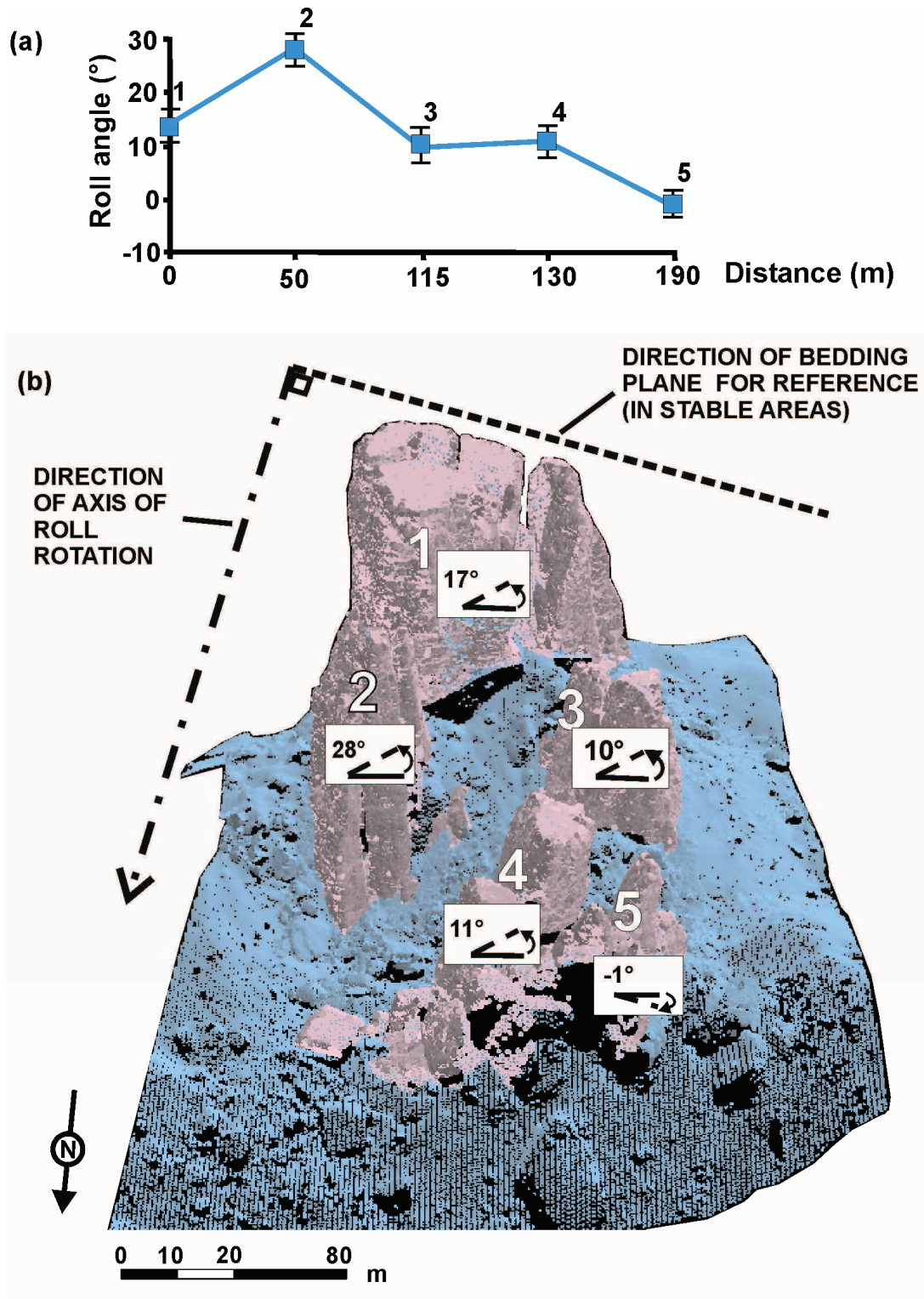


Fig. 6.15. Distribution of the roll angles. (a) Distribution as a function of the spatial distance among the centre of gravity of sectors (with respect to sector 1) projected along an ESE–WNW profile. Sectors are labeled on the top of the graph. (b) Sketch of the inferred roll angles indicating the rotation around an axis parallel to the direction of the reference bedding plane of each sector, rendered on the point cloud.

6.6. Discussion of the results and conclusion

In this study a comparison of the joint sets in the Cinque Torri group has allowed angular relationships among sectors to be found, through consideration of the general rotations of local discontinuities inside the studied group with respect to the regional trend. The results of the rotation computation suggest that the factors influencing instability, as evident from the facets of the monoliths, are the main tectonic lineaments of the area, the strata attitude and the rheological contrast in the stratigraphic sequence. We can infer that the triggering factors of the spreading include exogenic agents such as changes in groundwater flow, freeze-thaw cycles, weathering and earthquakes (Beck, 1968; Radbruck-Hall, 1978; Bovis, 1982; Forcella and Orombelli, 1984; McCalpin, 1999; Ballantyne, 2002; Agliardi et al., 2009).

The structural control on lateral spreading of the Cinque Torri is highlighted by two different aspects: i) the major tension cracks following structural discontinuities as revealed by traditional field surveys, and ii) the tectonic framework influencing the trajectories and extent of gravitational movements. This last point has been observed in the 3D scale analogue physical models proposed by Bachmann et al. (2004), where the presence of pre-existing large scale fractures (such as faults or shear zones) has little effect on slope instability except when they are combined with shallow weak layers. In these models, as for this study area, the fractures mainly control the lateral extent of the slope failures (Fig. 2.1). The tectonic structures and their role in pre-conditioning rock failures have also been recently analyzed for the historic failures of the Hope Slide in British Columbia and for the Randa rockslides in Switzerland, (Brideau et al., 2009), suggesting that a rock mass damage assessment is important for interpretation and remedial treatment of rock instabilities.

The ongoing spreading process within the Cinque Torri group is only partly controlled by the bedding plane orientation as revealed by the results described in Section 6.5.2. Indeed, the yaw rotation angles are very inhomogeneous and in general do not show clear trends along or across the strata dip direction. These variations are probably linked to morphological anomalies in the slope, i.e. bulges related to the lateral spreading development, determining the differentiation of the rock system into rock monoliths. From the results of the rotation computation the yaw values show the highest degree of influence due to the lateral spreading phenomenon. The roll values, which indicate a nearly uniform rotation of sectors towards East (the only exception being sector 5, which has a mild rotation toward West), provides evidence against the presence of N-S trending folds faults underlying the gravitational phenomena. In addition, the general southward tilt rotation (pitch angle) increasing from North to South suggests a rotational component of the movement, and a probable differentiation of the sliding surface of the DSGSD into segments with different amounts of rotation (Fig. 6.14), as opposed to a planar sliding surface (Viero et al, 2010a). In this context, recent geophysical surveys conducted in the surroundings of the group testify as to the presence of structural steps related to the tectonic imprint inside the non-rotated formation below the top of the dolomite. The presence of these steps can act as a nucleus for the differentiation of the tower into discrete sectors. From the results of Table 6.4 the difference in yaw angle

values between sectors 2 and 4 is particularly evident and this behavior can be related to a middle-ridge structural high with an NE–SW direction located between the two sectors.

The results agree with, and substantially confirm, the hypothesis that the initial fragmentation of a former Dolomitic plateau, later separated into discrete rock cliffs (the Cinque Torri group among others), is the effect of the initial action of several tectonic phases together with deglaciation and erosive processes followed by post-glacial spreading. The variations from the regional trend provide a kinematic description of the gravitational movement of the Cinque Torri group, which can be interpreted as initially controlled by the inherited tectonic features and subsequently differentiated into sectors, most likely induced by deep seated ground deformation and local topographic anomalies related to the lateral spreading development.

Since our methodology has allowed only the final amount of the rotations experienced by each sector to be determined and not their actual rate through time, we are unable to provide a definitive prediction of the evolving phenomena. However we can assume that the yaw components will continue to be more conditioned by the lateral spreading phenomena as opposed to the structural anisotropy. The pitch rotations will maintain a southward tilting common to all the monoliths and in addition it is very likely that the lower pitch values of sectors 2 and 5 will attain the higher values of the surrounding sectors as a consequence of propagation of the rotational movement. The pitch rotations and the roll components will probably maintain the tilt toward East, suggesting that future collapses may follow an Eastern trajectory.

In conclusion, the proposed approach allows full utilization of the spatial density and accuracy of the information provided by terrestrial and aerial laser scanner data, and is able to recognize the relationships among the structural and geomorphological components of the studied rock system. Both the statistical robustness of the results and time efficiency are characteristics of the proposed method. Further developments to allow automatic recognition of stratigraphic horizons and computation of translation are possible. Finally, the method can be directly applied to each system affected by deep seated gravitational slope deformations where multi-scale information, i.e. detailed spatial data on the system and a metric spatial sampling data related to the surrounding environment, is available.

7. Rock properties extraction from point clouds and traditional field surveys

7.1. Introduction

Nowadays, exposed rock outcrops can be characterized geometrically through manual surveys and remote sensing techniques. The last are subdivided into two main categories: active and passive remote sensing. Among the passive and active remote sensing techniques, the most frequently used are close-range terrestrial digital photogrammetry and terrestrial laser scanning (TLS) respectively. The advantages of both techniques are described by many studies (e.g. Feng and Röshoff, 2004; Martin et al, 2007; Jaboyedoff et al., 2008). With respect to traditional, hand-made surveys, the remote sensing techniques have the main advantage to derive geometrical information by averaging on a larger area, significantly decreasing sampling bias.

The recent improvements in computer performance, as well as the development of dedicated software for generation of 3D models starting from digital photographs, have increased the use of analytical photogrammetry in rock faces analysis. Like other types of passive remote sensing techniques, photogrammetry makes use of a sensor that detects the reflection of (sun) light from the exposed rock face.

Differently from photogrammetry, laser scanning is an active remote technique, which is based on a time-of-flight principle to determine the distance to an object. Terrestrial applications of laser scanning have developed considerably in the last decade. In particular, TLS techniques are being increasingly used as a complement to traditional scanline and window mapping methods especially in case of discontinuities with persistence magnitudes greater than 3 m (Sturzenegger et al., 2009).

TLS techniques are nowadays a powerful tool to acquire accurate geometrical models of discontinuous rock masses and to detect relative displacements of unstable zones through the use of multi-temporal images (Teza et al., 2007). The acquired data are represented by a point cloud, made up by millions of points, characterized by x , y , z values and by intensity scalars or mapped RGB colorization via photo coupling. TLS provide realistic measurements of discontinuity orientation and the highest accuracy on discontinuity location, persistence and curvature as explained in Sturzenegger et al. (2009) therefore was the elected technique for the present research.

The first part of this chapter promotes an example of extraction of information on rock discontinuity from a point cloud by means of a semi-automated approach. This methodology was applied to the analysis of the geomechanical behavior of the Torre Inglese (2275 m a.s.l.) (Fig. 7.1), the pinnacle within the Cinque Torri group showing the most critical conditions of stability.

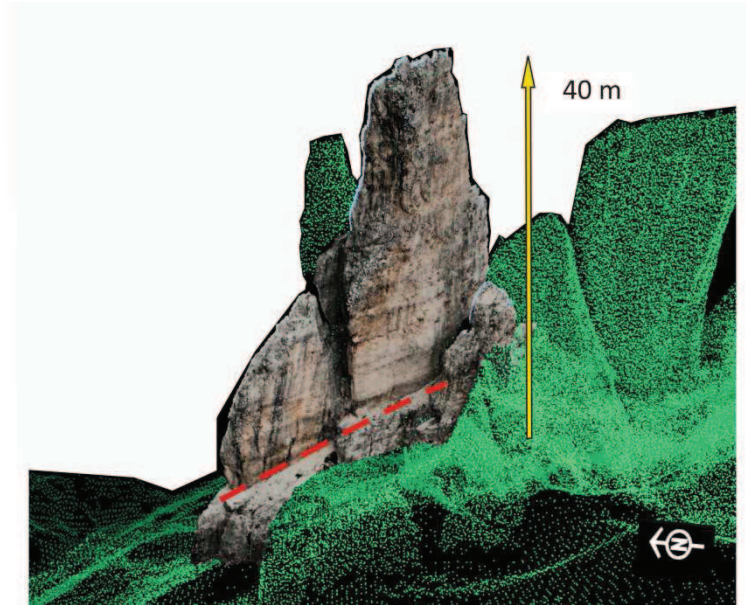


Fig. 7.1. The colored point cloud of the Torre Inglese pinnacle (PolyWorks package - Innovmetric). This potentially unstable monolith has a volume of about $10\,000\text{ m}^3$. Due to its critical condition a geodetic GPS antenna was installed on its top, while temperature and deformometer sensors were installed on main critical layering planes located in the lower part of the rock tower. A potential sliding surface corresponding to a bedding plane is highlighted on figure.

The applied methodology, initially proposed by Slob (2005), is based on TLS data processing by means of the experimental software Point Cloud Mapper (PCM), (Vosselman, 2004) and an additional MATLAB script (Slob, 2005), that allowed automated structural discontinuity analysis of the Torre Inglese. This software package was initially developed to process airborne laser data in order to detect planar geometric features such as roofs of buildings. As experienced in the present research, PCM can as well import and manipulate terrestrial laser datasets.

In the second part of the chapter, these elaborations are compared to the results of traditional methods for geotechnical classification of rock outcrops. With respect to topographical methods and the traditional scanline mapping, the point cloud-based approach shows higher accuracy and its remote acquisition promotes fast and safe surveys. Undoubtedly, the traditional field surveys should always be carried out since they provide reference values for validation purposes and fundamental information for rock mass properties determination.

Among the conventional (manual) field methods for measuring and assessing the geometric properties of discontinuities, the scanline survey was chosen for the Cinque Torri analysis. The advantage of the scanline survey is that orientation and, in particular, spacing data are gathered systematically. A second important aim of the collection of manual survey datasets is the definition of a reliable frame for comparison with the results provided by direct geotechnical analyses on intact rock specimens (Chapter 5). In this way, the rock mass properties of the involved lithotypes can be inferred.

7.2. Segmentation methodology

Point clouds can store geometric shapes, such as planes and cubic solids, in their spatial organization since each point is characterized by 3D coordinates defined with respect to a reference frame. The methodology applied in the present study allows an analysis of the point clouds to extract these geometric shapes. In order to accomplish this target, the point cloud is 'segmented', i.e. the data points are subdivided into sets according to common geometric criteria. With respect to the surface-reconstruction methods, the segmentation analysis has the advantages of a direct manipulation of the raw data points and of an automatic removing of the noise due to vegetation. This results in fast and accurate analyses.

In order to accomplish a spatial search of preferential direction of organization of the data, the initial point cloud is structured in a tree-fashion through a binary search (Bentley, 1975; Slob, 2005). In the present analysis a K-dimensional (K-D) tree structure is used (Fig. 7.2). This spatial search repeatedly subdivides the entire point cloud volume into balanced subcells, which means that all the subcells contains a similar number of points.

This method is particularly useful in the case of laser surveys on rock outcrops for which the acquired point cloud is frequently inhomogeneous, containing voids or sparse data. The 3D K-D tree method creates splitting planes which are perpendicular to the three coordinate axes. The main volume containing the entire point cloud is repeatedly split by such planes into several subcells until the smallest volume for a prescribed number of points is reached. This tree structure can perform a nearest neighbor search in a very fast manner. Since each subcell contains information about the nodes (laser points) and the splitting plane, by comparing the coordinates of the nodes, the spatial search indirectly interrogates the entire subcell and therefore, if needed, can improve the point cloud subdivision.

Once the point cloud is spatially organized, the segmentation approach can starts.

As above mentioned, in a point cloud the neighboring points are not connected to each other, but a spatial analysis, carried out by using PCM, determines whether there is a preferential direction of organization. In other words, when dealing with rock discontinuities characterization, the segmentation looks for points creating planar surfaces. More in details the method of segmentation, as explained by Maas et al.(1999) and further discussed in Slob (2005) has its mathematical basis in the 3D Hough Transform algorithm in combination with a Least-Squares evaluation. The coordinates of each node (i.e. point) and its neighbors are analyzed by these algorithms that verify if they are part of the same geometric shape. The identification of a common geometry does not involve the entire point cloud, but is restricted to the user-defined volume of data points around each subcell node, therefore resulting in fast computations.

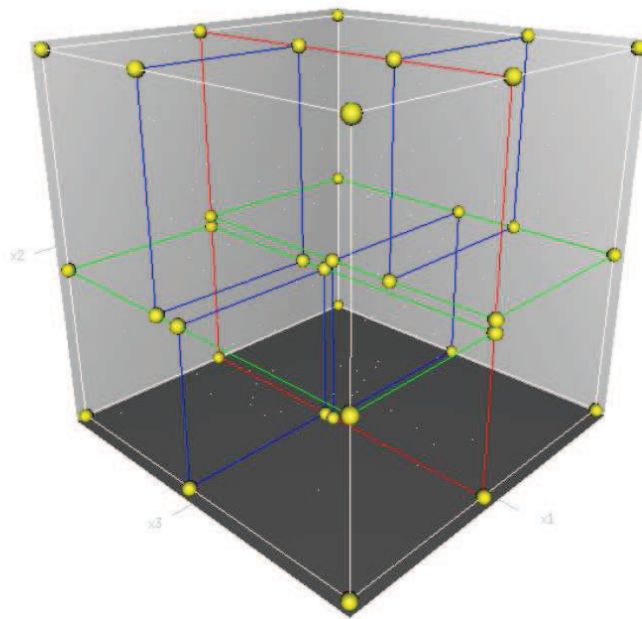


Fig. 7.2. Illustration of the (3-D) K-D tree splitting structure of the point cloud into subcells (Tyner, 2007)

The points classified as being part of a common geometry are then labeled with a distinctive code representing an independent plane. Since only few points can precisely match the detected feature, the software defines a threshold criteria through which create ranges of tolerance for each geometric property of the searched feature. If the user defined minimal number of points creating a geometric shape is found, all the selected points are labeled, therefore classified as part of that plane. These points are subsequently used as new node to improve the spatial search for that particular geometric shape. The segmentation process ends when all the points are classified or segmented into individual and independent planes.

Two algorithms are implemented in PCM software to compute segmentation, i.e. 3-D Hough transform and least square fitting.

The 3-D Hough transform algorithm is an extension of the original Hough transformation (Hough, 1962) and is able to recognize pre-defined geometric objects in complex data such as unorganized point clouds. This is obtained through a change of data domains. In practice, in the point cloud there are an infinite number of theoretical planes with different orientations that pass through any point. The goal of the transform is the determination, among all the potentials planes, of the plane which pass through most of the points. This is possible through a conversion of the of the laser data points from the 3-D space to 3-D Hough space in the form of a curved surface, and this requires a previous identification of plane parameters (Fig. 7.3). Once in the 3-D Hough space most of the curved surfaces intersect each other, a discontinuity plane is found and can be represented in the Cartesian space (initial domain).

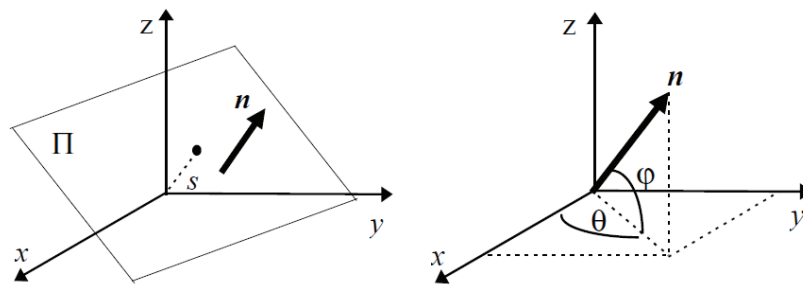


Fig. 7.3. Principle of the 3D Hough Transform. A plane Π is defined by a finite number of points with coordinates specified within a Cartesian coordinate system (O, x, y, z) . The 3D Hough Transform is based upon the principle of accumulating such points within a set of planes in R^3 . A plane $\Pi \subset R^3$ is uniquely defined by a triplet (s, θ, φ) . Marking all the points of the plane Π in Hough Space leads to a sinusoid curve. The intersections of two curves in Hough space denote the planes that are rotated around the line built by the two points. Consequently, the intersection of three curves in Hough space corresponds to the polar coordinates defining the plane spanned by the three points.

Inside PCM software the point cloud is subdivided into binary cells, volumes of laser points that can be potential surfaces. Each time, the curved surface representative of the laser point in the 3-D Hough space intersects the binary cell, the probability for that cell to be a plane increases. The cells containing the highest intersection points are potential planes in the point cloud. Cell parameters describe the plane made up by all the intersected points, therefore the lasts can be labeled as part of the same surface. This conversion shows similarities to the stereographic projects with the advantage also to discern among planes that have similar orientation but a different spatial location. The Hough transform is powered in PCM software through the Total Least Squares method.

The Least Square (LS) method is a very common statistical tool used to define (linear) regression relationships between variables. This method associates the characteristic function equation to the recognized planar surfaces on the principle of the best fit. Differently from the LS method, the Total Least Square Method uses an *orthogonal regression* to the fitted planar function to account of the errors associated to the three coordinates. In this way, a 3-D problem is solved in a 2-D subspace. In PCM software the simplification of the 3-D datasets into 2-D datasets, is achieved through the Principal Component Analysis (PCA) (Jackson, 1991) which creates a covariance matrix of the x, y, z coordinates of the total point cloud. PCA is a statistical technique that is frequently used in pattern recognition. The PCA method is appropriate for the 3-D laser scanner data, where there is no dependency among variables, and where all the variables are measured with a certain error.

By comparing the coordinates of all points by their respective covariance properties, it would in theory be possible to discover linear (planar) trends in the 3-D geometric data. In the PCA method, the datasets are subdivided into different classes on the base of their covariance with respect to an averaged trend. The first, second and third principal components are classified on the basis of the descending order of the eigenvalues associated to each eigenvector of the covariance matrix. A covariance matrix is positive semi-definite. This fact implies that its eigenvalues are non-negative.

To resume, the principle of the segmentation method implemented in PCM is based on the combination of the 3D Hough Transformation and Total LS Method which generates a region-growing strategy to assign the equation which mathematically determine each plane. More specifically, the region growing strategy is obtained through the following steps. Firstly, a spatial organization of the original point cloud data is provided through a (K-D) tree-based structure (Fig. 7.2) which allows a quick spatial search in the point cloud and therefore the efficiency of the direct segmentation approach. Then the 3-D Hough transform is used to select a good set of seed points from the point cloud that forms part of the plane. The seed plane is then “grown” interactively using a spatial search and then the new plane is every time optimized with Least Square (LS) estimation. The product of the segmentation process is a labeled point cloud, where points with the same label are part of the same discontinuity plane characterized by uniform color (Fig. 7.4.).

This approach provides the orientations of all the planes related to the point cloud, thus allowing the identification of the main discontinuity sets of the surveyed rock mass.

As a matter of fact, once the segmentation is reached, the rock discontinuities characterization is completed by determining their main geometrical properties of the rock discontinuities, the dip angle and the dip direction. Besides, through the interactive post-processing proposed by Slob (2005), it is possible to obtain other information such as plane size and plane equation parameters. As for the previous method, also at this stage no surface reconstruction is required since the segmented point cloud data is treated.

7.3. Results of the Torre Inglese rock discontinuities extraction

In June 2008, the pinnacle Torre Inglese was surveyed by a Riegl LMS Z420i (Riegl, 2011) terrestrial laser scanner, through six acquisitions of about 4 million of points each. The average spatial resolution related to the points of the cloud is about 5-10 cm at 200 m distance.

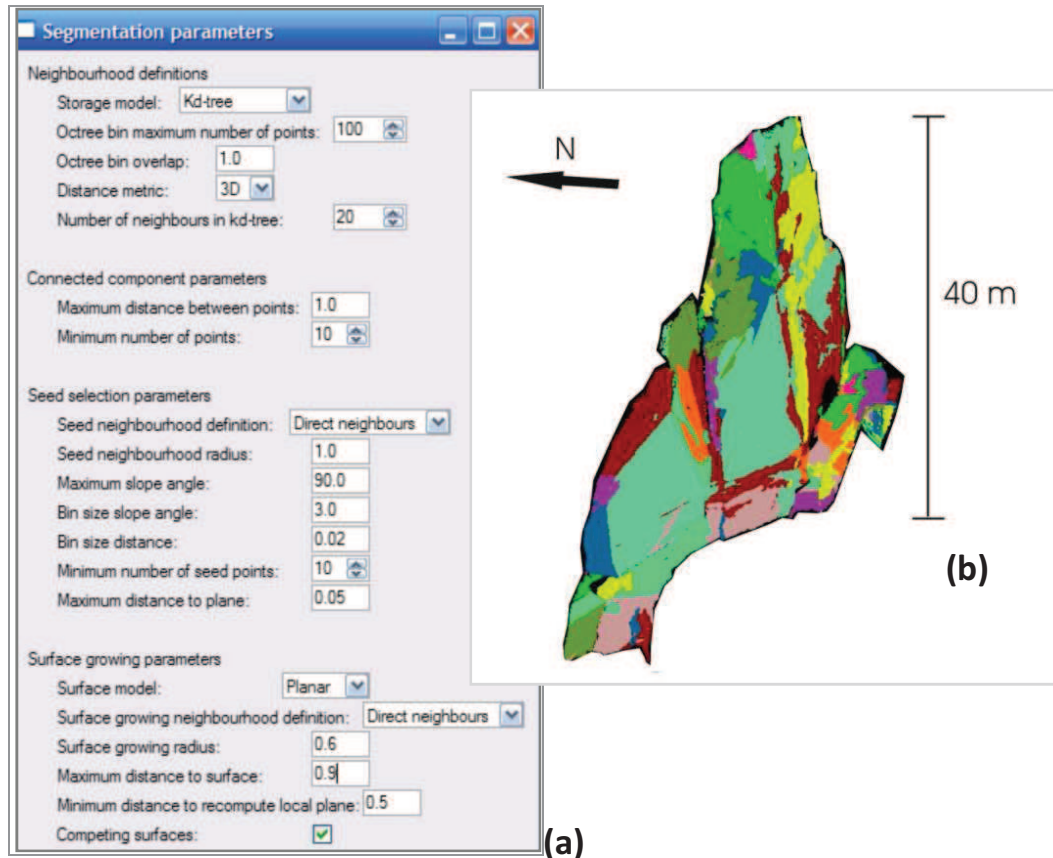


Fig. 7.4. PCM elaborations. Selected parameters for the segmentation analysis of the Torre Inglese point cloud (a). The segmented (classified) point cloud of the Torre Inglese pinnacle: each segmented set of points represents a potential discontinuity plane (b). (after Viero et al., 2009b)

In order to classify the point cloud, in PCM some parameters have to be settled up by using a window interface (Fig.7.4a). Firstly, the K-D tree partitioning model is chosen and subsequently some parameters ensuring the plane growing strategy are defined. In the present study, as the point cloud has an average resolution of 0.05-0.1 m, the maximum distance value is 1 m. This means that the spatial search will not account for points that are more than 10-20 times distance away from each other. Also the minimum number of points depends on the spatial resolution of the point cloud data and on the dimensions of the surveyed rock body. In the present case, since an average resolution of 0.05-0.1 m was obtained, a plane fitted on the basis of at least 10 points has a minimum size of about 10 cm^2 . In practice, this means that PCM accomplishes a spatial search for potential new seed point within a planar distance of 10 cm^2 . For the present case study, the elected methodology to select potential seed points is the direct neighbor criterion (Fig. 7.4a).

Once the potential seed points are found, they are converted to the Hough parameter space defined by three axes: the slope angle of the plane along X -axis, the slope angle of the plane along the Y -axis and the perpendicular distance of the plane to the origin. As Slob (2005) emphasizes, these axes have to be binned very carefully in order to generate reliable accumulator cells (growing planes). If the bin size is set too small, few planes are found, while an exceeding bin size can wrongly include different planes into a unique one. Also the bin size distance, which divides the Hough parameter axis into equal bins, can lead to the seam misleading accumulator criteria since the appropriate value should never been lower than the spatial resolution of the point cloud.

In general the good combination of values for the seed selection parameters requires some “trial and errors” based on the plots of the segmented point cloud (Fig. 7.4b).

In PCM, a point cloud filtering from outliers or noisy data is provided by two parameters: the “*minimum number of seed points*” and the “*maximum distance to plane*”. The first one generally is set to 10, a value that assures a corrected segmentation (Slob, 2005) independently from the point cloud characteristics. Conversely the second was set to 5 cm, the minimum spatial resolution of the point cloud, since it expresses the maximum orthogonal distance from the fitted plane to be accounted. In this way, noisy points such as vegetation are excluded from seeds identification.

Lastly, the plane growing parameters are selected on the basis of the spatial search criterion (direct neighbors) which accomplishes a spatial search around the previously defined seed points. This growth is gathered through the Total Least Squares estimation, which is a faster algorithm with respect to the Hough transform, but more influenced by outliers. Again, this spatial search is limited to a searching radius that should be taken similar to the seed selection radius. The computation time is strongly influenced by this parameter.

The parameter ‘maximum distance to surface’ filters some of the remaining noisy points from the re-computation of the plane and its value is slightly higher than the average precision of the ‘maximum distance to plane’ used in the Hough-based seed selection step.

The final selection of the optional parameter “*competing surfaces*” is extremely important for this analysis since it allows to re-evaluate previously labeled points, therefore it allows to evaluate if a point previously classified being part of a plane fit better to a new plane. This option is useful since it allows a better delineation of plane shape along edges and corners.

After the processing of the Torre Inglese point cloud, 72 labels or classes have been recognized on the base of 896873 input points; all these classes represent potential discontinuity planes (Fig. 7.4b).

7.4. Computation of plane orientation and geometry

Following the procedure proposed by Slob (2005) in order to derive orientation, equation and centroid of the found planes, the segmented point cloud is further processed. The labelled point cloud is indeed imported in MATLAB and stored in the form of matrices: a ($n \times 3$) matrix (B) that contains the original point cloud coordinates and a ($n \times 1$) matrix (L) that contains the label (plane) numbers. With the principal component analysis the normal vector n to the points in matrix C is computed, which enables to define the dip direction and dip angle of the found discontinuity planes.

The functions implemented in the script allow the following manipulations:

- Determination of the number of labels which equals the number of the found discontinuity planes.
- For each label, a subset matrix C of the matrix B is made by all point coordinates that belong to a particular discontinuity plane.
- Simple statistic for the found discontinuity planes such as number of points, mean coordinates and minimum and maximum extents of the plane in x, y, z directions (see Appendix C).
- Computation of the normal unit vector of the plane by means of principal component analysis. Such a normal vector represents the discontinuity orientation that can be plotted on stereoplots.
- From the components (a, b and c) of the normal vector of a plane can be derived as well as the orthogonal distance of the plane to the origin of the points coordinates. This parameter is fundamental to compute the normal set spacing.

The computed orientations of the planes are then imported into stereoplots to recognize the exiting rock discontinuity families. Totally six main discontinuities sets were manually clustered on Dips software (Rocscience, 2010) (Table 7.1, Fig. 7.5) on the basis of 10 planes initially recovered by the post-processing (Appendix C). In table 7.1 the mean results of the post-processing of the Torre Inglese labeled point cloud are reported.

Table 7.1. Properties of the main discontinuity sets of the Torre Inglese rock sector. Mean coordinates and the “equivalent” normal set spacing for each set are shown.

SET	Dip Dir (°)	Dip angle (°)	Plane equation parameters			
			a	b	c	d (m)
1	271	87	-0.99861	0.0173	0.049733	3863.8
3	31	83	0.50716	0.85387	0.11704	-6898
6	224	22	-0.26185	-0.26846	0.92702	423.0
7	328	84	-0.52123	0.84589	0.11308	-2631.1
8	186	90	-0.10291	-0.99468	0.003957	5712.7
9	10	88	0.16676	0.98561	0.027756	-5992.1

From the analysis of the stereoplot shown in Fig. 7.5, the found discontinuity sets can be directly linked to the regional tectonic. In this way, the fragmentation of the Cinque Torri group can be studied by restoring their attitudes on the basis of the rotational component analysis of the ongoing lateral spreading (Chapter 6). Among these it can be noticed the rotated N–S to NNW–SSE joints and faults, originated during the Mesozoic E–W extensional phase and frequently reactivated during the compressive Cenozoic Alpine orogeny with transcurrent movements ($31^\circ/83^\circ$, SET 3); the rotated alpine NW–SE synthetic Riedel conjugates of the previous sets ($186^\circ/90^\circ$, $10^\circ/88^\circ$, SETs 8-9), the perpendicular systems of fractures that can be associated to the gravitational phenomenon ($311^\circ/78^\circ$, $222^\circ/85^\circ$) and the strata bedding ($224^\circ/22^\circ$). The remaining sets, i.e. SETs 1-7 ($271^\circ/87^\circ$, $328^\circ/84^\circ$) are related to the gravitational phenomena (for details see Chapter 6, section 6.5.1). From this analysis, it results that there is no corresponding set that can be related, through rotation restoration, to the rock discontinuities families generated by the Alpine compressive phase (set C in table 6.3).

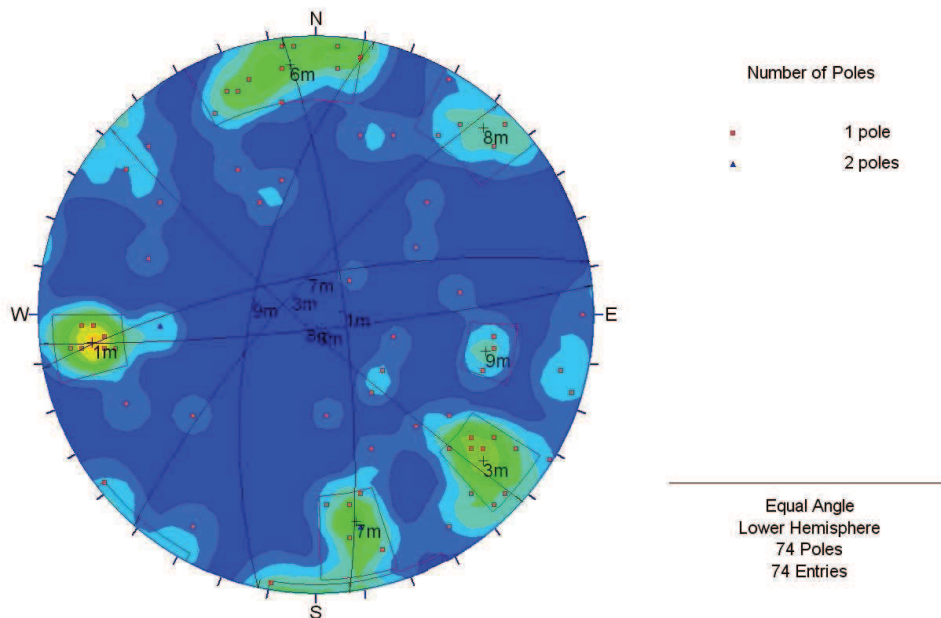


Fig. 7.5. Stereoplot of all identified discontinuity planes of the Torre Inglese monolith. Each discontinuity plane derives from a region growing process which accounts of hundreds of laser points.

Since the post-processing provides the plane equation parameters (a , b , c and d) to each clustered plane, and each plane is uniquely defined in the 3-D space, the normal set spacing can be derived. Differently from a manual scanline, the normal set spacing derived from point clouds cannot consider a linear direction, but should account for a 3-D space.

To carry out this calculation, Slob (2005) suggests the concept of “equivalent” normal set spacing by using the plane equations. This method directly uses the calculated distance parameter d . This distance is the perpendicular distance between the plane and the defined origin of the point cloud. By sorting the distances d of all the planes of the

same discontinuity set, the differences between consecutive values are the discontinuity spacing. The average of these values represents the mean "equivalent" normal set spacing of a particular rock discontinuity family. The term "equivalent" is chosen since this way for determining it differs from the methodology defined by Priest (1993).

The main difference between the two methods resides on the way in which the discontinuity spacing is calculated. In the conventional normal set spacing calculation, the planes are linearly projected to intersect a selected virtual scanline, while in the "equivalent" normal set spacing the distances are measured as projection of tangent circles of the planes with respect to the selected origin. This calculation is more straightforward respect the former since it does not require any mean normal set orientation to compute a virtual linear scanline, but only set coordinates centre is needed to define the origin O (Fig. 7.6).

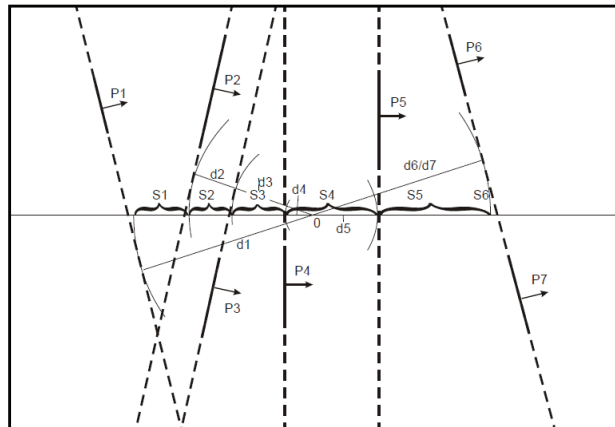


Fig. 7.6. Example of derivation of the "equivalent" normal set spacing based on the re-computation of the distance d values of the planes equations which depend on the selection of the set origin (O). S stands for normal set spacing (from Slob, 2005).

From the results of the "equivalent" normal set spacing calculation, it can be observed that the values range around 1m. This result is dependent to the chosen values for segmentation processing and describes only the major discontinuities present on the rock face at the scale of the rock pinnacle.

Table 7.2. Properties of the main discontinuity sets of the Torre Inglese rock sector. Mean coordinates and the "equivalent" normal set spacing for each set are shown.

SET	X mean	Y mean	Z mean	"Equivalent" normal set spacing (m)
1m	1,734,077.7	5,155,343.3	2241.0	1.3
3m	1,734069.4	5,155,343.9	2240.0	0.5
6m	1,734,077.3	5,155338.6	2245.0	0.7
7m	1,734,071.9	5,155,342.3	2234.8	1.1
8m	1,734075.1	5155337.9	2253.0	0.8
9m	1,734,066.0	5,155,335.0	2240.0	2.5

7.5. Traditional geomechanical reliefs in the study area

In this section, the main theoretical and practical aspects of a rock mass characterization in terms of intact rock and joint properties are described. Rock mass properties of local lithologies were determined through a combination of laboratory testing (Chapter 5) and rock mass evaluation. Laboratory testing involved uniaxial test, ultrasonic velocity pulse recordings on some of the involved lithotypes following the ASTM standards.

The rock mass characteristics were assessed in the field using Geological Strength Index, GSI (Hoek et al., 1995; Marinos et al., 2005) and Bieniawski's (1989) Rock Mass Rating (RMR₈₉) (Bieniawski, 1989). For each type of lithology, GSI values were evaluated as a range of values rather than a single value for each individual investigated site. Both classification methods are primarily based on the assessment of the geometric and mechanical properties of rock discontinuities.

Among the conventional (manual) field methods for measuring and assessing the geometric properties of discontinuities, the scan line survey was chosen for the Cinque Torri analysis (Fig. 7.7). The advantage of the scanline survey is that orientation and, in particular, spacing data are gathered systematically. As for the other traditional surveys, the final objective of the scanline mapping is to provide a basis for comparison with the information that results from direct geotechnical analyses on intact rock specimens and moreover to characterize the geometrical patterns of the surveyed rock surfaces.



Fig. 7.7. Evaluation of rock discontinuity orientation with geological compass during scanline mapping (Torre di Mezzo site, photo by S. Ceruffi).

7.5.1. Rock discontinuities

A rock discontinuity can be defined as a surface within a solid body which creates a solution of continuity. From a mechanical viewpoint, discontinuity surfaces are plane of weakness in the rock mass (Goodman, 1989).

Discontinuities rarely occur in a fully random manner, but generally are arranged in sets. There are various terms used to describe discontinuities. These terms are frequently used interchangeably, although often not correctly, thus creating some confusion. It is therefore useful to summarize here the different types of discontinuities that are investigated in this thesis:

- Bedding planes. They are discontinuity planes that separate successive layers of sedimentary or stratified rock. Bedding planes are the result of repeated sedimentation cycles with a change in sedimentary material and/or sedimentation rate. They frequently appear to represent periods of non-sedimentation or even erosion. Bedding planes are mostly well-defined discontinuity sets with often large lateral persistence.
- Joints. Joints result from changes in stress condition in the rock mass due to several geological processes. Along joints, by definition, no movement has taken place in geological time. However, when the rock mass is near or at the surface, movements along joints could be occurred. The term joint is then still used. Frequently, the terms fractures and joints are used interchangeably.
- Faults. These are discontinuities that frequently offset all other discontinuities through significant relative movement on either side of the fault. In the study site faults are frequent and are organized in systems on the base of common origin.

Since discontinuities play a very important role in the geomechanical behavior of a discontinuous rock mass, the characterization and classification of discontinuities are incorporated in most rock mass characterization and classification systems. Rock mass characterization systems assist in describing the rock mass in standard terms. Two main systems are used: the British Standard (BS 5930:1999) and the ISRM Basic Geotechnical Description (ISRM, 1981b). The British Standard system provides a qualitative system for describing discontinuities in terms of type, e.g. joints, faults, or bedding fractures. Additionally, the sizes and shapes of blocks that these discontinuities form in the rock mass can be described in a standardized way. With respect to the geometric discontinuity properties, the ISRM Basic Geotechnical Description (ISRM, 1981b) merely recommends the description of the discontinuity spacing. The more extensive ISRM (ISRM, 1978; 1981a) suggested methods for rock and discontinuity analysis recommends a quantitative description of the discontinuity properties, but does not provide formalized standards for doing this.

During field surveys rock discontinuities are generally described in terms of:

- Orientation is the most important geometric property, since it determines the anisotropy in the mechanical behavior of the discontinuous rock mass. The orientation of a discontinuity in 3-D space is uniquely defined by the dip direction

(azimuth) and dip angle. Measured orientations can be plotted using hemispherical projections, which will assist in the recognition of discontinuity sets.

- The spacing is defined as the distance between discontinuities determining, to a great extent, the block size distribution and therefore greatly influences the overall mechanical properties of the discontinuous rock mass. Two rock masses made up by the same lithology but characterized by completely different block size show different rock mass behaviors. Differently from spacing, the *set spacing* is the distance between a pair of adjacent discontinuities, from the same set, along a specified line, e.g., a scanline. The average of all sets spacing is the mean set spacing. The orientation of the scanline often produces some biases in the set spacing measurement, especially when a set is oriented almost parallel to the scanline, resulting in a great over-estimation.
- When the set spacing is measured perpendicularly to the direction of a set the spacing, a normal set spacing is derived. The mean normal set spacing and mean normal set spacing are good indicators of the block shape and size distribution in the rock mass and can be used as input to rock classification systems and numerical modeling programs.
- Persistence defines the continuation of discontinuity in different directions. The persistence of discontinuities greatly influences the mechanical behavior of rock masses. Blocks on either side of a non-persistent discontinuity are not likely to move unless the discontinuity extends and breaks through intact rock.
- Finally, another important rock property is the roughness. This property influences directly the shear strength of discontinuity itself. Surface irregularities on the discontinuity planes produce the discontinuity roughness.

7.6. Introduction to rock mass properties derivation

During last decades, the geotechnical and geomechanical modeling of rocks masses have been carried out by implementing computational schemes based on Mohr-Coulomb's theoretical criterion. In these situations it is crucial to distinguish between theoretical and real rock behavior, especially in the case of investigating rock masses rather than intact rocks.

Several authors pointed out the reliability of the Hoek & Brown's empirical criterion for the modeling of bulk rocks by testing intact rock specimens through direct or indirect tests. While the uniaxial test is an example of direct analysis which provides the required input data for rock modeling, the results of indirect analyses such as Schmidt hardness test require additional empirical correlations. Both direct and indirect methods are able to provide a reasonable geomechanical characterization of the intact rock. Nevertheless, the accuracies of the two methods are very different.

Another crucial aspect of rock modeling aimed to search of the analytical correlation between Mohr-Coulomb's theory and the Hoek & Brown's empiric criterion, is the quantification of the fundamental properties of friction angle ϕ and cohesion c .

The following paragraphs focus on the elected criteria and relationships for the determination of the properties of the rock mass. The principal input data are the

Schmidt hardness tests and results of the laboratory analyses (Chapter 5) carried out on representative sites or samples of Cinque Torri slope stratigraphy. In this way, the results of the direct tests can be introduced, together with qualitative classifications of rock masses, in the numerical models satisfying both Mohr-Coulomb and Hoek & Brown criteria.

7.6.1. Hardness testing of rocks

The Schmidt hammer was developed in the late 1940s as an index apparatus for non-destructive testing of concrete in situ. Since the early 1960s, this apparatus has been used in rock mechanics practice, leading to a quick and inexpensive measure of surface hardness that is widely used for estimating the mechanical properties of rock materials. The applications of this test include: the prediction of penetration rates for tunnel boring machines, determination of rock quality for construction purposes, and prediction of hydraulic erodibility of rock. This testing method is of limited use on very soft rock or very hard rock (unconfined compressive strengths less than approximately 1 MPa or greater than 100 MPa). As recommended by the ASTM standards, the results of this testing method are not intended for conversion to strength data suitable for design. Indeed, the evaluations derived by using this type of hardness test should be carefully handled. The severe influence of specimen/surface dimensions, surface smoothness, weathering and moisture content, testing data reduction and analysis procedures make the resulting values an estimate rather than a deterministic assessment of the rock properties.

The physical properties of the intact rocks depend on its microstructure in terms of minerals cleavage, grain boundaries and microfractures that influence directly the direction of failure (Willard and McWilliams, 1969).

Many empiric equations had been proposed to correlate the engineering properties of rock with its physical index properties. Deere and Miller (1966) performed an extensive study on large number of rock samples representative of the sedimentary, magmatic and metamorphic environment to develop an engineering classification system for the intact rock. They confirmed the above mentioned relationships through the formulations reproduced in Table 7.3, and they also concluded that rock strength and modulus properties are correlated better with Schmidt hardness than Shore hardness when the effect of unit weight of the rock is included. In Shalabi et al. (2007), a good relationship between the engineering properties of the intact rock and its hardness for dolomite, dolomitic limestone, and shale rocks specimen is found through statistical analyses.

In the present research, the rock properties are obtained from hardness test following Sachpazis (1990), who derived a strong relationship between the Unconfined Compression Strength, USC and Normalized Rebound number, NR, for carbonate rocks of known density. See Table 7.4, where the linear correlation coefficients $R = 0.96$ is obtained in this case.

Equation	R
$UCS = 461 \gamma - 52586$	0.604
$UCS = 1246HR - 34890$	0.880
$Et = (0.15 \gamma - 16.74) \times 10^6$	0.784
$Et = (0.259HR - 4.29) \times 10^6$	0.731
$UCS = 10(0.00014 \gamma HR + 3.16)$	0.943
$Et = 1395 \gamma HR - 2.94 \times 10^6$	0.847

Table 7.3. Correlation coefficients between rock hardness and both unconfined compressive strength and tangent modulus of rock (Deere and Miller, 1966). UCS: unconfined compressive strength, Et: tangent modulus at 0.5 UCS, γ : dry unit weight, HR: Schmidt hardness.

Correlated parameters	Regression equation	N.samples	R
UCS-NR	$NR = (UCS) * 0.2329 + 15.7244$	33	0.9178
Et-NR	$NR = (Et) * 0.5155 + 17.488$	33	0.7744
UCS-Et	$Et = (UCS) * 0.3752 + 4.479$	33	0.8151

Table 7.4. Correlations between Normalized Rebound number (NR) and both unconfined compressive strength and tangent modulus for dolostones, limestones and marls (Sachpazis, 1990).

For the Schmidt hardness tests, a L-type Proceq© Schmidt hammer with 0.735 N m of energy was used following the ISRM (1978a) and ASTM (2001) standards. The Schmidt hammer consists of a spring loaded piston which is automatically released onto the plunger when pressed orthogonally against a surface. Part of the impact energy of the piston is consumed largely by absorption, i.e. the work done in plastic deformation of rock material under the plunger tip, and transformation as heat and sound. The remaining energy represents the impact penetration resistance (or hardness) of the surface and enables the piston rebound. The harder the surface, the shorter the penetration time or depth and hence the greater the rebound. The distance traveled by the piston after rebound, expressed as a percentage of the initial extension of the key-spring, is called the rebound value (R) and is an index of surface hardness.

Tests were made directly in the field on the analyzed rock outcrops (Fig. 5.1, Appendices A-M) by performing the rebound test on the surfaces of the different discontinuities. According to Amaral et al. (1999), it is important to evaluate the variations of the measured data because they are strictly related to the material heterogeneity. Therefore, all 10 recording values are taken into account for the NR determination. Fig. 7.8 shows Schmidt hammer device during testing rock outcrops.



Fig. 7.8. Schmidt hammer device and types of analyzed rock discontinuities

An amount of 53 discontinuity rock surfaces were tested by means of the Schmidt hardness device. Among them, 5 lies on a Heiligkreuz rock outcrop. The surfaces were reasonably smooth and free of visible cracks, and the test impact points were almost coincident. The direction and versus of the hammer test influences the average rebound values. When the device is not vertical and directed downwards, the energy is differently decomposed due to the gravity influence, therefore the derived rebound values should be corrected to account for the energy loss. For each site the averaging rebound number was therefore normalized following the indication of Table 7.6. Since 10 measurements are repeated on each surface, an amount of 540 values are accounted for rock properties determination. The tested Dolomia Principale dolostones show an average NR of 50 while for Heiligkreuz carbonates it approximates 47.

Table 7.6. Corrections values for the determination of the Normalized Rebound number (NR) starting from the average Rebound number R derived from Schmidt hardness test.

Average R	Downwards $\alpha = -90^\circ$	Oblique $\alpha = -45^\circ$	Upwards $\alpha = 90^\circ$	Oblique $\alpha = 45^\circ$	Horizontal $\alpha = 0^\circ$
10	0	-0.8	/	/	-3.2
20	0	-0.9	-8.8	-6.9	-3.4
30	0	-0.8	-7.8	-6.2	-3.1
40	0	-0.7	-6.6	-5.3	-2.7
50	0	-0.6	-5.3	-4.3	-2.2
60	0	-0.4	-4.0	-3.3	-1.7

7.6.2. Scanline mapping and Rock Mass Rating

Scanline mapping, or line sampling, is a 1-D discontinuity mapping technique. The method consists of an imaginary or physical line placed, or drawn on, the exposed rock face. Discontinuity planes or traces of discontinuities that intersect this line are recorded with their properties and their intersection positions. Scanline mapping provide sufficiently detailed information on the individual discontinuities in each set that can be used in a probabilistic design (Priest and Hudson, 1981).

The length of the scanline should be chosen according to the average block size of the rock mass. A densely fractured rock mass requires a smaller scanline than a massive rock mass. According to Priest and Hudson (1976), the length of the scanline should be at least fifty times the mean discontinuity spacing in order to estimate the frequency of discontinuities to a reasonable degree of precision. The orientations of the scanlines are chosen in such a way that as many discontinuities as possible are intersected. Moreover, in order to minimize orientation sampling bias, the scanlines should preferably be chosen perpendicular to the main discontinuity set(s).

The features that are commonly recorded in a scanline survey include the following (Clayton et al., 1995):

- Intersection distance: This is the distance in meters (rounded to the nearest cm) along the scanline to the intersection point with the discontinuity. Where the face is irregular, it will be necessary to project the plane of fractures not in contact with the tape, so that the position of such fractures can be accurately recorded. In highly irregular faces, this method can lead to significant errors in the determination of joint spacing.

- Orientation: This is recorded by the dip direction and the angle of dip of the discontinuities.

- Semi-trace length: This is the distance from the intersection point on the scanline to the end of the discontinuity trace. There will be two semi-trace lengths associated with each discontinuity; one above and one below for a horizontal scanline, or one to the left and one to the right for an inclined or vertical scanline.

- Termination: This defines the way each semi-trace is terminated. The scheme recommended by ISRM (1978) could, for example, be used: '1' or '1' for a discontinuity trace that terminates in intact rock material; 'A' or '2' for a discontinuity trace that terminates at another discontinuity; and 'O' or '3' for a discontinuity whose termination is obscured or the trace extends beyond the limits of the exposure.

- Roughness: The shear strength of discontinuities depends greatly upon their roughness. Surface irregularities on the discontinuity planes produce the discontinuity roughness. The roughness may be visually estimated by using Barton's Joint Roughness coefficient (Barton, 1973) or any of the other observational methods.

The normal set spacing distribution and mean normal set spacing are usually the most important parameters to derive from the scanline data. In the present study, set spacings were calculated by subtracting each subsequent intersection distance (Appendices D-M) within the same discontinuity family. Such information was

introduced into the Rock Mass Rating system in order to infer in a second stage the rock mass properties.

The RMR, also called the Geomechanics classification system, was developed by the South African Council of Scientific and Industrial Research (CSIR) and proposed by Bieniawski (1989). Bieniawski developed a weighted rating system based on the algebraic sum of six rock mass properties (eq. 7.1):

$$RMR = R_s + R_{QD} + R_{dj} + R_{c_j} + R_w + R_{oj} \quad (7.1)$$

Where:

- R_s is strength of intact rock material (rating from 0 to 15)
- RQD is Rock Quality Designation
- R_{dj} is spacing of joints (rating 5 to 30)
- R_{c_j} is condition of joints (rating 0 to 25)
- R_w is groundwater conditions (rating 0 to 10)
- R_{oj} is joint orientation (rating 0 to -12)

In this classification system, geometric properties of discontinuities play a very important role; the RQD, the joint spacing (R_{dj}), and joint orientation (R_{oj}) are three geometric input parameters.

Among the terms included in the RMR classification, the RQD index nowadays defines a classification of rock discontinuities studied from boreholes. The RQD was originally developed as a rock mass classification system and also in this research is considered for such a purpose.

The RQD for the rock mass classification is defined as:

$$RQD\% = \frac{\sum l_i \geq 100mm}{L} \cdot 100\% \quad (7.2)$$

where l_i is the sum of the rock pieces longer than 10 cm and L is the scanline length.

By accounting all these factors, the RMR system provides a subdivision of the rock masses into distinct structural domains that should be analyzed separately. If supporting this classification with table reported on Fig. 7.9, all the domains are grouped into the single rock mass. Due to the homogeneous lithological and engineering properties of the analyzed lithologies, the dolostones ascribed to Dolomia Principale and the Heiligkreuz outcrops can be analyzed through the RMR classification.

A. CLASSIFICATION PARAMETERS AND THEIR RATINGS								
Parameter		Range of values						
1	Strength of intact rock material	Point-load strength index >10 MPa	4 - 10 MPa	2 - 4 MPa	1 - 2 MPa	For this low range - uniaxial compressive test is preferred		
		Uniaxial comp. strength >250 MPa	100 - 250 MPa	50 - 100 MPa	25 - 50 MPa	5 - 25 MPa	1 - 5 MPa	< 1 MPa
	Rating	15	12	7	4	2	1	0
2	Drill core Quality RQD	90% - 100%	75% - 90%	50% - 75%	25% - 50%	< 25%		
	Rating	20	17	13	8	3		
3	Spacing of discontinuities	> 2 m	0.6 - 2 . m	200 - 600 mm	60 - 200 mm	< 60 mm		
	Rating	20	15	10	8	5		
4	Condition of discontinuities (See E)	Very rough surfaces Not continuous No separation Unweathered wall rock	Slightly rough surfaces Separation < 1 mm Slightly weathered walls	Slightly rough surfaces Separation < 1 mm Highly weathered walls	Slickensided surfaces or Gouge < 5 mm thick or Separation 1-5 mm Continuous	Soft gouge > 5 mm thick or Separation > 5 mm Continuous		
	Rating	30	25	20	10	0		
5	Ground water	Inflow per 10 m tunnel length (l/m)	None	< 10	10 - 25	25 - 125	> 125	
		(Joint water press)/ (Major principal σ)	0	< 0.1	0.1 - 0.2	0.2 - 0.5	> 0.5	
	General conditions	Completely dry	Damp	Wet	Dripping	Flowing		
	Rating	15	10	7	4	0		
B. RATING ADJUSTMENT FOR DISCONTINUITY ORIENTATIONS (See F)								
Strike and dip orientations		Very favourable	Favourable	Fair	Unfavourable	Very Unfavourable		
Ratings	Tunnels & mines	0	-2	-5	-10	-12		
	Foundations	0	-2	-7	-15	-25		
	Slopes	0	-5	-25	-50			
C. ROCK MASS CLASSES DETERMINED FROM TOTAL RATINGS								
Rating	100 ← 81		80 ← 61	60 ← 41	40 ← 21	< 21		
Class number	I		II	III	IV	V		
Description	Very good rock		Good rock	Fair rock	Poor rock	Very poor rock		
D. MEANING OF ROCK CLASSES								
Class number	I		II	III	IV	V		
Average stand-up time	20 yrs for 15 m span		1 year for 10 m span	1 week for 5 m span	10 hrs for 2.5 m span	30 min for 1 m span		
Cohesion of rock mass (kPa)	> 400		300 - 400	200 - 300	100 - 200	< 100		
Friction angle of rock mass (deg)	> 45		35 - 45	25 - 35	15 - 25	< 15		
E. GUIDELINES FOR CLASSIFICATION OF DISCONTINUITY conditions								
Discontinuity length (persistence)	< 1 m		1 - 3 m	3 - 10 m	10 - 20 m	> 20 m		
Rating	6		4	2	1	0		
Separation (aperture)	None		< 0.1 mm	0.1 - 1.0 mm	1 - 5 mm	> 5 mm		
Rating	6		5	4	1	0		
Roughness	Very rough		Rough	Slightly rough	Smooth	Stickersided		
Rating	6		5	3	1	0		
Infilling (gouge)	None		Hard filling < 5 mm	Hard filling > 5 mm	Soft filling < 5 mm	Soft filling > 5 mm		
Rating	6		4	2	2	0		
Weathering	Unweathered		Slightly weathered	Moderately weathered	Highly weathered	Decomposed		
Rating	6		5	3	1	0		
F. EFFECT OF DISCONTINUITY STRIKE AND DIP ORIENTATION IN TUNNELLING**								
Strike perpendicular to tunnel axis				Strike parallel to tunnel axis				
Drive with dip - Dip 45 - 90°		Drive with dip - Dip 20 - 45°		Dip 45 - 90°		Dip 20 - 45°		
Very favourable		Favourable		Very unfavourable		Fair		
Drive against dip - Dip 45-90°		Drive against dip - Dip 20-45°		Dip 0-20 - Irrespective of strike°				
Fair		Unfavourable		Fair				

Fig. 7.9. Rock Mass Rating classification system (Bieniawski,1989)

7.6.3. Geological strength index (GSI)

The Geological Strength Index (GSI) was developed by Hoek and Brown (1997) to provide a quantitative evaluation of rock mass quality for engineering purposes. The GSI considers the structure and surface conditions of the rock mass, as depicted by Fig. 7.10.

GEOLOGICAL STRENGTH INDEX FOR JOINTED ROCKS (Hoek and Marinos, 2000) From the lithology, structure and surface conditions of the discontinuities, estimate the average value of GSI. Do not try to be too precise. Quoting a range from 33 to 37 is more realistic than stating that GSI = 35. Note that the table does not apply to structurally controlled failures. Where weak planar structural planes are present in an unfavourable orientation with respect to the excavation face, these will dominate the rock mass behaviour. The shear strength of surfaces in rocks that are prone to deterioration as a result of changes in moisture content will be reduced if water is present. When working with rocks in the fair to very poor categories, a shift to the right may be made for wet conditions. Water pressure is dealt with by effective stress analysis.		SURFACE CONDITIONS				
STRUCTURE		DECREASING SURFACE QUALITY → VERY GOOD: Very rough, fresh unweathered surfaces GOOD: Rough, slightly weathered, iron stained surfaces FAIR: Smooth, moderately weathered and altered surfaces POOR: Slickensided, highly weathered surfaces with compact coatings or fillings or angular fragments VERY POOR: Slickensided, highly weathered surfaces with soft clay coatings or fillings				
	INTACT OR MASSIVE - intact rock specimens or massive in situ rock with few widely spaced discontinuities	90			N/A	N/A
	BLOCKY - well interlocked undisturbed rock mass consisting of cubical blocks formed by three intersecting discontinuity sets	80	70			
	VERY BLOCKY - interlocked, partially disturbed mass with multi-faceted angular blocks formed by 4 or more joint sets		60	50		
	BLOCKY/DISTURBED/SEAMY - folded with angular blocks formed by many intersecting discontinuity sets. Persistence of bedding planes or schistosity			40	30	
	DISINTEGRATED - poorly interlocked, heavily broken rock mass with mixture of angular and rounded rock pieces				20	
	LAMINATED/SHEARED - Lack of blockiness due to close spacing of weak schistosity or shear planes	N/A	N/A			10

Fig. 7.10. Geological strength index (GSI) table (from Marinos and Hoek, 2001)

The GSI classification, first presented by Hoek and Brown (1980a, 1980b), is a method aimed to provide estimates of the strength of jointed rock masses. It is based upon an assessment of the interlocking of rock blocks and the condition of the surfaces between these blocks.

In the analysis of stability the Cinque Torri DSGSD, the input values for the rock mass properties are results mainly obtained from uniaxial compressive strength (σ_c), as well as on the RMR classification based on traditional scanline mapping. Both investigations focused on the exposed rock outcrops within the group of monoliths and its surroundings. The procedure to acquire these data is iterative and further rock material constants are needed. Due to the frequent impossibility to carry out adequate laboratory analyses, or when this information is needed before laboratory testing, reference tables can be used to estimate such values (Fig. 7.11).

Rock type	Class	Group	Texture			
			Coarse	Medium	Fine	Very fine
SEDIMENTARY	Clastic		Conglomerates *	Sandstones 17 ± 4	Siltstones 7 ± 2	Claystones 4 ± 2
			Breccias *		Greywackes (18 ± 3)	Shales (6 ± 2) Marls (7 ± 2)
	Non-Clastic	Carbonates	Crystalline Limestone (12 ± 3)	Sparitic Limestones (10 ± 2)	Micritic Limestones (9 ± 2)	Dolomites (9 ± 3)
		Evaporites		Gypsum 8 ± 2	Anhydrite 12 ± 2	
Organic					Chalk 7 ± 2	
METAMORPHIC	Non Foliated		Marble 9 ± 3	Hornfels (19 ± 4) Metasandstone (19 ± 3)	Quartzites 20 ± 3	
	Slightly foliated		Migmatite (29 ± 3)	Amphibolites 26 ± 6	Gneiss 28 ± 5	
	Foliated**			Schists 12 ± 3	Phyllites (7 ± 3)	Slates 7 ± 4
IGNEOUS	Plutonic	Light	Granite 32 ± 3 Granodiorite (29 ± 3)	Diorite 25 ± 5		
		Dark	Gabbro 27 ± 3 Norite 20 ± 5	Dolerite (16 ± 5)		
	Hypabyssal			Porphyries (20 ± 5)	Diabase (15 ± 5)	Peridotite (25 ± 5)
	Volcanic	Lava		Rhyolite (25 ± 5) Andesite 25 ± 5	Dacite (25 ± 3) Basalt (25 ± 5)	
		Pyroclastic	Agglomerate (19 ± 3)	Breccia (19 ± 5)	Tuff (13 ± 5)	

Fig.7.11. Table proposed by Marinos and Hoek (2001) to extract values and accuracy of constant m_i for intact rock, by rock group. The values in parentheses refer to estimates.

In this frame, the GSI classification is a factor within this iterative procedure rather than the elected method for assessing the strength of the studied rock masses. The equations that are introduced here following will clarify the role of GSI.

The field surveys on the study area concerned the most exposes rock type, i.e. the Dolomia Principale dolostones and the Heiligkreuz Formation.

In the present research, GSI index was first calculated from the RMR classification and then the resulted value was compared to the table of Fig. 7.10 for a qualitative validation:

$$GSI = RMR - 5 \quad (7.3)$$

Thus the GSI table (Fig. 7.3) was used as reference, in order to validate the results of the RMR classification which is related to the GSI from eq.(7.3).

In the following paragraph the results are presented.

7.6.4. Rock mass properties

The description of the rock mass properties of rocks requires field investigations and representative laboratory testing. Scanline mapping and hardness tests were carried out for the Dolomia Principale (DPR) and the Heiligkreuz formation (HKZ) outcrops. Therefore only a portion of the stratigraphical sequence was assessed through such methodologies.

From the analysis of the main results derived from scanline mapping, a similar mechanical behavior for the two analyzed lithologies emerges. As a matter of fact, if the rotational components of the lateral spreading are taken into account, 4 main rock discontinuity sets can be outlined for all the sites and similar mean values of normal set spacing is found (Fig. 7.12, Fig. 7.13).

The mean rebound results show higher values for the DPR outcrops respect to the HKZ outcrops, as reported on section 7.6.1. These results disagree with the uniaxial test outcomes that pointed out higher trends in UCS and Etan values for HKZ samples respect to DPR samples.

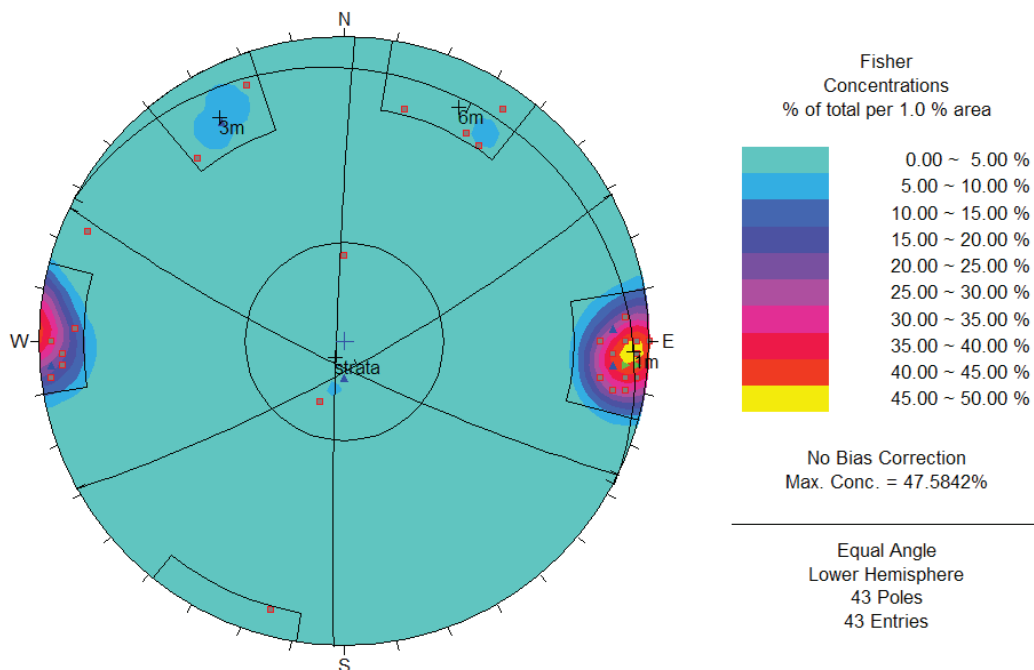


Fig. 7.12. Stereoplot of the rock discontinuities orientations analyzed during the scanline mapping of the Torre Grande site (Dolomia Principale (DP) outcrop) (Appendix D)

According to the results reported in tables D.2 and L.2 the rock outcrops show similar qualitative characteristics. In addition, the observations outlined a joint aperture varying between 0.001 m - 0.1 m and set spacing ranging between 0.15 - 1.5 m.

The overall scanline mapping shows that the (rotated) N-S to NNE-SSW is the most common rock discontinuity set. This statistics is biased by direction of the scanlines, which is frequently parallel to the strata direction. In order to obtain a reliable set spacing of this discontinuity system, a vertical scanline is preferred. In this way, the high angle discontinuity sets are only marginally intersected, but it would be almost normally intersected the strata bedding, which is actually the most frequent set in the rock faces.

Scanline mapping also outlined that the investigated discontinuities are characterized by a moderate joint roughness (mean Joint Roughness Coefficient JRC = 9) and by rare water percolation. If present, the joint filling has in general a clayey composition from cataclased to cemented.

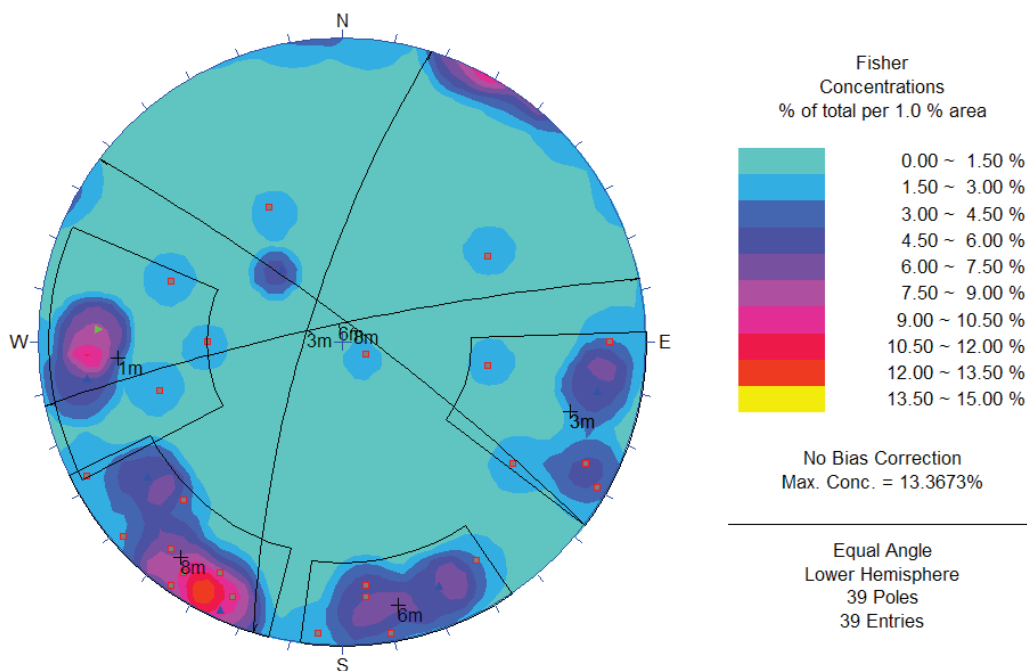


Fig. 7.13. Stereoplot of the rock discontinuities orientations analyzed during scanline mapping of the Nuvolau site (Heiligkreuz (HKZ) outcrop) (Appendix L)

The rock mass characteristics of the Dolomia Principale and Heiligkreuz Formation were estimated by introducing the information of field surveys according to the Bieniawski's (1989) Rock Mass Rating (RMR_{89}) classification. The RMR value determined for each lithology is based on the modified RMR^*_{89} , as described in Hoek et al. (1995), in which the groundwater is set to 'dry' conditions and the penalty for joint orientation is set to zero. These adjustments avoid double counting the effects of groundwater and joint orientation when deriving rock mass properties to be used in numerical analyses, where the influence of groundwater and adverse jointing are explicitly accounted for.

Rock mass properties for all the investigated lithologies were subsequently estimated using the empirical scaling relationships developed by Hoek et al. (2002) on the basis of relationships of strength and elastic properties outlined by the uniaxial test results.

The Hoek-Brown constant m_i is derived from triaxial testing on core samples, or estimated from a qualitative description of the rock material, as in Hoek and Brown (1997). This parameter is influenced by the frictional characteristics of the component

minerals in the intact rock sample and is directly correlated to the strength characteristics of rock. Alternatively, if no triaxial tests are available, an estimate of m_i can be obtained from the Fig. 7.11, where most of the values derived from triaxial tests reported on literature are reported.

Once the parameters UCS, RMR and GSI are defined, the mechanical properties of the rock mass can be estimated. For clarity, the calculations for determining the properties of DPR are provided with details, while the same parameters for the other rock types are summarized in Table 7.7.

Field surveys on the study area showed that, for a great extent, the high density dolostones of the Dolomia Principale forming the Cinque Torri group have similar properties of the Travenanzes dolostones layers (Fig. 2.6). The rock mass properties of this lithology can be derived from the known values of m_i , or constant of the intact rock, RMR and the deduced GSI. From Fig. 7.11 the value that can be attributed to this lithology ranges around ≈ 20 due to its high density respect common dolostones. For this lithotypes, the *Rock Mass Rating* (RMR) deduced from equation (7.1) according to table of Fig. 7.9 is about 80 and the *Geological Strength Index* defined as $GSI=RMR-5$ is therefore close to 75. With these input values, the rock constants m_b and s can be calculated from the following relations:

$$m_b = m_i e^{\frac{(GSI-100)}{28}} \approx 8.2 \quad (7.1)$$

$$s = e^{\frac{(GSI-100)}{9}} \approx 0.062 \quad (7.2)$$

Moreover, the maximum compression strength σ_{cm} is calculated taking into account the Griffith's theory in the empiric Hoek-Brown criterion:

$$\sigma_1 = \sigma_3 + \left(m_b \sigma_3 \sigma_c + s \sigma_c^2 \right)^{0.5} \quad (7.3)$$

and assuming σ_3 very small compared to σ_1 , thus $\sigma_3 \approx 0$ and $\sigma_1 \approx \sigma_{cm}$:

$$\sigma_{cm} \approx \sigma_c * (s)^{0.5} \quad (7.4)$$

where σ_c is the peak compression strength derived from uniaxial compression test (Chapter 5) and determines a σ_{cm} in the range of 21 MPa for the DP rock mass.

Consequently also the tensile strength σ_{tm} can be determined, by assuming for this calculation $\sigma_1 \approx 0$ and $\sigma_3 \approx \sigma_{tm}$:

$$\sigma_1 = \sigma_3 + \left(m \sigma_3 \sigma_c + s \sigma_c^2 \right)^{0.5} \quad (7.5)$$

$$\sigma_{tm} \approx \frac{\sigma_c}{2} * \left(m_b - \left(m_b^2 + 4s \right)^{0.5} \right) \quad (7.6)$$

For DPR, the mean resulting tensile strength is about 0.65 MPa.

Finally the Deformation modulus E_m is calculated from the modified Serafim and Pereira's relation:

$$E_m = \left(\frac{\sigma_c}{100} \right)^{0.5} * 10^{\frac{(GSI-10)}{40}} \quad (7.7)$$

while the friction angle of the rock mass is calculated from the following equation:

$$\phi = 0.5 * RMR + 5 \quad (7.8)$$

and for the DP it averages around 43°.

Finally, also the cohesion of the rock mass is computed according to the relation:

$$c = 0.005 * RMR \quad (7.9)$$

For the investigated DP rock faces, its mean values is 0.400 MPa.

At this point an intriguing aspect should be underlined. The direct tests carried out on rock specimens provide the needed parameters to calculate equations from (7.3) to (7.7). As seen in paragraph 7.6.1, a representative population of Schmidt hardness rebound values is available. Therefore, an estimate of the uniaxial compression strength of the intact DP and HKZ formation can be derived and compared with the results of the direct tests (see Chapter 5). This derivation has only an illustrative meaning, since for the numerical models treated on Chapter 8 only rock mass properties are used. To obtain the uniaxial compression strength from the mean rebound value, the formulation proposed by Sachpazis (1990) is used here:

$$\sigma_c = \frac{(N_R - 15.7244)}{0.2329} \quad (7.10)$$

Since, as previously reported in Sect. 7.6.1, the mean NR for DPR outcrops is 50, the calculated σ_c is 147 MPa. As expected, from the comparison with the results of the uniaxial tests (Sect. 5.5.1) a sensible overestimation appears. In Table 7.7 the measured and calculated properties for the investigated lithologies are summarized. From comparisons with literature, the found values are included in the averaging trends typical of sedimentary rocks. Again, attention should be played on the way these values were found, and their application in rock modeling. All these values are purely indicative due to the scarce number of analyzed samples and the fact that a scanline mapping has local representativeness only. These data highlight the existence of a relationships among lithologies in terms of strength and elastic properties rather than a reliable assessment of the properties of each lithology. Moreover, many values are inferred from the calculated ones by using the trends obtained from uniaxial tests and ultrasonic velocities tests.

Once the relationships between the parameters are captured, reliable models of the slope behavior for different conditions can be derived (see Chapter 8).

Table 7.7. Intact rock and rock mass properties derived from direct and indirect tests. The rock mass properties are calculated from Hoek –Brown (H-B) and Rock Mass Rating (RMR) equations. The * indicates inferred values from empiric calculations or from existing relationships for strength and elasticity among the investigated lithologies

INPUT:						
Intact rock properties	Units	DP	TVZ CARB	TVZ MUD	HKZ	DCS
Uniaxial compressive strength	[MPa]	86	86	60*	100	100*
Geological strength index (RMR*89)	[-]	75	75*	30*	80	80*
H-B constant, m_i	[-]	20*	20*	12*	21*	21*
Young's modulus, E	[GPa]	100	100*	20*	150	150*
Poisson ratio, ν	[-]	0.25	0.25*	0.30*	0.2	0.2*
Density, ρ	[kg/m ³]	2750	2750	2300*	2700	2800*
OUTPUT:						
Rock mass properties						
H-B constant, m_b	[-]	8.2	8.2	2.9	10.3	10.3
H-B constant, s	[-]	0.062	0.062	0.0004	0.1	0.1*
RMR cohesion, c	[MPa]	0.400	0.400*	0.175*	0.425*	0.425*
RMR friction angle, ϕ	[°]	43	43*	27*	43*	45*
Tensile strength, σ_{tm}	[MPa]	0.65	0.65*	0.0083*	0.97	0.97*
Deformation modulus, E_m	[GPa]	40	40*	2.5	56	56*

7.7. Results and conclusion

A reliable model of the potential instability phenomena in terms of both structural evolution and geometries is mainly based on a detailed representation of the rock body discontinuities.

During the last decade, 3-D terrestrial laser scanning has offered a great perspective for generating information on the geometric properties of rock outcrops in a fast and accurate way.

Despite the simplicity and effectiveness of conventional manual techniques for measuring orientation and spacing of rock discontinuities, the geometric information that is derived using manual surveys may often be biased, inaccurate and sparse.

Further, manual techniques are very labor-intensive and detailed mapping of rock faces is therefore often not feasible. Finally, the safety risk of working under a steep slope in often hazardous surroundings is another reason to reduce manual survey. Remote sensing is therefore a logical alternative to manual field surveys, since physical contact with the rock exposure can be avoided.

In the present chapter, the use of point clouds for deriving rock discontinuities geometrical properties is discussed. The method initially proposed by Slob (2005) is applied to a sector of the rocky group, the Torre Inglese pinnacle, with the goal of a classification of major rock discontinuities (with dimension in the order of the monolith facets). The main advantages of this methodology are: the entire rock surface is analyzed for discontinuity recognition, and no surface reconstruction is needed since the original point-cloud data are processed.

To perform the analysis, the PCM software package (Vosselman, 2004) was used. Initially, the unorganized point cloud is spatially structured in PCM by creating a tree-based data structure (K-D tree). This structure promotes the spatial search of common planar geometries among close points, the so-called region-growing strategy based on 3-D Hough transformation combined to a (Total) Least Squares Analysis for improving quality on the searching. The result of the segmentation is a classified (i.e. a segmented or labeled) point cloud (Fig. 7.4b), where points having similar labels belong to the same discontinuity plane. The combination of the PCM processing with a PCA post processing (section 7.4) provides an accurate and statistically representative acquisition of the geometrical pattern of fractured rock bodies (Appendix C) which is a specific parameter needed in rock stability analysis.

In figure 7.14 the stereoplots of rock discontinuities of the Torre Inglese pinnacle derived from point cloud segmentation (7.14a) and scanline mapping (7.14b) are shown. It can be observed that, despite the lower scattering of the scanline characterization, the last omits the discontinuity set '7m' (trend ENE-WSW), which in turn is well represented by the segmented point cloud data.

The comparison of the results of discontinuity spacing derived from traditional scanline and point cloud data processing shows significant differences in the set spacing evaluation but, nonetheless, some correlations are still possible. Differences are mainly due to the different nature of the above techniques: the scanline mapping concentrates only along a line, while the point cloud-based determination of set spacing accounts for all the discontinuity planes recovered within the point cloud. Therefore, it can be stated that the remote sensing methodology provides more representative information of the entire rock face. The disadvantage of the point cloud data processing for discontinuity properties assessment lies on the scale of investigation, which is directly related to the point cloud spatial resolution. It can be observed that the remotely recovered rock discontinuities are major discontinuities that subdivide the monolith surface into different faces. This derives in a data sub sampling with respect to estimates derived by the scanline mapping. Nonetheless, since the resulting rock discontinuity properties are imported into numerical models for slope behavior analysis (Chap. 8), the use of accurate and representative, even if less dense, discontinuity sets is advantageous as it can sensibly improve the computation time.

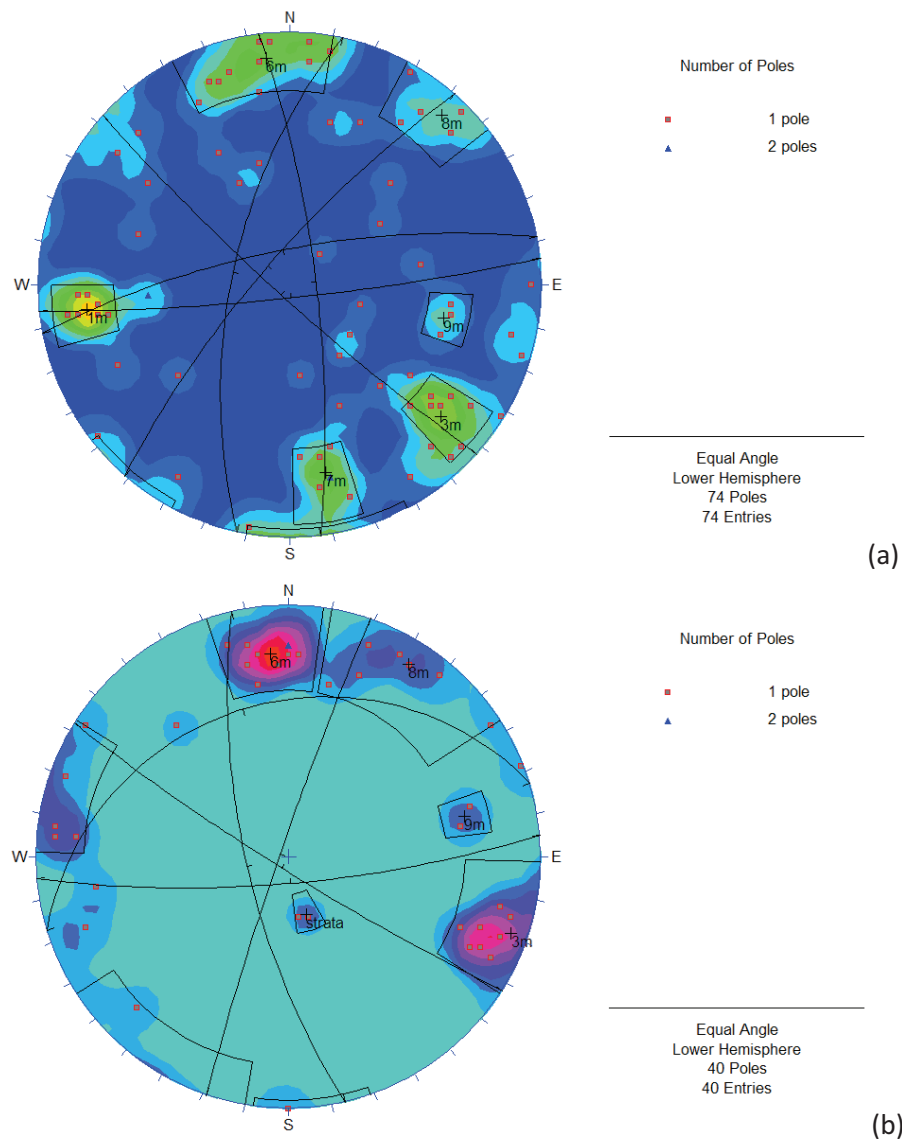


Fig. 7.14. Stereoplots of all the discontinuity planes found with segmentation of the point cloud data (a) and with the scanline mapping (b) for the Torre Inglese pinnacle. The color contours are pole densities.

The second part of the chapter deals to rock discontinuity and rock mass properties determination based on the results of traditional field surveys and laboratory tests. A reliable rock mass characterization is mainly based on direct test analysis carried out on a representative number of rock specimens. In the present research, only few rock tests were carried out for the assessment of intact rock properties. Unfortunately, in literature any reference value is reported for the specific investigated lithologies, but there exist only general classifications for limestones, dolostones and mudstones. In nature, rocks grouped into a certain category can show sensible differences in mechanical and physical properties according to a different mineral composition, porosity, fracturing grade, weathering and slope conditions. This leads to a wide range of variation. Thus the values reported on literature should be used as reference once direct or indirect test on rocks are carried out. If values on literature are directly used in

numerical models for slope behavior analysis, the elected values are arbitrarily chosen by the engineer, without any insurance about their reliability.

In the present research both direct and indirect tests were carried out in order to derive indicative values for the rock mass properties assessment. The calculation of rock mass properties is mainly based on Rock Mass Rating and Hoek & Brown empirical correlations.

The scarce number of direct and indirect observations prevents the creation a solid statistics of the main rock properties for each involved rock type. Nonetheless, the results provide indicative values of such properties and can highlight relationships among strength properties and elastic indexes. These relationships are indirectly validated by comparing the results of different test analyses (ultrasonic test, uniaxial test, Schmidt hardness test) and therefore can be used in numerical analysis for illustrative purposes. As a matter of fact, in Chapter 8 the numerical modeling is not implemented for slope stability assessment. The main aim instead is a qualitative evaluation of factors influencing the slope stability. A further important goal of numerical modeling consists in a verification of the interpretations derived in Chapter 6.

8. Numerical models of the Cinque Torri landslide: application and comparison of different approaches

8.1 Introduction to numerical modeling

Landslides result often in significant socioeconomic impact. The evaluation of the mechanisms and factors that influence slope stability is essential for the management of landslide prediction. The spatial information, geological, hydro-geological, and geomechanical properties together give the theoretical model for the investigated slope. Due to the general geological complexity of the slope mass and numerous factors and processes that may cause sliding, the analysis of landslides often requires an initial simplification of the slope conditions. Subsequently, investigations can be deepened through standard procedures and advanced technologies. For better understanding of slope failure or movement, underground conditions and mechanisms of slope instabilities need to be investigated. In this frame, numerical modeling can help in detecting where and how a particular hazard event is most likely to occur, and it may indicate the sensitivity for particular processes or factors that cause the slope instability. According to the general rules summarized in Stead et al. (2006) there are three main levels of sophistication in numerical analyses that should be considered for the slope modeling of a particular case study (Fig. 8.1). Level 'I' analyses include mainly limit equilibrium and kinematic techniques and are devoted to simple translational failures involving release on smooth basal, rear and lateral surfaces that produce progressive failure surface and /or asperity breakdown. Level 'II' analyses involve the use of continuum and discontinuum numerical methods, particularly useful for complex translational rock slope deformations that can be modeled by step-path failure mechanism that include degradation and failure of the intact rock bridges along the release surface and a significant component of brittle intact rock fracture. Finally level 'III' requires the use of hybrid continuum-discontinuum codes with fracture simulation capabilities and is particularly well suited to complex translation/rotational instabilities which comprise internal yielding, brittle fracturing and shearing in addition to strength degradation along release surfaces.

Since the processes leading to the Deep Seated Gravitational Slope Deformation (DSGSD) are far more complex than a simple balance of disturbing and resisting forces, it can be easily recognized limit equilibrium method (level I) is not sufficient. Limit equilibrium techniques neglect internal fracturing and deformations (Stead et al., 2006) that are common processes in the studied slope, while only active processes along the developing shear plane are computed.

The methodology applied for this study is derived from the combination and comparison of techniques ascribed from level II. By running numerical discontinuum techniques-level II, the controlling influence of joint on complex rock slope deformation is assessed and moreover is able to verify the effects of parameter variations on instability. The shear degradation in the form of sliding surface development and internal slide mass

deformation in case of non-planar failure surface are therefore included in such methods.

The use of distinct-element (UDEC, Itasca, 2004) and finite element (Plaxis, Brinkgreve et al., 2008) codes were used to investigate the present-day slope instability mechanisms therefore to create an effort for the interpretation derived from rotational analysis (Sections 6.5.2 and 6.6). In addition once the geometries of the instabilities are defined, the evaluation of the unstable rock volume can be achieved. The Cinque Torri slope presents a very heterogeneous stratigraphy that produces a high variable behavior from a geomechanical viewpoint. In this scenery both discrete and finite element codes are suitable since the former creates appropriate models for jointed rocks reproducing the deformation typical of fragile media while the latter is generally devoted to reproduce the ductile behavior of soil and soft rocks.

In particular, as experienced by Brideau et al. (2006), the combined use of distinct-element and finite element codes allows modeling of respectively the control exerted by both discrete structures and rock-mass strength and the stress-strain relations within the slope.

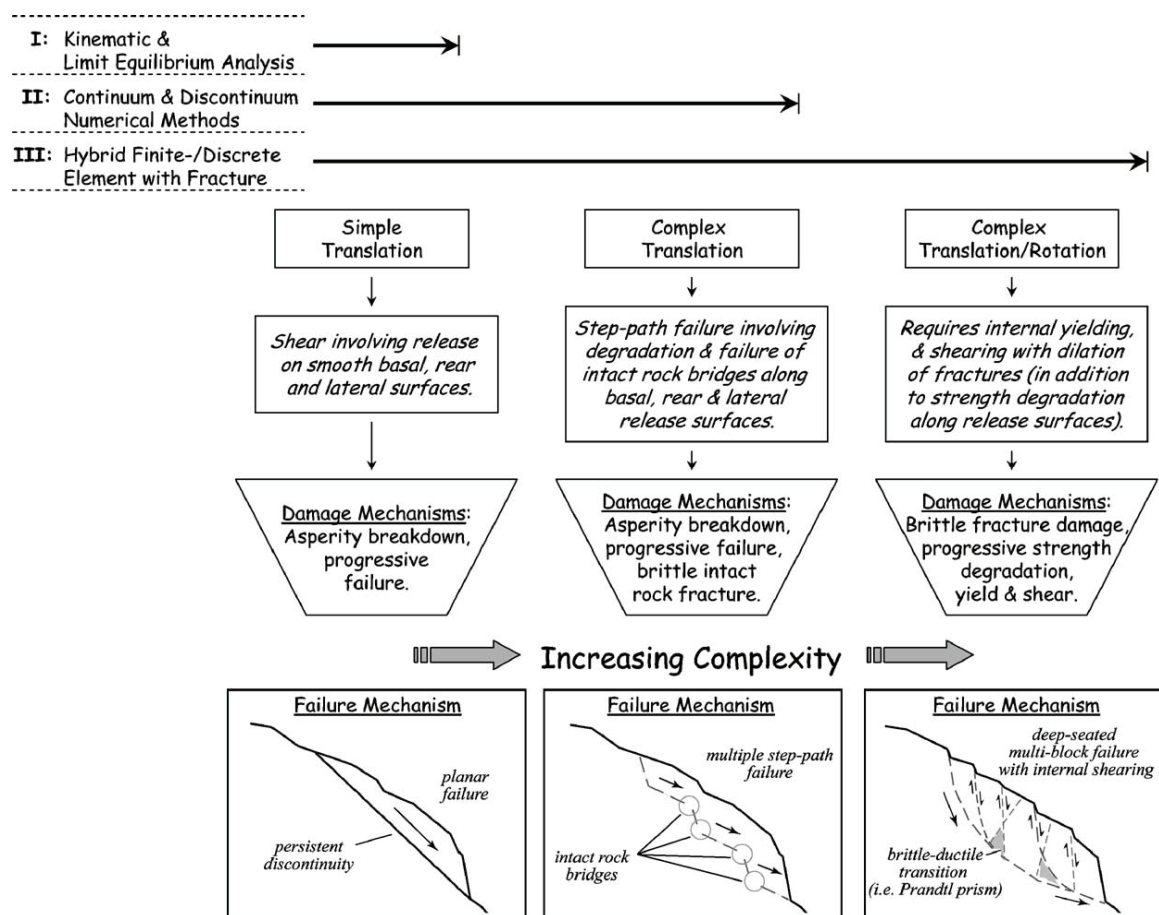


Fig. 8.1. Scheme of the types of numerical modeling in relation to the failure mechanism to be modeled (after Stead et al., 2006)

8.2 Classes and objectives of numerical modeling

The mechanics of large deep seated gravitational slope deformations has generally been reported as involving complex mechanisms and at time of writing only a few studies on this topic have been carried out using numerical techniques (Agliardi et al. 2001; Kinakin et al. 2005; Hurlimann et al., 2006). The experience on numerical modeling for landslide report that the main factors influencing the displacements of slopes are mainly the weathering processes, groundwater level, thickness and strength of the weak lithologies, inclination of slopes, rock discontinuities (Brideau et al, 2006; Chemenda et. al, 2009; Alejano et al., 2010; Conte et al., 2010; Welkner at al., 2010). In the case of the Cinque Torri landslide, the use of different models allows assessing and relatively speaking quantify the influence of the above mentioned factors to the overall instability. The main purposes of the numerical modeling are:

- a) Sensitivity analysis of the factors influencing the Cinque Torri DSGSD;
- b) Model creation of the DSGSD in terms of shape, dimensions and geotechnical relations among lithologies;
- c) Assessment and comparison of the results of the rotational components analysis (see Chapter 6) of the lateral spreading, occurring at the top of the DSGSD.

Because representative field data are limited at time of writing, especially concerning exact geotechnical and stratigraphic analyses and hydrogeological investigations, qualitative trends rather than quantitative values were expected from this modeling study.

With these principles the slope stability is assessed for different conditions and the most severe combination of slope settings can be determined.

8.3 Modeling with UDEC 4.1

UDEC (Itasca, 2004) is a distinct element code applied to slope stability analysis controlled by movements of joint-bounded blocks and/or intact rock deformation. This code has been used to investigate a wide variety of rock slope failure mechanism and is now in routine use in civil and mining engineering. Going into more details distinct element codes are suitable in analyzing from simple planar mechanisms (Costa et al., 1999), to complex retrogressive failures (Brideau et al., 2006) and rock avalanche failure surface (Welkner et al., 2010) and furthermore some cases of DSGSDs have been modeled (Agliardi et al, 2001; Hurlimann et al., 2005). Furthermore Udec can be also applied to verify results of Poisson ratio and rock mass strength coming from uniaxial tests as experienced by Singh et al. (2008). In all these cases, intact brittle fracture mechanisms are important components of the failures even if the distinct element code only imitates intact rock fracture, and do not follow basic principles related to such mechanic. Nevertheless the UDEC code has the advantage that it combines rigid with deformable blocks, and this is particularly interesting in the analysis of the Cinque Torri DSGSD. The output of the numerical models generally exhibit information about the ground movements, slide mechanism, acceleration, and stress and strain distribution and by interpreting these results the final comprehensive model can be achieved.

In order to carry out the Cinque Torri model uncertainties related to rock mass properties (Cohesion, Young's Modulus, Poisson's ratio, friction angle) assessment (Chapters 5 and 7) should be accounted therefore some initial simple tests are needed.

When dealing with very heterogeneous lithologies many aspects should be considered for the interpretation of the numerical modeling outcomes. Blocks with very low strength and stiffness properties show generally high sensitivity of displacements to the joint constitutive law or strength values. On the contrary, if the blocks have good quality, shearing of the interfaces is rather limited. In addition it should be pointed out that in case of the very weak lithotypes the overall stability of the rock body is mainly governed by the rock properties rather than the properties of joint discontinuities. This consideration is evident in cases when the number of joints is so high that the rock body behaves as a continuum rather than a discontinuous mass.

In the case of the complex geotechnical setting of the Cinque Torri slope, it is assumed that the displacement pattern in terms of position in the stratigraphic sequence is mainly controlled by the mechanical properties of the mudstone layers while the number of joints introduced in the rock layers controls the trend of the deformation.

To represent both rock and joints an elasto-plastic behavior is adopted by using a Mohr-Coulomb criterion which defines a linear relationship between stress and deformations.

When modeling slope behavior as suggested by Kinankin and Stead (2005) the choice of symmetrical ridge forms is not suitable for mountains affected by glacial erosion processes as for the Cinque Torri area, but generally valleys with a glacial history have only few symmetric ridges.

Taking into account also this aspect in the geometry setting, the adopted methodology is based on three levels of investigation (as reported on the scheme of Fig. 8.2):

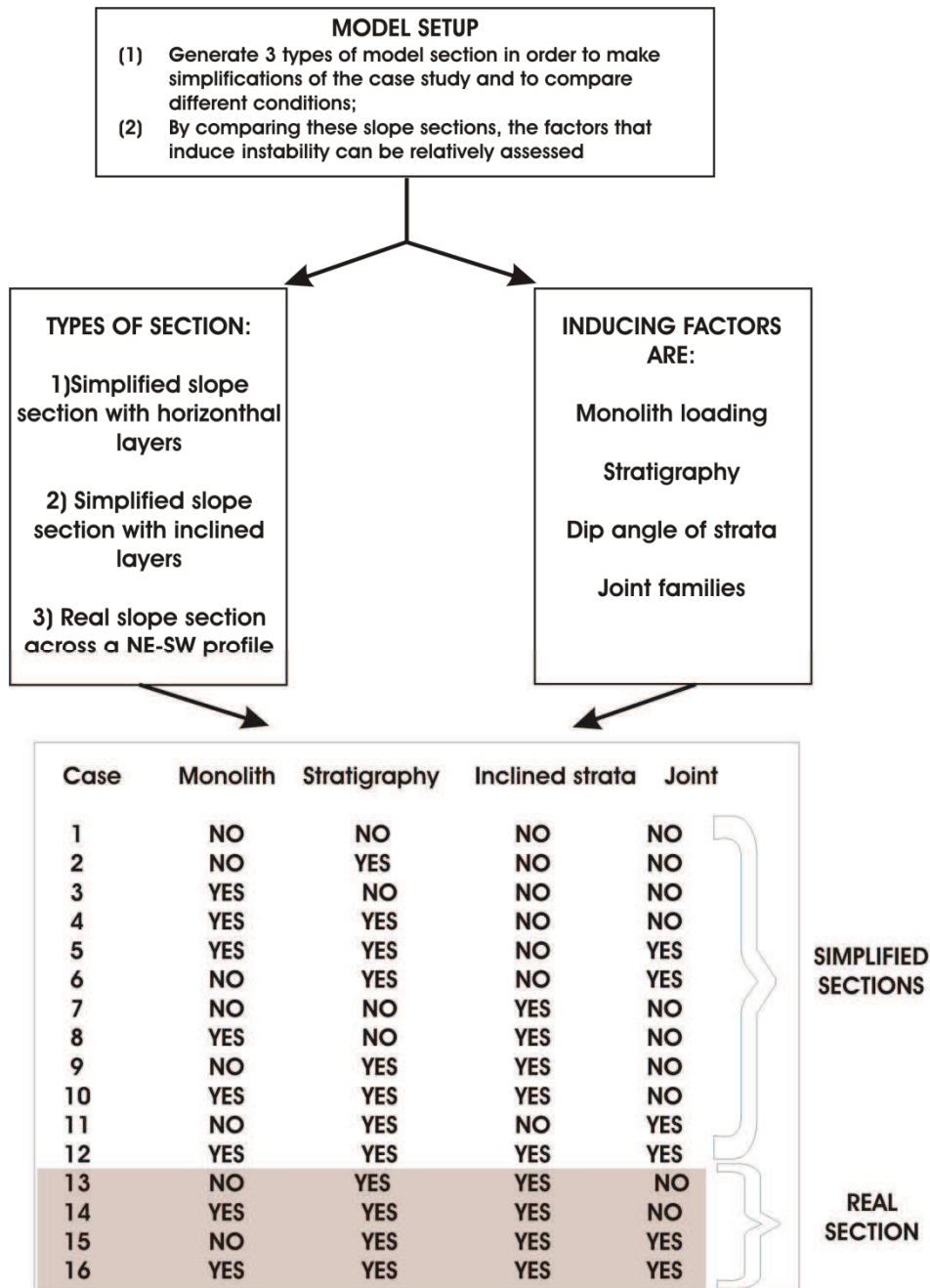


Fig. 8.2 Scheme of the adopted methodology for the numerical modeling of the Cinque Torri DSGSD.

- I. Simplified section with horizontal layers;
- II. Simplified section with inclined layers (as reality);
- III. NE-SW representative slope section along the immersion of strata N10°E (Fig.8.3 and 8.4).

For each case several conditions are modeled. In the final models, the following groups of the properties are defined: (i) parameters of the rock mass, (ii) parameters of the joints, (iii) applied stress due to the weight of the monoliths.

Before assessing the slope section model (III), two types of idealized theoretical sections, reproducing simplified stratigraphic sequence and shape of the slope are considered

first. The tests carried out on these models are useful to assess the influence of specific factors to the overall stability. Among the others stratigraphic and geotechnical heterogeneity, deep angle of the layers, weight of the monolith at the top and rock discontinuities influences are tested. The principle of the analysis is to get relative information of the stress and strain distributions by comparing different model settings. Therefore the lack of geotechnical and hydrogeological knowledge can be ignored thanks to a relative viewpoint derived mainly from the extraction of the principal stresses at the user's defined depth (see Sect. 8.3.1). By comparing the graphs of the stresses distribution along chosen horizons, the influence of each factor on the instability can be compared.

Another aspect of the modeling is devoted to the detection of the instability pattern that characterizes the Cinque Torri DSGSD and for this purpose a script based on the Shear Strength Reduction Method (Dawson, 1999) is applied.

By reducing the values of the strength in the slope section (case III) until the failure is reached, a possible deformation pattern is outlined and can be compared to the interpretation of the DSGSD geometries proposed in Section 6.5.2. Furthermore, if previous analyses and field investigations are accounted, some particular behaviors are expected for the real section model:

- pseudo-circular deformation with listric detachments and possible development of a shear sliding surface;
- plastic deformation within the mudstone layers;
- fragmentation of the hard lithologies (dolostones).

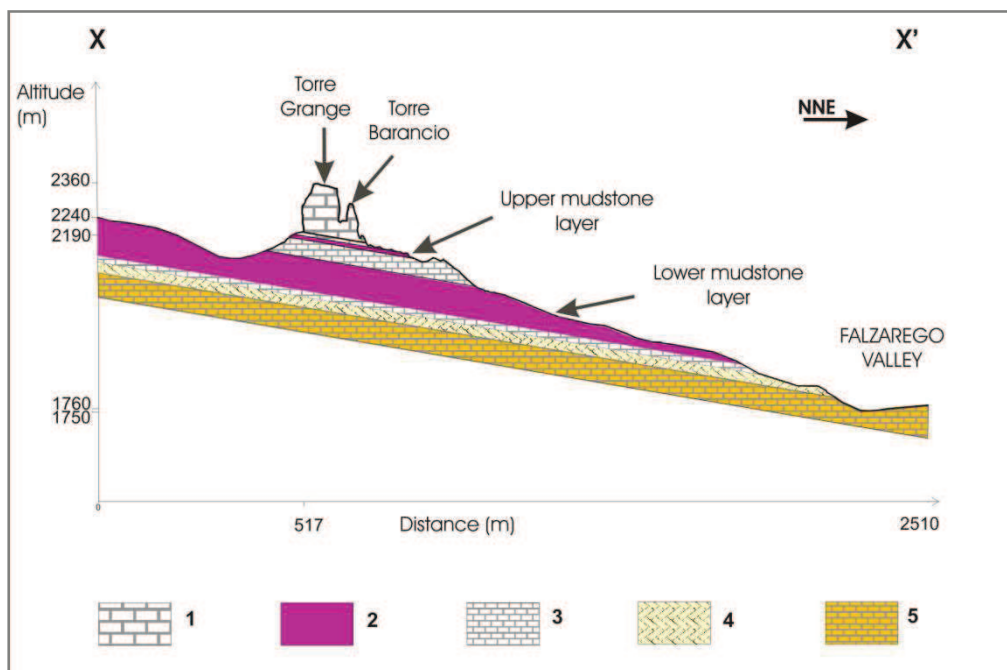


Fig. 8.3. Cross-section through the Cinque Torri slope showing the main geological features (the trace of the profile is shown on Fig. 8.4). Dolomia Principale –DPR dolostones (1), Mudstone layers of the Travenanzes formation –TVZ mudstones (2), carbonatic layers of the Travenanzes formation-TVZ carbonates (3), Heilgkreuz formation- HKZ carbonates (4), Dolomia Cassiana-DCS dolostones (5).

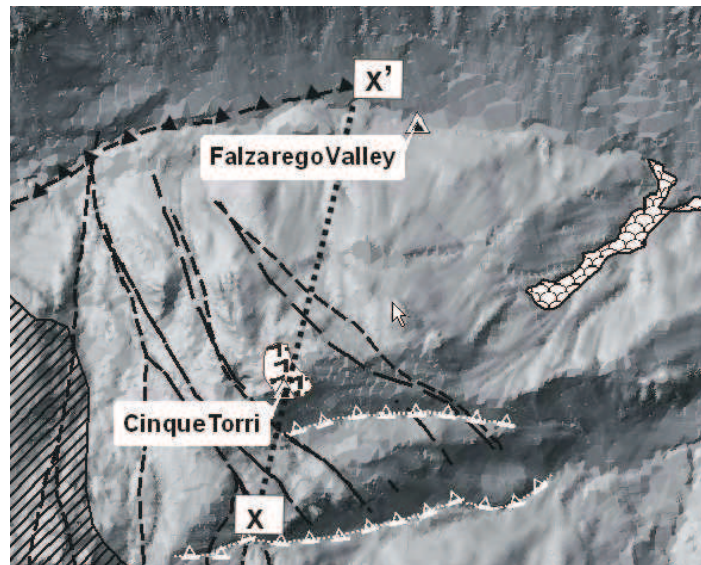


Fig. 8.4. Trace of the cross-section sketched on Fig. 8.3.

The effects of the natural topography on the stress distribution in a slope may have important implications for DSGSD development therefore some new features are expected from the models of the real slope section.

The influence of the water content both in terms of water table and snow melting should be included in the models in terms of pore water pressures. No direct information is available at time of writing, therefore the water influence is incorporated into the model indirectly by assuming dry unit weights for the permeable rock layers and wet unit weights for the mudstones layers. The study site is located on a mountain area where no permanent water table is expected. The abundant incomings of water related to seasonal snow melting and the numerous natural springs observed on the slope during field investigations suggest a rapid drainage from the fractured rocks at the top and a rapid decrease of infiltration within the mudstone layers.

Despite the qualitative purpose due to the uncertainties and simplifications of the chosen values for rock and joints properties and boundary conditions, all the proposed simulations are interesting and necessary because they demonstrate the capabilities of the modeling work to assess the effect of the expected influencing factors in the slope stability and to verify the reliability of previous hypotheses related to the failure mechanism.

When dealing with rock discontinuities numerical models have some limits in reproducing the geometries and frequencies recorded on field investigations and these limits reside in the pc memory assigned for computations. Since the required memory in processing numerical models is related to the complexity of the models themselves in terms of nodes, number of iterations for reaching equilibrium and structure of the investigated slope, the more are the joint families and their frequency, the higher are the time of processing and the required memory. Taken into account these considerations the spacing of the rock discontinuities in the model is calibrated on the basis of a factor of increment ranging from 40 to 7. The set spacing introduced in the models is therefore wider with respect the observed on field. None the less the chosen

values still represent a reliable reproduction of the structures that control the dynamic of the slope since the rock discontinuities that determine the fragmentation of the monoliths have a metric spacing.

As reported in Section 7.5, geomechanical reliefs, even if accurate and densely acquired, represent a small part of the whole rock body, therefore punctual information correlated by high uncertainties. When modeling the geometries of rock discontinuities a particular tool in UDEC allows reproducing a statistic variation of parameters like spacing, persistency, deep angle by assigning a standard deviation for each value. This particular approach assures a smoothing of the scale effect which often rises during modeling natural systems as rock slopes by taking into account the results of laboratory or local field tests.

8.3.1 Effect of the monoliths

The effects of the natural topography on the stress distributions in a slope may have important implications for the DSGSD development. Before going in trough details on the studied cases it would be necessary to introduce the concept of stress which is generally used to describe the intensity of internal forces in a body under the influence of a set of applied surface forces (Brady and Brown, 1985). The Mohr-Coulomb model is applied to studied cases. The failure envelope for this model corresponds to a Mohr-Coulomb criterion (shear yield function) with tension cutoff (tensile yield function) (Itasca, 2004).

Several models were set up with or without the presence of the monolith in cases of models with stratigraphy or with a homogeneous slope in order to compare stress and strain values. In this way the more favorable condition to instability is found and at the meantime the DSGSD features can be located within the modeled sections.

The stress produced by the monolith loading is considerable since for the section of Fig. 8.3 it ranges around 3700 KPa and 2700 KPa for the intersected Torre Grande monolith and the Torre Lusy monolith respectively. The stress propagation is also influenced by the reduction of the cohesion values simulating weathering and water saturation effects.

When assessing the role of the weight of monoliths an important aspect should be underlined: the numerical model defines the applied load as a stress boundary acting at the surface of the topography as an external force. The millions of year required for strata deposition and monolith formation due to erosive processes is not accounted by the model. This results in an overestimation of the involved stresses. Nevertheless, since the main objective of this modeling is not a displacements assessment neither a slope stability evaluation but a sensitivity analysis of the influencing factors of instability, the condition of higher stresses is more promising to underline even small differences among the analyzed cases.

The Udec models created to assess the Cinque Torri slope's sensitivity to the different triggering events are built using two simplified models and the present-day slope topography combined with the geology inferred from reference stratigraphic stations in the surroundings of the studied area. In Table 7.7 (Section 7.6) are summarized the

parameters for relevant materials included in the UDEC models for the rock mass properties of the involved lithologies.

The action of stresses related to the action of the monolith load is considered first.

In the case of uniform slope – with single lithology, the monolith weight induces a stresses regime as reported on Fig.8.5b. With respect to the case without monolith, the initial major principal stress increases by a factor of 8.5, therefore proving the influence of this force to the slope behavior. As a consequence, a slope similar to case of Fig. 8.5b is more prone to instability with respect case a (Fig. 8.5a).

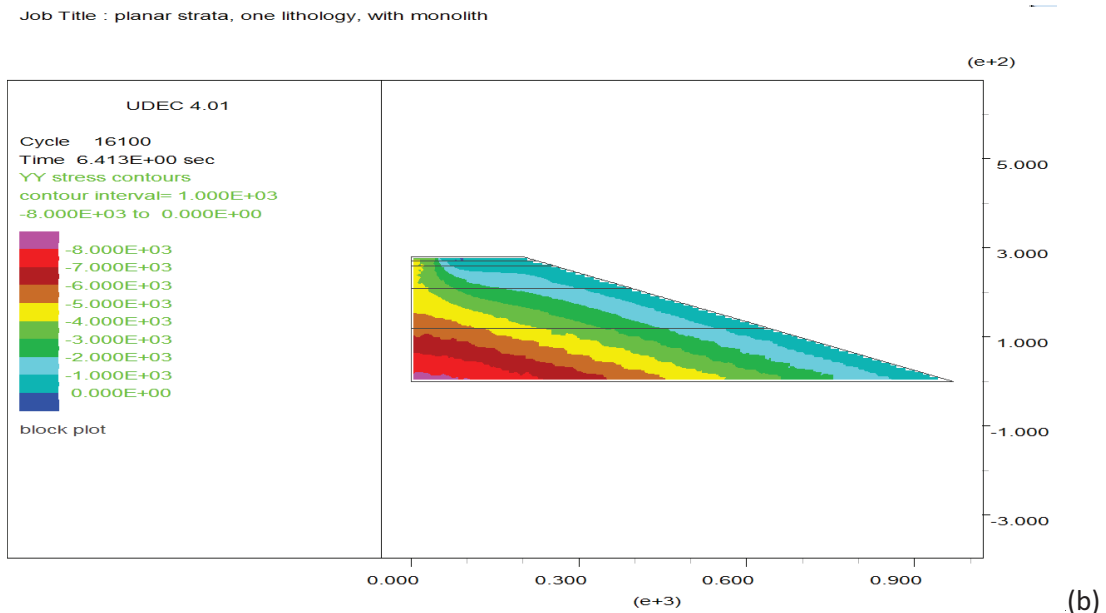
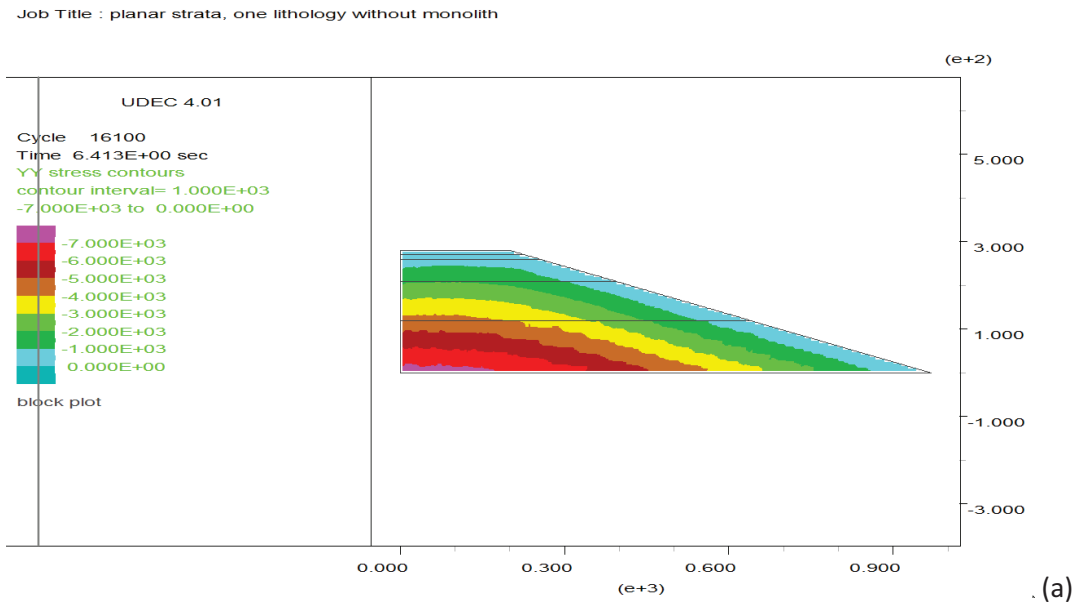


Fig. 8.5. Results comparison for the application of the monolith for the case of a simplified slope without stratigraphy before and after loading.

From the comparison of the stresses (σ_1 and σ_3) developed along the levels central horizons of the mudstone layers of the Travenanzes Formation, high values of the stresses are recorded especially for the deeper layer (Fig. 8.6b). This result is easily

explained by considering that for higher depth the stress due to the weight of the monolith is added to the stress due to weight of the above rock column.

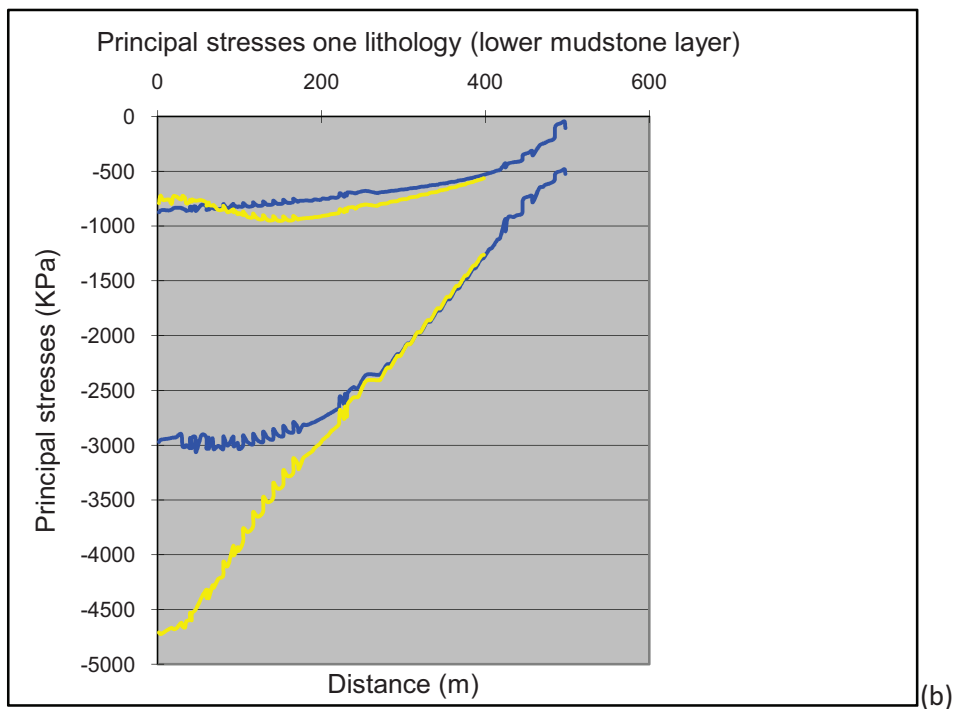
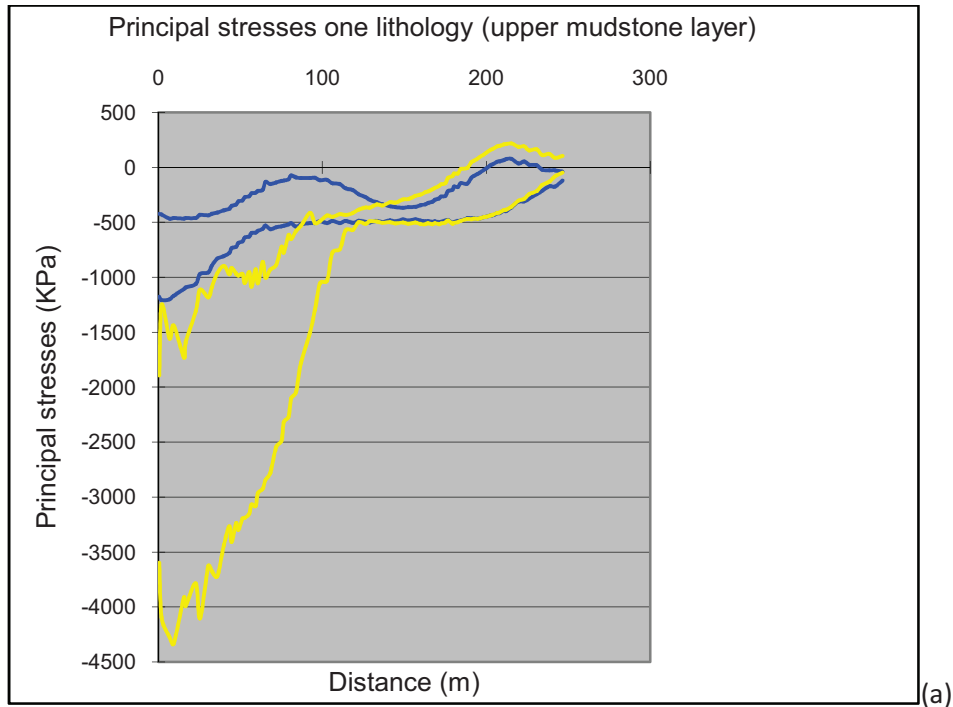


Fig. 8.6. Graphs of principal stresses (σ_1 e σ_3) extracted from key levels within the upper (a) and the lower (b) mudstone layers in the case of uniform slope without monolith (case 1, blue line) and in case of uniform slope with monolith loaded as boundary stress (case 3, yellow line).

Does the stratigraphy influence stress behavior?

By comparing stresses recorded along the central portions of the mudstone layers of the Travenanzas Formation a particular behavior is found. Despite the expectations, the

distribution of the principal stresses along the upper mudstone layer show a disperse trend and a wider peak for the case of the uniform slope compared to the case of stratified slope (Fig. 8.7a and b). This trend can be explained by citing the isotropic characteristic of the model without stratigraphy that, in case of stress application develop in a scarce organization of stress propagation and a minor dissipation of stresses due to the absence of interfaces (layers).

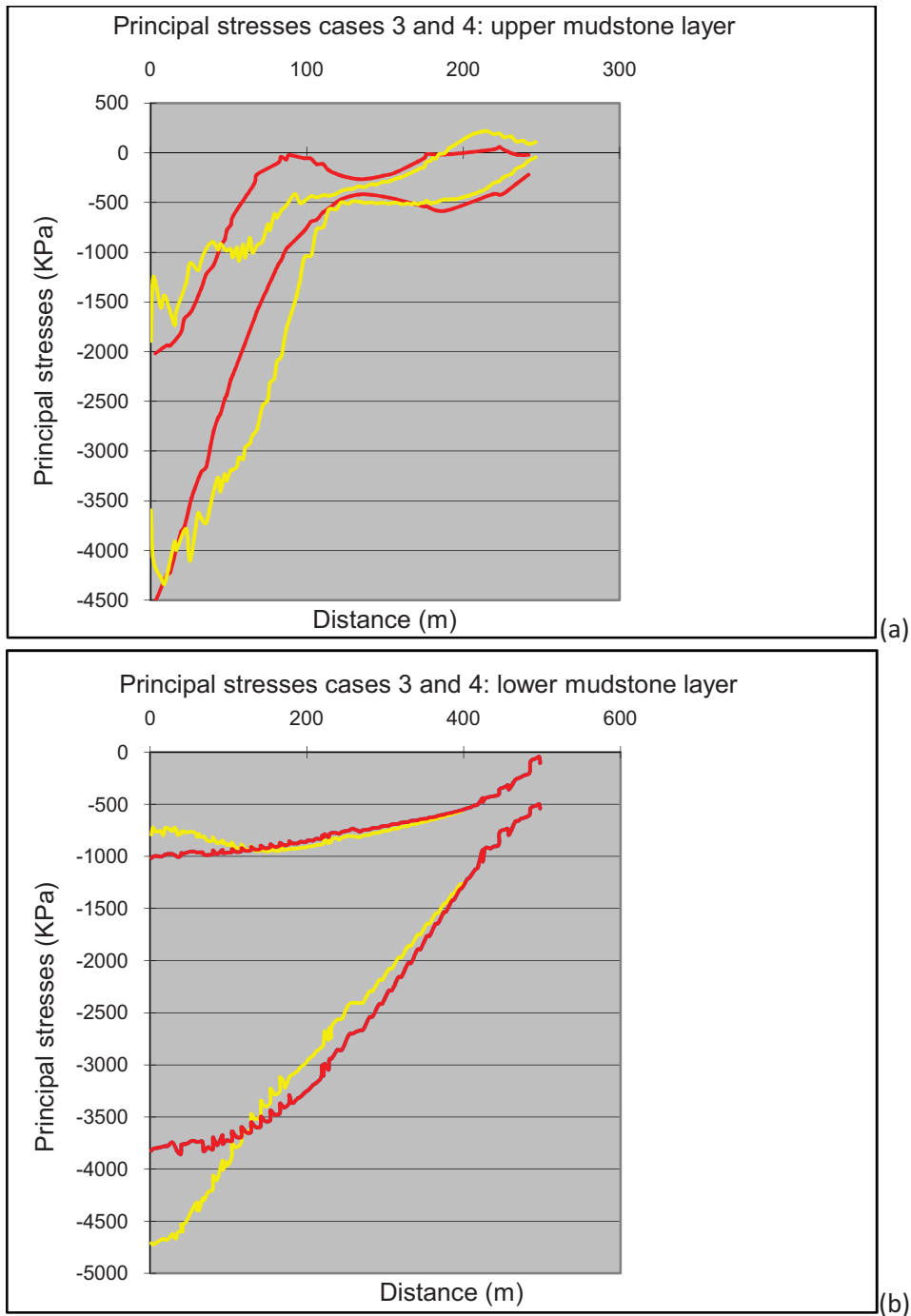


Fig. 8.7. Graphs of principal stresses extracted from key levels in the case of uniform slope with monolith as boundary stress (case 3, yellow line) and in case of planar stratigraphy and monolith loaded as boundary stress (case 4, red line) for the upper (a) and lower mudstone layer (b).

A different behavior is registered by principal stresses when taking into account the cases of absence of monolith as depicted by Fig. 8.8. Along the upper mudstone layer for the case of slope with stratigraphy (case 2, pink line) or uniform slope (case 1, blue line) the same values of σ_1 and σ_3 are recorded therefore suggesting that when no forces act on the slope, the stratigraphy has a minor influence in the overall stress distribution.

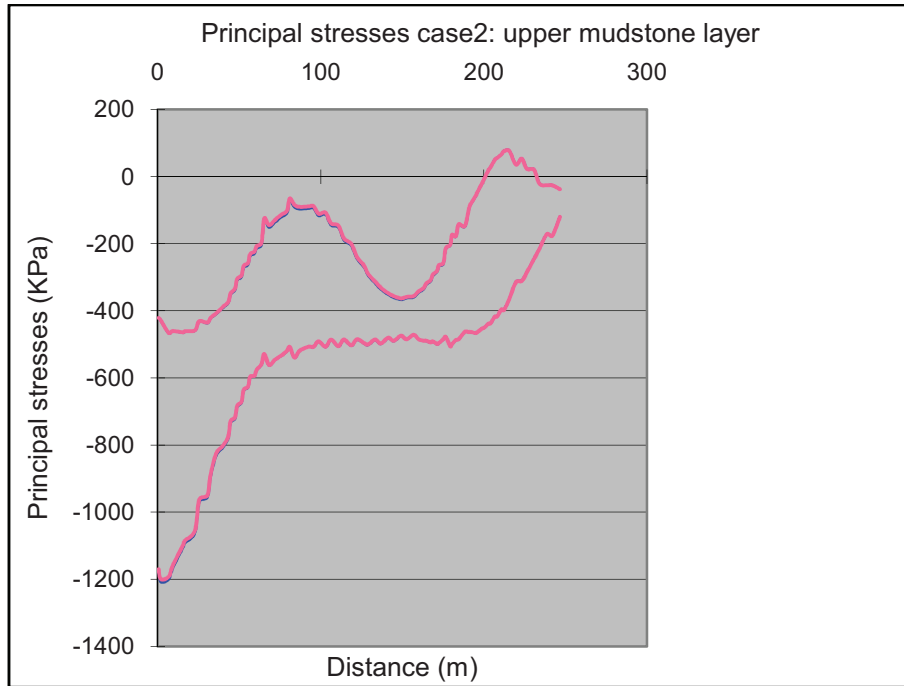
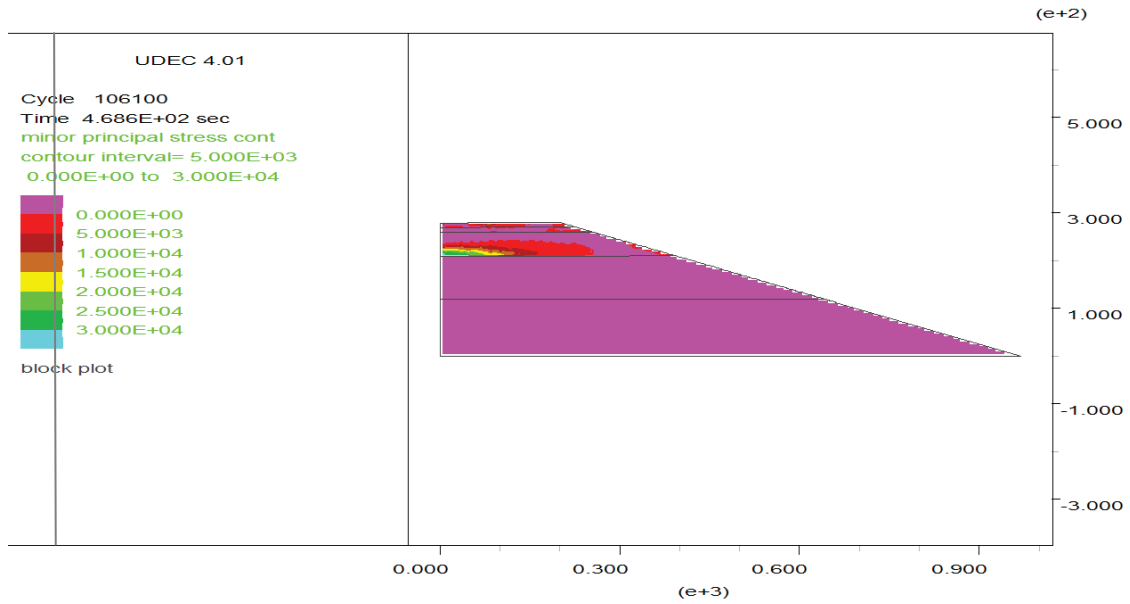


Fig. 8.8. Graphs of principal stresses extracted from key levels in the case of uniform slope without monolith (case 1, blue line) and in case of planar stratigraphy without monolith (case 2, pink line) for the upper mudstone layer.

In the case of simplified model with planar stratigraphy stress distribution within mudstone layer is not largely affected by the elastic modulus of the lithology. However, minimum principal stress in the first carbonate layer in the Travenanzes Formation shows marked tension due to bending of the carbonate plate (Fig. 8.9). This tensile stresses are reduced by introducing the joint families as shown in Fig.8.9b for case 5. The bending process typically occurs in situations where stresses are applied on brittle materials superimposed to a plastic medium; in such cases the volumetric compression under the force action corresponds to a tension on the margins of this volume (Fig. 8.10).

Job Title : horizontal stratigraphy with monolith



Job Title : horizontal jointed strata with monolith

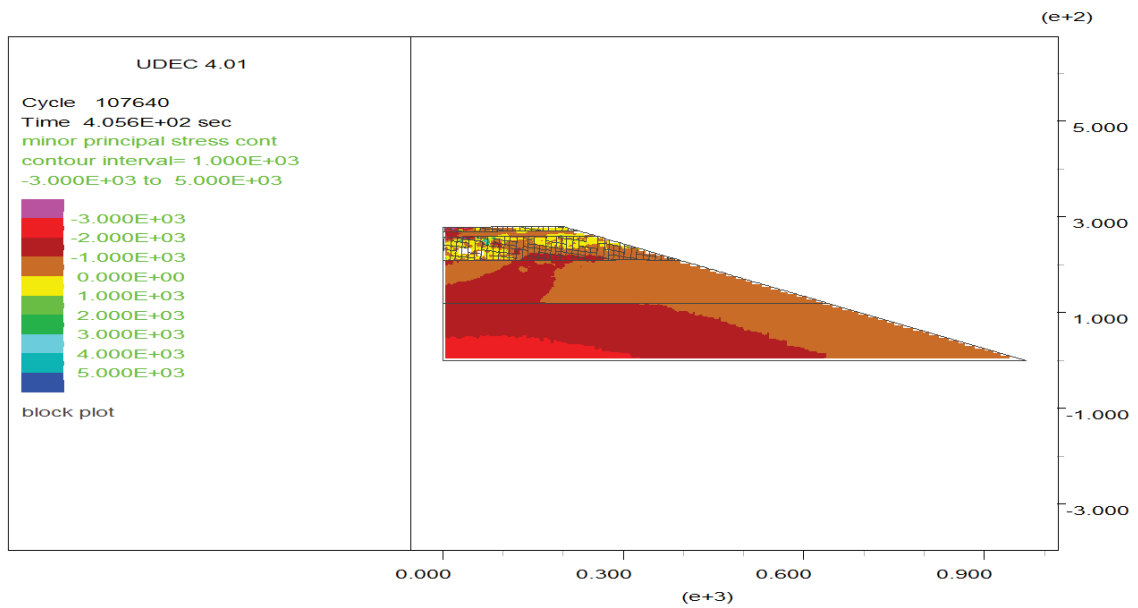


Fig. 8.9. Principal stresses difference result for the case of slope with a top monolith acting as boundary stress. In Fig. 8.8.a is shown the case of a simplified slope with planar stratigraphy (case 4) while Fig. 8.8.b shows the addition of joint families in the model (case 5) a sensible reduction of minor principal stresses is recorded.

Differently from the simplified cases, tensile stresses are observed also in the real section but they develop with small deviations due to the different modeled topography. Minor tensile stresses can be observed in the upper portion of the deeper mudstone layer (Fig. 8.11a).

Another tensile condition can be found for the case of the actual model without monolith; tensile stresses develop in counter scarp area in the southern part of the group (left side on Fig. 8.11a) as a consequence of the displacements directed towards the valley.

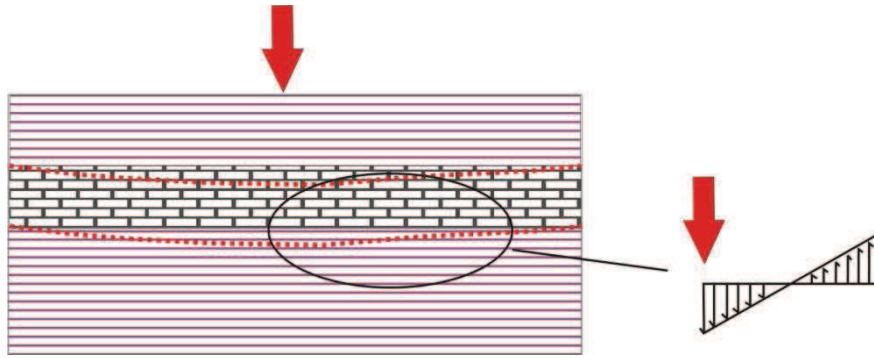
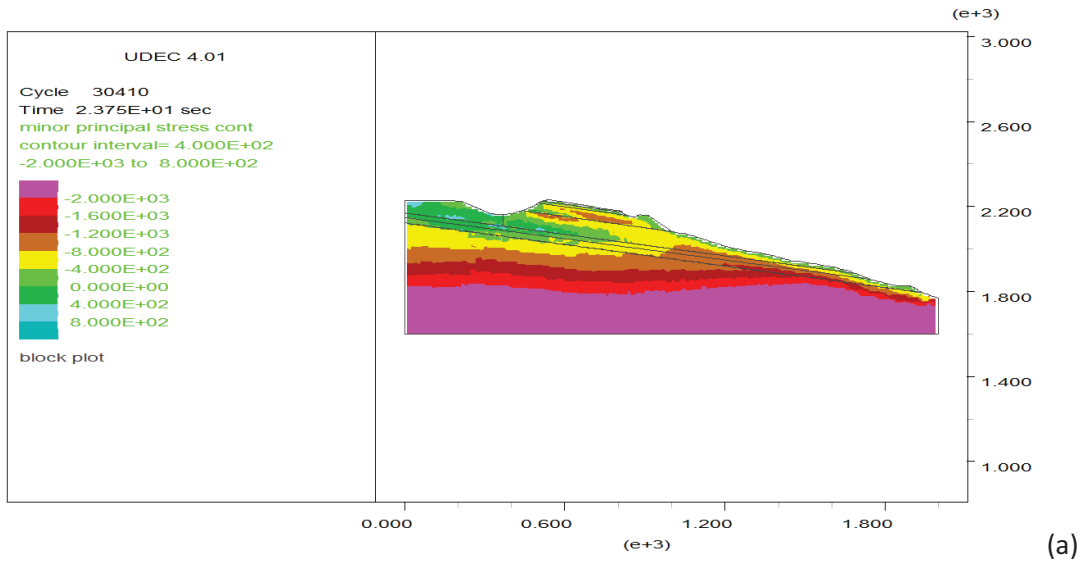


Fig. 8.10. Scheme of the bending mechanism when a local stress is applied on a heterogeneous sequence of strata.

Job Title : Cinque Torri real section, no monolith, no joints



Job Title : Cinque Torri real section, no monolith, no joints

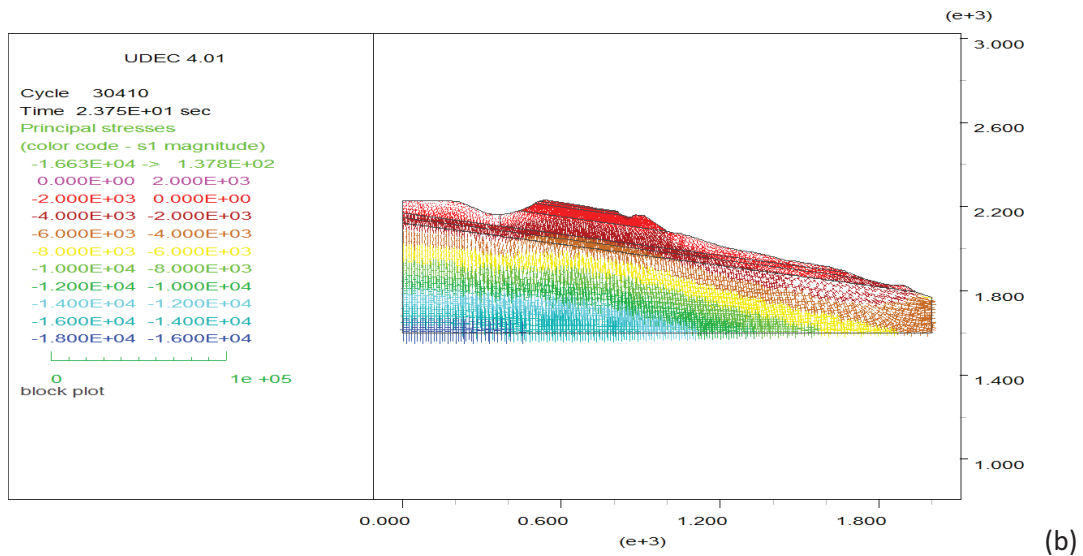


Fig. 8.11. Results for the case of real slope with inclined stratigraphy without monolith loading (case 13): principal stresses difference (a) and tensors principal stresses (b).

When introducing joint families as for the case 13, small tensile stresses develop. It can be therefore deduced that the tensile stresses acting among heterogeneous strata from a geotechnical viewpoint, should be related to a numerical artifact rather than a real physical-mechanical phenomenon. The graphs of the extracted principal stresses at selected horizons, offer a good explanation of the influence of the monolith load and another confirmation that probable failure surfaces will affect the deeper mudstone on the basis of the higher developed stresses.

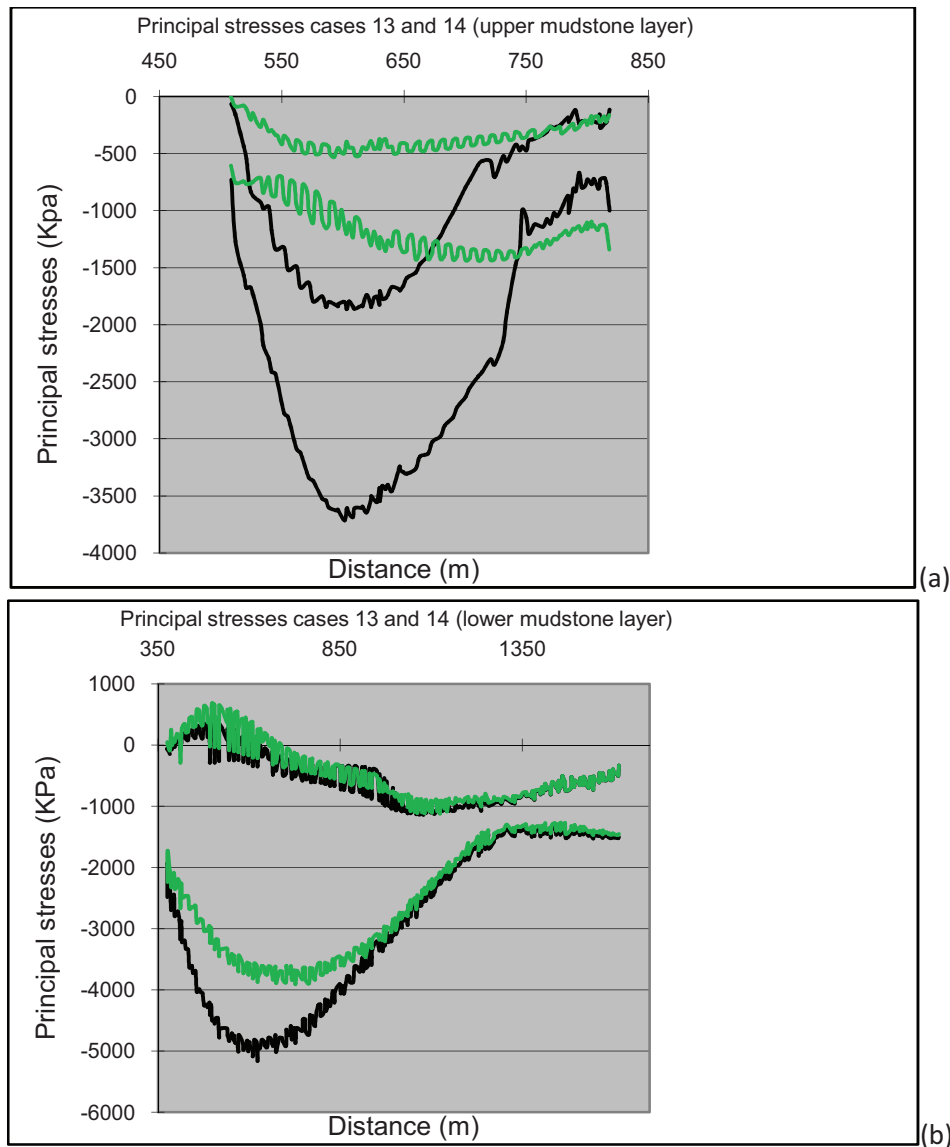
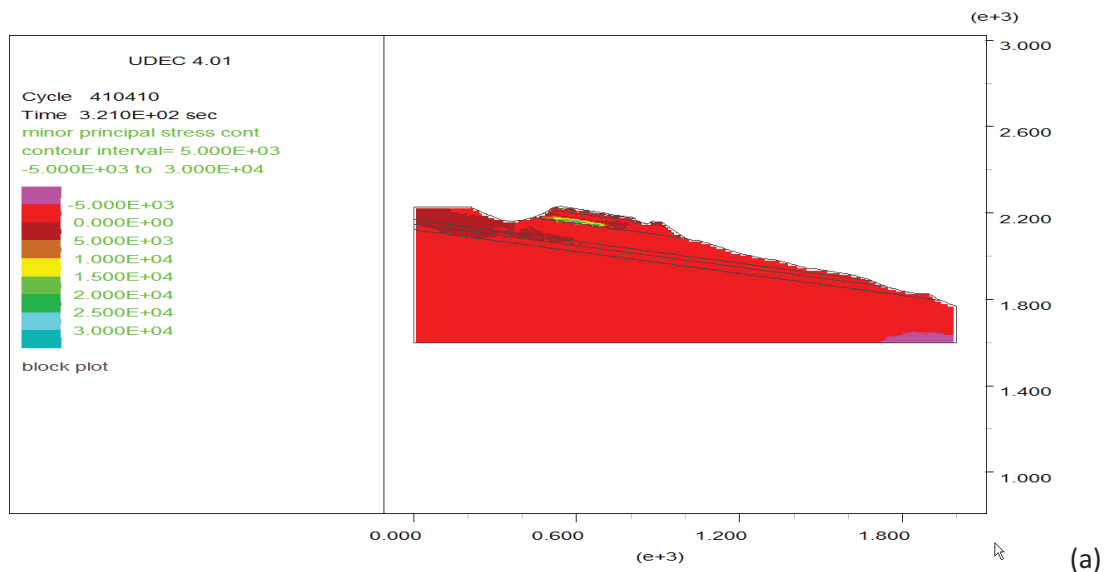


Fig. 8.12. Graphs of principal stresses extracted from key levels in the case of real slope without monolith (case 13, green line) and in case of real slope with monolith loaded as boundary stress (case 14, black line) for the upper (a) and the lower (b) mudstone layers.

Another tensile development occurs when the load of the monolith is accounted for the real model with no joint families in the rock units. The minimum principal stress in the first carbonate layer shows marked tension due to bending of the carbonate plate as happens in the case of simple model with horizontal stratigraphy (see Fig. 8.13).

Job Title : Cinque Torri real section, with monolith, no joints



Job Title : Cinque Torri real section, with monolith, no joints

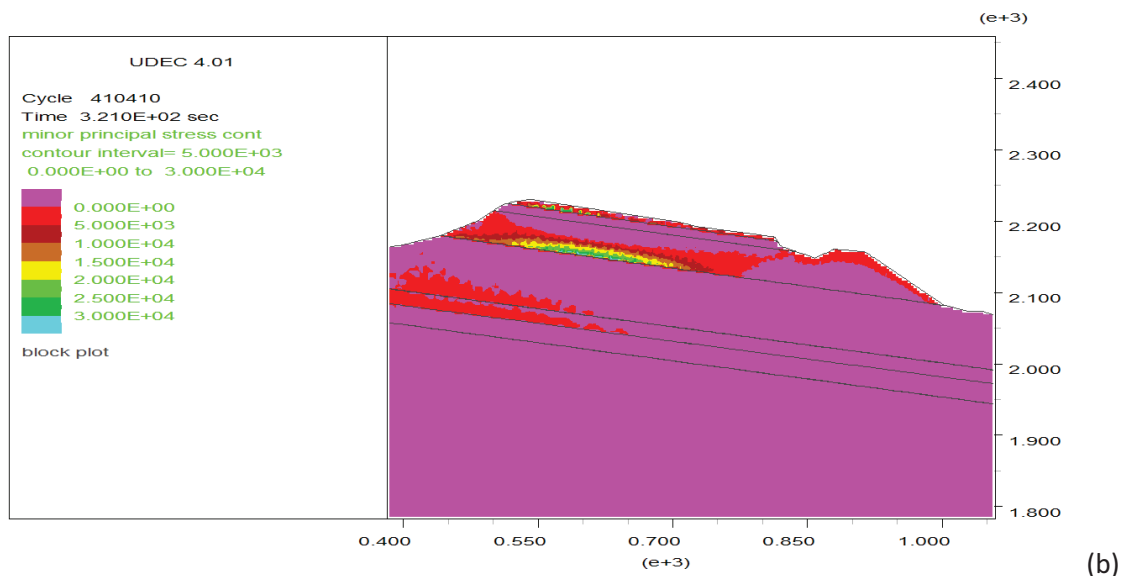


Fig. 8.13. Resulting principal stresses after application of the monolith for the case real slope section with stratigraphy without joint families (case 14). General view (a) and particular of the topmost sector of the slope (b).

This stress scenery even if possible, is quite unrealistic for the setting of the Cinque Torri area. The principal reason is related to the fact that the bending processes regard continuum media with high elastic properties. This is not the case of the dolostones of the Travenanzes Formation which on the contrary are discontinuous rock bodies with moderate elastic values from the results of the laboratory tests. Also for this case in order to create a reliable representation of the Cinque Torri slope, the introduction of the joint systems prevents the tensile stresses development. Among the discontinuity families recovered by the traditional surveys and laser data treatment (Chaps. 6 and 7), only the three most frequent families are significant for the models. These discontinuities are the bedding set and two sub-vertical joint sets with direction parallel

to the main tectonic lineaments. One of these high angle discontinuity sets is not included in the model since its direction is parallel to the trace of the section. Discontinuity sets orientations refer to the values derived from scanline mapping on Torre Grande (Fig. 7.12, Sect. 7.6.4). Table 8.1 summarizes the relevant geometrical data for the discontinuity sets.

Joint set	Dip angle(°)	Trace length(m)	Gap(m)	Spacing(m)
Bedding	10 ± 5	50 ± 20	10 ± 5	10 ± 3
Set NW-SE	87 ± 2	50 ± 20	2 ± 0.5	10 ± 2

Table 8.1. Selected values of joint properties for numerical models in UDEC (Itasca, 2004)

Table 8.2 reports the discontinuity properties estimated for the lithological contacts and rock discontinuities of the carbonatic levels (TVZ carbonates). These properties are based on Young's modulus and Poisson's ratio of the Travenanzes mudstones and are calculated through the followings relations:

$$JK_n = \left(K + \frac{4}{3}G \right) \Delta z_{\min} \quad (8.1)$$

$$JK_s = \frac{JK_n(1-2\nu)}{1-\nu} \quad (8.2)$$

where K and G are bulk and shear modules, respectively, of the block material, and Δz_{\min} is the smallest width of the zone adjoining the joint in the normal direction.

Joint family	Jkn [kPa/m]	Jks [kPa/m]	Jfric [°]	Jcohe [KPa]	Jten [KPa]
A	8.41E+05	4.81E+05	27	100	10
B	8.41E+05	4.81E+05	27	10	10
C	8.41E+05	4.81E+05	27	10	10

Table 8.2. Estimated range of discontinuity strength and stiffness parameters for the contact interfaces between different layers (A) and the first and second joint families introduced in the dolostones of the Travenanzes formation (B, C).

8.3.2 Effects of the stratigraphy and deep angle of layers

In the previous paragraph the role of horizontal stratigraphy in a simplified model is a dispersion of the values of stress and a widening of the relative peak. If the stratigraphy is not planar other important differences happen. Maximum shear stresses in the region outside the loading area in the real section model (case III) are higher than those of the planar model (see Fig. 8.14). This may be due to the effects of inclined layers.

The major principal stress is more close to horizontal than in the case with planar model and as well the minor principal stress is smaller than the correspondent of the planar model. Thus the maximum shear stress (stress difference) is larger in the case of real model (case III); implying that inclination of the layers may be the contributing factor that induces higher shear stresses.

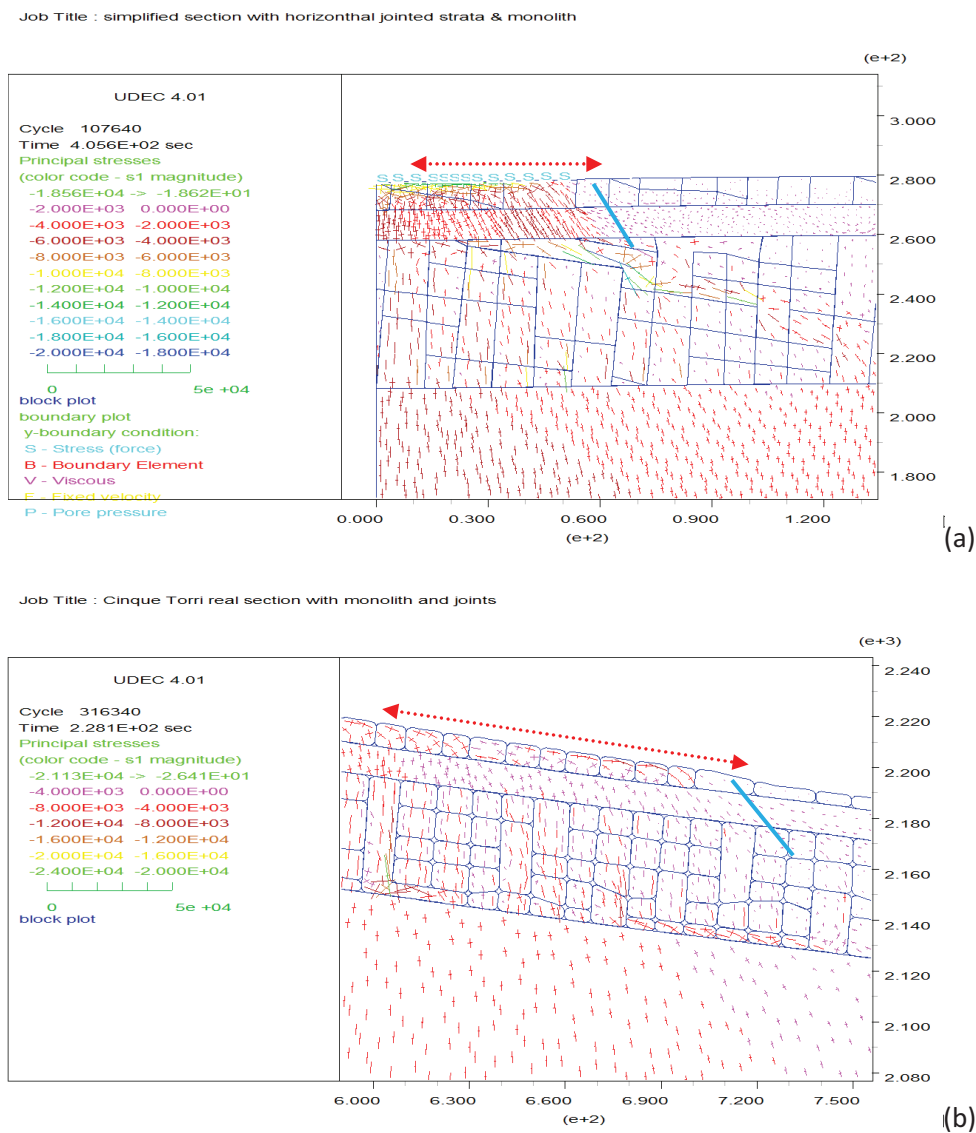


Fig. 8.14. Comparison of the resulting principal stress tensors after application of the monolith for the case of the simplified model with planar stratigraphy and joint families (case 6) (a) and the case of real slope section with stratigraphy and joint families (case 16)(b).

The different stress conditions can be explained taking into account that the tangent component of the stress increases from the planar to the stratigraphy cases, therefore the destabilizing forces increase accordingly. If in turn the influence of the joint is assessed by comparing the principal stresses for the simplified cases 10 and 12, it can be easily discovered that higher values of σ_1 develop within the lower mudstone layer (Fig. 8.15b) directly below the surface of action of the monolith stress.

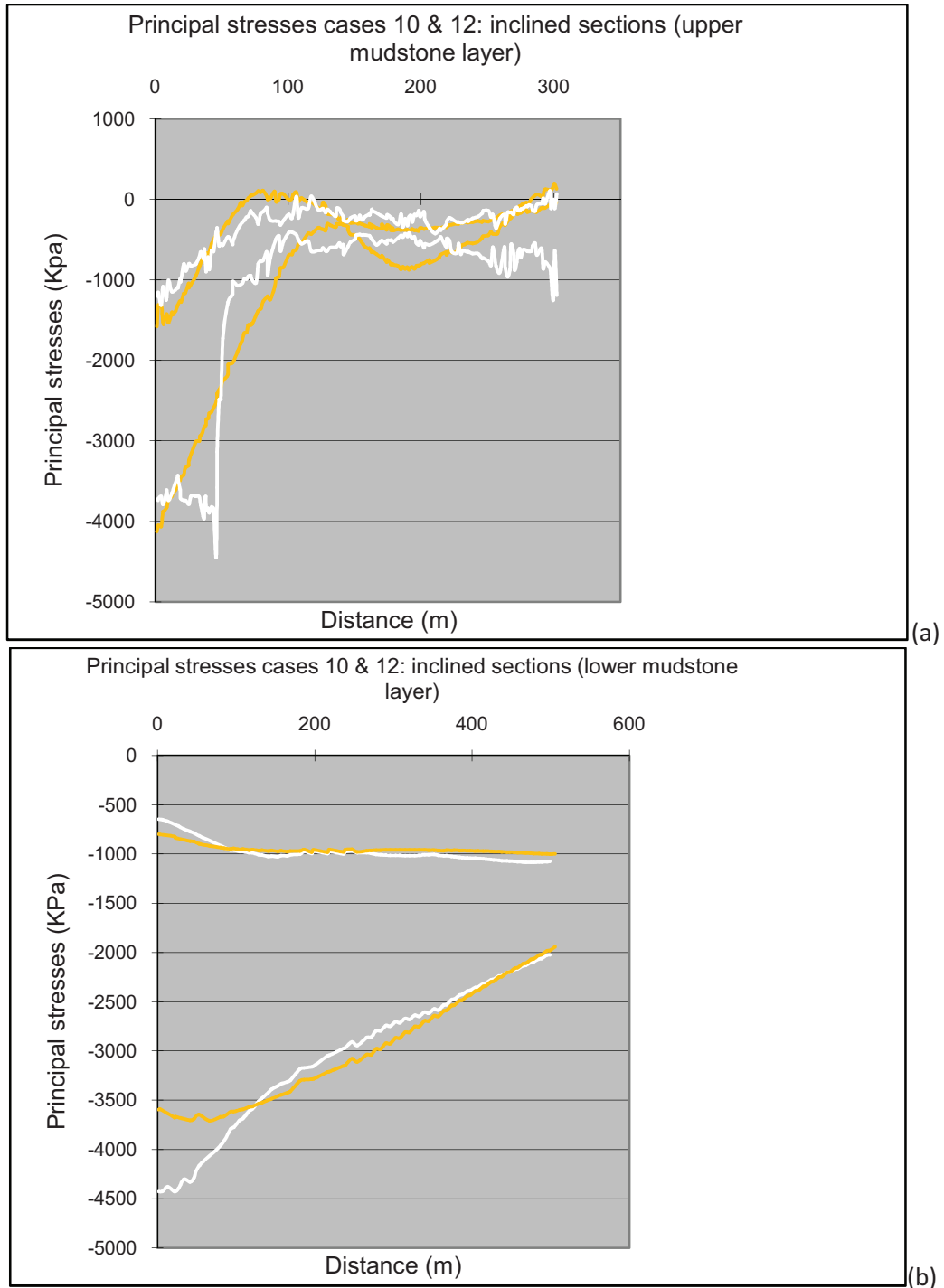


Fig. 8.15. Comparison of the resulting principal stresses recorded within the upper (a) and the lower (b) mudstone layer for the case of the simplified model with inclined stratigraphy without joint families (case 10) and the case the simplified model with inclined stratigraphy with joint families (case 12).

8.3.3 Shear strength reduction method

The Shear Strength Reduction Method (SSRM) was applied to the studied models in order to verify the deformation pattern of the DSGSD and make a comparison with these results with the rotational analysis interpretations (Chapter 6, Section 6.5.2).

In the analysis of slope stability, mechanical properties of blocks and joints should be accounted (Hurlimann et al.,2006; Nichol et al.,2002). In case of lithologies with low strength properties the displacements are driven mostly by the entire rock mass while for lithologies characterized by high quality, limited deformation starts along the existing discontinuities. In addition, when the slope as for the Cinque Torri case is made by a heterogeneous stratigraphy, the effect of the geological interfaces is considerable.

A staged analysis was performed to simulate strength degradation through incremental lowering of the rock mass cohesion and friction angle for the case of real section with stratigraphy. This modeling induces the loss of coherence in the units of the Travenanzes Formation through plastic deformation processes. This approach can be useful when the lack of geotechnical data does not allow carrying out a proper slope stability analysis and therefore a reliable evaluation of the relationship between resisting and destabilizing forces (i.e. factor of safety) for a defined condition of the slope. In such a frame the intent is to move towards a better recreation of the shapes and features of the instability by assuming that post-glacial processes and the seasonal changes in groundwater pressures are the key factors that may have reduced internal strengths.

The method of shear strength reduction is organized in two main stages (Fig. 8.16):

- Stage1: Definition of the reduction ratio and preliminary test to verify the sensitivity of the model to the changes.
- Stage 2: increase the reduction ratio until a clear shape of deformation is reached.

The most unstable areas are thus selected.

The results indicate that a reduction of the cohesion and friction of the layers within the TVZ formation of three orders of magnitude principally causes the development of a circular deformation zone right below the monolith represented by an external stress loading (Fig. 8.17).

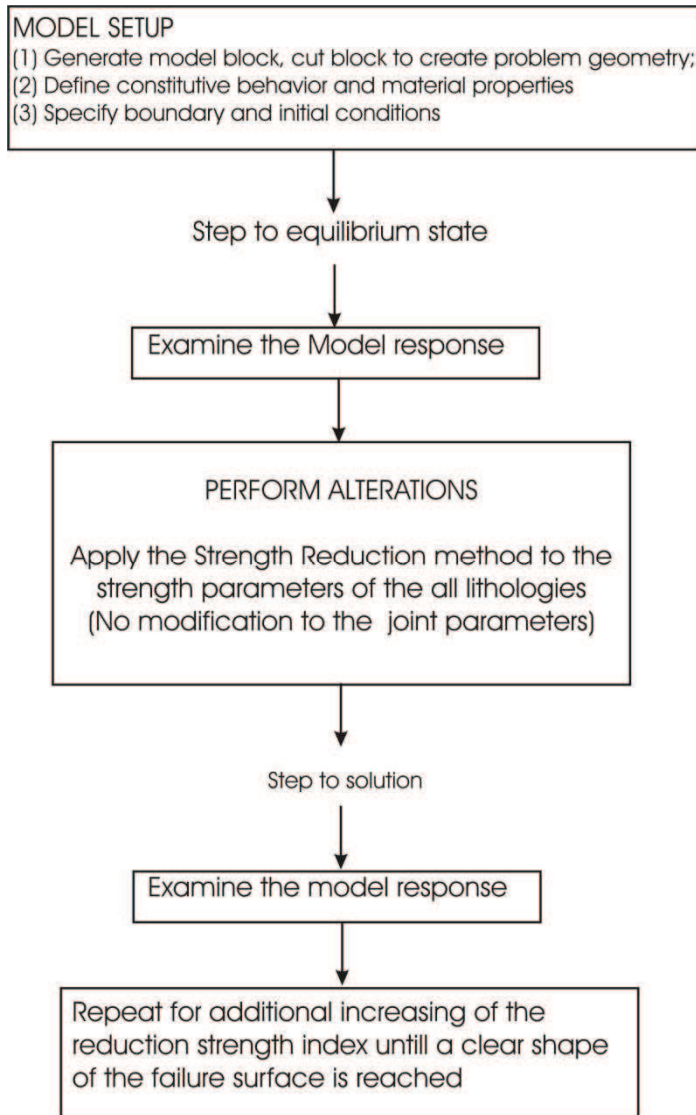
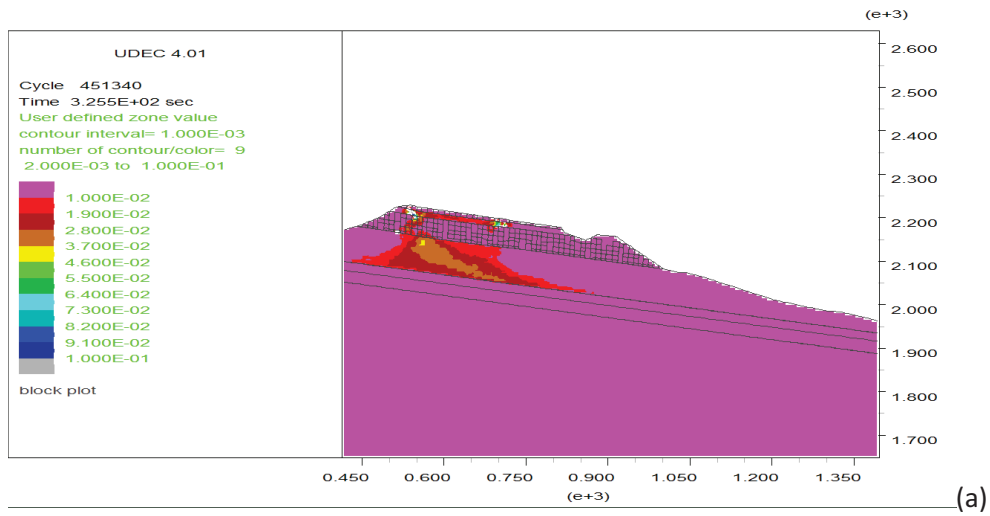


Fig. 8.16. Scheme of the adopted methodology for the Shear Strength Reduction method of the Cinque Torri DSGSD

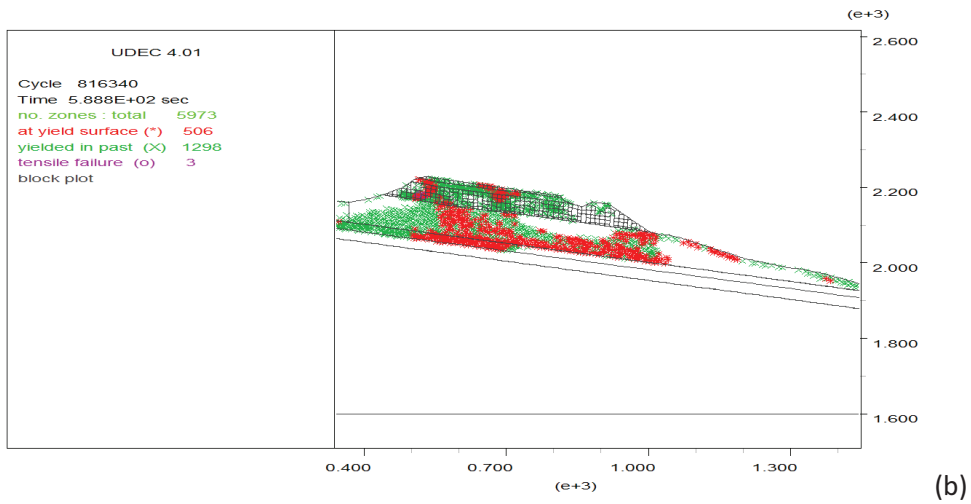
Fig. 8.17a represent the strain of the model zones while in Figs. 8.17b,c the plasticity state of the nodes composing the model is plotted. By comparing these results some differences are noticed. It is recommended to take into major account the results from strain computation since they represent an interpolation among close nodes thus a general behavior, which smoothes the effect of local variations.

By reducing the strength of the model with uniform properties, propagation of shear failure zone was found to develop from uppermost edge of the monolith towards the center of the section with a circular shape. In addition, when applying the SSRM to a slope section with stratigraphy, the output deformation features have a pseudo-circular shape in the topmost part, while below they follow a planar shape. This implies a significant influence of strata orientation. In addition other factors such as presence of weak surfaces and joint families in the TVZ carbonate layers may lead to generation of a pseudo-circular deformation which can develop into a sliding surface.

Job Title : Cinque Torri SSRM



Job Title : Cinque Torri DSGSD SSRM



Job Title : Cinque Torri SSRM

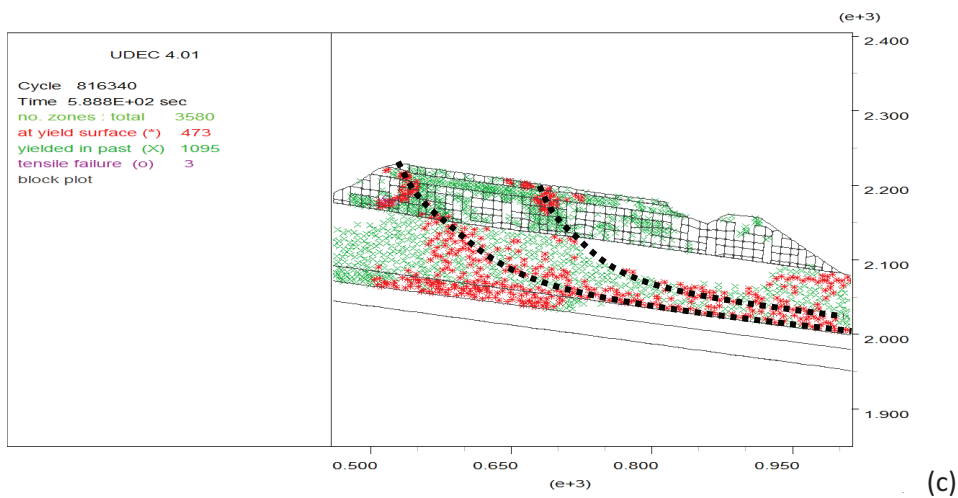


Fig. 8.17. Plots of zone strain (a) and plastic point (b, c) after application of the monolith and reduction of shear strength (RF =1500) for the case of real slope section with stratigraphy and joint families (case 16).

The results of all the examined case reduce significantly the present-day geotechnical properties but give a realistic impression of the morphologies observed on fields (the counterscarps and minor slides within the top slope) and a good correlation with the interpreted mechanisms from the rotational components analysis (Chapter 6). The SSRM represents a support to these interpretations improving the understanding of the global deformation pattern of the slope without any quantitative purpose to calculate absolute exact movements or instability conditions.

The analytical solutions showed that even if both the mechanical properties of the rock and the buried geological setting of the slope are important in predicting final stress-strain distribution, the qualitative analysis of deformations can as well be achieved by forcing the system to collapse.

8.3.4 Results of the numerical models in UDEC

The numerical models run in UDEC (Itasca, 2004) is intended to improve some aspects referring to the general understanding of the Cinque Torri DSGSD by introducing field and laboratory data in simplified numerical models. The site investigations and the results of the rotational components (Chapter 6) suggest that the deep deformation can develop from a complex circular deformation zone, but at present-day there is not available direct information on the instabilities affecting the slope. In order to improve the knowledge of both the pattern of the slope deformation and the influence of the different geological, morphological and structural features, 2D distinct element modeling has been carried out simulating the stratigraphy and influencing forces of the rock slope. The Cinque Torri slope is located at a river valley that was subjected to glacial erosion during Pleistocene and to the subsequent decompression of valley walls after ice retreat. These processes were indirectly analyzed into the models to account for the evolving stress history and decreasing of the internal strength. In addition, during modeling, focus was set on the effect of four different factors on stress and strain distribution: (1) monolith loading, (2) strata heterogeneity, (3) dip angle of strata, (4) rock discontinuities.

From the analyses of the influencing factors of the DSGSD some considerations have been pointed out:

- a. in the cases of absence of monolith, the influence of stratigraphy on stress and strain distribution is negligible (Fig.8.8);
- b. in the cases of the presence of monolith the strata act as constraint for the stresses distribution (the peak of the principal stress for the upper mudstone layer show less dispersion with respect the homogeneous slope cases) (Fig. 8.7a)
- c. both for the upper and the lower mudstone layers high principal stresses are recorded, therefore possible movements can start at the top and develop until the bottom of the lower mudstone layer (as expected).
- d. by comparing the values of the recorded principal it can be deduced that in the lower TVZ mudstone layer possible failures are more likely to occur respect the condition of the upper TVZ mudstone layer.

- e. from a first analysis of the II model (inclined case) an important role is played by the inclination of the strata (higher values for the shear components) even if the mean dip angle is only 10 degrees. Stress shows higher values and wider peaks in the inclined cases (Fig. 8.15).
- f. the presence of rock discontinuities within the carbonatic layers reduce the tensile stress development (Fig.8.9) and influences the deformation zone propagation (Fig. 8.17b).

The calculations of the Shear Strength Reduction Method show that this approach of simulating the stress history of the site is a powerful even if qualitative approach for the prediction of the instability features. The comparison of the outcomes of this approach and the interpretations derived by the rotational components analysis agree with the presence of a pseudo-circular deformation zone which develops from the upper toe of the monolith contact towards the interface between the lower mudstone layer and the lower carbonate layer of the Travenanzes Formation.

8.4 Modeling with Plaxis 8.5

Among the different method of numerical models, stress-deformation analysis has been commonly conducted through distinct or finite element numerical methods and used to understand many cases of slope instabilities involving among others incoherent and cohesive soils.

Plaxis (Brinkgreve et al., 2008), is a finite element package, enabling two-dimensional analysis of deformation and stability in geotechnical engineering. Geotechnical applications require advance constitutive models for the simulation of the non-linear, time-dependent and anisotropic behavior of soil and/or rock.

DSGSDs are generally characterized by small displacements in the range of few centimeters per year and due to their nature the use of finite elements stress deformation analysis is a suitable approach. In such physical simulation process, the physical system is first idealized to a mathematical model represented by mathematical equations based on continuum mechanics. The mathematical model is then transformed to a discrete model using the finite element method. Finally, the discrete model is solved for the physical system in the form of discrete solutions such as displacements, stress and strain (Brinkgreve et al., 2008; Chang et al., 2010). The finite element method treats a continuum as an assemblage of discrete elements with nodes. The link between nodal displacements and displacements at any point is established by shape functions for interpolation. Thus, the nodal displacements, stresses and strains at integration points of elements can be introduced to comply with the equations of the continuum concept (Brinkgreve et al., 2008).

$$\varepsilon = Lu \quad (8.3)$$

where ε is a strain vector, L is the matrix of a differential operator, and u is a displacement vector.

$$\sigma = S\varepsilon \quad (8.4)$$

where σ is a stress vector and S is a stress-strain matrix.

$$L^T \sigma + f = 0 \quad (8.5)$$

Where L^T is a transpose of the differential operator and f is a vector of body force.

$$M\ddot{u} + C\dot{u} + ku = F \quad (8.6)$$

Where M is a mass matrix, C is a damping matrix, K is a stiffness matrix and F is a load vector. In particular from the equation (8.6) derives that the difference between the external force vector and the internal reaction vector should be balanced by a stress increment.

The frequent non-linear relation between stress and strain requires a global iterative procedure to satisfy the equilibrium conditions (eq.4) and some defined boundary conditions are then needed.

Plaxis (Brinkgreve et al, 2008) is a geotechnical software based on the finite element method for solving deformation and stability problems pertaining to slopes, embankments, foundations, and excavations. The software can also be used to analyze site response, soil-structure interaction, and slope problems under earthquake loading.

The FEM modeling idealizes and discretizes the physical systems to a discrete model. Then, the discrete model is solved to obtain the discrete solution. The solution error is significant, and the error is mainly from idealization and discretization. In the numerical modeling of a natural slope, it is inevitable to simplify the underground conditions as homogenous strata for establishing the geometry model. As reported in other works (Lin et al., 2008; Chang et al., 2010), although the model parameters are given accordingly to extensive investigations, uncertainty remains. An attempt to decrease these uncertainties is to fix the known parameters and to assess the slope stability with different values of the most uncertain parameters such as strength of the cohesive layers and the water level.

8.4.1 Plaxis elaborations

The Cinque Torri DSGSD is modeled in terms of a two-dimensional plane strain condition. The section X-X' (Fig. 8.3, 8.4) used for the DEM modeling is treated also for the FEM modeling. As for the DEM cases also for this elaboration the slope is simplified to seven strata ascribed to the Travenanzes Formation (TVZ) at the top, followed by the Heiligkreuz Formation (HKZ) and the basal DolomiaCassiana (DC) (Fig. 8.18).

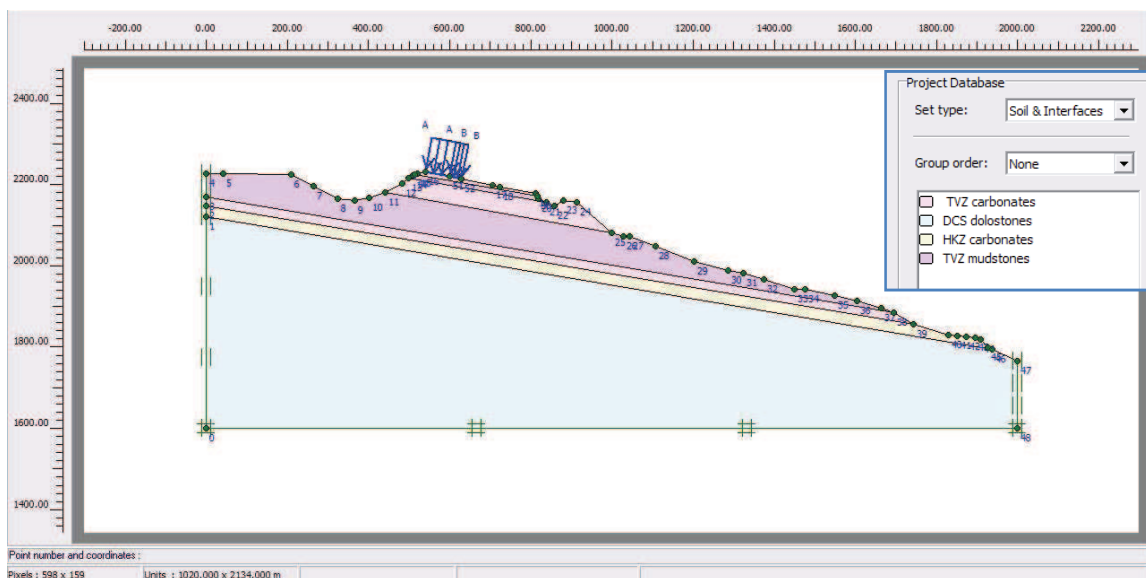


Fig. 8.18. PLAXIS numerical model of the Cinque Torri DSGSD. Model setup of the geometries, materials and applied load. The trace of the section is sketched on Fig. 8.4.

The model is discretized in a mesh made up by triangular elements linked on each other by nodes. Every modeling code require a computation time which is function of the number of element of subdivision of the initial model therefore, as for the Cinque Torri model, a very fine mesh corresponds to a longer computation time but guarantees accurate solutions. With the attempt to make comparisons with the UDEC elaborations the same rock parameters, conditions as well as uncertainties are considered. The geological interfaces also in this model are expected to have low friction angles due to the natural soaking in groundwater typical at the contact between heterogeneous lithologies. Hence the strength properties of the less competent lithologies are used as

input value in the model. The uncertain groundwater conditions induce to set the water level at the bottom of the section and to assign saturated conditions only for the cohesive layers as previously settled for the UDEC models. With such a solution the most severe conditions are analyzed.

Modeling in Plaxis requires, after a first set up of the geometries and the parameters for materials, the initial stress calculation through the equilibrium of the self-weight of the geomaterials, followed by the pore pressure calculation and, as final step, the application of the external stresses due to the weight of monoliths.

The model investigates the stress-strain behavior in the Cinque Torri slope by assigning an elasto-plastic Mohr-Coulomb constitutive criterion for the mudstone layers and a rock-jointed model for carbonatic layers and the parameters summarized in Table 7.7 (Section 7.6).

There are many criteria to model the mechanical behavior of soils and soft rocks and the related accuracy differs and for example, for the case of the Hooke's law of linear, isotropic elasticity, the stress-strain relationship is sometimes too simplistic and therefore not sufficiently accurate since it considers few input parameters, i.e. Young's modulus, E , and Poisson's ratio, ν . More information should be accounted in order to capture the essential features of soil and rock behavior.

In the Mohr-Coulomb model five input parameters are considered, i.e. E and ν for soil elasticity, φ and c for soil plasticity and ψ as an angle of dilatancy. This model represents a "first-order" approximation of soil or rock behavior and is particularly recommended when first approaching the analysis or when the material properties are not well classified as for the Cinque Torri case.

In the case of an anisotropic elasto-plastic model as the Jointed Rock model, plasticity can only occur in a maximum of three shear directions (shear planes), each characterized by its own strength parameters φ and c . The intact rock is considered to behave fully elastic with constant stiffness properties E and ν . Reduced elastic properties may be defined for the stratification direction as for the present application (Table 8.2).

Properties of jointed materials are conditioned by their anisotropies. As a result, they may respond differently when subjected to particular oriented conditions as the monolith loading. In this frame, a distinction between elastic anisotropy and plastic anisotropy should be highlighted. Elastic anisotropy refers to the use of different elastic stiffness properties in different directions. Plastic anisotropy may involve the use of different strength properties in different directions, as considered for the Jointed Rock model. The JR model is an anisotropic elastic perfectly-plastic model, suitable to simulate the behavior of discontinuous rock layers. Discontinuities are represented by stratification and major joints. The intact rock is considered to behave as a transversely anisotropic elastic material, quantified by five parameters and a direction. In the major joint directions it is assumed that shear stresses are limited according to Coulomb's criterion. Upon reaching the maximum shear stress in such a direction, plastic sliding will occur. In PLAXIS JR model up to three sliding planes can be defined, and arbitrarily the direction of plane 1 coincides with the direction of stratification. The model moreover is particularly useful when modeling joint families with spacing smaller to the overall slope

dimension. Each plane is characterized by the strength parameters c_i , ϕ_i , ψ_i and $\sigma_{t,i}$. On each discontinuity plane a local Coulomb condition applies to limit the shear stress, $|\tau|$. In addition, by introducing a tension cut-off criterion, the tensile stress on a plane is limited.

In the case of the mudstone layers on the TVZ formation, which enclose the maximum deformation in the DSGSD context, viscous effects such as creep and stress relaxation should be accounted. Generally soils and very soft rock types (strength in order of an incoherent medium) exhibit some creep and primary compression later followed by a certain amount of secondary compression. The latter phenomenon is most dominant in soft soils, as for example normally consolidated clays and silts. The Soft Soil Creep (SSC) model has been implemented in PLAXIS to analyze loading problems as cases of foundations and embankments but it is not appropriate in case of excavations problems for which instead a Mohr-Coulomb model is more representative (Brinkgreve et al, 2008). Since the Cinque Torri slope is affected by a local stress due to monolith loading thus a foundation-like condition, the SSC model seems to be the most promising approach.

Near-normally consolidated silts show in general high compressibility. From Chapter 5 the sampled mudstone layers are classified to have from medium to high compressibility in relation to an increase of clay content. This characteristic is therefore well reproduced by the SSC model which also can reproduce a linear stress-dependency of soil stiffness.

The advantage in applying this model to the mudstone layers of the Cinque Torri slope lays on the possibility to reproduce the creep behavior: when a stress acts on a clay/silt-rich slope, generally the primary compression is followed by a secondary compression which activated during a long period after the initial loading and it is a percentage of the primary compression. The higher is the initial compression the more developed is the creep.

The loading for the Cinque Torri slope is represented by the rock monoliths, which were not placed at one time in the present-day position (as an external pressure) but are probably the result of selective erosion, started during Post-glacial age, of a former carbonatic platform. It can be deduced that the layers of the slope under the Cinque Torri group underwent to a pressure release and subsequently, the new topographic setting determined new stress conditions. At this point a question arises: from postglacial age to present-day, layers have been normally consolidated? In other words, the monolith loading is inducing now a primary or a secondary compression? And distal deformations such as the reactivated mudflow can be ascribed more to the stress release due to slope unloading after glacial erosion or to a propagation of strain from the toe of the monoliths towards the surroundings? Which kind of mechanical changes are induced on lithotypes after a sudden tensional release? If the mudstone layers were over-consolidated before ice settlement, the following erosion and local loading produced probably normal-consolidation and therefore a significant creep of the unloaded slope.

The lack of information does not allow a certain answer, but if the attention is focused only on the present-day conditions, the primary compression of the monolith has been absorbed during the last 15.000 years thus, now the secondary compression is acting.

The latter is probably influenced by the changes in water content, that induce volumetric deformation in the soft mudstone layers of the Travenanzes Formation. These cyclic phenomena can be defined as creep, and the PLAXIS modeling focus also on it.

The main characteristics of the Soft-Soil-Creep model can be summarized as follow:

- Stress-dependent stiffness (logarithmic compression behavior);
- Distinction between primary loading and unloading-reloading
- Secondary (time-dependent) compression
- Memory of pre-consolidation stress
- Failure behavior according to the Mohr- Coulomb criterion.

The needed parameters are the failure parameters as in the Mohr-Coulomb model, that is the effective cohesion c , the friction angle, φ , and the dilatancy angle ψ . Typically for fine grained, cohesive soils, the dilatancy angle tends to be small, it may often be assumed that ψ is equal to zero. Moreover basic stiffness parameters, the modified swelling index k^* , the modified compression index λ^* and the modified creep index μ^* are specified. These three last parameters can be obtained both from an isotropic compression test and an oedometer test (Fig. 8.19).

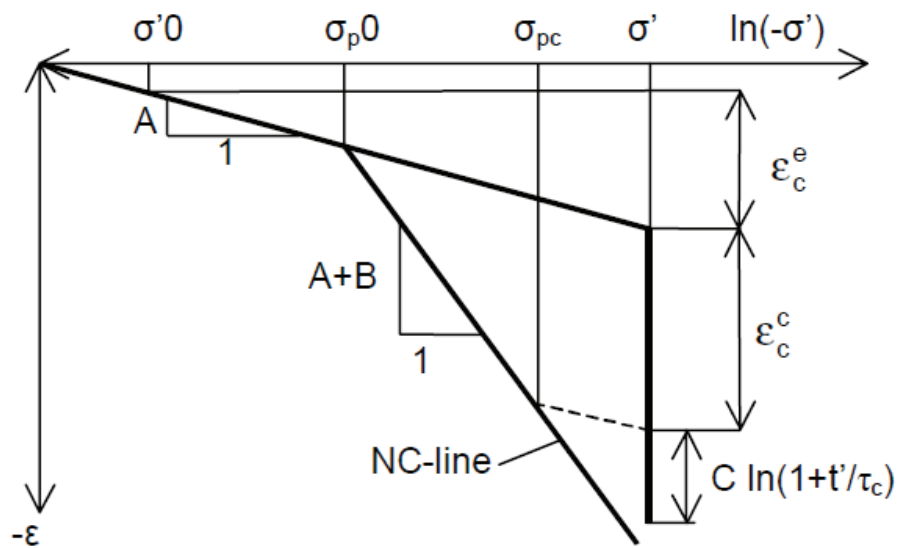


Fig. 8.19 Theoretical stress-strain curve derived from oedometer test. The slope of the Normal consolidation curve corresponds to the modified compression index. The elastic and creep component of the strain increments are underlined (after Brinkgreve et al, 2008).

If such tests can be carried out, the modified compression index λ^* equals to the slope of the normal-consolidation line (NC-line on Fig. 8.19):

$$\lambda^* = \frac{C_c}{2.3 (1+e)} \tag{8.7}$$

where C_c is the Compression index and e is the void ratio.

The slope of the unloading line (Fig. 8.19) is related to the modified swelling index k^* by the following relation:

$$k^* \approx \frac{2}{2.3} \frac{C_r}{(1+e)} \quad (8.8)$$

where C_r is the swelling index.

Finally the parameter μ^* derives from the volumetric strain on the long term plotted against the logarithm of time as shown on Figure 8.19:

$$\mu^* = \frac{C_\alpha}{2.3 (1+e)} \quad (8.9)$$

and C_α is the creep index that derives from a material constant C_B according to Garlanger (1972) from the relation:

$$C_\alpha = C_B (1 + e_o) \quad (8.10)$$

In the present study the chosen values has been fixed according to empirical criteria since no laboratory tests were available. For a rough estimate of these model parameters the correlation $\lambda^* \approx \frac{I_p (\%)}{500}$, where I_p is the plasticity index, and in addition to account that $\frac{\lambda^*}{\mu^*}$ is in the range between 15 to 25 and the general observation $\frac{\lambda^*}{k^*}$ is in the range from 5 to 10.

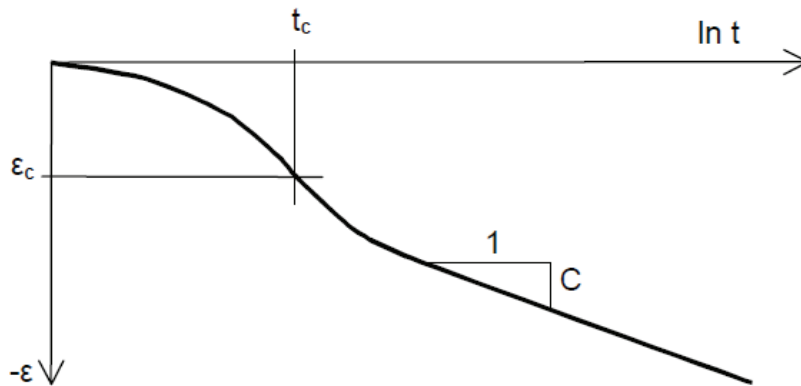


Figure 8.20 Consolidation curve derived from oedometer test with constant load. Consolidation strain ε_C is plotted as function of the logarithmic time (after Brinkgreve et al, 2008).

When analyzing results of the modeling care should be taken in the judgment of the reliability of the computational results since SSC model has some limitations due to the approximate nature of the modeling. Moreover when analyzing cycling loading soil dilatancy and debonding effects are not accomplished in the SSC model, but such limitations do not affect the Cinque Torri model.

8.4.2 Plaxis results

The interpretations of the numerical analyses carry out using PLAXIS software are constrained by geological knowledge of the area, field observations and the previous interpretative models obtained by the rotational components analysis (Chapter 6, Section 6.5.2) and UDEC modeling (Section 8.3.4). The most representative sections are shown in this paragraph.

In PLAXIS, tensile (normal) stresses are defined as positive whereas compression is defined as negative.

The Cinque Torri model investigates the stress-strain behavior of the slope as consequence of the monoliths loading. Deep deformation zone follow initially the dip angle of the high angle rock discontinuities (planes 1 and 2) and at higher depth it becomes parallel to a geological interface as reported in Figure 8.21b.

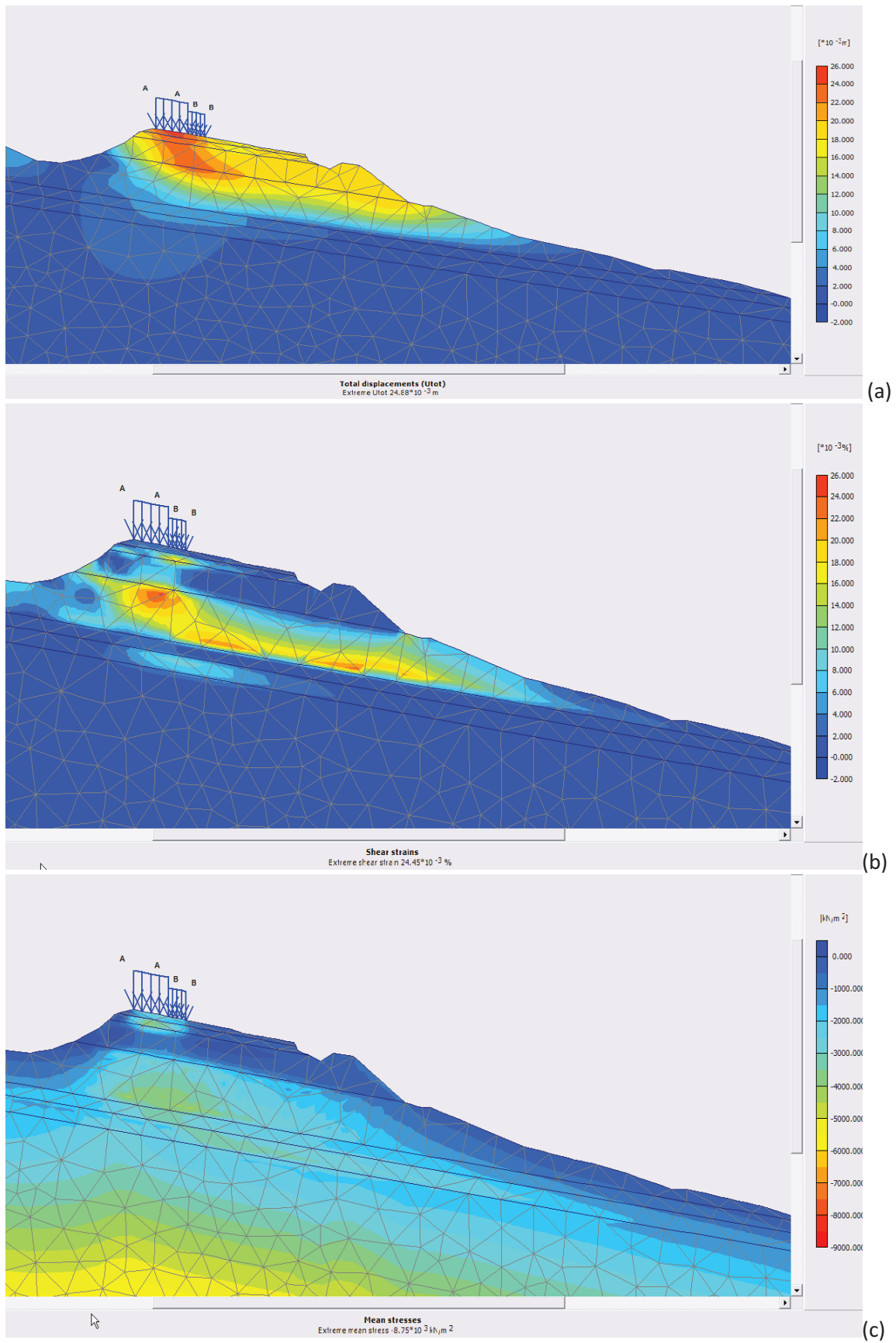


Fig. 8.21. PLAXIS numerical model of the Cinque Torri DSGSD. Total displacements (a), Shear strains (b) and mean stresses (c) after monolith loading displayed as shadings.

After the monoliths loading, the upper layers of the slope, right below the stress application, show significant deformation (Fig. 8.16b). Different zones of colors exhibit different displacements, and the boundaries of different zones represent possible limit of the slope deformations. The maximum deformation shown in yellow-orange (Fig. 8.21a) is organized along a curved zone which begins from the toe of the monolith and deepens toward the contact between the lower mudstone layer and the underlying TVZ carbonates. The maximum displacements concentrate at the top of the lower TVZ mudstone layer and are slightly greater than those in the upper part of the slope (Fig. 8.16 (a)) thus confirming the UDEC results. As for the DEM cases, the reasons of this behavior probably lies in different causes that can be summarized by the chosen values for strength parameters and the thickness of the slope along the profile.

According to the total displacements results (Fig. 8.16a), the maximum amount of movement occurring within the lower TVZ mudstone layer find agreement with the results obtained by UDEC computation and by field observations. The reactivation of the mudflow happened on 2009 detached from the eastern side of the Cinque Torri slope and interests mainly the lower mudstone layer (Fig. 2.6). Moreover the scarp of the mudflow is located at the contact between the middle TVZ carbonatic level and the lower (and thickest) mudstone layer of the TVZ formation. In addition, pseudo-rotational mechanism is delineated from the total displacements figure, supporting a deep deformation within the cohesive layers coupled by slides driven by the high angle rock discontinuities within the carbonates layers.

Because of the simplification of the geological condition and mechanical behavior of the strata, the numerical results are not intended to offer a quantitative assessment of stress and strain distribution or displacements but, as for the UDEC modeling, a tool for investigating the pattern of the deep deformation.

8.5 Results and discussion

The results of the field observation, rotational components analysis and numerical models suggest that the Cinque Torri DSGSD involves a complex mechanism incorporating components of plastic pseudo-circular deformation of the cohesive layers that induce vertical displacements of the brittle lithologies especially in the upper part of the slope.

The modeling carried out on a representative section of the Cinque Torri group following DEM and FEM principles basically provide similar results. This result can be related to the use of the same input values of rock properties, which seem to be more conditioning with respect to constitutive material models.

Both approaches outline a pseudo-circular deformation zone confined on the bottom by the lower carbonate layer of the Travenanzes formation.

By performing UDEC modeling for different cases of slope conditions (Section 8.3), it is found that there are three major factors that control the behavior of the Cinque Torri slope: and the weight of the monoliths, inclination of stratigraphy and the presence of rock discontinuities. The former acts by increasing the natural stress of the slope, while

the other factors influence the propagation of these stresses by increasing the action of destabilizing forces.

The reduction of the strength parameters in the stratigraphic sequence as simulation of weathering and post-glacial processes is a valid tool to analyze possible shape and features of the Cinque Torri deep deformation.

The interpretations derived from the structural analysis described on Chapter 6 (Section 6.5.2) and the results from the numerical modeling appear to support a deformation with pseudo-circular components developing under each monolith/rock sector in correspondence of poor rock-mass quality. The calculations show that a staged approach for simulating the failing processes of the slope by reducing strength values is appropriate since the input rock properties are probably overestimated. This overestimation derives from intact rock properties through empirical correlations which cannot account for all the characteristics of the rock mass.

In addition, the results present some limitations due to the impossibility to represent the real properties observed on field such as the discontinuity spacing and the 3D nature of the failure in 2D sections. Due to the presence of monoliths with different size subdivided into five sectors, a great variability in extension and stress/strain rates is expected. These limitations of the model reduce its capability to investigate the influence on the stability of the slope of the 3D geometry of the discontinuity sets that strongly influence the 3D distribution of stresses and strains and play an important role in the groundwater flow. However, the good correlation between the hypotheses rose from the rotational component analysis and the results of the numerical modeling suggest that the dominant mechanisms operative at the Cinque Torri landslide have been captured even if with limited input data (Chapters 5 and 7).

Future modeling should investigate the temporal evolution of the Cinque Torri slope. In particular, the influence of slope decompression due to the glacial retreat on the stability is one of the main point of interest and future back analysis should be carry out following this approach.

Once obtain more dense data concerning a geotechnical and hydrogeological characterization, another future perspective in the analysis of the Cinque Torri instability should be regarded to a probabilistic approach for the stability assessment. Such approach should be always used since it takes into account a statistic variation of the input values of the strengths parameters and boundary conditions as every slope experiences spatially and temporally due to the natural non-uniform behavior of weathering state of lithologies and seasonal variation of groundwater.

9. Conclusions

9.1. Analysis of the present-day setting

This thesis deals with the analysis of the gravitational phenomena of the Cinque Torri area (Cortina d'Ampezzo municipality, Belluno province, Italian Dolomites). Since several rock slope instabilities occurred in the recent period the present-day critical conditions of the entire slope is testified. In this frame, information about the slope setting is required in order to support suitable decisions for hazard mitigations.

Even if the rocky group is located on a mountain region isolated from villages and main infrastructures, the risk of possible new rock collapses or rock flows can severely affect the safety for many tourists who visit to the area during the year. The reasons of the popularity of the area reside on its magnificent scenery, the numerous climbing rock walls on the monoliths, the mountain paths along the restored trenches warfare dated back to the First World War, and the ski paths on the western side of the rock group. Moreover, the Cinque Torri area is the starting point of several excursion paths that reach important mountain sites in the surroundings (Averau Mount, Nuvolau Mount, Giau Pass).

During this PhD, the nature of the gravitational phenomena affecting the slope has been explored through non invasive technologies (Terrestrial and Aerial Laser Scanning, TLS and ALS, and Electrical Resistivity Tomography, ERT) and traditional methods (stratigraphical, geomechanical surveys and laboratory analyses of rock samples). All these approaches provide new insights on the instabilities affecting the area. Before this research, the involved phenomena were generally classified as lateral spreading developed over a Deep Seated Gravitational Slope Deformation (DSGSD), without deepening the investigations on slope conditions. Also in the previous studies, the stratigraphy is described as playing a central role in the dynamics of the rocky group, but no precise explanations on the role of the slope conditions for the uppermost group of rocky towers are given.

The first answer provided by this research is that the area is affected by a *DSGSD where heterogeneity of the geological sequence together with the complex tectonic activity recorded in the monoliths determine its instability. In addition, weathering processes as water action and freeze-thaw cycles, severely worsen the strength properties of the entire stratigraphy.*

The movements happening within the rock group are very slow and can be generally classified as tilt and rotations which may evolve into slidings and rock falls. The GPS monitoring system installed at the top of one the most unstable rock tower has not recorded yet any sensible movement. This result agrees with the typical low velocity of these phenomena.

The slope setting is the key that allow the complete characterization of a surface lateral spreading phenomenon. Nevertheless, due to the impossibility of carrying out direct investigations such as core drillings, an indirect approach was chosen in this study. This approach consists in ERT surveys combined with punctual passive seismic surveys. With

these methodologies, the near surface stratigraphy and the tectonic settlement were defined down to a depth of about 50-60 m below the surface, thus providing the structural patterns affecting the subsoil of the Cinque Torri DSGSD. The depth of the dolomitic root of the Cinque Torri was detected in the lateral part only, and therefore there is not a high definition of the lower contact behind the pinnacles. Nevertheless, the geophysical investigations allowed the recognition and location of the major faults as well as of the lithological contact geometries. In this way, the a priori geological information of the area was confirmed. The analysis of the outlined features supports the idea that the tectonic action in the Cinque Torri area produced substantial changes in the strata bedding orientation which may have favored tilts and rotations of the uppermost brittle carbonates. The geophysical surveys displayed structural steps within the slope stratigraphy as a result of the action of normal and inverse faults with metric vertical throw, which also promoted partial erosion of the stratigraphical sequence.

The slope behavior can be deciphered by creating a reliable slope model derived from accurate geometrical reliefs of the outcropped rocks, analysis of compositional, mechanical and physical properties of the involved lithotypes. A balance was struck between a dense sampling of the rock type of the area and the derivation of rock properties from literature. A combination of different laboratory analyses helped the identification of relationships between strength, composition and physical properties of the involved lithotypes.

The Cinque Torri slope is made up for a wide extent by Travenanzes Formation (TVZ), which includes mainly reddish mudstones with minor intercalations of peritidal dolostones, and the overlying Dolomia Principale, consisting of well-bedded white and grey cyclic dolomites (Fisher, 1964; Bosellini, 1967).

The results of laboratory tests carried out on samples of mudstone level within the TVZ formation aided the recognition of critical relationships between the compositional variables of silty-clay components and the geotechnical parameters such as compressibility of the ductile lithologies.

The results highlighted that the topmost mudstone levels (close to the Cinque Torri group) are characterized by higher clay content, as testified also by higher plasticity and compressibility. This behavior represents a predisposing factor for tilt, rotations and sliding affecting the Cinque Torri group. The high smectite minerals content revealed by the X-Ray Diffraction (XRD) analysis provides explanation for the typical slow movements of the Cinque Torri DSGSD. Smectite minerals can bear high water content owing to the microscopic structure of their interlayer space. This behavior increases the resistance to liquefaction of the smectite-rich lithotypes resulting in a stabilizing factor. Strength properties of the rock types were derived from uniaxial tests later validated through a comparison with ultrasonic velocity recordings. These values represent intact rock properties which were subsequently imported in formulation dedicated at deriving rock mass properties.

The overall characterization of the present day setting of the study area was introduced as data input in numerical models of the investigated slope, leading to some constraints in results interpretation.

9.2. Investigation of past movements through a novel methodology

Within this research, the role of the rock discontinuities is assumed to have capital importance since they enabled identification of spatial relationships among the spread monoliths and their surroundings. In other words, the discontinuities helped the study of the processes happened in the area until present.

The proposed approach allowed full utilization of the high spatial density and accuracy of the information provided by terrestrial and aerial laser scanner data. A multi-scale model of the study area was obtained from such information.

The extraction of spatial information from point clouds required an iterative procedure which adopts several software (Coltop-3D, Dips, Tectonics-FP, Georient, Polyworks, MATLAB scripts). Both statistical robustness of the results and time efficiency are characteristics of the proposed method.

The novel laser data-based analysis recovered angular components of the lateral spreading acting within the rocky group by relating common discontinuity sets among the monoliths and the reference stable areas. Distinct trends were discovered from the rotation computations, providing new interpretations of the DSGSD.

From the results of this computation, it is derived that the ongoing spreading process is only partly controlled by the bedding plane orientation. Morphological anomalies in the slope, i.e. bulges related to the lateral spreading development or tectonic detachments due to presence of normal faults, are the most influencing factors on the separation of the monoliths.

An intriguing aspect outlined from this analysis of the pitch angle component suggested that a rotational component of the movement occurred, with a probable differentiation of the sliding surface of the DSGSD into segments having different amounts of rotation (Fig. 6.14), as opposed to a planar sliding surface (Viero et al, 2010a).

All these outcomes and related interpretations were subsequently introduced in numerical models for validation purposes.

The results of the rotation computation suggest that the factors influencing instability are: the main tectonic lineaments of the area, plastic deformations of the mudstone layers, strata attitude and the rheological contrast in the stratigraphic sequence.

From the analysis of the tectonic relationships, significant horizontal translations of the rocky group due to the lateral spreading can be excluded. In the Torre Grande sector, the tectonic lineaments, which are antecedent to gravitational phenomena, can be identified both on the monolith facets and on the surrounding outcrops. This physical constraint assures that the position of monoliths bounded by fault remained approximately the same from the age of Alpine orogeny to present. This aspect together with the trends derived from rotational analysis also suggests that the entire rocky group did not undergo to significant horizontal translations.

An observation of the Cinque Torri area from a regional scale outlines that the tectonic lineaments influence both the rock dismantling and the probable limits of the former DSGSD (Fig. 9.1). According to observation derived from aerial photographs, the probable limits of the DSGSD coincide with the Falzarego thrust to the North, with the E-

W counterscarps to the South, with the NNW-SSE Mesozoic normal faults to the West and with the NE-SW trending mudflow to the East.

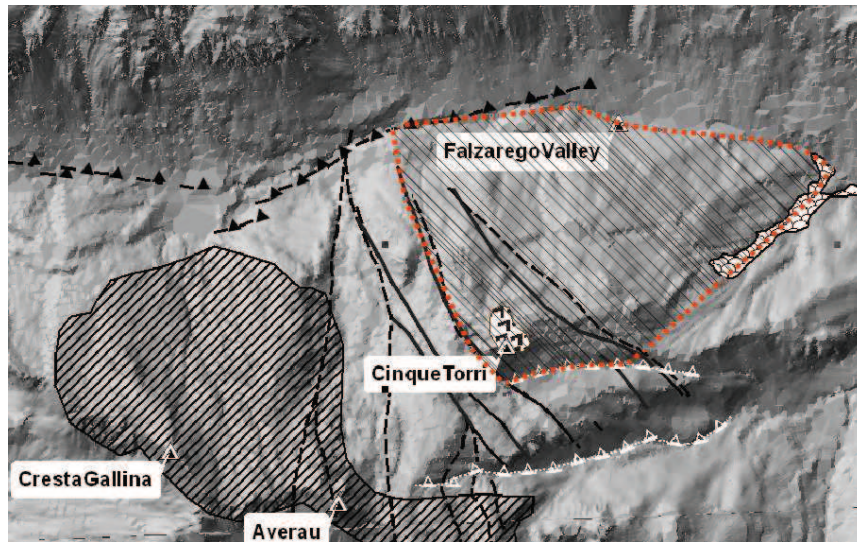


Fig. 9.1. Shaded relief map where the probable DSGSD extent is evidenced in red (the estimated surface is about 3 km²). Please refer to Fig. 2.1 for the legend of the symbols.

9.3. Interpretation of current and future instabilities

The numerical models run in UDEC (Itasca, 2004) and Plaxis (Brinkgreve et al, 2008) intended to improve some aspects related to the general understanding of the Cinque Torri DSGSD. The numerical models summarized the results of field surveys and laboratory analyses. The 2D distinct element modeling was carried out to simulate the influence of stratigraphy and acting forces on the rock slope stability. From these analyses, some important aspects of the Cinque Torri DSGDS were deduced:

- The stress due to the topmost rock masses leads the stratigraphical heterogeneity, and inclination of strata to act as constraint for the stresses distribution;
- For both the upper and the lower mudstone layers, high principal stresses are recorded. Therefore possible movements can start at the top and develop towards the bottom of the lower mudstone layer, as expected;
- The comparison of the developed stresses outlined that the modeled deformations reach the contact between the lower mudstone layer and the underlying dolostone of the Travenanzes formation;
- The presence of rock discontinuities reduce the tensile stress development within the dolostone layers of the Travenanzes formation and create a more definite shape of the deformation zone.

The outcomes of the numerical models substantially confirmed the interpretations derived from rotational components analysis. Both analyses suggested the presence of a circular deformation zone which originates from the upper toe of the monolith contact. Numerical models further deepen these interpretations testifying that the lower part of the deformation is limited by the interface between the lower mudstone layer and underlying carbonate layer of the Travenanzes formation. This important inference is confirmed by field observations which revealed that the reactivation of the mudflow

happened on 2009 detached from the eastern side of the Cinque Torri slope in correspondence of the lower mudstone layer.

The results of the field observations, rotational components analysis and numerical modeling suggest that the Cinque Torri DSGSD involves a complex mechanism incorporating components of pseudo-circular deformation within the Travenanzes Formation which induce vertical and horizontal displacements of the upper part of the slope. At present-day, there is not available direct information on the failure mechanism affecting the slope and the present thesis cannot argue the present day slope stability conditions.

In order to improve the knowledge of slope deformation and influencing factors, as well as to investigate the weathering degree of lithotypes, analysis of core samples from drilling campaigns is desirable. With such an approach, representative rock mass properties of the materials directly involved in the gravitational phenomena will be derived and a direct assessment of slope stability will be gained.

From the results of numerical modeling, the total volume of rock involved in the overall DSGSD can be derived. If the surface extent of the Cinque Torri DSGSD shown in Fig. 9.1 is used together with the depth reached by the deformation on a representative profile of the slope (see Fig. 8.3), the total volume of the instable rock masses reaches 280 Mm³.

9.4. The use of accurate geometrical surveys

Thanks to TLS measurements, the geometry of an observed slope surface is characterized with great detail. The laser scanner techniques allow the acquisition of data in an entirely remote way, without any contact with the high-risk or hardly-accessible areas of a landslide. Artificial targets are necessary to provide a good georeferencing, but they can be placed in suitable points, out of the unstable area, characterized by low-risk conditions and/or (relatively) easily accessibility.

Within this research, laser data are used to recognize in accurate manner rock discontinuities and derive representative spatial information of them. Moreover, laser data are directly used as reference geometry for numerical modeling carried out by using UDEC and Plaxis software packages.

Future acquisitions on the Cinque Torri area will allow comparison of the surveyed topography, leading to the computation of the displacement field and the strain field following the methods proposed by Teza et al. (2007) and Teza et al. (2008b).

In this research, a comparison between laser-based and traditional analysis of rock discontinuities is provided (Chap. 7). The former method experienced to recognize more discontinuity families with respect to traditional scanlines, but recovers lower set spacing values. This is due to the different typology of examined rock discontinuities. In the case of point cloud analysis, discontinuity planes with dimensions of rack facets were recovered. The subsequent higher set spacing assessment with respect scanline mapping is due to the spatial resolution of the point cloud and the chosen segmentation criteria (see sections 7.2 and 7.3).

From the other side, a traditional scanline offer a very detailed analysis of discontinuity since it accounts all the intersected discontinuities along a line of few meters. Very dense set spacings (below 0.20 m) can therefore be measured from traditional surveys but, due to their local viewpoint, they do not assure a complete representation of all the existing discontinuity families. To prevent this bias several scanline mappings should be planned, following also different directions. This results in a time consuming, unsafe and costly survey.

In addition, when dealing with numerical modeling of rock instabilities, the higher the number of rock discontinuities introduced in the model, the longer is the computation time. In some cases a modeled rock body subdivided in a great number of blocks causes the convergence of the computation algorithm to fail.

Therefore, a balance was stroked between a reliable representation of the real characteristics of the rock mass and the computing limitations. In the present work, the modeled slope is about 1250 m long and a set spacing lower than 1 m was observed to decrease significantly the speed of the analysis. The introduction in the modeling of an increment factor for the sets spacing and rock mass properties for the involved lithologies assured reproduction of the geometry of the discontinuous rock masses and at the meantime, an additional worsening of the calculated rock properties.



Fig. 9.2. Cinque Torri group viewed from the shelter “Rifugio Scoiattoli” (Photo courtesy of C. Squarzoni). Red dotted lines indicate a recognized strata contact common among the rock monoliths. Red lines indicate the inferred translations of the monoliths due to the acting gravitational phenomena.

Future challenges in the use of point cloud- based surveys will be the analysis of vertical translational component of the spreading movements happening in the rock group, thus completing the characterization of the past movements happened until present. Field observations allowed ascertaining stratigraphical correlations among the monoliths by recovering common horizons in the constitutive dolostone layers (Fig. 9.2). This analysis can be validated numerically by measuring layers thicknesses by means of the detailed

terrestrial laser data. Once the stratigraphy of each rocky pinnacle will be completely achieved, correlations will be evaluated in order to find the vertical displacements necessary to correlate the common stratigraphical horizons among towers. Thus, a complete characterization of the lateral spreading in terms of rotational and translational components will further aid interpretations of the underlying DSGSD.

9.5. The hydrogeological setting of the area: future perspectives

Triggering factors of gravitational deformations are generally found among exogenic agents such as changes in groundwater flow, freeze-thaw cycles, weathering and earthquakes (Beck, 1968; Radbruck-Hall, 1978; Bovis, 1982; Forcella and Orombelli, 1984; McCalpin, 1999; Ballantyne, 2002; Agliardi et al., 2009).

As examined by Van Ash (1997), landslide triggering systems show complex responses in relation to geotechnical, hydrological, and climatological properties, and more research is needed to understand these relationships, especially when studying processes started in past climate conditions.

At time of writing, the most severe triggering factor affecting the Cinque Torri slope stability is the local hydrogeology. As widely known, increased water infiltration leads to a rise in water-pressure and thus a drop in effective stress.

Water content and circulation are mainly influenced by geology, rock discontinuities nature and composition of the pore water and air temperature. In order to clarify the actual role of water in the slope dynamics, appropriate investigations on the hydrology and storability are required. In the Cinque Torri slope the fracturing of the upper brittle lithologies allows water infiltration which may cause the softening of the underlying marly and clayey formation (Panizza et al., 1994). Along the mudstones layers, water content is probably stored during winter as ice lenses or continuous levels of ice that decrease the permeability of the host layers, leading to a significant decrease of the cohesion and strength of the layers themselves during the melting period.

Due to the presence of alternating lithologies showing geotechnical contrast, a non-uniform behavior is expected as a response of water infiltration. The presence of fractured rocks bounded by impermeable and deformed clay-rich layers determines significant water pressure increase. If relevant water adsorption events occur, plasticity, good adsorption capacity of the clay rich layers and consequent volume changes should be taken into account. A continuous water supply provided by constant rains and active snow melting was registered during the first months of 2009. These phenomena probably triggered the mudflow reactivation which broke off from in the eastern side of the Cinque Torri slope on May of the same year.

Pore water pressure may play an important role in the Cinque Torri instability, but at present neither water table monitoring data nor information about relation between pore water pressure and displacements are available. A continuous monitoring of the water circulation is therefore needed in correspondence of the main contacts between permeable and impermeable layers.

9.6. Applications and limitations

The results presented within this thesis proved that a multi-scale geometrical approach can help for the interpretation of past and present slope dynamics. The main principle guiding laser data treatment is the reconstruction of the recorded history on the patterns characterizing any kind of slope. In particular, rock discontinuities and relationships among them bear information on the initial setting and on the movements experienced by rock masses. These achievements are important for solving a more general question “What is the origin of the Cinque Torri group?”, thus “What are the processes that contributed to the formation of this well-known rocky group?”

In these chapters the reader could make a backwards journey from the present-day conditions to the beginning of the lateral spreading phenomena started after ice retreat. At present, the slope shows evidences of the activity of the lateral spreading, due to the recent Torre Trepbor monolith collapse and the mudflow reactivation. The overall DSGSD activity is slow (as typically shown by DSGSDs), but during the fierce phase, slope dynamics undergo to an exponential increasing of speed, which develops at a last stage in rock falls, rock slides and at the outer borders in collateral phenomena as mudflows.

In the past periods the slope conditions were completely different from the present ones. The tectonic activity determines the initial crumbling of a continuous carbonatic platform, later eroded and dismantled by ice erosion. In the author’s opinion, the most severe acting process for the instability of the slope was the ice retreat during post glacial age. The ice melting produced two main changes in the slope setting: first of all a significant increase of water supply and secondly a gradual relaxation of the glacial valley, i.e. the Falzarego valley (Fig. 9.1), due to the consequent loss of weight. The new stress conditions and significant water supply were immediately recorded by the lithotypes of the Cinque Torri slope. Slope instabilities began as natural and unavoidable phenomena needed to restore forces equilibrium among water pressures, internal strengths and gravity. In particular, instabilities in the studied slope propagated from the valley to the topmost sectors, propagating as a gradual removal of the lower ‘foundations’ of the slope. Due to these new conditions, an interlocking displacement towards valley floor began and is still acting in the slope.

Within this frame, the Cinque Torri group can be viewed as the final relict of this old processes that nowadays act in the slope as plastic deformations of the ductile lithologies and the spreading of the topmost brittle and fragmented rock masses. The slope gradient together with the local stratigraphy determine the complex rotational shape of the deep deformation zone as outlined by numerical modeling.

The main limitations related to the presented research concern numerical modeling and are both qualitative and quantitative.

In numerical models the set spacing introduced for rock discontinuities is chosen following practical criteria promoting computation efficiency. In section 9.4 the reasons of the chosen values are explained, as well as the favorable judgment of the laser data-based characterization. This approach, even if very accurate and characterized by high spatial resolution, cannot recognize sealed rock discontinuities whose 3D orientation cannot be captured. These discontinuities are important for the assessment of the rock

mass properties and, if not taken into account in numerical models, a probable overestimation of slope stability appears. A faster computation thus does not necessarily imply reliable results, and a good estimation of the rock mass properties requires trials devoted to evaluation of suitable correction factors. With this indirect approach, estimation of rock mass properties would take into account for the influence of rock discontinuities. In this way, reliable slope models, able to help the design of suitable countermeasures, can be obtained.

Another limitation to the present research is related to the fact that few rock samples were taken and analyzed mainly due to the schedule and objectives of this PhD thesis. If the number of analyzed samples and the corresponding representativeness in the rock mass are not enough, inaccuracies of the derived rock properties appear. Since future challenges will concern slope stability assessment, further investigations on the study site are needed. In particular, an adequate rock sampling for all the investigated lithologies will guarantee a robust statistical approach to the rock mass characterization. The availability of multi-temporal laser acquisition of the Cinque Torri slope, prior and subsequent the mudflow reactivation happened on 2009, can validate future rock mass characterization. In an inverse modeling approach, the observed slope conditions before and after instability (i.e. the mudflow) act as constraints. The modeling process thus allows iteratively recognizing the most suitable rock properties which guarantee to better simulate the observed final slope setting. The final comparison of the model-based characterization and the laboratory results will undertake a reliable rock mass characterization.

9.7. Concluding remarks

This PhD research attempted to give the first detailed analysis of the Cinque Torri DSGSD through traditional and recently developed techniques. Within these activities, the laser scanning-based method for rotations computation represents a novel methodology for the analysis of lateral spreading associated to DSGSDs. The additional comparison with the results of numerical modeling provides a comprehensive scheme of geometries and processes acting within the gravitational body. In this way, useful information for hazard assessment is obtained.

The results show important new insights on the present day slope dynamic. In particular, recent instabilities highlight the precariousness of slope conditions. Collateral phenomena do not directly injure any infrastructure or human activity, even if future reactivations and moving back of the crown with significant slope detachments could affect a private shelter and a close mountain path.

The results of rotations computation suggest that future rock collapses within the rock group will follow a direction towards East. Since single monolith volumes range from 20000 to 80000 m³, and the area registers several thousands of tourists accesses per year, hazard mitigation are required to guarantee human safety. The continuous differential GPS system installed on the top of the Torre Inglese pinnacle is at time of writing the only monitoring system able to provide continuous registration of movements of this unstable pinnacle with accuracy of few millimeters.

The main problem in assessing stability of the rocky group resides on its non-linear kinematics. The Cinque Torri lateral spreading is characterized by low velocities during the precursory phases and reaches instantaneous velocities during the fierce phase. This is the case reported for the Torre Trepbor collapse. Rock climbers reported that between 2003 and 2004 the monolith underwent to a metric tilting as recognized from field evidences. Fortunately, the collapse happened during the night, therefore without victims.

The inspection of the laser data surveys outlines other hazard evidences, as shown in Fig. 9.3. Many erratic boulders can be detected all around the group and they can be related to past and recent rock falls originated from the studied rocky group. The dimensions of these rock masses, the preferential trajectories involving proximal human structures (i.e. mountain shelter and mountain paths) and the availability of new rock masses from the source area (i.e. Torre Grande monolith) represent potential dangers to tourists and climbers.

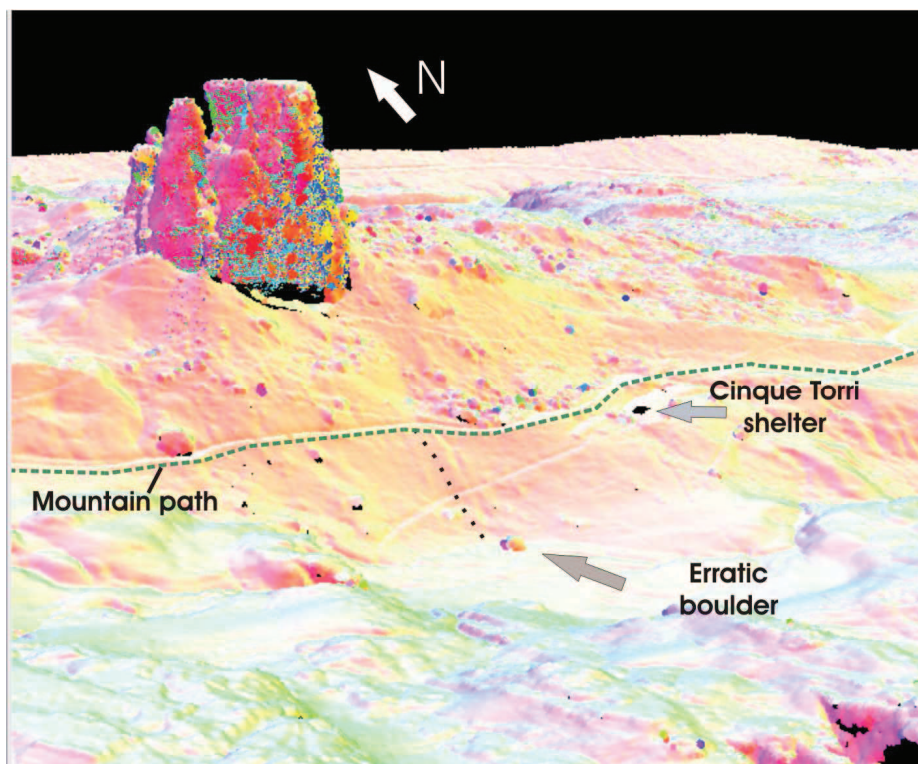


Fig. 9.3. View of the LS datasets (imported in Coltop-3D software) showing the imprint left by a erratic boulder with metric size.

In the author's opinion, it should be recommendable to deny the access of the area from about 200 m distance from the Cinque Torri group at least during May and June. These months represent the most crucial period for slope stability, since important water incomings due to seasonal rains are potentiated by continuous snow melting. The Cinque Torri group is an extraordinary site from natural, geological, hystorical viewpoints. Since future collapses are unavoidable, public authorities should prevent possible human injures by denying the access during late spring and support new investigations on the slope stability analysis.

References

- Abdullah, W.S., Al-Zou'bi, M.S., Alshhibli, K.A., 1999. Influence of pore water chemistry on the swelling behavior of compacted clays. *Applied Clay Science* 15, 447-462.
- Agliardi, F., Crosta, G., Zanchi, A., 2001. Structural constraints on deep-seated slope deformation kinematics. *Engineering Geology* 59, 83–102.
- Agliardi, F., Crosta, G.B., Zanchi, A., Ravazzi, C., 2009. Onset and timing of deep-seated gravitational slope deformations in the eastern Alps, Italy. *Geomorphology* 103, 113–129.
- Amaral, P.M., Rosa, L.G., Fernandes, J.C., 1999. Determination of Schmidt rebound hardness consistency in granite. *Int. J. Rock Mech. Min. Sci.* 36, 833– 837.
- Ambrosi, C., Crosta, G.B., 2006. Large sackung along major tectonic features in the Central Italian Alps. *Engineering Geology* 83, 183–200.
- ARPAV, 2010. Agenzia Regionale per la Prevenzione e Protezione Ambientale del Veneto. Rainfall data recordings at the Gilardon- Cortina d'Ampezzo, Faloria, Passo Falzarego weather stations for the period January 2000-2010. Private data transmission.
- Assereto, R., Brusca, C., Gaetani, M., Jadoul, F., 1977. Le mineralizzazioni Pb-Zn nel Triassico delle Dolomiti. Quadro geologico ed interpretazione genetica. *L'Ind. Miner.*, 28, 367-402. (in italian)
- ASTM D2845-05, Standard test method for laboratory determination of pulse velocities and ultrasonic elastic constants of rock, American Society for Testing Materials, 2005.
- Bachmann, D., Bouissou, S., Chemenda, A., 2004. Influence of weathering and preexisting large scale fractures on gravitational slope failure: insights from 3-D physical modelling. *Natural Hazards and Earth System Sciences* 4, 711–717.
- Badger, T.C., 2002. Fracturing within anticlines and its kinematic control on slope stability. *Environmental and Engineering Geoscience* VIII, 19–33.
- Ballantyne, C.K., 2002. Paraglacial geomorphology. *Quaternary Science Reviews* 21, 1935–2017.
- Beck, A.C., 1968. Gravity faulting as a mechanism of topographic adjustment. *New Zealand Journal of Geology and Geophysics* 11, 191–199.
- Bentley, J.L., 1975. Multidimensional binary search trees used for associative searching. *Communications of the ACM*, 18(9): pp. 509-517, September 1975.
- Bentley, L.R., Gharibi, M., 2004. Two- and three-dimensional electrical resistivity imaging at a heterogeneous remediation site. *Geophysics* 69, 674–680.
- Bergevin, R., Souci, M., Gagnon, H., Laurendeau, D., 1996. Towards a general multi-view registration technique. *IEEE Transactions on Pattern Analysis and Machine Intelligence* 18, 540–547.
- Bieniawski, Z.T., 1989. *Engineering Rock Mass Classifications: A complete Manual for Engineers and Geologists in Mining Civil and Petroleum Engineering*. John Wiley, New York, 272 pp.
- Bober, L., 1984. Landslide areas in the Polish Flysch Carpathians and their connection with the geological structure of the region. *Biuletyn Instytutu Geologicznego* 340, 115–158 (in Polish with English summary).
- Boehler, W., Heinz, G., Marbs, A., 2001. The potential of non-contact close range laser scanners for cultural heritage recording. In *Proceedings of CIPA 2001*

- International Symposium*, Potsdam, D, 18-21 September 2001. Available online at: <http://www.i3mainz.fh-mainz.de/publicat/cipa2001/cipa2001.pdf> (accessed: 12.12.2010).
- Bosellini, A., 1967. La tematica deposizionale della Dolomia Principale (Dolomiti e Prealpi Venete). *Boll. Soc. Geol. It.*, 86, 133-169. (in italian)
- Bovis, M.J., 1982. Uphill-facing (antislope) scarps in the Coast Mountains, southwest British Columbia. *Geological Society of America Bulletin* 93, 804–812.
- Brady, B.H.G., Brown, E.T., 1985. *Rock Mechanics for Underground Mining*. George Allen & Unwin, London.
- Breda, A., Massari, F., Meneguolo, R., Preto, N., 2006. An alluvial plain-sabkha-lagoon system in the Upper Triassic of the Dolomites, northern Italy. *EGU General Assembly 2006*, Wien.
- Brideau, M., A., Stead, D., Couture, R., 2006. Structural and engineering geology of the East Gate Landslide, Purcell Mountains, British Columbia, Canada. *Engineering geology* 84, 183-206.
- Brideau, M.-A., Yan, M., Stead, D., 2009. The role of tectonic damage and brittle rock fracture in the development of large rock slope failures. *Geomorphology* 103, 30–49.
- Casagrande, A., 1948. Classification and identification of soils. *Trans. Am. Soc. Civ. Eng.* 113, 901-930.
- Castellarin, A., Cantelli, L., Fesce, A., Mercier, J., Picotti, V., Pini, G., Prosser, G., Selli, L., 1992. Alpine compressional tectonics in the Southern Alps. Relationships with the N-Apennines. *Annales Tectonicae* 6, 1, 62-94.
- Castellaro, S., Imposa, S., Barone, F., Chiavetta, F., Gresta, S., Mulargia, F., 2008. Georadar and passive seismic survey in the Roman Amphitheatre of Catania (Sicily). *Journal of Cultural Heritage* 9, 357-366.
- Castellaro, S., Mulargia, F., 2009. Vs30 estimates using constrained H/V Measurements. *Bull. Seism. Soc. Am*, 99 (2).
- Chang, K. T., Wan, S., Lei, T. C., 2010. Development of a spatial decision support system for monitoring earthquake-induced landslides based on aerial photographs and the finite element method. *International Journal of Applied Earth Observation and Geoinformation* (in press).
- Chemenda, A.I., Bois, Bouissou, T.S., Tric, E., 2009. Numerical modelling of the gravity-induced destabilization of a slope: The example of the La Clapière landslide, southern France. *Geomorphology* 109, 86-93.
- Clayton C. R. I., Matthews M.C., Simons N.E., (1995). *Site Investigation*. Second Edition. Blackwell Science, Oxford. 584 pp.
- Constable S.C., Parker R.L. and Constable C.G.; 1987: Occam's inversion: a practical algorithm for generating smooth models from electromagnetic sounding data. *Geophysics* 52, 289–300.
- Conte, E., Silvestri, F., Troncone, A., 2010. Stability analysis of slopes in soils with strain-softening behaviour. *Computers and Geotechnics* 37, 710-722.
- Cruden, D.M., Varnes, D.J., 1996. Landslide types and processes. In: Turner, A.K., Schuster, R.L. (Eds.), *Landslides, Investigation and Mitigation*, Transportation Research Board, Special Report 247. National Academy Press, Washington D.C., pp. 36-75.
- Dahlin, T., 1996. 2-D resistivity surveying for environmental and engineering applications. *First break* 14, 275-283.

- Dahlin, T., Bernstone, C., Loke, M.H., 2002. A 3-D resistivity investigation of a contaminated site at Lernacken, Sweden. *Geophysics* 67, 1692–1700.
- Daily, W., Owen, E., 1991. Cross-borehole resistivity tomography. *Geophysics* 56, 1228-1235.
- Dawson, E.M., Roth, W.H., Drescher, A., 1999. Slope stability analysis by strength reduction. *Geotechnique* 49, 835-840.
- Deere, D.U., Miller, R.P., 1966. Engineering classification and index properties for intact rock. Tech. Report. Air Force Weapons Lab., New Mexico, No. AFWL-TR-65-116.
- Demant, D., Renardy, F., Vanneste, K., Jongmans, D., Camelbeeck, T., Megrahoui, M., 2001. The use of geophysical prospecting for imaging active faults. In: the Roer Graben, Belgium. *Geophysics* 66, 78–89.
- Doglioni, C., 1992. Relationships between Mesozoic extensional tectonics, stratigraphy and Alpine inversion in the Southern Alps. *Eclogae Geol. It.*, 8, 35-36.
- Dramis, F., Sorriso-Valvo, M., 1994. Deep-seated gravitational slope deformations, related landslides and tectonics. *Engineering Geology* 38, 231–243.
- Feng, Q., Sjögren, P., Stephansson, O. and Jing, L. 2001. Measuring fracture orientation at exposed rock faces by using a non-reflector total station. *Engineering Geology* 59, 133-146.
- Feng, Q.H., Röshoff, K., 2004. In-situ mapping and documentation of rock faces using a full-coverage 3D laser scanner technique. *International Journal of Rock Mechanics and Mining Sciences* 41 (3), 139–144.
- Fisher, A., 1964. The Lofer cyclothems of the Alpine Triassic. Symposium of cyclic sedimentation, D. Merriam (ed.), Bull., 169, 107-150, Geol. Surv of Kansas.
- Forcella, F., Orombelli, G., 1984. Holocene slope deformations in Valfurva, Central Alps, Italy. *Geografia Fisica e Dinamica Quaternaria* 7, 41–48.
- Franceschi, M., Teza, G., Preto, N., Pesci, A., Galgaro, A., Girardi, S., 2009. Discrimination between marls and limestones using intensity data from terrestrial laser scanner. *ISPRS Journal of Photogrammetry and Remote Sensing* 64, 522–528.
- Fröhlich, C. and Mettenleiter, M. 2004. Terrestrial Laser Scanning – New Perspectives in 3-D Surveying. *International Archives of Photogrammetry, Remote Sensing and Spatial Information Sciences*, Vol XXXVI – Part 8/W2, October 2004.
- Fuller, J., 2009. SpinCalc function at MATLAB central. Available online at: <http://www.mathworks.co.uk/MATLABcentral/fileexchange/authors/31368> (accessed on 31.05.2010).
- Garlanger, J.E., 1972. The consolidation of soils exhibiting creep under constant effective stress. *Geotechnique* 22, 71-78.
- Georient, 2010. Structural Geology — Mapping/GIS Software. Holcombe Coughlin Oliver. Available online at: <http://www.holcombe.net.au> (accessed on 31.05.2010).
- Gill, D.E., Corthesy, R., Leite, M. H., 2005. Determining the minimal number of specimens for laboratory testing of rock properties. *Engineering geology*, 29-51.
- Goodman, R.E., 1989. Introduction to rock mechanics. Second edition. New York etc.: Wiley & Sons, 1989. - 562 p.
- Gratchev, I.B., Sassa, K., Osipov, I. V., Sokolov, V.N., 2006. The liquefaction of clayey soils under cyclic loading. *Engineering Geology* 86, 70-84.
- Greaves, T. 2004. Inside Laser Scanners. Position. October/November 2004. South Pacific Science Press International, Alexandria, N.S.W, Australia. Issue 3:pp 50-52.

- Gunther, T., Rucker, C., Spitzer, K., 2006. Three-dimensional modelling and inversion of dc resistivity data incorporating topography - II. Inversion. *Geophysical Journal International* 166, 506–517.
- Guzzetti, F., Cardinali, M., Reichenbach, P., 1996. The influence of structural setting and lithology on landslide type and pattern. *Environmental and Engineering Geosciences* 2, 531–555.
- Hassan, M., Burdet, O., Favre, R., 1995. Ultrasonic measurements and static load tests in bridge evaluation. *NDT&E International* 28 (6), 331–337.
- Hoek, E. and Brown, E.T., 1980a. *Underground excavations in rock*. London, Inst. Min. Metall.
- Hoek, E. and Brown, E.T. 1980b. Empirical strength criterion for rock masses. *J. Geotech Engng. Div., ASCE*, 106 (GT 9), 1013-1035.
- Hoek, E., Kaiser, P.K., Bawden, W.F., 1995. *Support of Underground Excavations in Hard Rock*. Balkema, Rotterdam, 215 pp.
- Hoek, E., Carranza-Torres, C.T., Corkum, B., 2002. Hoek-Brown failure criterion- 2002 edition. In: Hammah, et al. (Ed.), *Proceedings of the Fifth North America Rock Mechanics Symposium (NARMS-TAC)*. Toronto, 7-10 July 2002. University of Toronto Press, pp. 267-273, vol.1.
- Hough, P.V.C., 1962. Method and means for recognizing complex patterns. U.S. Patent 3069654.
- Hurlimann, M., Ledesma, A., Corominas, J., Prat, P. C., 2006. The deep-seated slope deformation at Encampadana, Andorra: Representation of morphologic features by numerical modelling. *Engineering Geology* 83, 343-357.
- Innovmetric, 2010. PolyWorks software package technical data. <http://www.innovmetric.com/polyworks/3D-scanners/home.aspx> (accessed on 31.11.2010).
- ISRM, 1978a. Barton, N., Rengers, N., et al.: Suggested Methods For the Quantitative Description of Discontinuities, *International Society for Rock Mechanics, Int. J. Rock Mech. Sci. & Geomech. Abstr.*, Vol. 17, pp 69-76, 1978.
- ISRM, 1978b. Suggested methods for the quantitative description of discontinuities in rock masses. *Int. J. Rock Mech. Min. Sci. Geomech. Abstr.*, 15, pp. 319-368. 243
- ISRM, 1981a. *Rock characterization, testing and monitoring, ISRM suggested methods*. Ed. E. T. Brown. Pub. Pergamon Press, Oxford. 211 pp.
- ISRM, 1981b. Suggested Methods, Suggested method for determining sound velocity, in: E.T. Brown (Ed.), *ISRM Suggested Methods*, Pergamon Press, Oxford, 107–110.
- ITASCA Cons. Group INC., 2004. UDEC code-vers. 4.1, Minneapolis-Minnesota, 2004.
- Jaboyedoff, M., Baillifard, F., Couture, R., Locat, J., and Locat, P., 2004. New insight of geomorphology and landslide prone area detection using DEM, in: *Landslides: Evaluation and Stabilization*, edited by: Lacerda, W. A., Ehrlich, M., Fontoura, A. B., and Sayão, A., Taylor & Francis, London, 191–198.
- Jaboyedoff M., Metzger R., Oppikofer T., Couture R., Derron M.-H., Locat J. Turmel D., 2007. New insight techniques to analyze rock-slope relief using DEM and 3D-imaging cloud points: COLTOP-3D software. In Eberhardt, E., Stead, D and Morrison T. (Eds.): *Rock mechanics: Meeting Society's Challenges and demands* (Vol. 1), Taylor & Francis. pp. 61-68.

- Jaboyedoff, M., Oppikofer, T., Minoia, R., Locat, J., Turmel, D., 2008. Terrestrial LIDAR investigation of the 2004 rockslide along Petit Champlain Street, Québec City (Québec, Canada). Proceedings: 4th Canadian Conference on Geohazards, 20–24 May, Québec, Canada.
- Jaboyedoff, M., Couture, R., Locat, P., 2009. Structural analysis of Turtle Mountain (Alberta) using digital elevation model: toward a progressive failure. *Geomorphology* 103, 5–16.
- Jackson, J. E. 1991. *A User's Guide to Principal Components*, John Wiley and Sons, Inc., p. 592.
- Kaya, A., 2009. Relating equal smectite content and basal spacing to the residual friction angle of soils. *Engineering Geology* 108, 252-258.
- Kellogg, K.S., 2001. Tectonic controls on a large landslide complex: Williams Fork Mountains near Dillon, Colorado. *Geomorphology* 41, 355–368.
- Kinakin, D. and Stead, D., 2005. Analysis of the distributions of stress in natural ridge forms: implications for the deformation mechanisms of rock slopes and the formation of sackung. *Geomorphology* 65, 85-100.
- Kleczkowski, A., 1955. *Osuwiska i zjawiska pokrewne*. Wydawnictwa Geologiczne, Warszawa, pp. 1–94.
- LaBrecque, D.J., Miletto, M., Daily, W., Ramirez, A., Owen, E., 1996. The effects of noise on Occam's inversion of resistivity tomography data. *Geophysics* 61, 538–548.
- Lambe, T.W., Whitman, R.V., 1979. *Soil Mechanics*. SI version. Wiley, New York.
- Lichti, D. D., Gordon, S. J. and Stewart, M. P., 2002. Ground-based laser scanners: operations, systems and applications, *Geomatica*, 56(1), pp. 21 - 33.
- Lichti, D.D., Jamtsho, S., 2006. Angular resolution of terrestrial laser scanners. *The Photogrammetric Record* 21, 141–160.
- Lin, M.L., Lo, C.M., Chang, W.C., Dong, J.J., Huang, A.B., Lin, C.P., Chang, K.T., Lee, J.F., 2008. Site investigation of a large landslide triggered by the Chi-Chi earthquake, Taiwan. In: *The 3rd International Conference on site characterization*, Taipei, Taiwan. April 1-4, 2008, 449-452.
- Maas, H.G., Vosselman, G., 1999. Two algorithms for extracting building models from raw laser altimetry data. *Journal of Photogrammetry & Remote Sensing*, 54, 153-163.
- Markley, F.L., 1980. Parametrization of the attitude. In: Wertz, J.R. (Ed.), *Spacecraft Attitude Determination and Control: Chapter 12, Three-axis Attitude Determination Methods*. Springer, Berlin Heidelberg New York, pp. 410–420.
- Marescot, L., Loke, M.H., Chapellier, D., Delaloye R., Lambiel C. and Reynard E., 2003. Assessing reliability of the 2D resistivity imaging in mountain permafrost studies using the depth of investigation index method. *Near Surface Geophysics*, 57-67.
- Marinos, P., Hoek, E., 2001. Estimating the geotechnical properties of heterogeneous rock masses such as flysh. *Bull. Eng. Geol. Env.* 60, 85-92.
- Marinos, V., Marinos, P., Hoek, E., 2005. The geological strength index: applications and limitations. *Bulletin of Engineering geology and Environment*, 64, 55-65.
- Martin, C.D., Tannant, D.D., Lan, H., 2007. Comparison of terrestrial-based, high resolution, LiDAR and digital photogrammetry surveys of a rock slope. In: Eberhardt, E., Stead, D., Morrison, T. (Eds.), *Proceedings 1st Canada–U.S. Rock Mechanics Symposium*, Vancouver, May 27–31, 2007, pp. 37–44.

- Massironi, M., Bistacchi, A., Dal Piaz, G.V., Monopoli, B., Schiavo, A., 2003. Structural control on mass-movement evolution: a case study from the Vizza Valley, Italian Eastern Alps. *Eclogae Geologicae Helvetiae* 96, 85–98.
- Matsuura, S., Asano, S., Okamoto, T., 2008. Relationship between rain and/or meltwater, pore-water pressure and displacement of a reactivated landslide. *Engineering Geology* 101, 49–59.
- McCalpin, J.P., 1999. Criteria for determining the seismic significance of sackungen and other scarp-like landforms in mountainous regions. In: United States Government Printing Office (Ed.), *Techniques for Identifying Faults and Determining their Origins*. U.S. Nuclear Regulatory Commission, Washington, pp. 255–259.
- Meglis, I.L., Chow, T., Martin, C.D., Young, R.P., 2005. Assessing in situ microcrack damage using ultrasonic velocity tomography. *International Journal of Rock Mechanics and Mining Sciences* 42 (1), 25–34.
- Menotti, R. M., Pasuto, A., Silvano, S., Siorpaes, C., Soldati, M., 64 1990. Guida alle escursioni del IV seminario DGPV, Cortina d'Ampezzo _Bl., 25–28 settembre 1990. Gruppo Informale Deformazioni Gravitative Profonde di Versante. Istituto di Geologia Applicata del CNR, Padova, 22 pp.(in italian)
- Metzger, R., Jaboyedoff, M., Oppikofer, T., Viero, A., Galgaro, A., 2009. Coltop3D: A New Software for Structural Analysis with High Resolution 3D Point Clouds and DEM. In: *Proceedings of the Frontiers + Innovation CSPG CSEG CWLS Convention*, Calgary, Alberta (Canada), 4-8 May 2009.
- Morelli, G., and LaBrecque, D. J., 1996, Robust scheme for ERT inverse modeling: *European Journal of Environmental and Engineering Geophysics* 2, 1-14.
- Nakamura, Y., 1989. A method for dynamic characteristic estimation of subsurface using microtremor on the ground surface. *Quarterly Report of Railway Technology Research Institute* 30, 25-33.
- Nemcok, A., 1972. Gravitational slope deformation in high mountains. *Proceedings of the 24th International Geology Congress*, Montreal. 24th International Geology Congress, Ottawa, pp. 132–141.
- Neri, C., Gianolla, P., Furlanis, S., Caputo, R., Bosellini, A., 2007. Carta Geologica d'Italia alla scala 1:50000, foglio 029 Cortina d'Ampezzo, and Note illustrative. APAT, Roma, pp. 1–200. (in italian)
- Nguyen, F., Garambois, S., Chardon, D., Hermitte, D., Bellier, O., Jongmans, D., Subsurface electrical imaging of anisotropic formations affected by a slow active reverse fault, Provence, France. *Journal of Applied Geophysics* 62, 338–353.
- Nichol, S.L., Hungr, O., Evans, S.G., 2002. Large-scale brittle and ductile toppling of rock slopes. *Canadian Geotechnical Journal* 39, 773-788.
- Nogoshi, M., Igarashi, T., 1970. On the propagation characteristics of microtremors. *J. Seism. Soc. Jpn*, 23, 264-280.
- Ohlmacher, G.C., 2000. The Relationships between geology and landslide hazards of Atchinson, Kansas, and vicinity. *Curr. Res. Earth Sci.* 244 (3), 1-16.
- Olayinka, A.J., Yaramanci, U., 1999. Choice of the best model in 2-D geoelectrical imaging: case study from a waste dump site. *European Journal of Environmental and Engineering Geophysics* 3, 221-244.

- Oldenburg, D. W., and Li, Y., 1999. Estimating depth of investigation in dc resistivity and IP surveys. *Geophysics* 64, 403-416.
- Oppikofer, T., Jaboyedoff, M., Keusen, H.-R., 2009a. Collapse at the eastern Eiger flank in the Swiss Alps. *Nature Geoscience* 1, 531–535.
- Oppikofer, T., Jaboyedoff, M., Blikra, L., Derron, M., 2009b. Characterization and monitoring of the Åknes rockslide using terrestrial laser scanning. *Natural Hazard and Earth System Sciences* 9, 1003–1019.
- Optech, 2010. Airborne surveying: ALTM Airborne Laser Terrain Mapper <http://www.optech.ca/prodaltm.htm> (accessed on 31.05.2010).
- Optech, 2011a. Brochure “Complete solution for Airborne Surveying”. Pdf file available at: http://www.optech.ca/pdf/Airborne_Brochure_100915_Web.pdf. (accessed on 22.12.2010)
- Optech, 2011b. Brochure “Gemini. Summary specification sheet”. Pdf file available at: http://www.optech.ca/pdf/Gemini_SpecSheet_100908_Web.pdf. (accessed on 22.12.2010)
- Panizza, M., Pasuto, A., Silvano, S., Soldati, M., 1994. Temporal occurrence and activity of landslides in the area of Cortina d'Ampezzo (Dolomites, Italy). *Geomorphology* 15, 311–326.
- Panizza, M., Pasuto, A., Silvano, S., Soldati, M., 1996a. Landsliding during the Holocene in the Cortina d'Ampezzo Region, Italian Dolomites. In: B. Frenzel, J.A. Matthews, B. Glaser & M. M. Weib (Eds.), *Rapid mass movement as climatic evidence for Holocene times. Palaoklimaforschung/Paleoclimate Research*, p. 19.
- Panizza, M., Pasuto, A., Silvano, S., Soldati, M. 1996b. Temporal occurrence and activity of landslides in the area of Cortina d'Ampezzo (Dolomites, Italy) In: M.Soldati (Ed.) *Landslides in the European Union. Geomorphology* 15, 311-326.
- Pesci, A., Teza, G., Ventura, G., 2008. Remote sensing of volcanic terrains by terrestrial laser scanner: preliminary reflectance and RGB implications for studying Vesuvius crater (Italy). *Annals of Geophysics* 51, 619–631.
- Pettitt, W.S., King, M.S., 2004. Acoustic emission and velocities associated with the formation of sets of parallel fractures in sandstones. *Proceedings of SINOROCK Symposium, Paper1A* 25.
- Priest, S.D. and Hudson, J.A. 1976. Discontinuity spacings in rock, *Int. J. Rock Mech. Mm. Sci. and Geomech. Abstr.*, 13, 135—148.
- Priest, S.D. and Hudson, J.A. 1981. Estimation of discontinuity spacing and trace length using scanline surveys. *Int. J. Rock Mech. Min. Sci. & Geomech. Abstr. Vol 18*, pp. 183-197.
- Priest, S.D. 1993. *Discontinuity Analysis for Rock Engineering*, Chapman and Hall, London, 473 pp.
- Radbruch-Hall, D., 1978. Gravitational creep of rock masses on slopes. In: Voight, B. (Ed.), *Rockslides and Avalanches — Natural Phenomena: Developments in Geotechnical Engineering, Vol. 14*. Elsevier, Amsterdam, pp. 608–657.
- Reshetyuk, Y. 2006. Investigation and calibration of pulsed time-of-flight terrestrial laser scanners. Licentiate thesis in Geodesy. Royal Institute of Technology (KTH). Department of Transport and Economics. Division of Geodesy. 100 44 Stockholm. October 2006.
- Riegl, 2010a. Laser scanner Riegl LMSZ-420i technical specifications. Available online at: http://www.riegl.com/uploads/tx_pxpriegldownloads/10_DataSheet_Z420i_09-12-2009.pdf (accessed on 31.05.2010).

- Riegl, 2010b. Viewer, acquisition, and processing software RiSCAN PRO. Available online at: http://www.riegl.com/uploads/tx_pxriegldownloads/11_DataSheet_RiSCAN_PRO_27-11-2008_02.pdf (accessed on 31.05.2010).
- Rocscience, 2010. Dips, v 5.0. Graphical and Statistical Analysis of Orientation Data. Technical data available at: <http://www.rocscience.com/downloads/Dips.asp> (accessed on 31.05.2010).
- Rucker, D. F., Levitt, M. T., Greenwood, W. J., 2009. Three-dimensional electrical resistivity model of a nuclear waste disposal site. *Journal of applied geophysics* 69, 150-164.
- Sachpazis, C.I., 1990. Correlating Schmidt hardness with compressive strength and Young's modulus of carbonate rocks. *Bull. Int. Assoc. Eng. Geol.* 42, 75–83.
- Sack, D.A., Olson, L.D., 1995. Advanced NDT methods for evaluating concrete bridges and other structures. *NDT&E International*, 28 (6), 349–357.
- Shalabi, F. I., Cording, E.J., Al-Hattamleh, O.H., 2007. Estimation of rock engineering properties using hardness tests. *Engineering Geology*, 90, 138–147.
- Shönborn, G., 1999. Balancing cross section with kinematic constrains: The Dolomites (northern Italy). *Tectonics* 18, 3, 527-545.
- Singh, M., Singh, B., 2008. High lateral strain ratio in jointed rock masses. *Engineering Geology* 98, 75-85.
- Slob, S., Hack, H.R.G.K. and Turner, A.K. 2002. An approach to automate discontinuity measurements of rock faces using lasers scanning techniques. In: *Proceedings of ISRM International Symposium on Rock Engineering for Mountainous Regions – Eurock 2002*, Funchal, 2002 November 25-28th, 87-94.
- Slob, S., 2005. Automated rock mass characterization using 3-D terrestrial laser scanning. PhD thesis, Delft University, Delft, The Netherlands.
- Slob, S., van Knapen, B., Hack, R., Turner, K., Kemeny, J., 2005. A method for automated discontinuity analysis of rock slopes with 3D laser scanning. *Transportation Research Record* 1913, 187–208.
- Soldati M & Pasuto A., 1991 –Some cases of deep seated gravitational deformations in the area of Cortina d'Ampezzo (Dolomites). Implications in environmental risk assessment. In : M.Panizza, M. Soldati & M.M. Coltellacci (Eds.), *European Experimental Course on Applied Geomorphology 2: Proceedings*. Istituto di Geologia, Università degli studi di Modena, 91-104.
- Stead, D., Eberhardt, E., Coggan, J.S., 2006. Developments in the characterization of complex rock slope deformation and failure using numerical modelling techniques. *Engineering Geology* 83, 217-235.
- Summa, V., Tateo, F., Gianossi, M.L., Bonelli, C.G., 2010. Influence of clay mineralogy on the stability of a landslide in Plio-Pleistocene clay sediments near Grassano (Southern Italy).
- Sturzenegger, M., Douglas, S., 2009. Close-range terrestrial digital photogrammetry and terrestrial laser scanning for discontinuity characterization on rock cuts. *Engineering Geology*, (in press).
- TectonicsFP, 2010. Software for Structural Geology. Available online at: <http://www.tectonicsfp.com> (accessed on 31.05.2010).

- Teza, G., Galgaro, A., Zaltron, N., Genevois, R., 2007. Terrestrial laser scanner to detect landslide displacement fields: a new approach. *International Journal of Remote Sensing* 28 (16), 3425-3446.
- Teza, G., Atzeni, C., Balzani, M., Galgaro, A., Galvani, G., Genevois, R., Luzi, G., Mecatti, D., Noferini, L., Pieraccini, M., Silvano, S., Uccelli, F., Zaltron, N., 2008a. Ground-based monitoring of high-risk landslides through joint use of laser scanner and interferometric radar. *International Journal of Remote Sensing* 29, 4735–4756.
- Teza, G., Pesci, A., Genevois, R., Galgaro, A., 2008b. Characterization of landslide ground surface kinematics from terrestrial laser scanning and strain field computation. *Geomorphology* 97, 424–437.
- Tripathy, S., Subba Rao, K.S., Fredlund, D.G., 2002. Water content-void ratio swell-shrink paths of compacted expansive soils. *Canadian Geotechnic Journal* 39, 938-959.
- Tyner, B. 2007. Packages: K-D trees. <http://www.stat.purdue.edu/~btyner/packages.html>.
- Uchida, E., Ogawa, Y., Maeda, N., T. Nakagawa, 1999. Deterioration of stone materials in the Angkor monuments, Cambodia. *Engineering Geology* 55, 101–112.
- UNESCO, 2010. The list of the World heritage sites. <http://whc.unesco.org/en/list/1237>. (accessed on 31.05.2010).
- Van Asch, T.W.J., 1997. The temporal activity of landslides and its climatological signals. In: Matthews, J.A., Brunsten, D., Frenzel, B., Glaßer, B., Weiß, M.M. (Eds.), *Rapid Mass Movement as a Source of Climatic Evidence for the Holocene*. *Palaeoclimate Research*, vol. 19. Gustav Fischer, Stuttgart, pp. 7 – 16.
- Varnes, D.J., Radbruch-Hall, D., Varnes, K.L., Smith, W.K., Savage, W.Z., 1990. Measurement of ridge-spreading movements (sackungen) at Bald Eagle Mountain, Lake County, Colorado 1975–1989. U.S. Dept. of the Interior, U.S. Geological Survey Open-File Report 90-543. 13 pp.
- Viero, A., Galgaro, A., Oppikofer, T., Metzger, R., Jaboyedoff, M., 2009a. Structural and geomechanical pattern recognition using terrestrial and airborne laser scanner techniques. Oral presentation. In: *Proceedings of the Natural Hazard session -EGU General Assembly, Geophysical Research Abstracts, Wien (Austria), 19-24 April 2009*.
- Viero, A., Vosselman, G., Slob, S., Galgaro, A., Hack, H.R.G.K., 2009b. Automatic analysis of terrestrial laser data: the application to a rock cliffs instability in the Dolomites (Eastern Alps- Italy. In: *Proceedings of the 6th EUREGEO- European Congress on Regional Geoscientific Cartography and Information systems, Munich, Bavaria (Germany), 9-12 June 2009*.
- Viero, A., Teza, G., Massironi, M., Jaboyedoff, M., Galgaro, A., 2010a. Laser scanning-based recognition of rotational movements on a deep seated gravitational instability: The Cinque Torri case (North-Eastern Italian Alps). *Geomorphology*, 122, 191-204.
- Viero, A., Teza, G., Massironi, M., Jaboyedoff, M., Galgaro, A., 2010b. A new method to derive rotational components of recent lateral spreadings: a laser scanning application. Oral presentation. In: *Proceedings of Natural Hazard session -EGU General Assembly, Geophysical Research Abstracts, Wien (Austria), 2-7 May 2010*.
- Vosselman, G., Gorte, B.G.H., Sithole, G. and Rabbani, T. 2004. Recognizing structure in laser scanner point clouds. *The International Archives of the Photogrammetry, Remote Sensing and Spatial Information Sciences*. vol. 46, part 8/W2, Freiburg, Germany, October 4-6, pp. 33-38.

- Welkner, D., Eberhardt, E., Hermanns, R.L., 2010. Hazard investigation of the Portillo Rock Avalanche site, central Andes, Chile, using an integrated field mapping and numerical modelling approach. *Engineering Geology* 114, 278–297.
- Willard, R.J., McWilliams, J.R., 1969. Microstructural techniques in the study of physical properties of rock. *International Journal of Rock Mechanics. Min. Sci.* 6, 1–12.
- Wise, D.J., Cassidy, J., Locke, C.A., 2003. Geophysical imaging of the Quaternary Wairoa North Fault, New Zealand: a case study. *Journal of Applied Geophysics* 53, 1-16.
- Wyllie, D.C., Mah, C.W., 2004. *Rock Slope Engineering: Civil and Mining* — Spon Press/ Taylor & Francis Group, London and New York.
- Yalcin, A., 2007. The effects of clay on landslides: a case study. *Applied clay sciences* 38, pp. 77-85.
- Yasar, E., Erdogan, Y., 2004. Correlating sound velocity with density, compressive strength and Young modulus of carbonate rocks. *International Journal of Rock Mechanics and Mining Sciences* 41 (5), 871–875.

Appendices

Appendix A. Rock samples properties

ID	Sample name	f (mm)- diameter	L (mm)- length	weight (g)	volume (mm ³)	r (g/cm ³)	L/f	area (cm ²)
1	HKZ 1	37.8	92.4	286.	103457	2.76	2.4	11.19
2	HGZ 1 (perp strata)	37.6	73.6	227.	81601	2.78	2.0	11.08
3	5T 1	37.7	95.6	295.	106667	2.76	2.5	11.15
4	T M 1 (obliq)	37.7	80.6	249.	90043	2.76	2.1	11.18
5	T M (perp strata)	37.7	67.9	212.	75798	2.79	1.8	11.16
6	AV1 (pll strata coarse)	37.8	75.4	225.	84669	2.66	2.0	11.23
7	AV1 (pll strata fine)	37.8	78.3	232.	87719	2.65	2.1	11.20
8	AV1 (pll strata fine)	37.3	93.4	209.	101948	2.05	2.5	10.91

This table shows the main physical properties of the rock samples tested by means of ultrasonic and uniaxial tests (Chap. 5.).

Appendix B. Direction Cosine Matrix for Euler angles determination

A rotation R can be always conceived as rotation by a specified angle α about a specified vector $\hat{\mathbf{v}}$, called Euler vector. Such a representation has the advantage of a clear physical interpretation, but four parameters (vector components and angle) are necessary and redundancy therefore exists (a rotation can be completely characterized by three parameters only), trigonometric functions are involved and the rotation axis is undefined if $\alpha = 0$.

The direction cosine matrix (DCM) is a representation particularly useful in those cases where the triads associated to the initial $(\hat{\mathbf{i}}, \hat{\mathbf{j}}, \hat{\mathbf{k}})$ and final $(\hat{\mathbf{i}}', \hat{\mathbf{j}}', \hat{\mathbf{k}}')$ reference frame are known. The DCM related to this transformation is

$$R = \begin{bmatrix} \hat{\mathbf{i}}' \cdot \hat{\mathbf{i}} & \hat{\mathbf{i}}' \cdot \hat{\mathbf{j}} & \hat{\mathbf{i}}' \cdot \hat{\mathbf{k}} \\ \hat{\mathbf{j}}' \cdot \hat{\mathbf{i}} & \hat{\mathbf{j}}' \cdot \hat{\mathbf{j}} & \hat{\mathbf{j}}' \cdot \hat{\mathbf{k}} \\ \hat{\mathbf{k}}' \cdot \hat{\mathbf{i}} & \hat{\mathbf{k}}' \cdot \hat{\mathbf{j}} & \hat{\mathbf{k}}' \cdot \hat{\mathbf{k}} \end{bmatrix}. \quad (\text{B.1})$$

This representation has the advantages that no singularities can appear, no trigonometric functions are involved, and the product rule for successive rotations is very simple (it is simply the matrix product). Nevertheless, six of the nine parameters are redundant, and a physical interpretation of the result is not always clear.

Another representation involves a sequence of three rotations around independent axes. Several possible sequences can be considered. Particularly used in analytic studies is the sequence 3-1-3, where a rotation by the angle ψ about the z axis, $R_z(\psi)$, is followed by $R_x(\theta)$ (about the rotated the x-axis) and, finally, by $R_z(\phi)$ (about the rotated z-axis). Nevertheless, in the problem addressed in the article, the sequence of Euler angle rotations that better represents the rotation is 3-2-1, like the case of aircraft attitude control. The rotation R is therefore represented by $R = R(\phi, \theta, \psi) = R_x(\phi)R_y(\theta)R_z(\psi)$, where ϕ , θ , and ψ are the roll, pitch and yaw angle respectively. Since the elementary Euler angle rotations are

$$R_x(\phi) = \begin{bmatrix} 1 & 0 & 0 \\ 0 & \cos \phi & \sin \phi \\ 0 & -\sin \phi & \cos \phi \end{bmatrix},$$

$$R_y(\theta) = \begin{bmatrix} \cos \theta & 0 & -\sin \theta \\ 0 & 1 & 0 \\ \sin \theta & 0 & \cos \theta \end{bmatrix},$$

$$R_z(\psi) = \begin{bmatrix} \cos \psi & \sin \psi & 0 \\ -\sin \psi & \cos \psi & 0 \\ 0 & 0 & 1 \end{bmatrix}, \quad (\text{B.2})$$

the result is

$$R = R(\phi, \theta, \psi) = \begin{bmatrix} \cos \theta \cos \psi & \cos \theta \sin \psi & -\sin \theta \\ -\cos \phi \sin \psi + \sin \phi \sin \theta \cos \psi & \cos \phi \cos \psi + \sin \phi \sin \theta \sin \psi & \sin \phi \cos \theta \\ \sin \phi \sin \psi + \cos \phi \sin \theta \cos \psi & -\sin \phi \cos \psi + \cos \phi \sin \theta \sin \psi & \cos \phi \cos \theta \end{bmatrix}. \quad (\text{B.3})$$

Thanks to its advantages of clear physical interpretation and absence of redundant parameters, the Euler angle representation is used in analytic studies, acquisition of input data or presentation of output data in many problems involving rotations, and onboard attitude control of a 3-axis stabilized spacecraft. Disadvantages are the facts that trigonometric functions are involved, singularities can appear for some θ angles, and no convenient product rules exist.

The fact that the rotation group in the 3D space is not Abelian (i.e. not commutative) must be taken into account. In particular, if the Euler angle representation is used and a sequence is chosen, this choice must be maintained in all the computations. The inverse of the rotation $R = R_x(\phi)R_y(\theta)R_z(\psi)$ is $R^{-1} = R_z(-\psi)R_y(-\theta)R_x(-\phi)$. Other possible representations of a rotation exist, e.g. the Euler parameters (based on quaternion algebra), but are unnecessary in this study.

Appendix C. Post processing results after segmentation of the Torre Inglese point cloud

Plane number	Dip direction (°)	Dip angle (°)	Plane equation parameters			XMEAN	YMEAN	ZMEAN	SIZE	Number of points	
			a	b	c						d (m)
1m	271	87	-0.99861	0.0173	0.049733	3863.8	4074	5340.8	2254	91.5	349
2m	110	66	0.85834	-0.30381	0.41346	-2814	4086.3	5345.6	2250.7	6.2	383
3m	31	83	0.50716	0.85387	0.11704	-6898	4078.1	5346.3	2261.7	22.2	2979
4m	262	55	-0.80961	-0.12061	0.57444	2658.7	4079.8	5324.1	2239.6	7.9	2688
5m	52	59	0.67714	0.53025	0.51021	-6727.5	4079.9	5323.9	2237.9	3.6	1053
6m	224	22	-0.26185	-0.26846	0.92702	423.0	4076.5	5326.6	2237.7	16.1	3884
7m	328	84	-0.52123	0.84589	0.11308	-2631.1	4080	5325.1	2239.3	4.4	387
8m	186	89	-0.10291	-0.99468	0.003957	5712.7	4082.3	5329.9	2247.1	19.9	11452
9m	10	88	0.16676	0.98561	0.027756	-5992.1	4075.2	5327	2238.7	7.7	2572
10m	190	85	-0.17707	-0.98067	0.083259	5760	4077.7	5327.4	2238.9	3.3	481

This table summarizes, for each segmented plane the most important geometrical properties imported in the calculation of set spacing.

Appendix D. Exposure data Site 1 – Torre Grande, Cinque Torri group

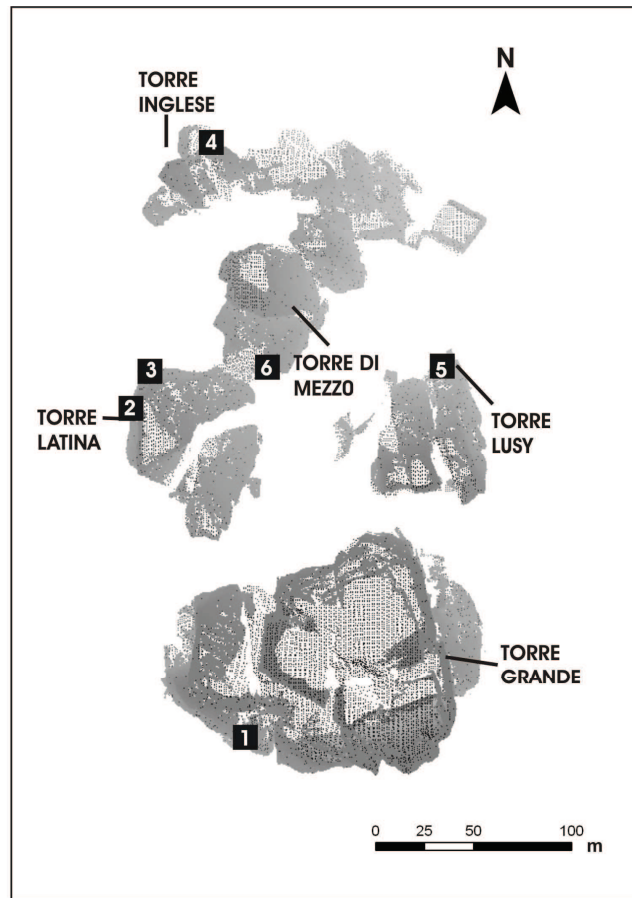


Figure D.1. Location map Site 1 (Torre Grande site) on the point cloud data.



Fig. D.2. Approximate position of the horizontal scanline at the basement of the western side of the Torre Grande: Site 1. The trace of the scanline is drawn-in by hand. The horizontal scanline survey was done from left to right over 5.00 metres.

Scanline data

Table D.1. Horizontal scanline (Torre Grande, Site 1)

Rockface orientation		345°/85°	Rockface width	50 m
Scanline orientation		58°/20°	Scanline length	5.00 m
Intersection distance (m)	Dip direction(°)	Dip(°)	Semi-trace length (m)	R (Schmidt hammer test)
0.05	275	89	5.00	
0.11	270	87	5.00	
0.15	273	89	5.00	
0.18	280	83	1.20	
0.27	276	85	1.40	
0.53	277	89	2.50	49-49-50-44-45-45-53-46-51-52
0.59	274	85	1.50	
0.60	216	85	1.40	
0.72	275	82	1.40	
0.75	275	89	1.30	
0.75	20	25	5.05	46-56-60-62-69-65-59-60-58-62
0.88	275	85	2.00	
0.94	271	86	2.00	
0.96	270	90	2.00	
1.00	273	82	2.00	
1.10	276	84	2.00	
1.20	5	15	6.00	
1.25	15	85	0.30	
1.25	210	76	2.50	
1.30	275	89	4.00	
1.40	277	80	4.00	
1.60	280	85	4.00	
1.60	5	15	6.00	
1.71	278	86	4.00	
1.82	159	84	1.50	
1.89	88	85	4.00	
1.98	93	84	4.00	50-60-58-46-48-38-50-55-57-53
2.20	216	75	2.10	
2.27	86	89	3.50	
2.35	151	80	1.50	
2.58	86	89	3.60	
2.90	83	90	3.50	
3.00	89	88	5.50	
3.88	113	84	4.50	
3.88	195	76	4.50	54-57-51-59-53-51*-52-52-54-55
4.10	143	75	3.50	
4.25	151	80	4.80	
4.25	178	31	6.00	
4.37	268	82	4.50	
4.64	265	85	4.50	
4.80	270	80	4.50	
4.88	268	82	4.50	
5.00	86	85	3.50	

	Set 1	Set 2	Set 3	Set 4
Mean dip direction (°)	272	206	028	151
Mean dip angle (°)	87	81	007	80
Number of observations N	29	4	4	5
Mean normal set spacing (m)	0.17	0.53	1.06	0.85

Table D.2. Summary statistics of the scanline surveys done on the Torre Grande exposure (Site 1).

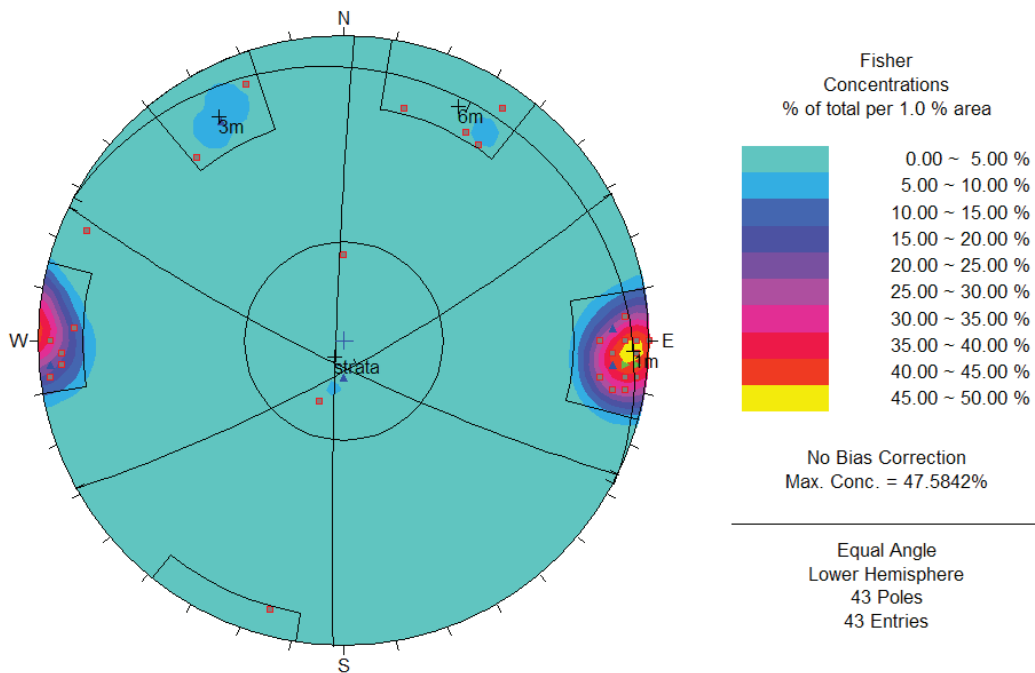


Fig. D.3. Stereoplot of the rock discontinuities orientations analyzed during the scanline mapping of the Torre Grande site

Appendix E. Exposure data Site 2 – Torre Latina, Cinque Torri group

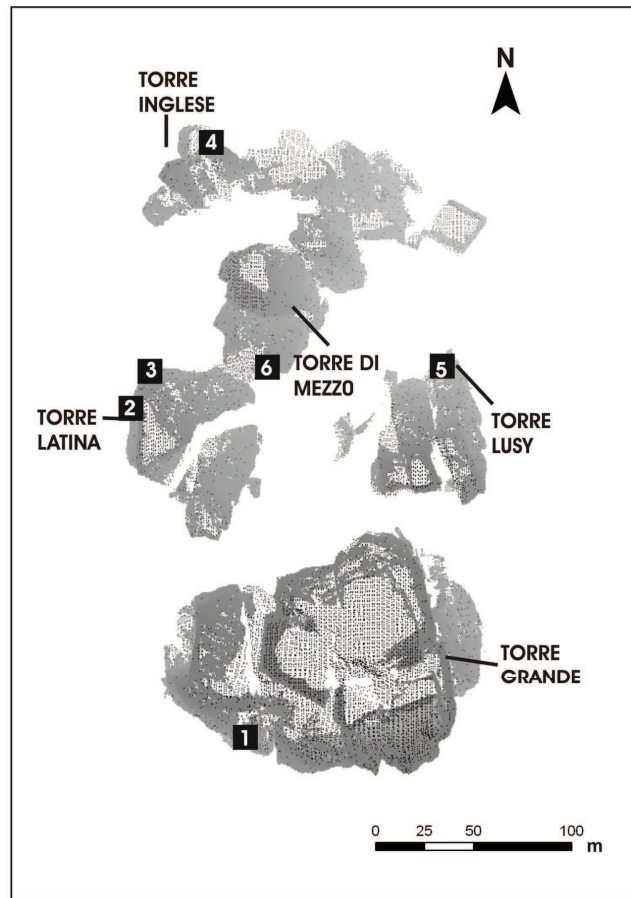


Figure E.1. Location map Site 2 (Torre Latina pinnacle) on the point cloud data.



Fig. E.2. Approximate position of the horizontal scanline at the basement of the western side of the Torre Latina pinnacle: Site 2. The trace of the scanline is drawn-in by hand. The horizontal scanline survey was carried out from left to right over 5.00 meters.

Scanline data

Table E.1. Oblique Scanline (Torre Latina, Site 2)

Rock face orientation		280°/90°	Rock face width		15 m
Scanline orientation		10°/15°	Scanline length		5.20 m
Intersection distance (m)	Dip direction(°)	Dip(°)	Semi-trace length (m)	R (Schmidt hammer test)	
0.04	340	7	3.60	26-27-26-21-19-26-28-22-24-20	
0.16	355	75	0.80		
0.28	355	75	2.30		
0.30	270	85	1.20	39-38-42-35-39-42-38-42-38-46	
0.33	358	75	2.60		
0.44	3	77	2.60		
0.55	90	85	1.70		
0.55	2	71	0.80		
0.55	270	10	4.20		
0.71	11	75	2.30		
0.80	10	73	0.60		
0.89	12	79	0.60		
0.89	82	73	0.55	46-46-46-47-46-47-46-45-45-48	
0.94	11	75	0.20		
1.11	10	78	1.50		
1.60	11	68	1.91		
1.70	10	70	1.40		
1.85	92	83	1.20	59-59-58-52-52-50-57-52-48-48	
1.97	1	80	1.40	45-48-47-49-47-51-50-48-45-48-47	
2.33	15	80	2.50		
2.35	320	25	2.60		
2.45	168	64	0.40	49-53-53-48-50-54-38-51-50-60-40-48	
2.50	17	78	2.00	22-20-28-28-20-18-20-21-35-39-34-26	
2.90	355	80	4.50		
3.05	1	56	1.40		
3.10	5	63	1.40		
3.18	170	68	0.11		
3.24	357	65	1.40		
3.37	6	70	1.40		
3.48	10	75	1.40		
3.60	19	75	2.20		
3.75	354	70	2.30		
3.98	349	85	1.50		
4.00	95	80	2.05	54-50-54-48-46-46-50-52-55-54	
4.12	345	87	1.50		
4.30	355	82	1.00		
4.48	85	85	1.00		
4.65	356	80	0.60		
4.82	360	78	0.60		
5.20	355	80	3.50		

	Set 1	Set 2	Set 3	Set 4
Mean dip direction (°)	3	89	312	169
Mean dip angle (°)	75	83	13	66
Number of observations N	29	6	3	2
Mean normal set spacing (m)	0.15	0.27	0.28	0.60

Table E.2. Summary statistics of the scanline surveys done on the Torre Latina exposure (Site 2).

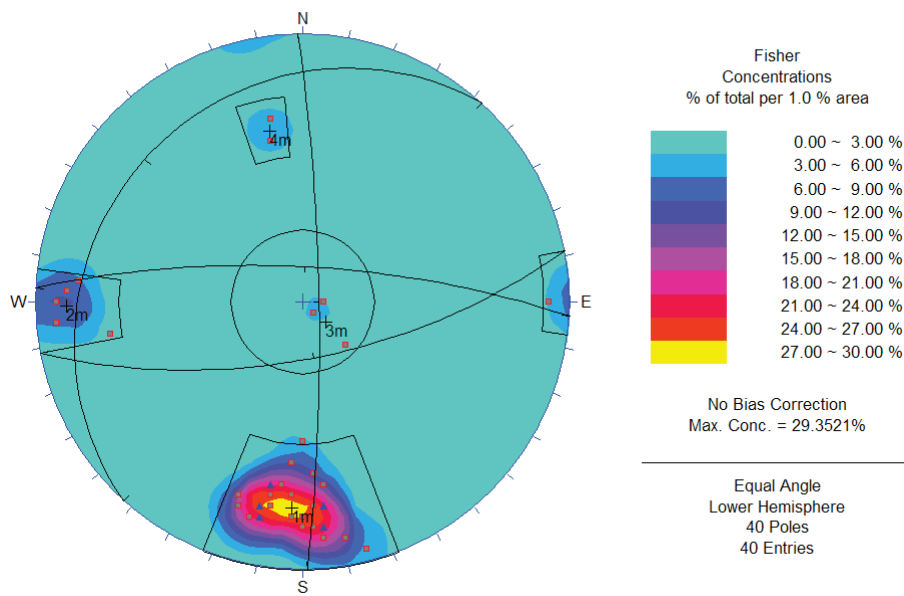


Fig. E.3. Stereoplot of the rock discontinuities orientations analyzed during the scanline mapping of the western side of the Torre Latina pinnacle

Appendix F. Exposure data Site 3 – Torre Latina, Cinque Torri group

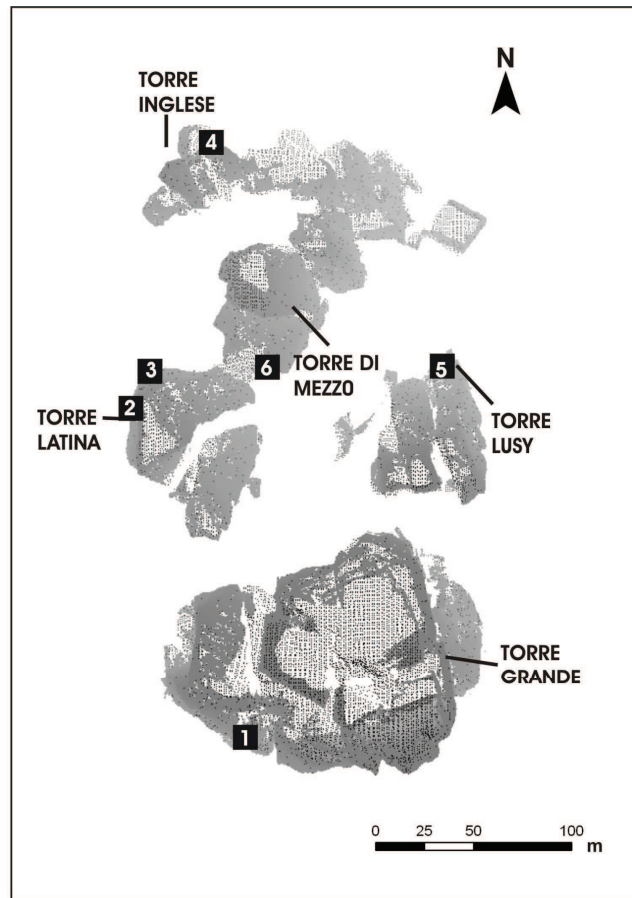


Figure F.1. Location map Site 3 (Torre Latina pinnacle) on the point cloud data.



Fig. F.2. Approximate position of the oblique scanline at the basement of the northern side of the Torre Latina pinnacle: Site 3. The trace of the scanline is drawn-in by hand. The survey was carried out from left to right over 5.00 meters.

Scanline data

Table F.1. Oblique Scanline (Torre Latina, Site 3)

Rock face orientation		350°/78°	Rock face width	20 m
Scanline orientation		160°/18°	Scanline length	5.05 m
Intersection distance (m)	Dip direction(°)	Dip(°)	Semi-trace length (m)	R (Schmidt hammer test)
0.20	90	90	2.20	
0.36	65	85	2.20	
0.44	68	82	2.40	
0.51	85	80	2.40	
0.57	80	85	2.25	
0.62	90	85	2.45	
0.90	275	87	1.40	
0.92	343	72	2.30	68-42-59-41-57-64-57-69-61-58
0.98	296	81	1.30	
1.00	10	85	0.50	38-38-36-39-39-43-43-38-41-44
1.03	262	85	0.80	
1.12	259	86	1.20	
1.20	2	75	0.80	
1.21	253	90	0.60	38-42-38-39-43-39-42-45-44-47
1.23	280	78	6.00	
1.24	80	85	1.25	
1.40	70	85	0.90	
1.41	290	85	1.00	
1.55	50	75	1.30	
1.61	67	82	1.50	
1.85	221	68	1.70	
1.86	84	84	1.90	
1.92	275	90	1.80	
1.93	25	67	1.50	
2.01	89	90	0.75	
2.20	289	80	0.25	
2.29	22	80	0.20	
2.31	22	80	0.20	
2.55	241	80	0.60	
2.70	1	80	0.20	
2.71	100	86	0.15	
2.90	100	90	0.15	
3.00	205	5	8.00	
3.20	90	80	4.00	
4.10	200	9	4.00	
4.70	100	85	4.50	
5.05	260	75	2.05	

	Set 1	Set 2	Set 3
Mean dip direction (°)	202	87	9
Mean dip angle (°)	7	90	77
Number of observations N	2	26	7
Mean normal set spacing (m)	0.18	0.05	0.34

Table F.2. Summary statistics of the scanline surveys done on the Torre Latina exposure (Site 3).

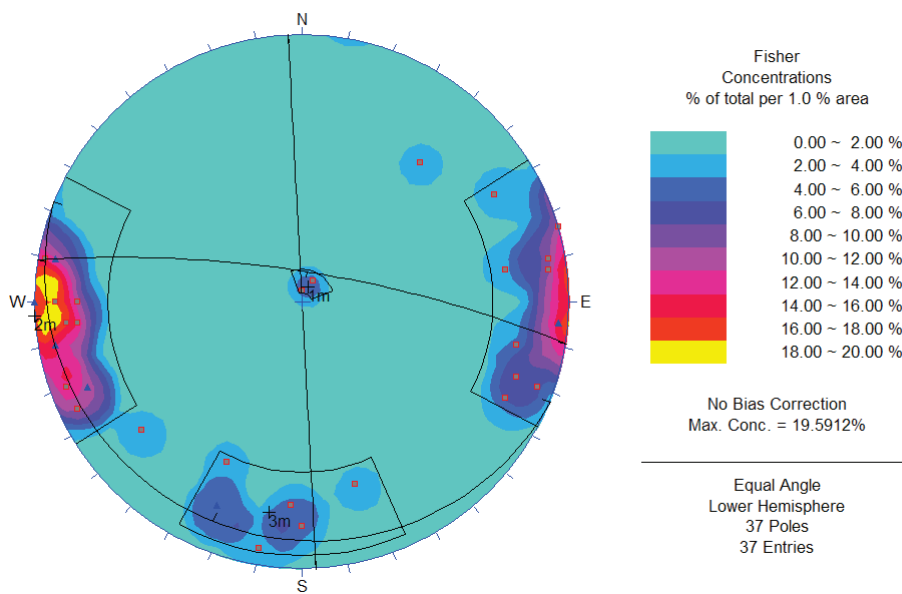


Fig. F.3. Stereoplot of the rock discontinuities orientations analyzed during the scanline mapping of the northern side of the Torre Latina pinnacle

Appendix G. Exposure data Site 4 – Torre Inglese, Cinque Torri group

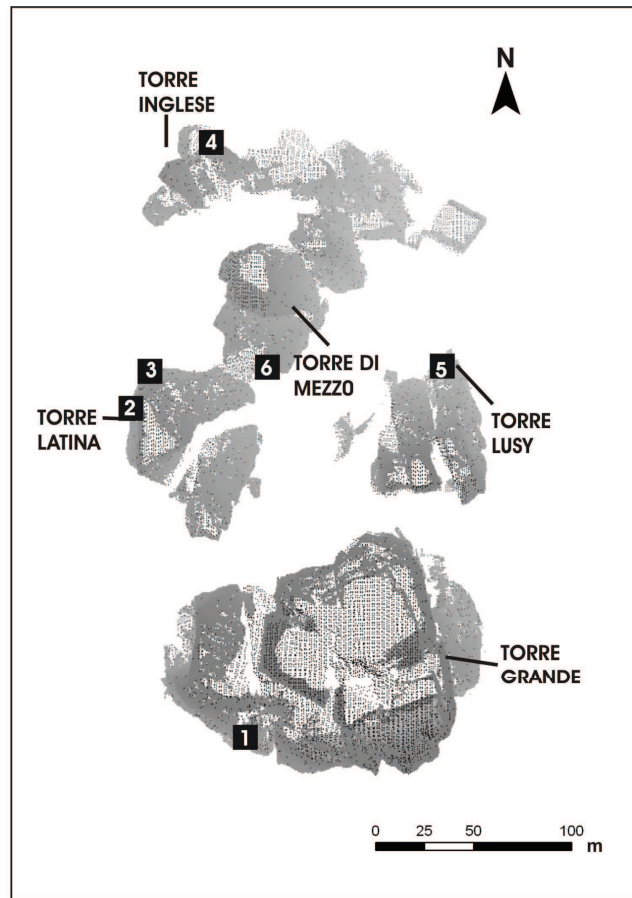


Figure G.1. Location map Site 4 (Torre Inglese pinnacle) on the point cloud data.



Fig. G.2. Approximate position of the oblique scanline at the basement of the northern side of the Torre Inglese pinnacle: Site 4. The trace of the scanline is drawn-in by hand. The survey was carried out from left to right over 4.00 meters.

Scanline data

Table G.1. Oblique Scanline (Torre Inglese, Site 4)

Rock face orientation		165°/68°	Rock face width	20 m
Scanline orientation		155°/24°	Scanline length	4.12 m
Intersection distance (m)	Dip direction(°)	Dip(°)	Semi-trace length (m)	R (Schmidt hammer test)
0.00	70	80	0.30	
0.10	164	81	0.15	
0.12	170	80	0.15	
0.25	250	90	1.90	
0.30	342	29	4.50	
0.35	140	67	0.09	
0.60	220	85	2.20	
0.65	1	90	2.00	
0.90	296	81	1.30	
0.91	208	85	4.00	
1.05	95	80	4.00	
1.20	45	80	4.00	
1.25	80	75	1.40	
1.27	200	83	1.70	
1.30	236	90	1.90	
1.47	95	85	1.10	
1.48	200	76	4.00	
1.60	98	86	2.00	
1.70	177	75	3.00	
1.75	345	26	5.00	50-51-50-52-53-48-47-48-51-48
1.85	284	83	1.50	
1.90	213	85	3.50	
1.93	285	85	3.50	53-48-53-52-48-48-50-46-50-47
2.23	110	86	2.50	
2.24	260	70	2.50	
2.28	255	72	2.50	
2.55	180	76	1.05	
2.75	193	70	0.90	
2.80	123	88	0.90	
2.93	180	80	2.50	
3.10	168	75	1.60	
3.32	296	76	1.90	
3.45	294	72	1.90	
3.45	182	78	1.90	
3.46	180	80	1.80	
3.57	290	79	1.90	
3.64	170	70	1.80	
3.65	298	83	1.90	
4.10	172	78	1.80	
4.12	290	83	1.80	

	Set 1	Set 5	Set 6	Set 7	Set 6
Mean dip direction (°)	343	257	175	289	212
Mean dip angle (°)	27	71	78	86	84
Number of observations N	2	2	11	13	8
Mean normal set spacing (m)	0.37	0.11	1.12	0.01	0.01

Table G.2. Summary statistics of the scanline surveys done on the Torre Inglese exposure (Site 4).

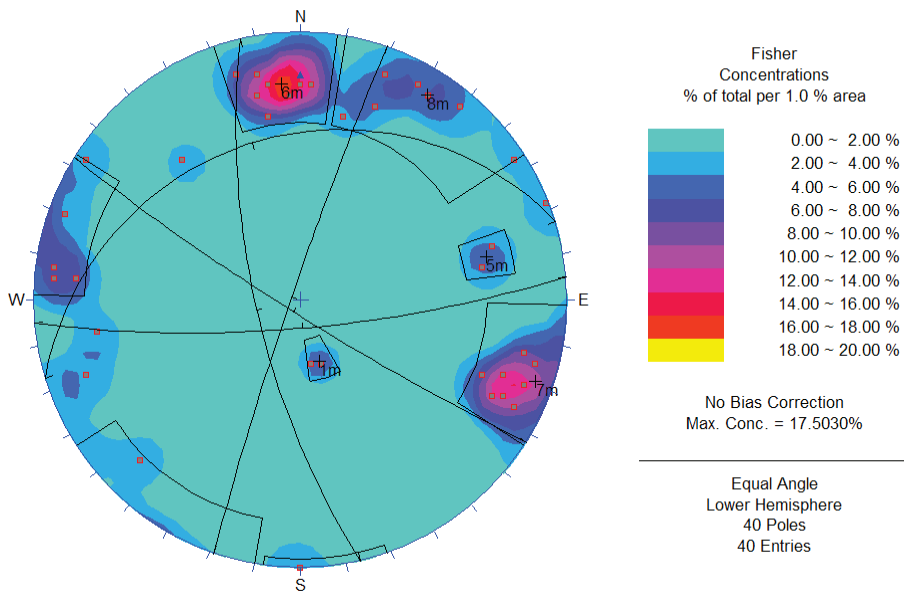


Fig. G.3. Stereonet of the rock discontinuities orientations analyzed during the scanline mapping of the northern side of the Torre Inglese pinnacle

Appendix H. Exposure data Site 5 – Torre Lusy, Cinque Torri group

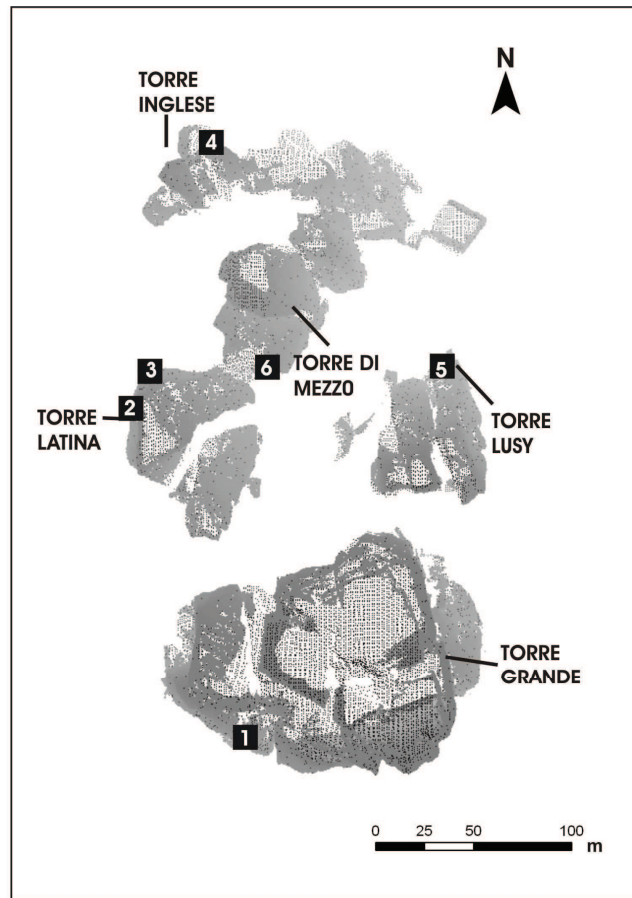


Figure H.1. Location map Site 5 (Torre Lusy pinnacle) on the point cloud data.



Fig. H.2. Approximate position of the oblique scanline at the basement of the northern side of the Torre Lusy pinnacle: Site 5. The trace of the scanline is drawn-in by hand. The survey was carried out from left to right over 4.85 meters.

Scanline data

Table H.1. Oblique Scanline (Torre Lusy, Site 5)

Rock face orientation		66°/84°	Rock face width		20 m
Scanline orientation		28°/26°	Scanline length		4.85 m
Intersection distance (m)	Dip direction(°)	Dip(°)	Semi-trace length (m)	R (Schmidt hammer test)	
0.00	92	88	42.00		
0.02	20	6	2.20		
0.05	330	74	0.17		
0.17	150	79	0.04		
0.20	50	78	0.14	44-46-50-56-48-50-40-48-46-46 (48)	
0.30	326	81	0.35		
0.35	250	5	0.70		
0.45	320	80	0.55		
1.30	344	80	60.00		
1.40	344	80	60.00		
1.50	344	80	60.00		
1.67	235	30	1.00		
1.74	80	78	0.21		
1.75	330	88	0.25		
1.78	24	70	0.45		
1.80	260	30	4.20		
1.90	92	77	0.20		
2.00	153	86	0.10		
2.30	96	84	0.70	54-54-52-54-54-54-48-54-53-54	
2.40	30	5	3.10		
2.42	160	87	0.50		
2.90	20	86	0.40		
3.00	327	88	0.50		
3.05	294	65	0.25		
3.25	180	64	0.65		
3.50	30	84	0.25		
3.75	144	88	0.80	54-55-55-54-54-52-49-50-49-47	
3.80	144	88	0.80		
3.90	144	88	0.80		
3.91	209	20	3.20		
4.00	144	88	0.80		
4.10	209	20	3.20		
4.20	332	90	0.55		
4.30	332	90	0.55		
4.40	200	77	0.65		
4.45	332	90	0.55		
4.50	62	76	0.40		
4.55	326	81	0.50	46-49-44-40-46-34-43-40-44-42	
4.60	326	81	0.50		
4.70	326	81	0.50		
4.75	326	81	0.50		
4.80	60	80	0.40		
4.85	326	81	0.50		

	Set 1	Set 2	Set 3	Set 4	Set 5
Mean dip direction (°)	236	330	90	57	25
Mean dip angle (°)	13	86	82	78	80
Number of observations N	7	23	4	3	3

Table H.2. Summary statistics of the scanline surveys carried out on the Torre Lusy exposure (Site 5).

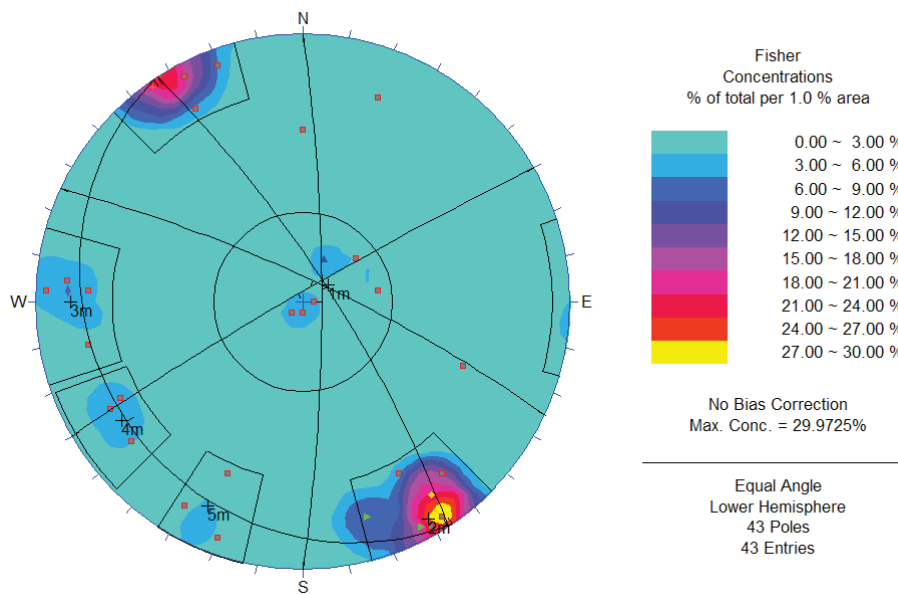


Fig. H.3. Stereoplot of the rock discontinuities orientations analyzed during the scanline mapping of the eastern side of the Torre Lusy pinnacle

Appendix M. Random analyses of main rock discontinuities of the Torre Grange and Torre Inglese pinnacles

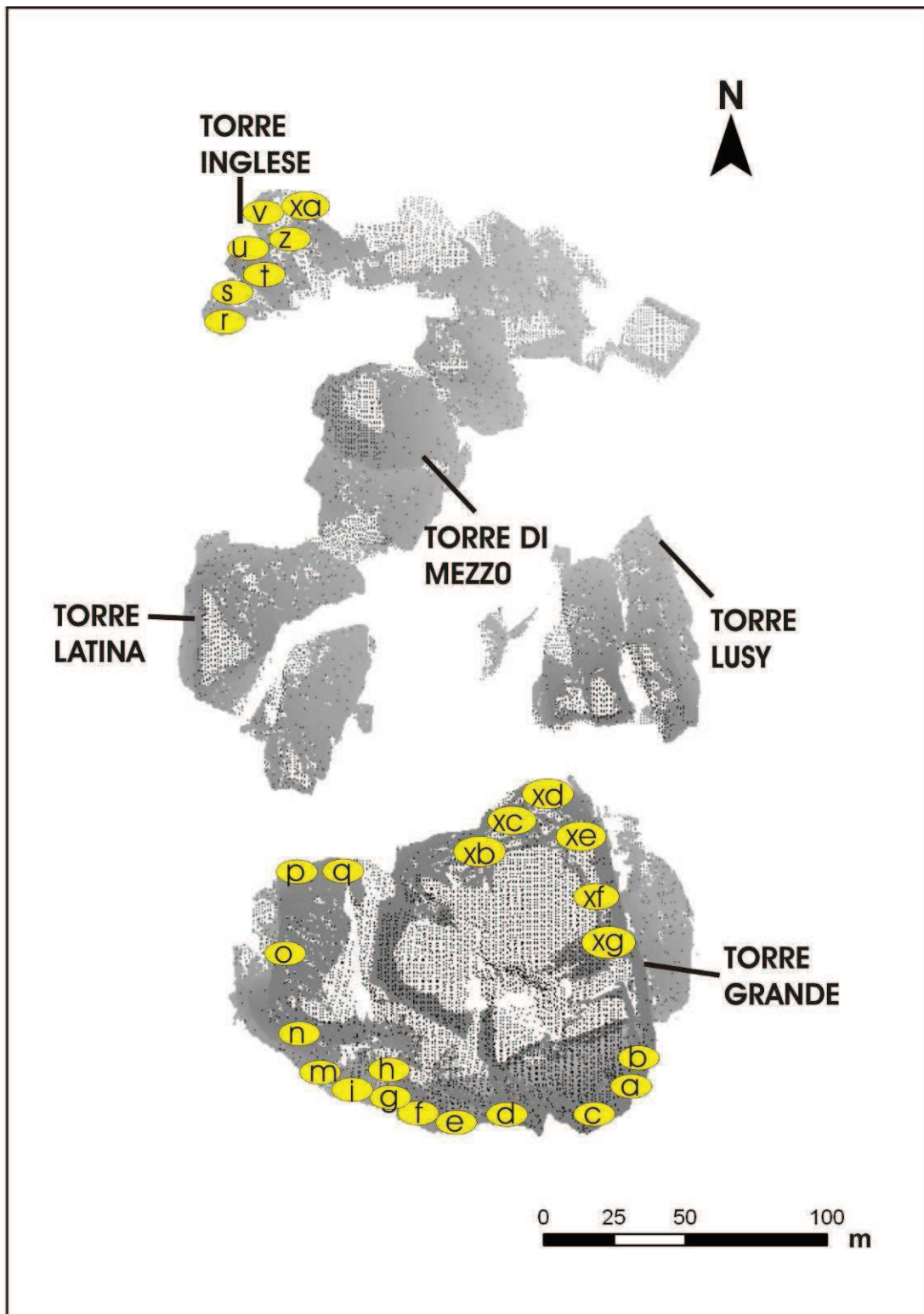














Fig. M.1. Map view of the filtered Cinque Torri point cloud with location of a random joint characterization carried out through geological compass and Schmidt hardness test.




Field campaigns 20 June 2008

SITE	Joint attitude	Schmidt hammer rebound number (R) and orientation device	
a	<p>N63°E/ 84°</p> <p>(N150°E/ 78°)</p>	<p>54 , 69, 57, 53, 50, 50, 48, 48, 49, 50, 58</p> <p>61, 64, 61, 60, 65, 58, 68, 70, 66, 69</p>	
b	<p>Strata bedding</p>	<p>43, 52, 50, 49, 51, 54, 41, 41, 43, 45, 39</p> <p>45, 46, 41, 42, 36, 43, 38, 36, 38, 40, 45</p>	
c	<p>205°/7°</p>	<p>/</p>	



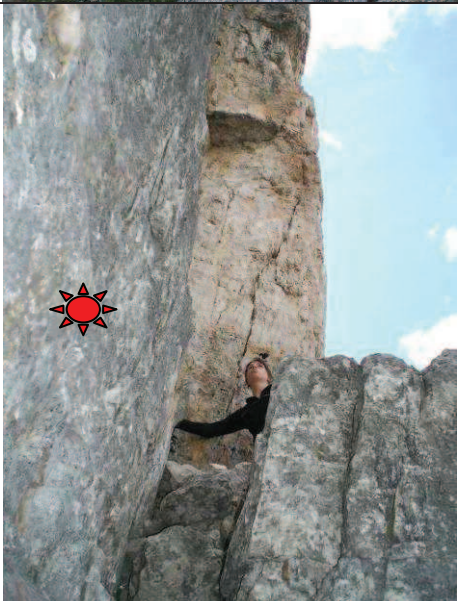
d	7°/90°	60, 60, 57, 61, 42, 54, 57, 58, 48, 60, 59, 62	
e	Strata bedding N13°W/14° joint N 56°E/88°	63, 63, 60, 57, 60, 61, 62, 59, 56, 55	
f	264°/85°	70, 68, 67, 70, 70, 52, 66, 68, 64, 60, 65	

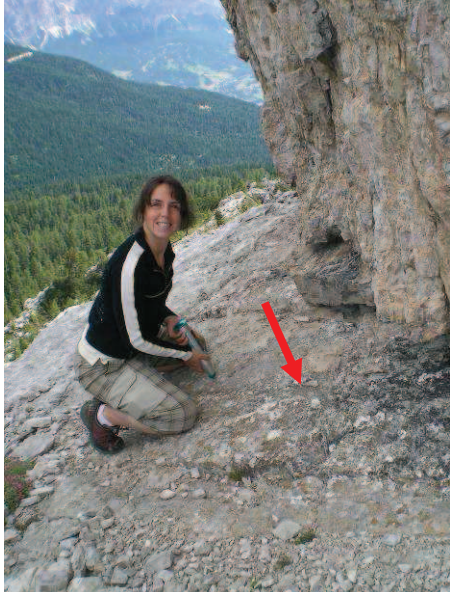
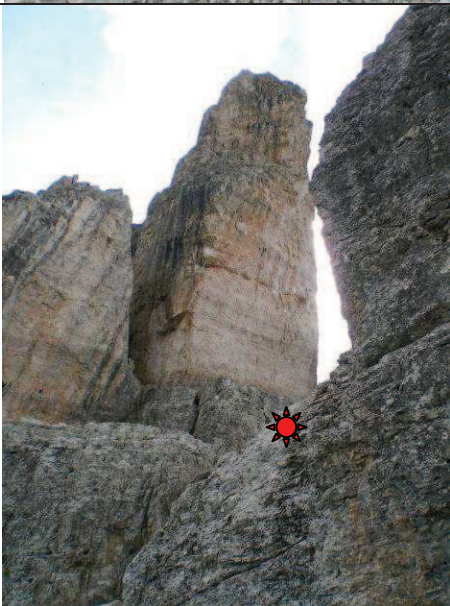

g	263°/90°	52, 54, 52, 58, 45, 46, 52, 50, 48, 45	
h	70°/82°	56, 50, 52, 58, 60, 61, 70, 70, 69, 62, 69 53, 53, 58, 63, 65, 61, 63, 59, 54, 58, 55	
i	188°/78°	52, 55, 48, 58, 62, 61, 61, 59, 65, 59, 62	

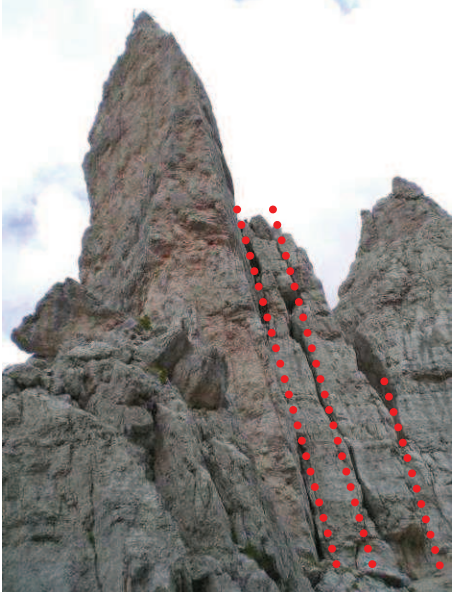

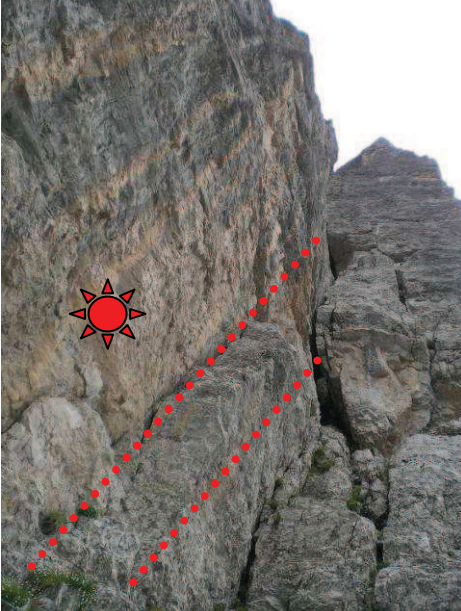
l	145°/82°	51, 45, 46, 58, 56, 48, 46, 46, 54, 55, 51, 56	
m	72°/85°	49, 50, 48, 52, 57, 50, 57, 49, 50, 49	
n	268°/86°	48, 46, 49, 49, 40, 48, 56, 42, 55, 45	



o	228°/65°	56, 54, 58, 57, 54, 52, 50, 52, 53, 53 60, 48, 49, 48, 58, 61, 68, 68, 70, 60	
p	262°/82°	52, 60, 50, 62, 68, 67, 58, 67, 66, 54	
q	178°/85°	52, 62, 63, 62, 50, 68, 56, 60, 58, 60	


Field campaign 24 July 2008

SITE	Joint orientation	Schmidt hammer rebound number (R) and orientation device	
r	335°/22° Strata bedding	52, 68, 52, 62, 66, 52, 54, 54, 54, 58 59, 60, 62, 60, 58, 56, 54, 52, 54, 52, 56, 58 (block below strata)	
s	75°/76°	48, 50, 44, 45, 53, 46, 44, 45, 50, 54	
t	275°/88°	/	

<p>u</p>	<p>Strata bedding</p>	<p>55, 40, 44, 54, 68, 52, 66, 66, 64, 50, 62, 68, 54</p>	
<p>v</p>	<p>Fault surface western side Torre Inglese</p>	<p>70, 60, 66, 52, 58, 60, 66, 62, 60, 54, 58</p>	
<p>z</p>	<p>Joint at the base of the Torre Inglese (north-western side)</p>	<p>58,59,60,56,60,61,59,56, 57,60,58</p>	

<p>Xa</p>	<p>Parallel discontinuity system 80°/80°</p>	<p>/</p>	
<p>Xb</p>	<p>90°/82°</p>	<p>68,68,72,72,64,72,73,70, 70,68</p>	
<p>Xc</p>	<p>255°/90°</p>	<p>/</p>	

Xd	Eastern side Torre Grande N85°/85°	/	
Xe	Rock discontinuity 340°/75°	/	

<p>xf</p>	<p>85°/85°</p>	<p>/</p>	
<p>xg</p>	<p>Eastern side of the Torre Grande 335°/85°</p>	<p>/</p>	